

INVOLVEMENT OF THE GABA_A RECEPTOR IN CALCIUM-DEPENDENT TOXICITY OF
METHYLMERCURY IN DEVELOPING AND AGED CEREBELLUM

By

Aaron Blackwood Bradford

A DISSERTATION

Submitted to
Michigan State University
in partial fulfillment of the requirements
for the degree of

Biochemistry and Molecular Biology - Environmental Toxicology - Doctor of Philosophy

2013

ABSTRACT

INVOLVEMENT OF THE GABA_A RECEPTOR IN CALCIUM-DEPENDENT TOXICITY OF METHYLMERCURY IN DEVELOPING AND AGED CEREBELLUM

by

Aaron Blackwood Bradford

Methylmercury (MeHg) is an environmental neurotoxicant of concern because of its bio-accumulation in marine ecosystems and the susceptibility of developing cerebellum to toxicity. MeHg accumulates in the central nervous system with a long latency to toxicity and excretion. It induces permanent motor dysfunction through selective toxicity in cerebellar granule cells (CGCs), with developing CGCs being a particular target. Though the exact pathways by which MeHg induces neuronal death and dysfunction are not fully characterized, one of the common, central pathways by which it is hypothesized to act is through disruption of intracellular calcium concentration ($[Ca^{2+}]_i$). $[Ca^{2+}]_i$ is kept low in neurons and small changes are critical for neuronal signaling. Disruption of these concentrations occurs in several cell models, characterized as an irreversible increase in $[Ca^{2+}]_i$ over time. We sought to characterize disruption of $[Ca^{2+}]_i$ in cerebellar slices, which retain many characteristics of whole tissue. One pathway by which methylmercury may act on intracellular calcium is through the γ -aminobutyric acid type A receptor (GABA_AR), a normally inhibitory receptor that is excitatory in developing CGCs and possibly in axons and presynaptic terminals. This excitation is coupled to influx of $[Ca^{2+}]_i$ and is critical to developmental migration of neurons and to neurotransmitter release. The interaction of GABA_AR s with MeHg is partially characterized by electrophysiology and there are several experiments that suggest certain subunits of the receptors are associated with cell and developmental susceptibility. We hypothesized that both MeHg and GABA_AR s could have effects on $[Ca^{2+}]_i$ in CGCs in acutely-isolated slices of cerebellum and that these effects would be dependent on age and GABA_AR subunit expression. To monitor $[Ca^{2+}]_i$ we used

concentration-dependent fluorophores and imaging on confocal and epifluorescent microscopes. We first tested for $[Ca^{2+}]_i$ changes in neonatal rat, a model frequently used previously for MeHg toxicity studies. In neonatal rat CGCs, MeHg caused a concentration-dependent increase in $[Ca^{2+}]_i$ -dependent fluorescence within minutes. These fluorescence increases included up to about 2-fold in mature CGCs compared to starting fluorescence and up to about 3-fold increase in susceptible developing CGCs. Muscimol, a GABA_AR agonist, and bicuculline, a GABA_AR antagonist, are both able to reduce the effects of MeHg on $[Ca^{2+}]_i$. MeHg is able to increase $[Ca^{2+}]_i$ in cerebellar slices from mice as well, and a knockout of the GABA_AR $\alpha 6$ subunit is able to increase the susceptibility of CGCs, particularly developing CGCs, with similar 2-3 fold increases in fluorescence. Muscimol and bicuculline reduce MeHg effects in these mice as well. Compared to developmental toxicity, aging and lifelong exposures to MeHg have not been characterized nearly as fully, and as part of a comprehensive study, the effects of MeHg and several other $[Ca^{2+}]_i$ -dependent mechanisms were tested with these fluorescence microscopy approaches. Acute application of MeHg appears to cause 2-fold increases in fluorescence that are not dependent on age or chronic treatment. However, chronic treatment with MeHg appears to be able to increase both spontaneous and induced Ca^{2+} activity in slices, and chronic treatment with isradipine appears to reduce this activity, indicating chronic, non-lethal concentrations can have subtle effects on Ca^{2+} -dependent mechanisms. Finally, this dissertation provides some characterization of spontaneous $[Ca^{2+}]_i$ transients in slices, indicating age and genotype have effects on spontaneous CGC activity. Altogether, the results of this dissertation indicate that GABA_AR s have a partial role in the toxicity of MeHg as a pathway by which MeHg appears to be able to disrupt $[Ca^{2+}]_i$ as interference by GABA_AR modulators and alterations to subunit expression also alter MeHg effects on $[Ca^{2+}]_i$. MeHg exposure may in turn alter GABA_AR signaling as indicated by changes to muscimol responses in chronically-exposed mice.

Copyright by
AARON BLACKWOOD BRADFORD
2013

This dissertation is dedicated to everyone that believed I could do it. Having learned stagecraft in high school and college, I am especially thankful to anyone and everyone that worked behind the scenes to make sure that I could continue, with or without my knowledge.

ACKNOWLEDGMENTS

First I need to thank my family. My parents, grandparents and extended family encouraged my pursuits of education and science from an early age and always kept me going even when I faltered. I want to thank my wife for caring for me at my worst and always pushing me to get on with things. I want to thank my grandpa Blackwood, he didn't get to see me accomplish this, but I think he knew it was where I was headed and would be proud to see the high levels of achievement in the family. I want to thank my little sister Nora for always thinking the science I am doing is interesting and cool.

I want to thank Dr. William "Bill" Atchison and my thesis committee for carefully considering my proposal and experiments, and always being able to come up with interesting suggestions and corrections. I also want to thank everyone for pushing me to produce a complete dissertation, rather than settling for a Masters' thesis when the possibility came up.

I want to thank the Center for Integrative Toxicology, including its directors Dr. Roth and Dr. Kaminsky as well as the support staff, for taking me on as a fellowship student and always finding a way to support me when I needed it. I want to thank MSU's Institute for Cyber-Enabled Research and Dr. Colbry for providing extensive imaging training, and MSU's Center for Statistical Training and Consulting for extensive statistical training. I want to thank Dr. Sisk and Dr. Schneider for training in writing.

I want to thank my friends, particularly my fellow graduate students both inside and outside the laboratory. I might seem like an introvert, but laughing, socializing, venting and griping are still needed. I hope I was as generous, kind, honest, fun and loyal with my friends as they were with me.

TABLE OF CONTENTS

LIST OF FIGURES	X
KEY TO SYMBOLS AND ABBREVIATIONS	XX
CHAPTER ONE: INTRODUCTION	1
A) BACKGROUND	2
a. Methylmercury	2
i. MeHg in the environment	2
ii. MeHg in human health	3
iii. MeHg chemistry and mechanisms	7
iv. MeHg toxicity susceptibility and resistance	12
b. Calcium	15
i. Calcium signaling and regulation	15
ii. Calcium and neurotransmission	17
iii. Calcium in development and aging	18
iv. MeHg and calcium	20
c. Cerebellum	22
i. Cerebellar circuitry	22
ii. Cerebellum growth and neuron development	23
d. GABA _A receptors	26
i. GABA _A receptor structure and function	26
ii. GABA _A receptor signaling	30
iii. GABA _A receptors and calcium	32
iv. GABA _A receptor pharmacology	33
v. GABA _A receptors during development	35
vi. GABA _A receptor disorders and toxicology	37
B) OBJECTIVES AND RATIONALE	39
a. Hypothesis and aims	39
b. Ca ²⁺ imaging in cerebellar slices from rats and mice as a model for MeHg toxicity	40
CHAPTER TWO: METHYLMERCURY-ASSOCIATED INCREASES IN FLUO4 FLUORESCENCE IN NEONATAL RAT CEREBELLAR SLICES ARE DEPENDENT ON GRANULE CELL MIGRATIONAL STAGE AND MODULATED BY GABA_A RECEPTORS.	45
A) Abstract	46
B) Introduction	47
C) Materials and methods	50
Chemicals and solutions	50
Acute slice preparation	51
Confocal microscopy	52
Image analysis and statistics	56
D) Results	65

	Visualization of layers and cytotoxicity	65
	Acute MeHg slice treatment	66
	Muscimol and bicuculline treatment with MeHg	72
E)	Discussion	78
CHAPTER THREE: ACUTE METHYLMERCURY TREATMENT INCREASES FLUO4 FLUORESCENCE IN NEONATAL MOUSE CEREBELLAR SLICES AND IS DEPENDENT ON GABA_AR α6 SUBUNIT EXPRESSION, MIGRATIONAL STAGE AND GABA_AR MODULATION		
83		
A)	Abstract	84
B)	Introduction	86
C)	Materials and methods	89
	Chemicals and solutions	89
	Animal care and genotyping of transgenic animals	89
	Acute slice preparation	92
	Confocal microscopy	92
	Image analysis and statistics	93
D)	Results	97
	Visualization of layers	97
	Acute MeHg paired treatment in (+/+) and (-/-) mice	100
	Muscimol and bicuculline paired treatments with MeHg	102
E)	Discussion	112
CHAPTER FOUR: COMPARATIVE Ca²⁺ EFFECTS OF CHRONIC EXPOSURE OF ADULT MICE TO MeHg OR ISRADIPINE		
117		
A)	Abstract	118
B)	Introduction	120
C)	Materials and methods	124
	Chemicals and solutions	124
	Animal care and treatments	125
	Tissue collection	126
	High-speed imaging	128
	Confocal microscopy	132
	Statistics	133
D)	Results	137
	Confocal Ca ²⁺ imaging	137
	High-speed Ca ²⁺ imaging	143
E)	Discussion	154
CHAPTER FIVE: HIGH-SPEED Ca²⁺ IMAGING REVEALS SPONTANEOUS Ca²⁺ TRANSIENTS IN CEREBELLAR SLICES FROM YOUNG AND OLD MICE		
158		
A)	Abstract	159
B)	Introduction	161
C)	Materials and methods	163
	Chemicals and solutions	163
	Animal care and use	163
	Image acquisition and treatment	164

D)	Results	166
	Visualization of CGCs	166
	Spontaneous Ca ²⁺ transients	166
E)	Discussion	175
CHAPTER SIX: SUMMARY AND CONCLUSIONS		180
	Summary and conclusions	181
REFERENCES		195

LIST OF FIGURES

- Figure 1.1 Schematic representation of neuronal MeHg targets and the central action of $[Ca^{2+}]_i$ in normal neuronal function and toxicity. This schematic represents an axon terminal, but many of these mechanisms are present throughout a neuron. MeHg acts on Ca^{2+} channels (such as VGCCs), metabotropic receptors that signal through IP_3 (such as the M3 muscarinic receptor), and the $GABA_A$ receptor at the surface of neurons (red arrows). MeHg is also able to enter cells and act on proteins such as the mitochondrial transition pore (mPTP), but the exact mechanisms of entry are unclear (dashed red arrow); $[Ca^{2+}]_i$ is normally increased transiently through several mechanisms, such as Ca^{2+} -dependent Ca^{2+} release from ER through ryanodine receptors, but MeHg increases $[Ca^{2+}]_i$ beyond normal levels (black arrows). The action by which MeHg can increase $[Ca^{2+}]_i$ through $GABA_A$ receptors is unclear, but may be dependent on VGCCs through depolarization or other mechanisms (dashed black line). Some Ca^{2+} may be buffered by Ca^{2+} binding proteins in the cytosol, but excess Ca^{2+} is normally taken up by the ER through Ca^{2+} -ATPases such as the smooth endoplasmic reticulum Ca^{2+} ATPase (SERCA), and may be expelled from the cytoplasm by other ATP-dependent mechanisms, both of which require ATP from the mitochondria (blue arrows). The normal actions of increased $[Ca^{2+}]_i$ include regulating vesicle release, neuronal motility during development, and regulation of gene expression, but the excess of Ca^{2+} from MeHg actions can cause excess neurotransmitter release, aberrant gene expression, and can activate several enzymes involved in apoptosis, such as lipases and calpains (magenta arrows). For interpretation of the references to color in this and all other figures, the reader is referred to the electronic version of this dissertation. 10
- Figure 1.2 Schematic of CGC migration and maturation in the cerebellum. CGCs migrate from the base of the developing cerebellum through several stages (gray arrows) during the third trimester in humans and the first two postnatal weeks in rodents, both of which are considered to be the most susceptible periods for MeHg toxicity in each group. CGC precursors (orange) migrate along the surface of the cerebellum, accumulate in a temporary layer termed the external granule (or germinal) layer (EGL) and divide. Division terminates for these CGC precursors, and the resulting CGCs then migrate down Bergmann glial processes (green) through the molecular layer (ML) where PCs are developing extensive dendrites (blue). Migration stops, and the CGCs put out axons that travel back through the ML and produce parallel fibers which synapse onto PC dendrites. All stages of migration and maturation are dependent on finely-tuned Ca^{2+} oscillations and regulation by expression of surface receptors such as $GABA_A$ Rs (Komuro and Rakic, 1998). CGCs express mostly $\alpha 2$ subunit-containing $GABA_A$ Rs during development, while expressing mostly $\alpha 6$ in maturation (Takayama and Inoue, 2004). PCs express $\alpha 3$ subunits during development and $\alpha 1$ at maturation. Adapted from Atchison 2005. 24

Figure 1.3 Cartoon depiction of the GABA_A receptor, a heteropentameric ion channel that conducts Cl⁻. *In vivo* it typically forms a unit from two α (from 6 subtypes), two β (from 3 subtypes), and one additional subunit, including γ and δ . GABA_ARs have two GABA binding sites, located at the interface of α and β subunits, which based on binding studies are also the location of the agonist muscimol and antagonist bicuculline binding sites. The construction of these interfaces controls GABA binding and thus the physiology of the receptor. An additional site where benzodiazepines (BZs) bind and potentiate GABA activation is located between α and γ subunits, so GABA_ARs without γ subunit are insensitive to these modulators. Synaptic scaffolds such as gephyrin bind to certain subtypes of GABA_ARs, clustering them inside synapses, whereas others such as those containing $\alpha 6$ can be found spread around the membrane. The direction of ion flow depends on the Cl⁻ gradient. An inward gradient is present at most post-synaptic domains and most mature cells and activation produces hyperpolarization and thus inhibition of activity. However, in developing neurons there is no extrusion of Cl⁻ through potassium-chloride co-transporter (KCC2), and thus the gradient is outward, so activation causes depolarization. This reversal of the gradient may also be present in some locations of mature cells, such as axons. 28

Figure 2.1 **A** A representative pseudocolor fluorescent image of an acutely-isolated cerebellar slice from PND9 rat showing modified fluo4/ethD-1 live/dead cytotoxicity assay, post-incubation control. Images are from internal folds of the developing cerebellum. Images show maximum fluo4 and ethD-1 fluorescence values by pixel. Approximate pial surface of an inner fold is indicated by a white line and other boundaries are indicated by dashed lines. EthD-1 (red), an indicator of dead cells, and Fluo4AM (green), an indicator of relative intracellular calcium concentration, do not colocalize. Scale bar represents 30 μ m. **B** Representative image from separate slice from the same cerebellum after one additional h in ACSF supplemented with 20 μ M MeHg. **C** EthD-1 mean pixel staining (% pixels \pm SEM) comparison of layers post-incubation in fluo4 and ethD-1 (n=5), with an additional 1 h incubation in ACSF (n=3) or with an additional 1 h incubation in 20 μ M MeHg ACSF (n=3). Abbreviations: EGL, external granule layer; ML, molecular layer; IGL, internal granule layer. 53

Figure 2.2 40x grayscale examples of cerebellar slices before (-10) and after (40 min) treatment with MeHg. Images show projection of maximum fluo4 fluorescence by pixel. **A** Fluorescence does not change over the course of imaging in control slices. **B** MeHg increased fluorescence in all layers, with the signal from many cells saturating the detector. Scale bars are 60 μ m in all images. Surfaces and boundaries are indicated as with Figure 1.1. White arrows indicate examples of cells with extinguished fluorescence by the end of treatment. 57

Figure 2.3 Relative fluo4 fluorescence intensity (F/F₀) in CGCs by histological layer in slices from neonatal rat cerebellum exposed to concentrations of MeHg continuously for 30 min. Control MeHg concentrations did not change

fluorescence significantly. Continuous perfusion of ACSF with 0 μM (\circ , $n=5$), 1 μM (∇ , $n=3$), 5 μM (\blacktriangle , $n=5$), 10 μM (\blacklozenge , $n=6$) or 20 μM MeHg (\bullet , $n=4$) were compared in **A**, the EGL, **B**, the ML, and **C**, the IGL. Significant differences are indicated from untreated control (*) and between 20 μM and 10 μM treatments (#) at the same time point. Intensity values are expressed in arbitrary units (mean \pm SEM). 60

Figure 2.4 Cell density per $(100 \mu\text{m})^2$ for CGCs monitored for fluo4 fluorescence intensity, in each layer (EGL, ML and IGL), for tissue treated with different concentrations of MeHg. Fluorescent CGCs were more dense in the EGL and IGL layers than in the ML. At higher MeHg concentrations, fluorescent CGCs in the EGL were more dense than in IGL, but at lower concentrations, density was higher in the IGL. Within the EGL, fluorescent cell density increased significantly with greater concentrations of continuous MeHg treatment, non-overlapping letters are significantly different comparisons ($P<0.05$). Paired comparisons were made between each concentration of MeHg by layer. Significantly different pairs within each layer are indicated by different letters ($P<0.05$). n for each treatment is the same as in Figure 2.3. 62

Figure 2.5 Fluorescent cell loss “extinguished” counts from slices during treatment with several concentrations of MeHg over 30 min. Cells extinguished when they lost significant fluo4 fluorescence between time points. Fluo4 fluorescence loss was occasionally associated with visible lysis of cells, so presumably all fluorescence loss is associated with cell death. Comparisons were made between each concentration of MeHg and untreated control, no comparisons were significantly different ($P>0.05$). 64

Figure 2.6 Effect of bicuculline and MeHg on relative fluo4 fluorescence intensity (F/F_0) of CGCs by histological layer. Untreated controls (\circ , $n=5$) and 20 μM MeHg alone (\bullet , $n=5$) are the same as in Figure 2.3. Bicuculline pulses (arrows, 10 μM) with 20 μM MeHg (\square , $n=4$) were compared to bicuculline alone (\square , $n=3$) and MeHg alone. Significant difference are indicated from bicuculline control (*) and from MeHg alone (#) at that time point, $P<0.05$. Intensity values are expressed in arbitrary units (mean \pm SEM). 68

Figure 2.7 Cell density (per $(100 \mu\text{m})^2$) for CGCs monitored for fluo4 fluorescence intensity, in each layer (EGL, ML and IGL) and density for the total tissue, for tissue treated with two concentrations of MeHg (0 and 20 μM) and two concentrations of bicuculline (0 and 10 μM). CGCs were more densely distributed in the EGL and IGL layers than in the ML. Paired comparisons were made between each concentration of MeHg by layer. Significantly different pairs within each layer are indicated by different letters ($P<0.05$). Values are mean \pm SEM, for the same n as described in Figure 2.6. 70

Figure 2.8 Percentage of “extinguished” cells in experiments comparing MeHg and

bicuculline treatment. Comparisons were made between 20 and 0 μM MeHg treatments, between bicuculline alone and 0 μM MeHg, between bicuculline alone and bicuculline combined with 20 μM MeHg, and between bicuculline combined with MeHg and 20 μM alone. Significantly different pairs within each layer are indicated by different letters ($P < 0.05$). Values are mean \pm SEM, for the same n as described in Figure 2.6. 71

Figure 2.9 Effect of muscimol and MeHg on relative fluo4 fluorescence intensity (F/F_0) of CGCs by histological layer. Untreated controls (\circ , $n=5$) and 20 μM MeHg alone (\bullet , $n=5$) are the same as in figure 3. Muscimol pulses (arrows, 100 μM) with 20 μM MeHg (\square , $n=4$) were compared to muscimol alone (\triangle , $n=3$) and MeHg alone. Significant difference are indicated from muscimol control (*) and from MeHg alone (#) at that time point, $P < 0.05$. Intensity values are expressed in arbitrary units. 74

Figure 2.10 Cell density (per $(100 \mu\text{m})^2$) for CGCs monitored for fluo4 fluorescence intensity, in each layer (EGL, ML and IGL) and density for the total tissue, for tissue treated with two concentrations of MeHg (0 and 20 μM) and two concentrations of muscimol (0 and 100 μM). CGCs were more densely distributed in the EGL and IGL layers than in the ML. Paired comparisons were made between each concentration of MeHg by layer. Significantly different pairs within each layer are indicated by different letters ($P < 0.05$). Values are mean \pm SEM with n the same as described in Figure 2.9. 76

Figure 2.11 Percentage of “extinguished” cells in experiments comparing MeHg and muscimol treatment. Comparisons were made between 20 and 0 μM MeHg treatments, between muscimol alone and 0 μM MeHg, between muscimol alone and muscimol combined with 20 μM MeHg, and between muscimol combined with MeHg and 20 μM alone. Significantly different pairs within each layer are indicated by non-overlapping letters ($P < 0.05$). Values are mean \pm SEM with n the same as described in Figure 2.9. 77

Figure 3.1 Representative images of frames of interest and labeled layers from (-/-) mouse cerebellar slices. Images are from two slices; both slices are from the same (-/-) mouse. Detailed description of assigning boundaries is discussed in Chapter Two materials and methods. Layers and boundaries from surface of cerebellum (solid line) include the external granule layer (EGL), the EGL-ML interface (dotted line), the molecular layer (ML), the Purkinje layer (dashed line) and the internal granule layer (IGL). The left images are prior to administration of MeHg, and right images are the last image taken from respective series. The top slice was treated with only ACSF (0 μM MeHg, untreated control) for 55 min, the bottom slice was treated to 20 μM MeHg in ACSF for 55 min. Untreated control had little change to fluorescence, but 20 μM treatment increased fluorescence ~2-fold in the EGL in this example, with smaller increases in the ML and IGL. Scale bar is equal to 50 μm . Images are summary projections of ~30 scans through the depth of the slice, intensity values are adjusted to the value histogram of the first image.

Images are cropped to remove blank space around edges from image registration. 95

Figure 3.2 Time course of effects of MeHg on fluo4 fluorescence in cerebellar slices from neonatal $\alpha 6$ (+/+) and (-/-) mice. Mean fluo4 fluorescence intensity was compared between 0 (untreated control, Con) and 20 μM MeHg (MeHg) in (-/-) (circles, n=5) and (+/+) (squares, n=6) mice over 55 min of treatment. Each of the three developmental layers are shown separately. MeHg is applied continuously for the duration of the experiment starting at t=0 (20 μM , black; 0 μM , white). MeHg treatment causes a rapid increase in fluo4 fluorescence in all layers and genotypes, with the largest change in the (-/-) EGL. * represents time points that are significantly greater than pretreatment ($P < 0.05$) and ** represents time points that are significantly greater than pretreatment as well as greater than the paired, untreated time point ($P < 0.05$). 98

Figure 3.3 Extinguished cell percentages as found in paired mouse cerebellar slices treated with 0 (ACSF) and 20 μM MeHg (MeHg) from (-/-) (white bars) and (+/+) (black bars) mice. Extinguished cells are cells that rapidly and significantly lose fluo4 fluorescence intensity as compared to the normal variation during treatment. These cells are removed from time course intensity traces and tallied. In these MeHg treatments, only the CGCs in (+/+) IGL significantly extinguish as compared to their untreated paired slices (*, $P < 0.05$) 101

Figure 3.4 Time course of effects of MeHg and muscimol on fluo4 fluorescence in cerebellar slices from neonatal $\alpha 6$ (-/-) mice. Mean fluo4 fluorescence intensity was compared between 20 μM MeHg (MeHg, white circles) and 20 μM MeHg with 100 μM muscimol pulses (Muscimol, black circles) in (-/-) mice over 55 min of treatment (\pm SEM, n=5). Each of the three developmental layers are shown separately. MeHg is applied continuously for the duration of the experiment starting at t=0 and muscimol is pulsed into the feed for 60 s at 9.5, 19.5, 29.5, 39.5 and 49.5 min (arrows). MeHg alone causes a rapid increase in fluo4 fluorescence in all layers in a manner similar to previous paired experiments in (-/-) mice. Muscimol pulses reduced this effect immediately and kept fluo4 fluorescence near baseline for the duration of experiments. * represents time points that are significantly greater than pretreatment ($P < 0.05$). 104

Figure 3.5 Time course of effects of MeHg and muscimol on fluo4 fluorescence in cerebellar slices from neonatal $\alpha 6$ (+/+) mice. Mean fluo4 fluorescence intensity was compared between 20 μM MeHg (MeHg, white circles) and 20 μM MeHg with 100 μM muscimol pulses (Muscimol, black circles) in (+/+) mice over 55 min of treatment (\pm SEM, n=5). Each of the three developmental layers are shown separately. MeHg is applied continuously for the duration of the experiment starting at t=0 and muscimol is pulsed into the feed for 60 s at 9.5, 19.5, 29.5, 39.5 and 49.5 min (arrows). MeHg alone causes a rapid increase in fluo4 fluorescence in all layers in a manner similar to previous paired experiments in (+/+) mice. Muscimol pulses reduced this effect in all layers and kept fluo4 fluorescence near baseline for the duration of experiments in the EGL and ML. *

represents time points that are significantly greater than pretreatment (P<0.05). 106

Figure 3.6 Time course of effects of MeHg and bicuculline on fluo4 fluorescence in cerebellar slices from neonatal $\alpha 6$ (-/-) mice. Mean fluo4 fluorescence intensity was compared between 20 μ M MeHg (MeHg, white circles) and 20 μ M MeHg with 10 μ M bicuculline pulses (Bicuculline, black circles) in (-/-) mice over 55 min of treatment (\pm SEM, n=5). Each of the three developmental layers are shown separately. MeHg is applied continuously for the duration of the experiment starting at t=0 and bicuculline is pulsed into the feed for 60 s at 9.5, 19.5, 29.5, 39.5 and 49.5 min (arrows). MeHg alone causes a rapid increase in fluo4 fluorescence in all layers in a manner similar to previous paired experiments in (-/-) mice. Bicuculline pulses reduced this effect immediately and kept fluo4 fluorescence near baseline for the duration of experiments in the IGL. * represents time points that are significantly greater than pretreatment (P<0.05). 108

Figure 3.7 Time course of effects of MeHg and bicuculline on fluo4 fluorescence in cerebellar slices from neonatal $\alpha 6$ (+/+) mice. Mean fluo4 fluorescence intensity was compared between 20 μ M MeHg (MeHg, white circles) and 20 μ M MeHg with 10 μ M bicuculline pulses (Bicuculline, black circles) in (+/+) mice over 55 min of treatment (\pm SEM, n=6). Each of the three developmental layers are shown separately. MeHg is applied continuously for the duration of the experiment starting at t=0 and bicuculline is pulsed into the feed for 60 s at 9.5, 19.5, 29.5, 39.5 and 49.5 min (arrows). MeHg alone causes an increase in fluo4 fluorescence in all layers in a manner similar to previous paired experiments in (+/+) mice. Bicuculline did not reduce the effect in any layers, but also did not increase fluo4 fluorescence in the ML compared to pretreatment. * represents time points that are significantly greater than pretreatment (P<0.05). 110

Figure 4.1 Example frames of interest from confocal fluo4 time course imaging. Slices were imaged through 45 min of continuous perfusion with 20 μ M MeHg in 6 month chronically-treated mice. All images are from the same batch of animals. Images are registered, rotated and cropped for clarity; scale bar equals 50 μ m. **A.** Slices of cerebellum are from four 9 month old animals treated chronically for 6 months with, in order, standard food and water (O), 6.25 ppm MeHg in drinking water (M) with standard food, 2 ppm isradipine in food (I) with standard water, and the combination of MeHg in water and isradipine in food (M/I). MeHg application over 45 min increases relative fluo4 fluorescence in CGCs in the IGL by about 2-fold within 45 min, the duration of observation, in all 4 chronic treatment groups. **B.** Expanded frame of interest from group O after 45 min of continuous MeHg perfusion. Image highlights processes in the ML that become apparent with MeHg treatment (arrows), infrequent PC fluorescence (boxes), and non CGC cells in the ML (circles). 135

Figure 4.2 Mean relative fluo4 fluorescence intensities as measured from confocal time course image series of cerebellum slices from 6 month chronically-treated mice.

Slices from untreated control (O, n=11, white circles), MeHg-treated (M, n=11, black circles), isradipine-treated (I, n=9, white triangles), and combination MeHg- and isradipine-treated (M/I, n=11, black triangles) were imaged at 5 min intervals for 50 min with one pretreatment scan and 10 images with 20 μ M MeHg flowing over the slices. All acute MeHg treatments caused about a 2-fold increase in relative fluo4 fluorescence in CGCs (\pm SEM) and reached significance compared to pretreatment by 20 min of imaging ($P < 0.05$), but were not significantly different from one another ($P > 0.05$). 138

Figure 4.3 Mean relative fluo4 fluorescence intensities of CGCs in slice during 20 μ M MeHg exposure over 45 min from 12 month chronically-treated mice. Traces are from acute treatments of 0 μ M MeHg (untreated controls, white circles) and 20 μ M MeHg (black circles) applied in the bath ACSF solution to cerebellum from 15 month old mice chronically treated for 12 months. Paired comparisons were made between matching time points (*, $P < 0.05$). **A.** Acute treatments of mice receiving no chronic MeHg or isradipine (Group O). Acute MeHg treatment (n=16) significantly increased fluorescence above no MeHg treatment (n=5). **B.** Acute treatments of mice receiving chronic 6.25 ppm MeHg in water and no isradipine (Group M). Acute MeHg treatment (n=16) significantly increased fluorescence above no MeHg treatment (n=7). **C.** Acute treatments of mice receiving no MeHg and 2 ppm isradipine in diet (Group I). Acute MeHg treatment (n=13) increased fluorescence above no MeHg treatment (n=5), but only at one intermediate time point. **D.** Acute treatments of mice receiving both 6.25 ppm MeHg in water and 2 ppm isradipine in diet (Group M/I). Acute MeHg treatment (n=17) did not significantly increase fluorescence above no MeHg treatment (n=6) during observation. 139

Figure 4.4 Mean relative fura-2 ratio values for acute 25 μ M AMPA, 50 μ M NMDA + 10 μ M glycine and 40 mM KCl applications measured from high-speed (0.5 Hz) time course image series in cerebellar slices from 9 month old mice. Mice were treated chronically for 6 months with MeHg or isradipine. Separate lines represent different chronic treatments, including no MeHg and no isradipine (Group O, black line, n=13, representative +SEM shown), MeHg and no isradipine (Group M, red line, n=11), isradipine and no MeHg (Group I, blue line, n=11), and both MeHg and isradipine (Group M/I, magenta line, n=11). Treatments are in order, and consisted of treatment for 2 min, with approximately 20 s to reach the bath, imaging for an additional 8 min and a 2 min wash between imaging. **A.** AMPA treatment of slices, all four chronic treatment groups responded to the treatment (*, $P < 0.05$ compared to baseline). Several stayed above baseline ratio, while group M/I returned during the imaging period. **B.** NMDA treatment of slices, following AMPA. No population-wide change in fluorescence occurred. **C.** KCl treatment, following NMDA. Only group O showed a significant, population-wide change in fluorescence ratio during treatment. 144

Figure 4.5 Mean relative fura-2 ratio values for acute 25 μ M AMPA, 50 μ M NMDA + 10 μ M glycine and 40 mM KCl applications measured from high-speed (0.5 Hz)

time course image series in cerebellar slices from 15 month old mice. Mice were treated chronically for 12 months with MeHg or isradipine. Separate lines represent different chronic treatments, including no MeHg and no isradipine (Group O, black line, n=15 representative +SEM shown), MeHg and no isradipine (Group M, red line, n=17), isradipine and no MeHg (Group I, blue line, n=14), and both MeHg and isradipine (Group M/I, magenta line, n=15). Treatments are in order, and consisted of treatment for 2 min, with approximately 20 s to reach the bath, imaging for an additional 8 min and a 2 min wash between imaging. **A.** AMPA treatment of slices, all four chronic treatment groups responded to the treatment (*, P<0.05 compared to baseline). All stayed above the baseline ratio for the duration of the imaging period. **B.** NMDA treatment of slices, following AMPA. No population-wide change in fluorescence occurred. **C.** KCl treatment, following NMDA. All four chronic treatment groups showed significant responses to treatment, and all were temporary. 146

Figure 4.6 Mean relative fura-2 ratio values from acute ACSF control, 100 μ M muscimol and 10 μ M bicuculline applications as measured from high-speed (0.5 Hz) time course image series in cerebellar slices from 15 month old mice. Mice were treated chronically for 12 months with MeHg or isradipine. Separate lines represent different chronic treatments, including no MeHg and no isradipine (Group O, black line, n=5, representative +SEM shown), MeHg and no isradipine (Group M, red line, n=6), isradipine and no MeHg (Group I, blue line, n=4), and both MeHg and isradipine (Group M/I, magenta line, n=6). Treatments are in order, and consisted of treatment for 2 min, with approximately 20 s to reach the bath, imaging for an additional 8 min and a 2 min wash between imaging. **A.** ACSF control treatment (no change from pretreatment) of slices. Both chronically MeHg-treated groups (M and M/I) showed significant responses during this treatment (*, P<0.05 compared to baseline). **B.** Muscimol treatment of slices. Both chronically MeHg-treated groups showed significant increases in fluorescence, including the largest increase of any treatment in Group M. **C.** Bicuculline treatment of slices, showing no significant changes from baseline. 152

Figure 5.1 Example of two spontaneous events and KCl depolarization from a young (+/+) mouse cerebellar slice loaded with fluo4-AM. Images are registered, cropped and contrast enhanced for clarity. Images were captured at 60x magnification; the scale bar equals 100 μ m. Two nearly simultaneous events in the IGL are depicted in the first two images. The first image is just before the events and the second at the peak intensity. Arrows indicate the two cells showing the events. This slice was later treated with high [KCl] ACSF for the purposes of depolarizing the slice. Peak depolarization is depicted in the third image. The two cells that displayed spontaneous transients were depolarized by this treatment, as were most cells in the slice. 167

Figure 5.2 Representative fluo4 intensity traces from cells in three groups. Each trace is normalized to the mean intensity value of the individual trace, so units are

relative. The first group is traces from young (PND 4-14) GABA_AR α6 (+/+) mice while the second is traces from young (-/-) mice. The third set includes traces from older mice (22 months) from a separate line, so they are considered (+/+) for the purposes of these results. Some qualities of the traces can be seen from these examples. Note that several spontaneous events are repeated in young animals and the fluo4 events in aged animals were much more protracted. . . . 168

- Figure 5.3 Slice characteristics from total cell and active cell regions of interest (ROI). Parameters from the automated event counter included cell counts and unique event ROIs, allowing a count of total cells as well as active cells. Because of the differences between layers in young (Y) and aged (A) mice, these counts are not divided into layers or corrected to calculate cell density as has been performed in previous experiments in this dissertation. No significant differences were found in comparisons of total cell count. Young α6 (+/+) and (-/-) slices showed 13-33% active cells while aged slices only showed about 4% compared to total fluorescent cells, which is significantly fewer (P<0.05). 170
- Figure 5.4 Mean fluo4 intensity of events within frames of interest in slices from α6 (+/+) and (-/-) genotypes and young and old age groups. Event parameters were calculated relative to the mean value of an ROI over all time points, so values are relative. Even though it appeared that (+/+) A had lower overall intensity, there were no significant differences. 171
- Figure 5.5 Cumulative distribution of event durations in slices from α6 (+/+) and (-/-) genotypes and young and old age groups. Events were distributed into 1 sec bins and plotted cumulatively up to 100% and out to the longest duration of 174 sec. Because of the relative differences in number of total events, young mice have a smoother distribution. Statistics were run comparing the largest % difference between distributions and comparing to the critical difference (D) calculated from event counts and standard deviation (σ). Slices from young (-/-) mice had significantly more short duration events than (+/+) mice, while slices from aged (+/+) mice had significantly more long duration events. 172
- Figure 5.6 Mean frequency of events in slices from α6 (+/+) and (-/-) genotypes and young and old age groups. Frequency was calculated from the total events over total time, with some total times reduced to just pretreatment time to focus on the spontaneous events. All slices had at least one significant event. Events occur about every 20 s in young (+/+) slices, about every 4 s in young (-/-) slices and about every 150 s in (+/+) aged slices. 174
- Figure 6.1 Cartoon depiction of GABA_AR and MeHg interactions with [Ca²⁺]_i as highlighted by results of this dissertation. MeHg acts through GABA_ARs in part to increase [Ca²⁺]_i in all CGCs and all developmental stages. Both muscimol and bicuculline reduce MeHg effects on [Ca²⁺]_i through GABA_ARs, apparently by desensitization in the case of muscimol and direct inhibition by bicuculline. Loss of α6 subunits is disruptive to developing granule cells, possibly through increased neurotransmission associated with mature CGCs with local synapses or

possibly through alterations in GABA_AR expression. [Ca²⁺]_i-dependent cell death, through enzyme activation, rundown of ATP and aberrant nuclear signaling, is present, but not significant compared to regular handling. Chronic MeHg appears to alter responses to muscimol, indicating a role for changes in GABA_AR surface expression, such as through internalization, as well as possible changes in gene expression of GABA_AR subunits (dashed arrows). 182

KEY TO SYMBOLS AND ABBREVIATIONS

5-HT3 - 5-hydroxytryptamine (serotonin)

ACSF - artificial cerebrospinal fluid

ALS - Amyotrophic lateral sclerosis

AMPA - 2-amino-3-hydroxy-5-methyl-5-isoxazole propionic acid

ANOVA - analysis of variance

ATP - adenosine 5'-triphosphate

BDNF - brain-derived neurotrophic factor

BZ - benzodiazepine

$[Ca^{2+}]_e$ - extracellular calcium concentration

$[Ca^{2+}]_i$ - intracellular calcium concentration

$[Ca^{2+}]_m$ - mitochondrial calcium concentration

Ca^{2+} - calcium ion

CaM - calmodulin

CaMK - calmodulin kinase

cAMP - cyclic adenosine monophosphate

CF - climbing fiber

CGC - cerebellar granule cell

Cl^- - chloride ion

CNQX - 6-cyano-7-nitroquinoxaline-2,3-dione

CNS - central nervous system

dNTP - deoxynucleotide triphosphate

DMSO - dimethyl sulfoxide

EDTA - ethylene-diamine-tetra-acetic acid

EGL - external granule (or germinal) layer

EPA - Environmental Protection Agency

ER - endoplasmic reticulum

erk - extracellular related kinase

eth-D1 - ethidium homodimer

Fluo 4 NW - fluo 4 no wash

Fura-2 AM - fura-2 acetoxymethylester

GABA - γ -aminobutyric acid

GABA_A or GABA_AR - GABA type A receptor

GAD - glutamic acid decarboxylase

GAT - GABA transporter

GCaMP - Green fluorescent protein-CaM protein

h - hour(s)

Hg²⁺ - mercury ion

Hz - hertz (s⁻¹)

IGF-1 - insulin-like growth factor 1

IGL - internal granule layer

IP₃ - inositol-1,4,5-triphosphate

iPSP - inhibitory post-synaptic potential

K⁺ - potassium ion

KCC2 - potassium-chloride co-transporter

LTD - long term depression

LTP - long term potentiation

M3 - muscarinic receptor type 3

mapk - mitogen associated protein kinase

MEK1 - mapk/erk kinase 1

MeHg - methylmercury

min - minute(s)

ML - molecular layer

ml - milliliter

mo - month(s)

mRNA - messenger RNA

μ - micro

mPTP - mitochondrial transition pore

nAChR - nicotinic acetylcholine receptor

NCX - sodium-calcium exchange transporter

NKCC1 - sodium-potassium-chloride co-transporter 1

NMDA - N-methyl-D-aspartate

NSF - n-ethylmaleimide sensitive factor

PC - Purkinje cell

PCB - poly-chlorinated biphenyl

PCR - polymerase chain reaction

PCMB - 4-chloromercuribenzoic acid

PF - parallel fiber

PKC - protein kinase C

PLC - phospholipase C

PMA - phenylmercury acetate

PMCA - plasma membrane Ca^{2+} ATPase

PND - post-natal day

RfD - reference dose

ROI - region of interest

ROS - reactive oxygen species

SEM - standard error of the mean

SERCA - smooth endoplasmic reticulum Ca^{2+} ATPase

sIPSC - spontaneous inhibitory post-synaptic current

SNARE - soluble NSF attachment receptor

TPEN - N,N,N',N'-tertrakis-(2-pyridylmethyl)ethylenediamine

VGCC - voltage-gated Ca^{2+} channel

Zn^{2+} - zinc ion

CHAPTER ONE

INTRODUCTION

A) Background

a. Methylmercury (MeHg)

i. MeHg in the environment

Methylmercury (MeHg^+ , henceforth abbreviated MeHg) is an organic heavy metal ion formed from the addition of a single methyl side group to inorganic elemental mercury (Hg or Hg^{2+}). Inorganic mercury in the environment can be the result of many natural and anthropogenic sources, including volcanic eruptions, erosion, mining, coal and oil burning, and is typically deposited in bodies of water through precipitation in rain and runoff over land. In water, inorganic mercury is toxic and irritable to many single-celled organisms, and is converted to its methylated form. While this MeHg form is less toxic to some organisms, it is more lipophilic and more difficult for multicellular organisms to excrete, leading to bioaccumulation up the marine food chain (US EPA, 1997). Fish that consume microorganisms and plankton are least likely to accumulate MeHg, but predatory fish such as tuna and swordfish are likely accumulators. Even further, marine mammals at the top of the food chain have the largest concentrations of all, and may have additional accumulated toxicants, such as dioxins and polychlorinated biphenyls (PCBs) accumulating in their tissues. Consumption of these mammals such as whales and seals, is not usually considered because of its rarity, but is important for some populations (Debes, et al., 2006).

A few other forms of organic mercury exist, mostly compounds produced by advanced chemistry techniques. These include ethylmercury, which has been an ingredient used in dental amalgam, and dimethylmercury, a more lipophilic and toxic compound than MeHg that is not considered an environmental contaminant. There are also several compounds of mercury that display some of the characteristic chemistry and toxicity of mercury, including 4-chloromercuribenzoic acid (PCMB), a protease inhibitor that reacts with protein thiol groups,

and phenylmercury acetate (PMA), a discontinued fungicide, disinfectant and paint preservative. While these toxicants have their own profiles and are of interest in the study of mercury toxicity, they will only be noted when necessary.

ii. MeHg in human health

Because of the bioaccumulation of MeHg in the marine food chain, it is primarily a concern of low doses through seafood consumption, but it is necessary to note other exposures and their importance to understand MeHg exposure and toxicity. A handful of medical reports indicate that MeHg exposure through occupational handling of mercury compounds and possible aerosols trace the medical characterization of mercury poisoning to the early half of the 19th century (Hunter and Russell, 1954, Magos and Clarkson, 2006). Though the exact mixture of metals in these cases was not always clear, neurotoxicity was noted alongside liver and renal failure. In particular, imprecise motor control and gait disturbance, termed ataxia, was a common sign of neurological damage. Ataxia was correlated with degeneration of the cerebellum, as determined by postmortem histology as well as early animal experiments. Additional characteristics associated with MeHg poisoning included paresthesia (peripheral sensory loss), disarthria (slurred speech), dysphagia (difficulty swallowing), constricted vision, and tremors. In human and mammalian exposures, many symptoms can take several months to manifest, indicating a latency for MeHg toxicity. Some MeHg is excreted through the hair and is dependent on concentration, so suspected cases of MeHg poisoning can be extrapolated backwards to the highest concentration, and with sufficient hair a history of exposure can be constructed.

The first major mass poisoning traced to MeHg occurred in the 1950s in a region of Japan around the Minamata Bay (Takeuchi, et al., 1962). Hundreds of people in the area began to show a severe neurological disorder characterized by motor dysfunction, sensory and visual

losses. This disorder was termed Minamata Disease. Through comparisons with occupational MeHg exposures, it was hypothesized that MeHg was the cause, later confirmed through blood and hair analysis. The source was eventually traced to industrial waste from a local chemical company dumping MeHg into the bay, where the toxicant had bioaccumulated in the local fish stocks over several years. As with occupational exposures, the Minamata exposure caused preferential loss of cerebellar granule cells (CGCs) (Takeuchi, 1968, Tokuomi, et al., 1982). Visual degeneration was attributed to damage in the occipital lobe, and peripheral sensory nerve damage was also noted. This mass exposure was also of note because it was also the first event that highlighted one of the hallmarks of MeHg poisoning, developmental toxicity. Fetal Minamata disease, a cerebral palsy-like disorder, was found not long after the adult disorder was characterized (Harada 1978). It was later determined to be a result of MeHg absorbed and concentrated in the placenta, a mechanism that was unheard of at the time, but has been shown to be an attribute of several lipophilic and bioaccumulative toxicants since. No abnormalities in the exposed mothers of the infants were noted, and there was a delay of about 6 months between birth and notable abnormalities such as loss of muscle tone, convulsions, mental retardation, hyperactivity, disarthria, and slowed growth. In 15 years of followup, some symptoms recovered, particularly in mild cases, but intelligence was not improved and many of the more severely-affected children died within that time. Many umbilical cords were kept from the Minamata exposure and analyzed for MeHg concentration when techniques were developed (Akagi, et al., 1998). This analysis indicated that cord blood in affected infants contained about 216 $\mu\text{g/L}$, and it was then estimated that women pregnant with affected children consumed MeHg at about 225 $\mu\text{g/day}$.

A second mass exposure event occurred in Iraq in the 1970s through a much different source (Bakir, et al., 1973). Relief shipments of grain sent to the country after a crisis contained

seed grain coated in MeHg and ethylmercury, common fungicides at the time. The grain bags warned about proper handling and planting of the seeds, as the fungicides were meant to wash off over germination. Through various errors, including delays that brought the seed in after planting season and siphoning of the aid onto the black market, warnings were not read and the seed was frequently used in flour instead. Concentrations of the fungicide in this food were much higher than in the exposures in Minamata, so toxicity was more acute and more widespread around the country. Through monitoring of the aftermath, it was extrapolated that severe cases of the exposure included as much as 5 ppm (20 μ M) MeHg in blood. As with the Minamata event, exposed pregnant women with few to no symptoms frequently gave birth to severely affected children (Amin-Zaki, et al., 1974).

While there has not been any major exposure event of the size or severity of Minamata or Iraq since, MeHg is still an area of concern, particularly in fish-consuming populations around the world. Also, due to the developmental susceptibility noted in exposures, special attention has been paid to neurological function in infants, children and adolescents (Castoldi, et al., 2008). Two major ongoing studies have monitored MeHg exposure and low dose effects for several decades. In the Seychelles Islands, located north of Madagascar in the Indian Ocean, locals are almost entirely dependent on fish diets, and almost the entire population receives regular health checks that include monitoring MeHg (Davidson, et al., 2008). In the Faroe Islands, located between Scotland and Iceland in the Arctic Ocean, fish diets are supplemented by marine mammals which may also accumulate persistent organic pollutants such as dioxin and PCBs (Debes, et al., 2006). The Seychelles study has found few neurological differences in its cohorts, possibly due to the beneficial nutrients of fish protein. The Faroe study has found significant detrimental neurological effects from the combination of pollutants in whale meat, enough to repeatedly call for the end of whale consumption.

As with many environmental toxicants, regulators have formulated a reference dose (RfD) of 4-5 $\mu\text{g/L}$ in blood and approximately 1 $\mu\text{g/g}$ in hair for MeHg through integration of the epidemiological research (US EPA, 1997). The RfD is approximately 1/10th of the concentration found to cause minor developmental delays in the Iraq exposure. Blood and hair measures of MeHg, which cannot distinguish between types of Hg exposure, are typically used. Blood concentrations are best for determining MeHg concentration immediately, but hair concentration offers several advantages. MeHg is concentrated in hair when excreted and hair grows at a constant rate, so past MeHg exposure can be tracked. Because of the ease of hair monitoring, several smaller studies have included monitoring indigenous populations in North America, in the general population of Europe, and miners and indigenous populations in the Amazon that may be exposed to fumes and runoff from gold mining operations. While more specific correlation of brain and blood biomarkers for MeHg exposure and neurotoxicity has been shown in laboratory animals, biomarkers such as muscarinic receptor activity and monoamine oxidase activity have shown mixed effectiveness in predicting outcomes in humans (Roda, et al., 2012) so direct measurements remain the standard. The data at the time of the EPA report indicated that about 10% of the population exceeded the RfD regularly, with as much as 3 fold excess in regular fish consumers. Because of a relative lack of specific cases involving children and pregnant women, the RfD is based on the general population. Recent studies of seafood consumption indicate that in European females of child-bearing age, about 11% of consumers are still getting levels of MeHg above the RfD while 44% are not getting the recommended amounts of beneficial fatty acids associated with fish consumption (Strom, et al., 2011). As many populations of fish do not contain an adequate balance of MeHg versus beneficial nutrients, future recommendations for fish consumption may need to take this into account.

iii. MeHg chemistry and mechanisms

While MeHg and Hg^{2+} do not appear much different chemically as ions, the methyl group addition produces an ion capable of making much longer and weaker bonds with targets (Tai and Lim, 2006). This results in a number of important chemical differences. First, MeHg has high affinity to bind sulfhydryl groups, including cysteine (Cys) and methionine (Met) groups on many proteins. Second, this chemical bond is weak and labile, meaning that though the ion is bulky, interactions are likely to be temporary. Together this binding pattern makes MeHg likely to bind and interact with many proteins, and it makes MeHg a particularly difficult toxicant to characterize. Though research on MeHg has been intense for many decades, the exact suite of interactions and mechanisms by which it causes toxicity still have not been determined.

Interactions with sulfhydryl groups appear to be critical for the comparative efficiency of MeHg to pass the blood-brain barrier and placenta, because when bound to L-Cys or L-Met, MeHg is able to pass through amino acid transporters easily (Aschner and Aschner, 1990, Kerper, et al., 1992). Unlike MeHg, Hg^{2+} is primarily toxic to liver and kidneys, in part due to inefficient passage through the blood-brain barrier. Despite this major difference, MeHg is still ten-fold more toxic to cultured CGCs than Hg^{2+} , meaning that additional differences in entering cells or interactions with cell signaling pathways must exist (Gasso, et al., 2001). Interaction with sulfhydryl groups also makes MeHg an easy target for glutathione-based excretion, but its lability may allow it to escape this cleanup, especially once outside the blood stream (Choi, et al, 1996).

While the passage of MeHg through the blood-brain barrier allows it to accumulate in the central nervous system (CNS), MeHg also accumulates in cells. Though MeHg is charged, there is ample evidence that it is able to enter cells, where it is able to act directly on mitochondria and cytosolic signaling cascades (Atchison and Hare, 1994, Limke and Atchison, 2002). Proteomic

analysis of CGCs indicates that MeHg may be able to alter expression of mitochondrial proteins and cytoskeletal proteins critical for migration (Vendrell, et al., 2007, Vendrell, et al., 2010). As with other metals, some of this permeability may come from the simply entering through the pores of ionotropic receptor channels, such as voltage-gated calcium channels (VGCCs) (Atchison, 1987). However, altering the concentration of extracellular calcium (Ca^{2+}) or using ions other than Ca^{2+} in order to compete with MeHg ions does not alter the effects of the toxicant, so other mechanisms of MeHg cell permeability must exist (Traxinger and Atchison, 1987). Just as it passed through the blood-brain barrier, MeHg may be able to pass into cells while bound to amino acids or other transported molecules, or, if incorporated into a small enough non-polar molecule, MeHg could pass directly through the membrane. Once inside, MeHg could interact with many signaling cascades, and could only be removed by scavengers such as glutathione or n-acetylcysteine (Aremu, et al., 2008). Despite evidence that MeHg enters cells and may even accumulate, many of the most critical actions of MeHg appear to happen at the surface of neurons.

Once inside the CNS, MeHg is able and likely to encounter many cell surface receptors, and due to its lability, it can interact with available sulfhydryl groups. In many cases, MeHg is able to alter both activity of a wide array of neuronal receptors directly and expression of these receptors through signaling cascades. Because it is present both inside and outside the cell, MeHg is able to interact with many more sites on these receptors than an extracellular toxicant. The interaction of MeHg and neuronal receptors is a major area of interest of the Atchison laboratory. In particular, a number of receptors that are able to alter the intracellular concentration of Ca^{2+} ($[\text{Ca}^{2+}]_i$) are known to be targets of MeHg (Figure 1.1). MeHg alters the activity of some of these, including VGCCs (Marty and Atchison, 1997, Sirois and Atchison, 2000, Hajela, et al., 2003), and the muscarinic M3 receptor, a metabotropic receptor that

regulates Ca^{2+} release from internal stores (Limke, et al., 2003, Limke, et al., 2004). Ligand-gated Ca^{2+} -permeable channels, such as N-methyl-D-aspartate (NMDA), 2-amino-3-hydroxy-5-methyl-isoxazole propanoic acid (AMPA) and kainate receptors, may also be affected by MeHg, either directly altering their activity or by changing their expression (Juarez, et al., 2005, Basu, et al., 2007, Johnson, et al., 2011). These are by no means the only receptors or mechanisms by which MeHg acts. However, the presence of many surface receptor targets of MeHg that are capable of altering $[\text{Ca}^{2+}]_i$ and its signaling suggest a collective mechanism, changes to Ca^{2+} homeostasis, by which MeHg can act. As with many possible mechanisms of MeHg toxicity, these interactions require further scrutiny to understand under what conditions they contribute or are affected by MeHg toxicity.

One receptor stands out as needing further consideration. In electrophysiological study elucidating the receptors in susceptible cells that respond to low concentrations of MeHg, the γ -aminobutyric acid type A GABA_A receptor (GABA_AR) was found to be a target (Yuan and Atchison, 1997, Yuan and Atchison, 2003, Yuan and Atchison, 2007). Further study suggested that GABA_ARs could be involved with MeHg toxicity in a Ca^{2+} -dependent manner (Herden, et al., 2008). GABA_ARs fit well with a $[\text{Ca}^{2+}]_i$ model for MeHg toxicity due to several different factors. First, though they are generally considered inhibitory, GABA_AR activation is still frequently associated with Ca^{2+} influx through secondary mechanisms, and activation may actually be excitatory under some conditions (Owens, et al., 1996, Eilers, et al., 2001, Brodinsky, et al., 2003). Second, GABA_ARs are heterogeneously constructed, with many different combinations of subunits and responses to ligands (Brickley, et al., 1996, Saxena and MacDonald, 1996). The expression of specific GABA_ARs frequently matches characteristics of MeHg toxicity, such as cell and developmental susceptibility. Third, GABA_ARs are closely

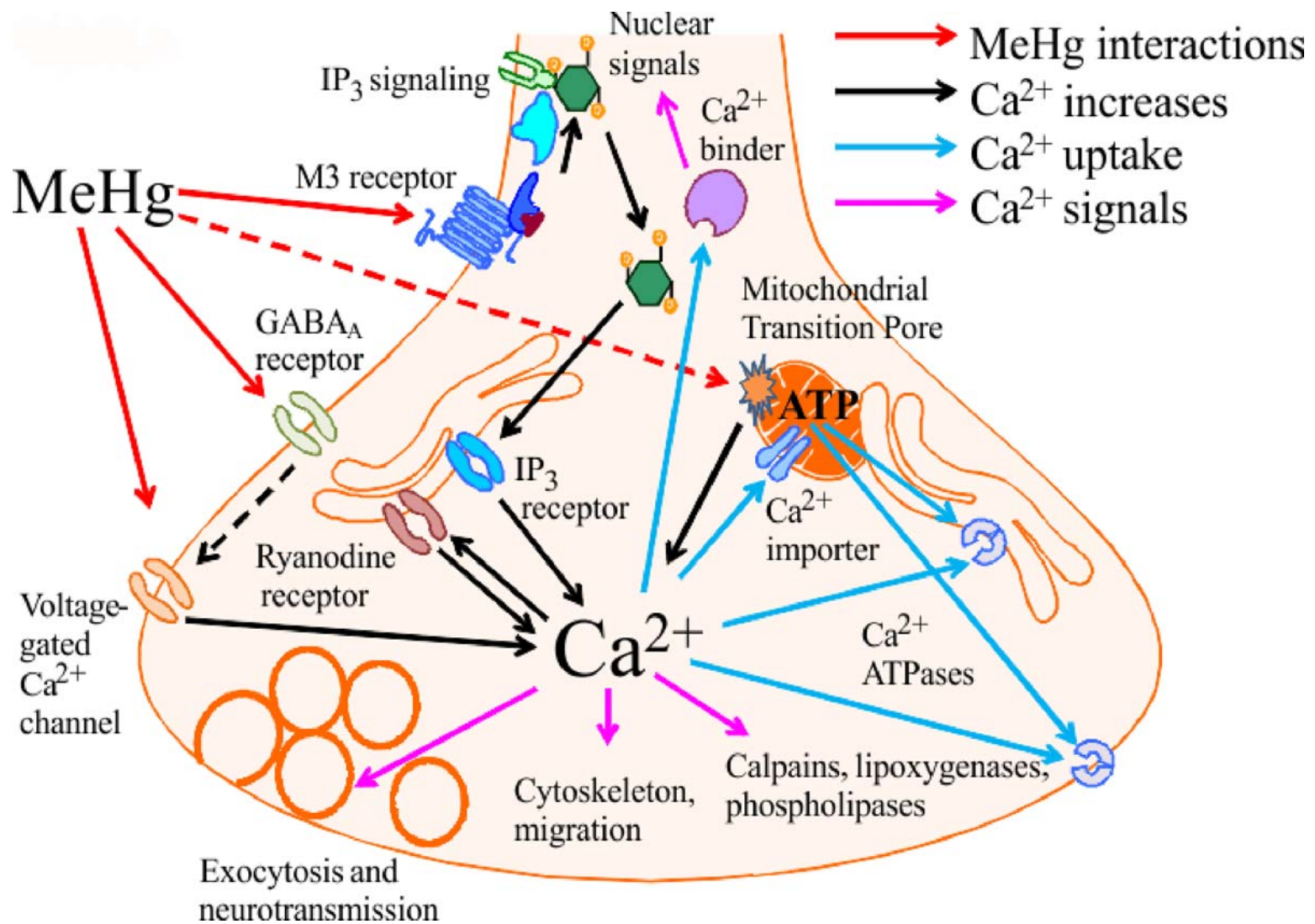


Figure 1.1. Schematic representation of neuronal MeHg targets and the central action of $[Ca^{2+}]_i$ in normal neuronal function and toxicity.

Figure 1.1 (cont'd). This schematic represents an axon terminal, but many of these mechanisms are present throughout a neuron. MeHg acts on Ca^{2+} channels (such as VGCCs), metabotropic receptors that signal through IP_3 (such as the M3 muscarinic receptor), and the GABA_A receptor at the surface of neurons (red arrows). MeHg is also able to enter cells and act on proteins such as the mitochondrial transition pore (mPTP), but the exact mechanisms of entry are unclear (dashed red arrow). $[\text{Ca}^{2+}]_i$ is normally increased transiently through several mechanisms, such as Ca^{2+} -dependent Ca^{2+} release from ER through ryanodine receptors, but MeHg increases $[\text{Ca}^{2+}]_i$ beyond normal levels (black arrows). The action by which MeHg can increase $[\text{Ca}^{2+}]_i$ through GABA_A receptors is unclear, but may be dependent on VGCCs through depolarization or other mechanisms (dashed black line). Some Ca^{2+} may be buffered by Ca^{2+} binding proteins in the cytosol, but excess Ca^{2+} is normally taken up by the ER through Ca^{2+} -ATPases such as the smooth endoplasmic reticulum Ca^{2+} ATPase (SERCA), and may be expelled from the cytoplasm by other ATP-dependent mechanisms, both of which require ATP from the mitochondria (blue arrows). The normal actions of increased $[\text{Ca}^{2+}]_i$ include regulating vesicle release, neuronal motility during development, and regulation of gene expression, but the excess of Ca^{2+} from MeHg actions can cause excess neurotransmitter release, aberrant gene expression, and can activate several enzymes involved in apoptosis, such as lipases and calpains (magenta arrows). For interpretation of the references to color in this and all other figures, the reader is referred to the electronic version of this dissertation.

associated with other receptors and are critical for regulation of neuronal excitability and neurotransmission (Long, et al., 2009). In whole brain, alterations in neurotransmission can be as toxic for surrounding cells as direct toxicity. MeHg affects three unique components of CGC neurotransmission, GABA_ARs, M3 muscarinic receptors, and a K⁺ leak current. All three contribute to an increase in glutamate release (Atchison, 2005). MeHg also inhibits glutamate uptake (Aschner, et al., 1990, Yin, et al., 2007), so with increased glutamate release and decreased uptake, MeHg can be considered toxic through glutamate excitotoxicity. Through other changes to neurotransmitter and modulator release, such as changes to brain-derived neurotrophic factor (BDNF), MeHg is capable of altering neuroprotection throughout the brain (Onishchenko, et al., 2008).

iv. MeHg toxicity susceptibility and resistance

Despite widespread brain and nerve toxicity displayed in major exposure events, MeHg shows a progressive neurotoxicity, with certain parts of the brain affected at lower concentrations than others. The cerebellum is a target, as are dorsal root ganglia in the spinal cord, and parts of the visual cortex, all of which degrade before regions such as the cerebral hemispheres. This is most clearly shown in post-mortem histology of both humans and laboratory animals (Hunter and Russell, 1954, Takeuchi, 1968, Sakamoto, et al., 1998). Because it is one of the larger brain structures that can be targeted by even small concentrations of MeHg, much of the toxicological characterization of MeHg has focused on the cerebellum. Within the cerebellum, cell-specific toxicity is also seen. In both acute and chronic MeHg exposure, there is a significant loss of CGCs while Purkinje cells (PCs), their synaptic targets, remain relatively intact (Edwards, et al., 2005). CGCs and PCs have many cellular differences that may account for the differences in their relative susceptibilities to MeHg toxicity. The most readily apparent difference is in size, CGCs are some of the smallest neurons in the brain while PCs are among

the largest. This size difference leads to a difference in buffering capacity, wherein CGCs are more likely to respond to a smaller ion flux than the larger PCs, and this difference is driven further by differences in expression of binding proteins and other typical cytosolic buffers (Gall, et al., 2005).

Many of the specific effects of MeHg are enhanced in developing animals. Even low-level MeHg exposure during pregnancy, ~1ppm as measured by maternal hair, subtly decreases the size of a newborn's cerebellum (Cace, et al., 2011). As suggested by the historical record of a latency period before overt toxicity in human infants, this latency period is reciprocated in animal studies of perinatal exposure (Sakamoto, et al., 1998). Toxicity in animals includes many of the same disorders and degeneration as seen in human exposures, including degeneration of the cerebellum, neocortex, striatum, brainstem and dorsal root ganglia, leading to hind limb paralysis and unsteady gait. Overt toxicity in this type of application is enhanced by lack of the critical metabolism and excretion protein metallothionein (Yoshida, et al., 2008). As with many toxicants, there is evidence that damage to liver and kidney occurs during MeHg exposure in young animals in addition to its effects on the CNS (Abdalla, et al., 2012). While most of the research focusing on the developmental effects of MeHg has focused on the time corresponding to the later susceptible periods of gestation in humans, MeHg may have other effects in early neuronal development (Xu, et al., 2010, Engel, et al., 2012).

The effects of MeHg on aged animals have not been as widely studied as developmental effects, but it is important to consider elderly susceptibility and the possibility that MeHg enhances neuronal degeneration (Weiss, 1990, Weiss, et al., 2002, Weiss, 2010). Enhanced effects of MeHg might come about by either direct effects due to declining protective mechanisms during aging or, in the case of developmental or lifelong exposure, prevention of the buildup of neurons and connections in the brain, leading to a smaller safe threshold above

neurodegenerative disorders. As an example of a direct effect that could enhance age-related decline, MeHg treatment decreases dopamine receptor density in hippocampal neurons (Coccini, et al., 2011). Dopamine signaling is important for motor control in the hippocampus and normally declines in aging, and this additional alteration by MeHg could enhance the risk of neurological disorders associated with dopamine, such as Parkinson's Disease. MeHg exposure also accelerates motor decline in a mouse model of familial Amyotrophic Lateral Sclerosis (ALS), suggesting that genetic susceptibilities for decline can be exacerbated by the toxicant (Johnson, et al., 2009). One study suggests that acute MeHg exposure does not enhance the typically monitored motor effects in normal populations of aged mice compared to younger adult exposure (Bellum, et al., 2012). But in zebrafish, it appears that in older, already deteriorating populations, acute exposure to MeHg is more toxic than exposure in young adults (Xu, et al., 2012). Compared to acute exposures, it is clear that chronic or perinatal exposure to MeHg causes motor deficits that are at least persistent into old age, and that some new deficits appear in geriatric animals, including deficits in visual and spatial discrimination and increased weight gain in geriatric rodents (Paletz, et al., 2007, Vitalone, et al., 2010).

Along with susceptibility, ability to resist MeHg toxicity may also elucidate mechanisms responsible for toxicity. MeHg-tolerant organisms indicate the importance of metabolism and clearance in protection from MeHg toxicity. *C. elegans* appears to show a resistance to the effects of MeHg on neurons, which may be due in part to induced expression of glutathione, heat shock proteins and metallothioneins, which can export or inactivate MeHg (Helmcke and Aschner, 2010). This induction leads to hormesis, wherein a small dose of MeHg applied induces a strong resistance to further applications. Several generations of flies can be selected to produce MeHg tolerant strains by using MeHg-supplemented food. When compared to non-tolerant populations with and without MeHg-containing food, several metabolic genes and one immune

gene were highlighted (Mahapatra, et al., 2010). Resistance appears in these studies to include antioxidant and inflammatory regulatory pathways.

b. Calcium

i. Calcium signaling and regulation

Just as MeHg has broad effects in the CNS, one of the mechanisms by which it can act, changes to $[Ca^{2+}]_i$ and other Ca^{2+} dynamics, is critical for a multitude of neuronal mechanisms. Because of these wide-ranging interactions, Ca^{2+} signaling will be related to other mechanisms of MeHg toxicity, primarily control of electrochemical gradients, cell death and neurotransmitter release, along with cell, developmental and aging susceptibilities that may be related.

In neurons, $[Ca^{2+}]_i$ is tightly regulated, with concentrations usually in the 100-200 nM range, while external Ca^{2+} ($[Ca^{2+}]_e$) in the 1-2 mM range, representing a 10,000 fold difference and establishing a strong chemical gradient, even though most of the ion is bound (Kass and Orrenius, 1999). While cytosolic $[Ca^{2+}]_i$ is maintained at these low concentrations, neurons also maintain stores of Ca^{2+} in organelles, both in the endoplasmic reticulum (ER) and in mitochondria. The ER maintains a dynamic store of Ca^{2+} at concentrations near $[Ca^{2+}]_e$, with uptake controlled by the smooth ER Ca^{2+} -ATPase pump (SERCA) and release regulated by inositol-phosphate 3 (IP_3) receptors. Typically mitochondria maintain concentrations of Ca^{2+} ($[Ca^{2+}]_m$) similar to the cytosol, but can rapidly take up the excess during stimulation, at about 0.5 $\mu M/s$ (Rizzuto, et al., 1994). Ca^{2+} levels in neurons and glia are also critical for metabolism, regulating glycolytic activity and ATP metabolism at rest or in active states (Pancani, et al., 2011). This baseline configuration of cytosolic and organellar $[Ca^{2+}]$ is considered homeostasis, and any regulatory mechanism that maintains it is homeostatic. Many stimuli can induce changes in one or more of these concentrations, however most are temporary. Influx of Ca^{2+} comes

primarily from two sources, neurotransmitter activation of receptors and membrane depolarization. Both neurotransmitter activation and membrane depolarization can propagate along the surface of neurons through IP₃-dependent release from ER and Ca²⁺-dependent Ca²⁺ influx from membrane receptors (Gleichmann and Mattson, 2011). Ca²⁺ is directly and continually removed from cytoplasm by SERCA and the plasma membrane Ca²⁺-ATPase (PMCA), which both require ATP. Large concentrations of [Ca²⁺]_i may also be extruded from neurons by the Na⁺/Ca²⁺ exchanger (NCX), which indirectly requires ATP to reestablish the sodium gradient. Frequent activity and influx of Ca²⁺ or low ATP increases [Ca²⁺]_i, which is taken up by mitochondria and signals a need for increased ATP production. Increased [Ca²⁺]_m is a signal of dysfunction, both as it reflects a high [Ca²⁺]_i and as increased ATP production can lead to increased production of reactive oxygen species (ROS).

As seen in the uptake of Ca²⁺ by mitochondria, Ca²⁺ can serve as both a signal for mechanisms to attenuate stress, as with the increase in ATP production, and as a stressor, inducing ROS production. In a similar manner Ca²⁺ signals both cell survival and cell death (Cerella, et al., 2010). If a neuronal insult, including toxicant exposure or excessive activation, is sufficient to induce rapid, strong increases of [Ca²⁺]_i, necrosis can occur. However, most stresses only induce apoptosis. Ca²⁺-dependent apoptosis is characterized by activation of several Ca²⁺-sensitive enzymes, including m-calpains, which break down many cytosolic proteins (Chan and Mattson, 1999, Demarchi and Schneider, 2007), and lipoxygenases and phospholipases, which break down lipids in the membrane and release inflammatory mediators (Exton, 1990, Tang, et al., 2007). Neurons rely on a close coupling of ER and mitochondria to maintain low [Ca²⁺]_i (Csordás, et al., 1999, Shoshan-Barmatz, et al., 2004). While Ca²⁺ is normally taken up by ER through SERCA, if this is overwhelmed or ATP is depleted, neurons must rely on mitochondrial uptake (Spät, et al., 2008, Ruiz, et al., 2009). Excess [Ca²⁺]_i taken up

by mitochondria can depolarize and overwhelm the organelle, leading to opening of the mitochondrial permeability transition pore (mPTP), which can release critical mitochondrial proteins and degenerate the mitochondria (Dahlem, et al., 2004, Denlaud, et al., 2008, Baumgartner, et al., 2009). Since ATP is already depleted, loss of mitochondria exacerbates the energy failure.

ii. Calcium and neurotransmission

All neurotransmitter release requires Ca^{2+} signaling and current models place a variety of Ca^{2+} channels in close proximity to vesicle pools (Chad and Eckert, 1984, Fogelson and Zucker, 1985, Westenbroek et al., 1995, Schneggenburger, et al., 2012). Typical neurotransmitter release occurs when a depolarizing action potential reaches the presynaptic membrane. This depolarization activates VGCCs in the membrane, inducing a large Ca^{2+} influx (Augustine, et al., 1985, Sabatini and Regehr, 1995,). This influx of Ca^{2+} is able to mechanically trigger neurotransmitter release directly (Stanley, 1993, Atlas, et al., 2001). This is because Ca^{2+} influx in close proximity to vesicles activates synaptotagmin I in vesicular soluble n-ethylmaleimide sensitive fusion (NSF) attachment receptor (SNARE) complexes and causes rapid (μs -ms) vesicle fusion and release (Geppert, et al., 1994, Xu, et al., 2007, Chapman, 2008).

Neurotransmitter release is regulated in part through differences in VGCC expression at presynaptic and postsynaptic sites in different types of synapses (Jones and Heinemann, 1987, Doroshenko, et al., 1997, Catterall and Few, 2008). These differences in expression are also important for neuronal plasticity, the stored response level of a neuron based on previous activity, including long-term depression (LTD) and long-term potentiation (LTP) (Pelkey, et al., 2006, Wankerl, et al., 2010). Defects in $\text{Ca}_v2.1$, the major presynaptic VGCC in the CNS, underlie familial migraine and two forms of ataxia (Ophoff, et al., 1996, Zhuchenko, et al., 1997). These ataxias are characterized by excitotoxic loss of CGCs similar to losses seen in

MeHg poisoning, suggesting excitotoxic alterations to neurotransmission may be a major factor in MeHg neurotoxicity.

iii. Calcium in development and aging

Ca^{2+} signaling is critical for some early neuronal developmental steps (Leclerc, et al., 2012), but is critical for neuronal migration and axon elongation (Zheng and Poo, 2012). Ca^{2+} dependence for neuronal migration was first described in CGCs, and is the most characterized (Komuro and Rakic, 1992, Komuro and Rakic, 1993, Komuro and Kamada, 2005). Ca^{2+} imaging of these cells indicates repeated, somatic increases and decreases of $[\text{Ca}^{2+}]_i$, Ca^{2+} oscillations, with forward progress during high $[\text{Ca}^{2+}]_i$ and rest at low concentration. These transients are mediated through NMDA receptors and VGCCs (Rossi and Slater, 1993, Komuro and Yacubova, 2003), which in intact brain are activated by a depolarizing current through GABA_A Rs and ambient GABA (Brodinsky, et al., 2003). Ca^{2+} signaling within the cells during migration is dependent on several pathways, including phospholipase C (PLC), protein kinase C (PKC), cyclic AMP (cAMP), and calmodulin kinases (CaMKI and CaMKII) (Kumada and Komuro, 2004). Many of these signals produce locomotion through interactions with the cytoskeleton (Rakic et al., 1994). When CGCs in organotypic slice culture are treated with caffeine or thimerosal, a mercury-containing compound, both increase neuronal $[\text{Ca}^{2+}]_i$ continuously, but the effects are dependent on stage of migration, and both are able to reverse migration at some stages that normally have low $[\text{Ca}^{2+}]_i$ (Kumada and Kumoro, 2004). Most inhibitors of Ca^{2+} oscillations, and many agents that simply disrupt $[\text{Ca}^{2+}]_i$, including MeHg and nicotine, decrease both Ca^{2+} oscillations and migration, while modulators that increase spike frequency, such as cAMP activation and insulin-like growth factor 1 (IGF-1) signaling, restore migration, both *in vitro* and *in vivo* (Mancini, et al., 2009, Fahrion, et al., 2012). Directional cues may also be encoded in Ca^{2+} gradients across migrating neurons. Ethanol is able to interrupt

these cues, possibly through actions on GABA_ARs, leading to disruption in turning of CGCs during migration and ectopic expression of the neurons (Kumada et al., 2010). Complete block of Ca²⁺ oscillations, as demonstrated in many of these studies, is a signal to neurons to cease migration, both in normal migration and when agents are added, and mature neurons are rarely found with regular changes to [Ca²⁺]_i compared to migration.

Changes to Ca²⁺ dynamics, have been hypothesized as a risk factor for many neurodegenerative diseases, including Alzheimer's and Parkinson's, but are also a hallmark of aging neurons (Landfield and Pitler, 1984, Toescu and Vreugdenhil, 2010). Aged neurons display increases in VGCCs, increased Ca²⁺ release from stores, and changes to Ca²⁺ buffering (Thibault and Landsfield, 1996, Ouanounou, et al., 1999, Nicholls, 2004, Gant, et al., 2006). Several types of neuron also have significant increases in baseline [Ca²⁺]_i in aged brains compared to younger brains, including CGCs and some hippocampal neurons (Thibault, et al., 2001, Xiong, et al., 2002). Perhaps more importantly, some presynaptic terminals in aged animals have increased [Ca²⁺]_i, indicating a mechanism for increased neurotransmitter release (Tonkikh, et al., 2006, Tonkikh, et al., 2009). As [Ca²⁺]_i is tied to cell metabolism and ATP production, ATP reserves are typically lower in aging neurons (Mattson, et al., 2009). Even a slight increase in baseline [Ca²⁺]_i attributable to basic variations and polymorphisms could contribute to declines by requiring more ATP use to recover from each event (Stutzmann, 2007). Because of this decreased ATP pool and decreased buffering of [Ca²⁺]_i, aging brains have been hypothesized to be chronically depolarized, leading to degeneration of synapses and nerve terminals, and contributing to age- and disease-related declines in function (Marczynski, 1998). While [Ca²⁺]_i increases in normal brain aging contribute to some of these declines in synaptic function, remodeling and plasticity, actual cell death and neurodegeneration requires additional insults, such as genetic disorders, excessive stimulation or injury, that increase [Ca²⁺]_i further

(Brewer, et al., 2007, Sun, et al., 2008). Further increases of baseline $[Ca^{2+}]_i$ in these models lead to activation of many of the lipases, kinases and phosphatases associated with cell death.

iv. MeHg and calcium

MeHg directly modulates several neuronal membrane receptors and channels, including VGCCs (Sirois and Atchison, 1996). MeHg also activates the M3 muscarinic receptor, a metabotropic receptor that, via IP_3 signaling, is able to rapidly release ER Ca^{2+} stores (Hare and Atchison, 1995, Limke, et al., 2004). Acute MeHg exposure can also open the mPTP, releasing additional stores (Limke and Atchison, 2002). Through these mechanisms, MeHg induces sustained and irreversible dysregulation of $[Ca^{2+}]_i$. This is seen in Ca^{2+} imaging of many different types of cells, with an initial phase of Ca^{2+} entry into the cytosol from internal stores, followed by a second phase of entry from extracellular sources (Hare, et al., 1993, Marty and Atchison, 1998, Edwards, et al., 2005). The second phase can be blocked by extracellular Ca^{2+} chelation, but the first phase is irreversible (Hare and Atchison, 1995, Marty and Atchison, 1997). In separately cultured CGCs and PCs, MeHg causes increases in $[Ca^{2+}]_i$ in both cell types, but the effect was delayed in PCs compared to CGCs at the same concentrations. In cerebellar slices from rats, MeHg increases $[Ca^{2+}]_i$ in CGCs as well as diffusely in many intact processes, while PCs in slice do not respond visibly (Yuan and Atchison, 2007). This increase in $[Ca^{2+}]_i$ corresponded with increased spontaneous vesicular release.

A surge in neurotransmitter release is another mechanism characteristic of acute MeHg toxicity in neurons and synaptosomes (Atchison, 1986, Minnema, et al., 1989, Kalisch and Racz, 1996,). Mitochondrial uptake of Ca^{2+} as well as Ca^{2+} blockers are able to reduce this surge (Levesque and Atchison, 1988, Levesque, et al., 1992, Denny and Atchison, 1996). Since CGCs are the most susceptible neurons to dysregulation of $[Ca^{2+}]_i$ by MeHg and also release glutamate as a neurotransmitter, it is possible they contribute to enhanced glutamate in the cerebellum.

Glutamate is toxic to CGCs through NMDA receptor activation, which feeds back into increased $[Ca^{2+}]_i$ (Eimerl and Schramm, 1991). MeHg inhibits glutamate uptake in astrocytes, the main scavenger of the neurotransmitter, further enhancing the concentration of this excitatory neurotransmitter (Aschner, et al., 1990, Moretto, et al., 2005). MeHg also enhances release of amino acid signaling molecules from astrocytes, potentially contributing to other toxic signaling cascades throughout the brain (Aschner, et al., 1995).

Irreversibly high increases in $[Ca^{2+}]_i$ can occur after many toxic insults, including glutamate, MeHg and repeated high K^+ depolarizations, and these increases precede other cell death markers, such as cell membrane permeation (Tymianski, et al., 1993, Ding, et al., 2011). These $[Ca^{2+}]_i$ increases are capable of inducing acute necrosis of some neurons immediately, but it is more notable as inducing delayed apoptosis in many more exposed neurons (Castoldi, et al., 2000). Apoptosis is typically $[Ca^{2+}]_i$ -dependent, and Ca^{2+} blockers are able to protect against MeHg neurotoxicity by blocking some Ca^{2+} influx in both *in vitro* and *in vivo* models (Sakamoto, et al., 1996, Edwards, et al., 2005). While protective, these blockers are only temporarily effective, if MeHg is not removed, block only delays toxicity.

Zinc ions (Zn^{2+}), may be an additional factor in MeHg toxicity. Zn^{2+} is released by MeHg treatment, as indicated by changes in the Ca^{2+} insensitive wavelength of the Ca^{2+} fluorophore Fura-2, and from chelating released divalent cations (Denny, et al., 1993, Denny and Atchison, 1994). Several possible sources of Zn^{2+} release from MeHg exposure exist, including release from proteins due to MeHg interference with thiol groups (Tao and Lim, 2006, Gibon, et al., 2010). For example, scaffolding proteins Shank2 and Shank3 are involved in the formation of postsynaptic densities (PSDs). Removal or release of Zn^{2+} degenerates PSDs (Grabrucker, et al., 2011). Though a direct effect has not been characterized, MeHg degenerates similar PSDs (Castoldi, et al., 2000). Once released, intracellular Zn^{2+} is itself toxic to neurons, in part through

disruption of mitochondrial ATP production and possibly by contributing to the depolarization of mitochondria and opening of the mPTP (Manev, et al., 1997, Sensi, et al., 2000, Jiang, et al., 2001, Isaev, et al., 2012). Extracellular Zn^{2+} may be important as well. Much of the Zn^{2+} in the brain is found in vesicles, but compared to the rest of the brain, it is unclear if this is an important pool available in the cerebellum (Wall, 2005). Golgi cell interneurons are the only cell in the cerebellum with the appropriate transporters to load Zn^{2+} into vesicles (Wang, et al., 2002). Golgi synaptic release of Zn^{2+} may modulate CGCs through inhibition of NMDA and $GABA_A$ Rs (Schmid, et al., 1999, Erreger and Traynelis, 2008, Amico-Ruvio, et al., 2011). Extracellular Zn^{2+} may actually be protective against MeHg, by inducing signaling cascades in astrocytes that produce metallothioneins, a scavenger of MeHg (Aschner, et al., 1998).

c. Cerebellum

i. Cerebellar circuitry

The cerebellum has relatively few different types of cells and a fairly uniform structure. The basic circuit of the cerebellum was famously described in the 1960s (Eccles, et al., 1967). In the cerebellar cortex, the only two typical neurons are the small, numerous CGCs and the large PCs, which are known for their large and heavily branched dendrites. While the cerebellar circuit is considered a simple circuit by many, complex combinations of spike activity and silent intervals suggest that more complicated activity may be prevalent in cerebellar learning (De Zeeuw, et al., 2011). CGC axon to PC dendrite synapses, which are glutamatergic, excitatory synapses, are important in procedural skills and memory, particularly through the Ca^{2+} -dependent synaptic plasticity associated with LTP and LTD. Mutations regulating both are detrimental to skill acquisition (Ito, 2008, Schonewille, et al., 2010). In addition to parallel fibers, climbing fibers enter the cerebellum from neuronal circuits in the spinal cord, sensory and motor cortexes, vestibular system (balance), red nucleus (motor coordination), and superior

colliculus (optical and sensory coordination). These climbing fibers form glutamatergic synapses and act on PC dendrites as well. CGCs receive excitatory glutamatergic synapses from mossy fibers originating from outside the cerebellum, while also receiving feedback GABAergic inhibition from Golgi cell interneurons, circuits that have been characterized much further from the original hypotheses (Ito, 2006). Additional internal circuits, such as regulation by Basket and Stellate interneurons, Lugaro cell regulation of Golgi cells, and Unipolar Brush cell synapses with CGCs in some regions of the cerebellum can also regulate cerebellar circuitry, but climbing fibers and mossy fibers remain the major inputs to the cerebellum, while PC axons are the only output. Both parallel fibers and climbing fibers act on many different PCs, parallel fibers synapse on scores of PCs in parallel, while climbing fibers may branch to about 10 PCs with many synapses on each. These multiple connections between populations of CGCs and PCs lead to groups of the neurons acting in concert, so even though PC axons are the only output of the cerebellum, the concerted output to the deep cerebellar nuclei and the system that provided the input is strong.

ii. Cerebellum growth and neuron development

Cerebellar development starts in the neural tube of the embryo, with the definition of midbrain and hindbrain, and proceeds with the formation of the rhombic lip and roof plate, where accumulating neuronal precursors migrate and build the structure of the cerebellar cortex (Hashimoto and Hibi, 2012). Migrating PCs radiate into the developing cerebellum and form a thick layer near the surface of the developing cerebellum (the pial surface). At the same time, CGC precursors migrate tangentially along the surface and form a transient layer, called the external granule or germinal layer (EGL), where precursors divide and form immature CGCs (Figure 1.2). As the cerebellum builds up with this influx of cells, PCs spread until they form a monolayer of cells. Spatial constraints require that this layer folds the cerebellum into its

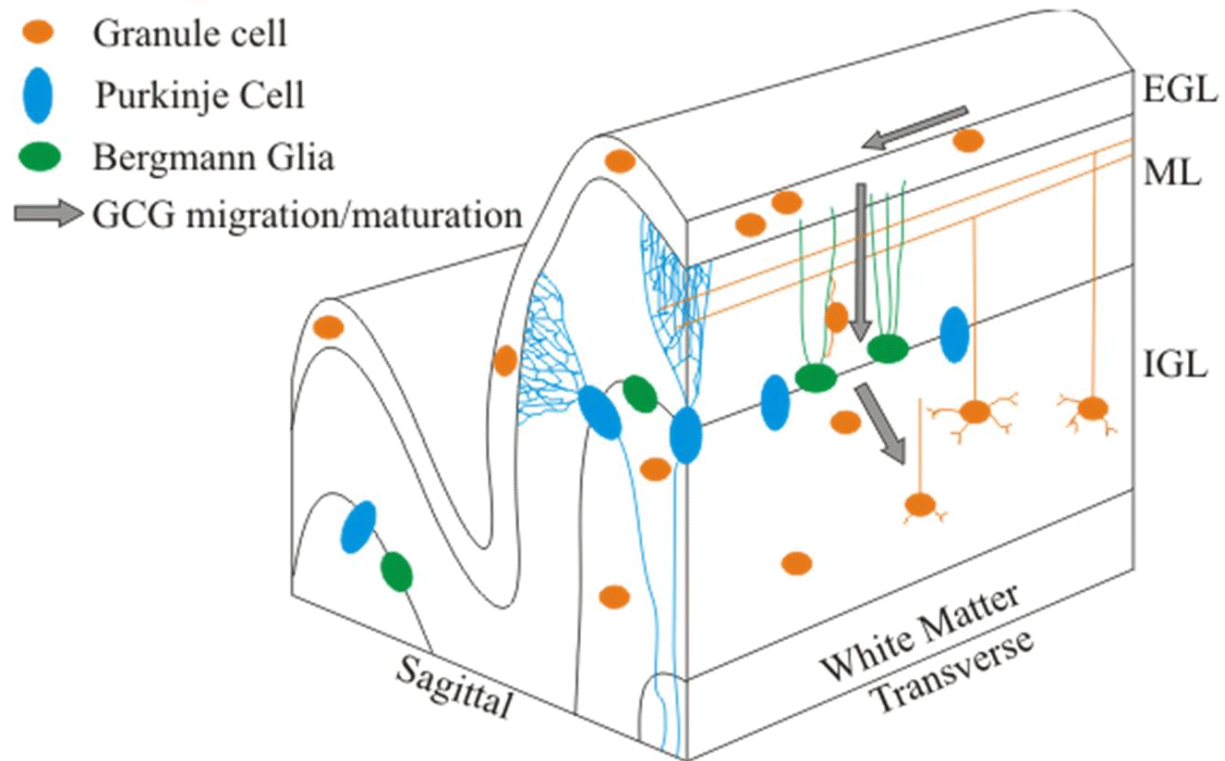


Figure 1.2. Schematic of CGC migration and maturation in the cerebellum. CGCs migrate from the base of the developing cerebellum through several stages (gray arrows) during the third trimester in humans and the first two postnatal weeks in rodents, both of which are considered to be the most susceptible periods for MeHg toxicity in each group. CGC precursors (orange) migrate along the surface of the cerebellum, accumulate in a temporary layer termed the external granule (or germinal) layer (EGL) and divide. Division terminates for these CGC precursors, and the resulting CGCs then migrate down Bergmann glial processes (green) through the molecular layer (ML) where PCs are developing extensive dendrites (blue). Migration stops, and the CGCs put out axons that travel back through the ML and produce parallel fibers which synapse onto PC dendrites. All stages of migration and maturation are dependent on finely-tuned Ca^{2+} oscillations and regulation by expression of surface receptors such as GABA_A Rs (Komuro and Rakic, 1998). CGCs express mostly $\alpha 2$ subunit-containing GABA_A Rs during development, while expressing mostly $\alpha 6$ in maturation (Takayama and Inoue, 2004). PCs express $\alpha 3$ subunits during development and $\alpha 1$ at maturation. Adapted from Atchison 2005.

characteristic shape. The development of PC dendrites builds up a layer between the PCs and EGL, the molecular layer (ML). As this occurs, CGCs that have finished dividing switch from tangential migration to a radial migration inward, through the ML and past the PCs to a new layer between the PCs and deep cerebellar white matter, the inner granule layer (IGL) (Figure 1.2). From the IGL, CGCs send out an axon into the ML, which bifurcates into an axonal structure termed a parallel fiber (PF). Because all PFs are roughly parallel, they extend toward the right and left hemispheres. PFs produce synapses on many PC dendrites along their path, and because CGCs greatly outnumber PCs, PCs receive many PF synapses on their complex dendritic trees.

Cerebellar growth in humans accelerates during the second half of gestation during migration of cerebellar neurons and construction of cerebellar circuits (Scott, et al., 2012). The cerebellar structure is fragile during this time; premature birth greatly increases the likelihood of cerebellar damage and motor deficits in infants (Volpe, 2009). Human cerebellar development continues after birth, including a nearly two-fold increase in volume during the period between 3-13 mo, outpacing whole brain growth (Choe, et al., 2012). Some additional CGC migration appears to occur at least until age 4, and possibly longer. During early growth spurts, cerebellar neuronal precursors are rapidly dividing and multiplying. Defects in cerebellar precursors typically lead to less growth in the cerebellum, leading to cerebellar hypoplasia or even aplasia, as seen in Joubert syndrome (Doherty, 2009). These are also periods of intense synaptic formation and remodeling (Castejon, et al., 2004). Defects in developmental migration can occur in various genetic disorders and some forms of autism (Métin, et al., 2008, Laure-Kamionowska and Maslinska, 2011). Normally, neurons that either do not reach their destination or do not stop die by apoptosis due to a lack of synaptic input. However, in these genetic disorders, clusters of CGCs can survive in white matter or PCs scatter in many parts of the cerebellar layers.

Migration and growth of the cerebellum is clearly a fragile period, and injury is possible through mechanisms such as premature birth, so toxic insults are potentially devastating. Even low-level MeHg exposure during pregnancy, ~1 ppm as measured by maternal hair, subtly decreases the size of a newborn's cerebellum (Cace, et al., 2011). While injection of MeHg in mice after weaning does induce motor defects, treatment during gestation and pre-weaning causes more severe deficits, even if treatment is ended at weaning (Huang, et al., 2011). MeHg treatment is also able to delay CGC migration through a Ca^{2+} -dependent mechanism (Mancini, et al., 2009, Fahrion, et al., 2012). While developmental exposures are clearly susceptible to MeHg, MeHg is able to interfere directly at mature parallel fiber and climbing fiber synapses, blocking them completely through both presynaptic and postsynaptic mechanisms after an initial increase in excitation (Yuan and Atchison, 1999).

d. GABA_A receptors

i. GABA_A receptor structure and function

GABA_ARs are members of the family of Cys-loop receptors, which include nicotinic acetylcholine receptors (nAChRs), 5-HT₃ serotonin receptors, and glycine receptors (Olsen and Tobin, 1990, Olsen, et al., 1991, Tsang, et al., 2007, Tsetlin, et al., 2010). All Cys-loop receptors are pentameric membrane-spanning receptors with a central ion channel pore. GABA_ARs are generally formed from two α subunits ($\alpha 1-6$), two β ($\beta 1-3$) subunits and one of several available additional subunits ($\gamma 1$ or 2 , δ , ϵ , θ , or π), arranged with alternation of the α and β subunits, with the additional subunit located between an α and β (Jacob, et al., 2008) (Figure 1.3). The α and β subunits within a receptor do not even have to be the same numbered type (e.g. $\alpha 1\alpha 6\beta 2\beta 3\gamma 2$) (Sigel and Baur, 2000). The various combinations of subunits determine many characteristics of the receptor, including available binding sites, ligand affinity and the electrophysiological characteristics of the channel (Saxena and Macdonald, 1996, Dhulst, et al., 2009). Almost any

combination can be expressed *in vitro*, but in many of the expression systems there is no preference for construction, producing non-physiological receptors such as those with only α subunits. Many combinations still potentially exist *in vivo*, along with additional modifications such as splice variants and post-translational modifications allow neurons to tailor the exact purpose of GABA_ARs even down to specialized regional combinations in the membrane (Lo, et al., 2010). However, many of these potential constructions are not common, and many neurons have typical variants associated with them.

As with many neuronal receptors and channels, cytosolic domains are where most of the interactions with other proteins occur, as well as domains that can be modified by phosphorylation. Phosphorylation of GABA_AR subunits may be important for surface expression through stabilization. In PCs continually stimulated by the glutamatergic climbing fibers, GABA_ARs are dephosphorylated, leading to dissociation from GABA_AR associated protein (GABARAP) scaffold and decreased surface expression (Qian, et al., 2011). This relationship between phosphorylation and expression has been shown with the $\alpha 4$ subunit in other parts of the brain (Abramian et al., 2010). This change also increases activity of receptors with the $\alpha 4$ subunit by slowing run down. Several additional scaffolding proteins and interacting factors appear to be critical for forming GABA_AR complexes with other membrane and cytosolic components, such as post-synaptic domains. Gephyrin, while generally associated with glycine receptors, also forms scaffolds with GABA_AR subunits $\alpha 1$, $\alpha 2$, and $\alpha 3$ (Tretter, et al., 2012). Removal of the synaptic GABA_AR scaffold gephyrin reduces surface expression of both synaptic and extrasynaptic GABA_ARs, but it is unclear if this is due to a reduction in innervation and GABA spillover or another mechanism (Marchionni, et al., 2009). Further characterization of modifications of GABA_ARs as well as interactions with scaffolding proteins could elucidate

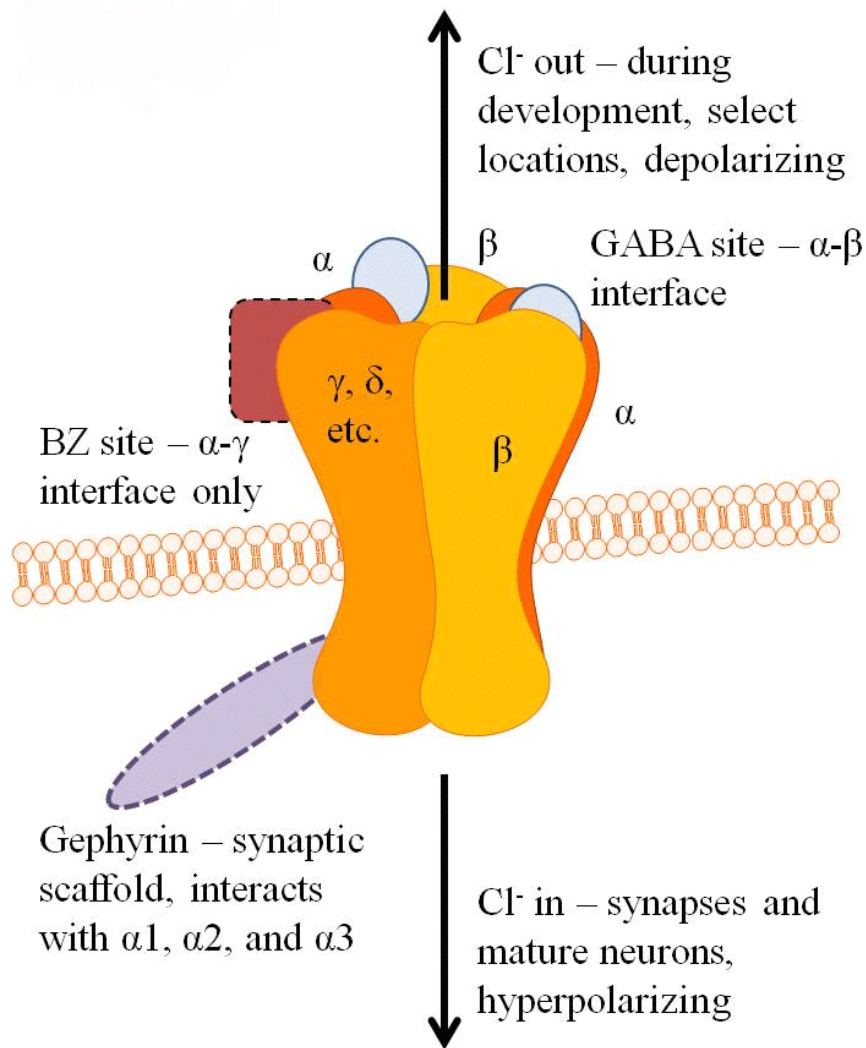


Figure 1.3. Cartoon depiction of the GABA_A receptor, a heteropentameric ion channel that conducts Cl⁻. *In vivo* it typically forms a unit from two α (from 6 subtypes), two β (from 3 subtypes), and one additional subunit, including γ and δ. GABA_ARs have two GABA binding sites, located at the interface of α and β subunits, which based on binding studies are also the location of the agonist muscimol and antagonist bicuculline binding sites. The construction of these interfaces controls GABA binding and thus the physiology of the receptor. An additional site where benzodiazepines (BZs) bind and potentiate GABA activation is located between α and γ subunits, so GABA_ARs without γ subunit are insensitive to these modulators. Synaptic scaffolds such as gephyrin bind to certain subtypes of GABA_ARs, clustering them inside synapses, whereas others such as those containing α6 can be found spread around the membrane. The direction of ion flow depends on the Cl⁻ gradient. An inward gradient is present at most post-synaptic domains and most mature cells and activation produces hyperpolarization and thus inhibition of activity. However, in developing neurons there is no extrusion of Cl⁻ through potassium-chloride co-transporter (KCC2), and thus the gradient is outward, so activation causes depolarization. This reversal of the gradient may also be present in some locations of mature cells, such as axons.

functional roles of the receptors, such as cross-talk in post-synaptic domains or functional pairing in presynaptic domains.

Unlike some other neuronal receptors, GABA_ARs can function both inside and outside of synapses. Even finer localization of GABA_ARs may be important in determining function, including synaptic and extrasynaptic receptors on dendrites, soma, axon and presynaptic sites. Localization of GABA_ARs is generally determined by α subunit composition, where $\alpha 1$ is almost always synaptic, whereas $\alpha 6$ and $\alpha 4$ are usually extrasynaptic (Nusser, et al., 1995, Olsen and Sieghart, 2009). Chimeras of these receptors with switched intracellular domains also switch localization (Wu, et al., 2012). Receptors with $\alpha 2$, $\alpha 3$ and $\alpha 5$ have not been as thoroughly characterized, although it appears that $\alpha 2$ and $\alpha 3$ can be found synaptically or extrasynaptically, while $\alpha 5$ is mostly extrasynaptic, even though it clusters similar to synaptic receptors. In many synapses, GABA_ARs may also be found on the presynaptic surface, and are critical in modulating neurotransmitter release (Engelman and MacDermott, 2004).

Several alterations to neuronal receptors, including certain GABA_AR subunits, can alter the expression of other combinations. Knockout of the $\alpha 6$ subunit of GABA_ARs selectively degrades the δ subunit without changing its mRNA expression, indicating that other receptor subunits are not able to construct surface receptors with δ *in vivo* (Jones, et al, 1997). In knockout mice, deletion of the GABA_AR $\alpha 6$ subunit in mice results in ~50% GABA_AR decrease overall in the cerebellum and the complete removal of surface δ subunits (Nusser, et al., 1999). AMPA and kainate receptors, additional ligand-gated Ca²⁺ channels in the CNS, can alter the expression of various GABA subunits through [Ca²⁺]_i-dependent mechanisms (Payne, et al., 2008). The *Stargazer* mouse, which has mutations of the AMPA receptor that regulates its trafficking as well as mutations to a VGCC subunit, also decreases GABA_AR $\alpha 6$ expression in CGCs, but increases $\alpha 1$ subunits expressed in synapses (Letts, et al., 1998, Payne, et al., 2007).

Unlike the $\alpha 6$ knockout, this mouse expresses considerable neurological dysfunction, and the compensation of $\alpha 1$ may contribute to them. Another VGCC mutant mouse, *tottering*, has deficits in neurotransmitter release and alterations to GABA_AR expression, particularly the GABA_AR $\alpha 6$ subunit (Tehrani and Barnes, 1995, Kaja, et al., 2007). These mutations and deficits indicate a strong link between VGCC and GABA_AR subunit expression.

ii. GABA_A receptor signaling

GABA_ARs in neurons, like glycine receptors, open to Cl⁻ with activation from their major ligand, in this case GABA (Lehoullier and Ticku, 1989). GABA is synthesized in neurons from glutamate by the enzymes glutamic acid decarboxylase 65 and 67 (GAD65 and GAD67). These enzymes are frequently used as a marker for GABAergic synapses. GABAergic synapses release GABA and produce inhibitory post-synaptic potentials (iPSPs) in their target neurons. GABAergic transmission is the primary inhibitory mechanism in the CNS. iPSPs are capable of interrupting action potentials and generally lowering excitability of target neurons. As with many other synapses, GABA is recovered from the synapse by high affinity GABA transporters (GAT) in nerve terminals where it can be reloaded into vesicles, or in surrounding glia, where it can be metabolized. Some synapses appear to have GABA_ARs arranged around synapses to detect overflow if too much GABA is released and escapes the synapse. GABA_ARs can be also found in synapses with other neurotransmitters, and GABA can be released from the same vesicles as other neurotransmitters or independent vesicle pools (Shrivastava, et al., 2011). When released in this manner, GABA is typically able to reduce the efficacy of the post-synaptic response through inhibitory action on post-synaptic GABA_ARs, indicating it takes part in fine tuning of response.

In addition to the standard inhibition characterized by phasic, synaptic inhibition, GABA_ARs can take part in a continual form of inhibition, termed tonic inhibition. When first described in maturing CGCs with no GABAergic synapse input, this form of inhibition was

found to account for as much as 99% of the inhibition of the cells (Brickley, et al., 1996). This tonic current is a result of extrasynaptic GABA_ARs containing $\alpha 6$ and δ subunits, which have unusually high affinity for GABA, low inactivation and little dissociation (Bianchi, et al., 2002). Expression of the $\alpha 6$ subunit in cells that do not normally express them produces extrasynaptic receptors capable of inducing tonic inhibition and inhibition of spontaneous and miniature iPSCs at synaptic sites (Wisden, et al., 2002). Tonic inhibition appears to be able to propagate through the cerebellum through large populations of Golgi cells releasing GABA both through synapses and into the extracellular environment. When large populations of CGCs are inhibited tonically in this manner, the collective glutamatergic release from parallel fibers onto PC dendrites is reduced, and the output of the cerebellum is reduced (De Schutter, 2002). Tonic and phasic inhibition appear to be independent of one another, In the thalamus, sustained activity of phasic inhibition as a form of LTD learning is able to alter individual cells, but not change response to extrasynaptic GABA_AR activation (Bright and Brickley, 2008). Phasic inhibition may thus be important for development of individual cells and memory, but tonic inhibition may be related to collective changes in larger populations of neurons in the brain.

Interestingly, the first suggested mechanism for tonic inhibition, that the extrasynaptic GABA_ARs were responsive primarily to GABA spilled from nearby synapses, has been overturned. Even with low ambient GABA, extrasynaptic GABA_ARs were found to be desensitized and unable to respond to spillover GABA from GABAergic glomeruli synapses (Bright, et al., 2011, Brickley and Mody, 2011). This appears to indicate that the normal mode of GABA_AR-mediated tonic inhibition requires only a very few of the receptors to be open, but for them to be open continuously, acting as hyperpolarizing channels and molecular shunts.

In CGC axons, it appears there may be some locations with high local $[Cl^-]_i$, leading to a reversal of the gradient and depolarization of the axon with GABA application simulating a

synaptic release (Pugh and Jahr, 2011). Despite the combination of depolarization and a resulting Ca^{2+} influx, these stimuli were rarely capable of initiating an action potential and releasing neurotransmitter. However, the increase in $[\text{Ca}^{2+}]_i$ did propagate along the axon all the way to the soma, increasing spontaneous release.

iii. GABA_A receptors and calcium

GABA_ARs have a complex set of secondary signals, many of which involve changes to $[\text{Ca}^{2+}]_i$. In cultures of CGCs from post-natal day (PND) 6-8 rats, GABA increases $[\text{Ca}^{2+}]_i$ through an L-type VGCC and depolarizes the neurons (Brodinsky, et al., 2003). Long-term culture with GABA induces neuritogenesis which is blocked by Ca^{2+} channel blockers as well as mitogen activated protein kinase (mapk) / extracellular-related kinase (erk) kinase 1 (MEK1) and calmodulin kinase II (CaMKII) blockers, suggesting several mechanisms of continuous GABA signaling. Phosphorylation of CaMKII and erk1 and erk2 also change with this GABA application. GABA activation in PCs induces a similar transient increase in $[\text{Ca}^{2+}]_i$ that is more pronounced in developing PCs. These transients are abolished by both bicuculline and VGCC block (Eilers, et al., 2001). Interestingly, positive allosteric modulators of GABA_ARs such as alcohol and pentobarbital inhibit the action of L-type VGCCs (Earl and Tietz, 2011). This is also the case in some neocortical nerve terminals, where GABA_AR activation and Ca^{2+} influx inhibits L-type VGCCs and neurotransmitter release (Long, et al., 2009). This makes clear that the eventual effect of $[\text{Ca}^{2+}]_i$ increases caused by GABA activation are dependent on the type of VGCC present in the nerve terminal. In cerebellar interneurons, it appears that GABA_AR activation can induce $[\text{Ca}^{2+}]_i$ increases without any concurrent depolarization or action of VGCCs, possibly through signals triggered by changes in osmotic pressure (Chavas, et al., 2004).

In CGC axons, muscimol activation of GABA_ARs is able to stimulate release of cytosolic glutamate without any changes to membrane potential or $[Ca^{2+}]_i$, indicating even more unexplored secondary signals (Raiteri, et al., 2001). Many of the effects of GABA_AR activation may be “sub-threshold”, acting in a manner that does not immediately alter the resting potential nor directly inducing depolarizations through Ca^{2+} influx (MacDermott et al., 1999). It appears that due to mechanisms such as VGCC activation, equilibration with HCO_3^- , and other secondary signaling events, that non-synaptic GABA_AR activation may have a net excitatory effect, rather than the presumed inhibitory effect (Kullman, et al., 2005). It will be critical in future studies to determine the conditions under which GABA activation is excitatory versus inhibitory, including the location on the cells, the existing localized Cl^- and Ca^{2+} concentrations, and the ligand used.

iv. GABA_A receptor pharmacology

GABA_ARs were originally mistaken for two receptors, one that responded to GABA and one that responded to benzodiazepines (BZs) such as diazepam and chlordiazepoxide, and was termed the BZ receptor (Lehoullier and Ticku, 1989). This may have been in part due to the fact that some GABA_ARs do not respond to BZs. This is due to the arrangement of ligand binding sites on the receptors, with the two GABA binding sites located between α and β subunits, while the BZ site sits between the α and γ subunit (Jacob, et al., 2008). When there is no γ subunit, as there is in extrasynaptic δ -containing receptors, there is no BZ site and so no BZ response. BZs are allosteric modulators of GABA_ARs, changing the receptor’s affinity and open dynamics. When bound by BZs, GABA_ARs open more frequently in response to GABA, but BZ binding alone is not enough to activate the receptors. BZs, through enhancing GABA signals, inhibit neurotransmission and neuronal activity throughout the brain, generally leading to anxiolytic and anesthetic results in mammals. Some of the effects of alcohol may be similar to BZs, due to

sharing a similar binding site on the GABA_AR, but this mechanism has not been well characterized yet due to the wide ranging effects of alcohol in the brain (Brickley and Mody, 2011).

Several agonists and antagonists of GABA_ARs have been used for many years in electrophysiological and biochemical recordings of GABA_AR activity. Muscimol is derived from many types of *Amanita* mushrooms, and is the major psychoactive component of the mushrooms. It is highly selective for GABA_ARs and binds the same sites as GABA, activating the receptors without altering the ambient GABA concentrations. Muscimol may have some subunit preference for extrasynaptic receptors due to a higher binding affinity, much like GABA does, but this preference has not been fully characterized (Chandra, et al., 2010). The agonist propofol acts through a binding site on the β subunit distinct from the GABA and muscimol site, and loreclazone and etomidate demonstrates preference for β 2- and β 3-containing receptors (Sanna, et al., 1995, Sanna, et al., 1996, Smith, et al., 2004, Drexler, et al., 2009). Bicuculline is derived from a plant alkaloid and induces seizures. It is a competitive antagonist for the GABA binding site and out-competes muscimol binding at effective concentrations. Bicuculline does not exhibit subunit specificity, but other antagonists, such as pore blocking competitive antagonists lanthanum (La³⁺), Zn²⁺ and furosemide, show preference for extrasynaptic receptors (Wafford, et al., 1996, Schmid, et al., 1999, Wall, 2002).

A diverse array of modulators is available or in development for modulation of GABA_ARs, some more effective on extrasynaptic receptors, but few have subunit specific effects (Belelli, et al., 2009). Compared to more general agonists, antagonists and allosteric modulators, subunit-specific modulators can produce widely different effects on GABA_AR signaling (Baur, et al., 2005, Khom, et al., 2010, Joksimovic, et al., 2013). One of these more recent classes of modulators for GABA_ARs is neurosteroids. As with BZs, many of these

molecules produce sedative effects, and neurosteroids are generally considered to be similar allosteric modulators of GABA_ARs, though they do not share the same binding sites. Despite multiple sites present for binding of neurosteroids, only one needs to be occupied for potentiation of the GABA_AR (Bracamontes, et al., 2011). With a homologous structure now available through ELIC1, additional interaction domains are being found for GABA_ARs, so many more modulators may be found soon (Varagic, et al., 2013).

Finally, there are a few modulators of other receptors in the CNS that may have effects of GABA_ARs as well. The AMPA receptor antagonist 6-cyano-7-nitroquinoxaline-2,3-dione (CNQX) appears to increase GABA-induced spontaneous currents in hippocampus and cerebellum, (Brickley et al., 2001). Not all antagonists of AMPA acted the same as CNQX and its derivatives, which were also able to increase sIPSC frequency. This change cannot be attributed to NMDA antagonism, as NMDA specific antagonists did not increase sIPSC frequency.

v. GABA_A receptors during development

One of the most interesting discoveries about GABA_ARs is that they are not always hyperpolarizing when activated. In fact, during development and migration in almost every neuron that expresses GABA_ARs, including CGCs, GABA_AR activation is directly depolarizing, due to a Cl⁻ concentration equilibrium that is positive compared to the cell resting potential (Owens, et al., 1996). As neurons migrate and mature, the electrochemical equilibrium potential becomes more negative, and the cells instead hyperpolarize with application of GABA. Expression of GABA_ARs also changes with migration and maturation. It appears that CGCs express mostly the $\alpha 2$ subunit in GABA_ARs during migration in the cerebellum whereas $\alpha 6$ rapidly becomes the dominant receptor type once they reach the IGL (Takayama and Inoue, 2004). In these same treatments, immature PCs appear to express more $\alpha 3$ subunits while mature

PCs have mostly $\alpha 1$ receptors. As with GABA_AR activation in adult neurons, activation of immature GABA_ARs also increases $[Ca^{2+}]_i$ through a VGCC-dependent mechanisms. This can be recapitulated in cultured CGCs from PND 6-8 rats, where GABA increases $[Ca^{2+}]_i$ through an L-type VGCC and depolarizes the neurons (Brodinsky, et al., 2003). When these CGCs are cultured in a depolarizing medium, simulating the formation of active synapses common in maturation, there is a gradual decrease in the depolarizing effect of GABA. Conversely, CGCs cultured in non-depolarizing medium can remain responsive for several days *in vitro*. Similarly, GABA reversal potentials change over PC development alongside CGCs, becoming more negative as the cells develop to a final equilibrium of -87 mV (Eilers, et al., 2001). Depolarization and increases in $[Ca^{2+}]_i$ increase δ subunit expression in CGCs, suggesting that migration and the IGL environment induces expression of extrasynaptic GABA_ARs (Gault and Siegal, 1997).

The critical point determining GABA_AR depolarization versus hyperpolarization appears to come from expression of the Potassium-Chloride Co-transporter type 2 (KCC2). KCC2 acts as a stop signal to many migrating neurons, as its expression in the membrane is able to reduce the efficacy of GABA-induced depolarization, which is a driving force of migration via Ca^{2+} oscillations (Bortone and Polleaux, 2009). Phosphorylation of KCC2 by protein kinase C (PKC) appears to be critical for its membrane trafficking and stability, indicating another regulatory step in maturation (Lee, et al., 2007). Because of its association with specific subtypes of GABA_AR expression and thus inhibition, alterations in KCC2 expression in the mature brain can be associated with epileptic seizures as well (Mao, et al., 2011). Once established, KCC2 surface expression can still be altered, as with ischemia, so the relative effects of GABA_AR activation and K^+/Cl^- transport may still change in adult and aging neurons (Galeffi, et al., 2004). Golgi cells are highly active during the migration of CGCs, and rat CGCs receive inhibitory Golgi

synapses in the IGL as early as PND 3 (Farrant and Brickley, 2003). Synaptic GABA could signal the end of migration for individual cells and promote KCC2 expression.

An argument has been made that depolarizing actions of GABA in developing neurons is an artifact of slicing and other preparations (Bregetovski and Bernard, 2012), but evidence from many model organisms and non-invasive techniques strongly refutes this (Ben-Ari, et al., 2012). Even the original discovery of tonic inhibition indicates that GABA depolarized the developing rat CGCs before they matured (Brickley, et al., 1996). This is perhaps best demonstrated, though, in live intact organisms. In early postnatal mice, when neurons can be imaged by two-photon microscopy while still in the live animal, depolarizing GABA is critical for migration of interneurons in the cortex, (Inada, et al., 2011).

vi. GABA_A receptor disorders and toxicology

Several disorders are associated with alterations to GABA_AR function or to general GABA signaling. Knockouts of several subunits of GABA_ARs display seizure phenotypes, typically caused by overactive signaling in discrete brain regions, indicating that GABA_AR signaling is critical for general function (Belelli, et al., 2009). Because of their inhibitory importance, GABA_ARs that are mutated in a way that prevents appropriate translation, folding, trafficking or function are associated with several types of epilepsy, including child *absence* epilepsy, Dravet syndrome, generalized epilepsy with febrile seizures plus, juvenile myoclonic epilepsy and severe myoclonic epilepsy in infancy (Macdonald, et al., 2010). Cerebellar and hippocampal GABA increases, as brought about by inhibition of GABA uptake through GABA transporter type 1 (GAT1), cause tremor, anxiety, and ataxia, both in knockout models and with the antiepileptic GAT1 inhibitor tiagabine (Chiu, et al., 2005). Alternatively, overexpression of GAT1 through a human mutation that decreases GAT1 degradation in turn decreases ambient GABA in the cerebellum and tonic inhibition (Egawa, et al., 2012). This in turn leads to a variety

of disorders, including developmental delay, lack of balance, speech impairment and epilepsy. This balance of GABA is critical to drugs that can alter the levels of GABA in the brain, such as tiagabine, so this must be taken into consideration for treatment strategies such as those for epilepsy (Houston, et al., 2012).

Several studies indicate direct effects of MeHg on GABA_ARs. At most relevant concentrations, MeHg potentiates activation of GABA_ARs, as indicated by larger amplitudes of spontaneous and evoked currents in the presence of ambient GABA (Arakawa, et al., 1991). Higher concentrations instead block GABA_ARs, indicating a possible mechanism that may explain aberrant results in some studies. MeHg, as well as Hg²⁺ and the sulfhydryl alkylating agent n-ethylmaleimide, potentiate binding of BZs to GABA_ARs, suggesting this is the immediate effect of MeHg on these receptors (Fonfria, et al., 2001). MeHg also shows subunit specificity in its action, acting on $\alpha 6$ -containing receptors at lower concentrations than on $\alpha 1$ receptors, significant changes to GABA_ARs occur at lower concentrations of MeHg than any other receptor, including VGCCs (Yuan and Atchison, 2003, Yuan, et al., 2005). These differences may contribute to different cell viability when comparing cells expressing mostly GABA_AR $\alpha 6$ subunits such as CGCs compared to cells expressing mostly $\alpha 1$, such as PCs or cortical neurons (Herden, et al., 2008).

Some regulation of GABA_ARs appears to occur due to internalization of the receptors, which can occur with both acute and chronic stress such as pregnancy, and appears to be due to excess activity (Maguire, et al., 2009, Poulter, et al., 2009). While toxic levels of activity frequently alter the surface expression of GABA_ARs and decrease GABA binding, this is not due to changes in membrane potential (Lyons, et al., 2001). Instead, it appears expression changes are mediated through increases in $[Ca^{2+}]_i$ and decoupling of GABA binding appears to relate to VGCC activation. Mink fed environmentally-relevant concentrations of MeHg for three months

showed decreases of GABA_AR expression up to 94% in cerebellum, along with decreased metabolic production of GABA and GABA receptor binding in other regions of the brain relevant to motor disorders (Basu, et al., 2010).

Some insight may also be gained by examining other toxicants that affect GABA_ARs. Dieldrin, a pesticide, antagonizes GABA_ARs as well as the structurally-similar glycine receptor. Long-term cell exposure to dieldrin antagonizes GABA and NMDA receptors and decreases surface expression of both, in turn reducing glutamate neurotransmission and excitotoxicity (Vale, et al., 2003, Babot, et al. 2007). Many of the effects of dieldrin can be directly reversed by the neurosteroid allopregnanolone, suggesting that neurosteroids are potent and lasting competitors for actions on GABA_ARs. When several chemicals and drugs of abuse were tested in neuronal cell cultures, assays for GABA_AR function, GABA uptake and cell membrane potential were the best indicators of neurotoxicity in humans (Galofre, et al., 2010).

B) Objectives and Rationale

a. Hypothesis and aims

Because of their individual interactions with Ca²⁺, we hypothesize that the interaction of MeHg and GABA_ARs will have effects on [Ca²⁺]_i in CGCs, and that these effects will be dependent on age and expression of receptor subunits. Previous experiments in the lab have begun to probe these interactions, through electrophysiology and other approaches (Yuan and Atchison, 2003, 2007, Mancini, dissertation, 2006). Direct interactions, through comparisons of cells with MeHg and GABA_AR modulators, or through comparisons of cells in different states, such as developing versus mature cells, have not been characterized thoroughly. Three projects were developed to characterize the interactions of MeHg and GABA_ARs as they relate to [Ca²⁺]_i in CGCs. The first, presented in Chapter 2, uses neonatal rats, the model for developmental toxicity used in this lab and others for many years. Neonatal mice are used in Chapter 3 in order

to introduce the additional factor of GABA_AR subunit knockout, in this case knockout of the $\alpha 6$ subunit, the expression of which marks another difference between developing and mature CGCs. Chronic, lifetime exposure is probed in mice in Chapter 4, including several Ca²⁺-dependent mechanisms in addition to GABA_AR modulation. Together these aims characterize the interactions of GABA_ARs, MeHg and Ca²⁺ in susceptible CGC populations of both developing and aging model populations.

b. Ca²⁺ imaging in cerebellar slices from rats and mice as a model for MeHg toxicity

From the background described, it is clear that the underlying mechanisms of MeHg toxicity, particularly mechanisms of selective neurotoxicity, remain elusive, and there are many potential approaches. One approach to studying MeHg toxicity is to model susceptible and potentially susceptible groups, including cell types and genotypes, against more resistant groups in the same environment. Thankfully, previous research has developed models and techniques that make this approach feasible. Slice culture has long been a convenient method for the study of electrophysiology, and has developed into a method for other forms of live study as well (Tashiro, et al., 2006). Finely cut slices of neural tissue from animals are able to maintain live, functional cells for several hours, and keep active synapses and other intercellular interactions once outside the brain. In cerebellar slices, we can examine and image CGCs, PCs and the other various cells and components in the cerebellum without the disruption that occurs with dissociation or similar approaches. Imaging in slice culture also allows for the possibility of examining in three dimensions, rather than in the relatively planar culture of cells. Computer modeling of the various components of cerebellar circuits reinforces the importance of working with a three-dimensional model as can be found in cerebellar slice culture (Berends, et al., 2004). Advances in these techniques are even capable of maintaining large cell populations for many

days in culture media (Mancini and Atchison, 2009), though much of the structure does eventually degrade.

One drawback of slice culture when compared to cell culture or live animal study is that the act of slicing by nature destroys and damages cells near the plane of the slice. This in turn leads to progressive degeneration of the slice over time (Kasischke, et al., 2001). In cerebellar slices, especially of immature cerebella, slicing is also rapidly toxic to PCs, in part due to a release of GABA from sliced cells (Rakotomamonjy, et al., 2011). Because we are interested more in CGCs, and because maintaining depolarized slices and using Ca^{2+} channel blockers or other inhibitors could interfere with our ability to measure Ca^{2+} accurately, we are using standard acute slice methods. These include important steps in slice culture incubation, including temperature control, rapid progression and precise concentrations of ions in buffering solutions that mimic cerebrospinal fluid to control osmolarity and reduce the actions of damaging ions released from cut cells. The initial concentrations of these artificial cerebrospinal fluid (ACSF) buffers are based on previous experiments in the lab (Yuan and Atchison, 2003, 2007). These protocols are updated and optimized as needed, particularly for handling tissue from older animals.

One goal of this dissertation is to examine different populations of cells that are considered more or less susceptible to MeHg yet reside within the same environment. This includes differences between CGCs and PCs, but primarily focuses on differences in cells at different stages of development. Conveniently, windows for the peak of CGC migration are 9-12 PND in rats and 8-11 PND in mice, as indicated by a comparative database (www.translatingtime.net, Clancy, et al., 2007, Workman, et al., 2013). With appropriate selection of images of slices from these animals, we can see CGCs in all stages, from dividing in the EGL, migrating in the ML, and maturing and forming synapses in the IGL. We can make

comparisons based on populations of these cells with treatments of MeHg. In addition to characterizing neonatal slice preparations, we had the opportunity to examine slice preparations from adult and geriatric mice through an overarching project involving chronic MeHg treatment in mice and co-treatment with a VGCC antagonist, isradipine.

Another goal of this dissertation is to examine a potential genetic susceptibility to MeHg, in this case a knockout of the GABA_AR subunit $\alpha 6$. Knocking out the $\alpha 6$ subunit causes a 50% overall reduction in GABA_AR expression in the cerebellum, no changes to synaptic $\alpha 1$ subunits, and no gross changes to phenotype (Nusser, et al., 1999). A permanent knockout of $\alpha 6$, caused by insertion of a neomycin cassette into the subunit gene, has been produced (Homanics, et al., 1997). It is of interest in this approach in part because though it has no obvious phenotype and no obvious difference in response to some agents thought to act on the subunit, we are certain of a difference in the selectivity of MeHg between extrasynaptic and synaptic GABA_ARs and we have evidence it acts preferentially on $\alpha 6$ receptors (Yuan and Atchison, 2003, Yuan, et al., 2005, Herden, et al., 2008). Recording from these animals would reinforce our data on the selectivity of MeHg, and characterize differences from other neurotoxicants acting on GABA_ARs.

While there are many approaches for imaging and biochemical analysis of cells in slice, in this dissertation, the approach chosen for imaging is live-cell Ca^{2+} fluorescence imaging. This approach uses live tissue and thus can elucidate changes over time in addition to special differences. $[\text{Ca}^{2+}]_i$ is clearly important to the toxicity of MeHg, and we have evidence of major changes to $[\text{Ca}^{2+}]_i$ as shown by Ca^{2+} fluorescence imaging in several cell types and preparations, including neuroblastoma-glioma cultures, synaptosome preparations and CGC cultures (Hare, et al., 1993, Denny, et al., 1993, Marty and Atchison, 1997, Marty and Atchison, 1998). Additionally, we have evidence of $[\text{Ca}^{2+}]_i$ increases throughout the cerebellum in slices, but

these responses need further characterization, (Yuan and Atchison, 2007). Such characterization includes determination of what concentrations of MeHg are effective in these slices over various periods of time as well as whether or not the time course of MeHg disruption of $[Ca^{2+}]_i$ can be modulated by agents that affect Ca^{2+} signaling.

This Ca^{2+} imaging approach allows for exploration of some additional hypotheses as well. The $GABA_A$ R connection to $[Ca^{2+}]_i$ is unclear, but may be dependent on the same cellular and developmental differences as MeHg toxicity susceptibility and has some clear connections to the toxicity itself. Therefore, we seek to characterize this interaction in these slice preparations through the use of the nonspecific agonist muscimol and antagonist bicuculline.

There are generally two approaches to loading fluorescent Ca^{2+} probes into neurons, bolus injection and bulk loading (Yuste, et al., 2011). While injection appears to produce the best sensitivity to changes in fluorescence, bulk loading highlights many cells and structures, and is more in line with our needs. Bulk loading of acetoxymethyl (AM) esters can be uneven depending on temperature and cell type, and some cells and techniques also produce inactive fluorescent intermediates, so it is important to have controls and optimize protocols (Cannell and Cody, 2006). Thankfully, this research group has had many years experience working with bulk loading of fluorescent probes, and has developed and optimized these techniques already.

Another drawback in Ca^{2+} imaging is that intense laser light produces reactive oxygen species in neurons, so it is critical to reduce light intensity and duration to avoid phototoxicity (Knight, et al., 2003). Careful attention is paid in this dissertation to techniques that can reduce phototoxicity, especially where phototoxicity can directly contribute to changes in fluorescence of both the cells and the fluorophores. Confocal laser light intensity is kept to a minimum, while the shutter system on the epifluorescence microscope minimizes illumination time. Where

possible, control treatments were run with only the illumination and untreated perfusion buffers in order to establish baseline levels of fluorescence and cell death during experiments.

Finally, with large numbers of cells and complex treatments over time, it becomes time consuming to identify and track Ca^{2+} imaging experiments over time manually, so automated cell identification and tracking is valuable (Wong, et al., 2010). Techniques used in this dissertation include both manual and automated approaches, depending on the bulk and complexity of data used. The automation techniques used may be important for further study, as the complexities involved in comparisons that must be made to characterize MeHg toxicity are increasing.

CHAPTER TWO

**METHYLMERCURY-ASSOCIATED INCREASES IN FLUO4 FLUORESCENCE IN
NEONATAL RAT CEREBELLAR SLICES ARE DEPENDENT ON GRANULE CELL
MIGRATIONAL STAGE AND MODULATED BY GABA_A RECEPTORS.**

A) ABSTRACT

Methylmercury (MeHg) induces permanent motor dysfunction through damage to the cerebellum in mammals and is of environmental concern due to bioaccumulation in diets and enhanced developmental susceptibility. MeHg induces neuronal cell death, particularly in developing cerebellar granule cells (CGCs). The critical mechanisms by which MeHg is toxic and selective for cell type are unclear. MeHg treatment alters current through many neuronal channels and disrupts divalent cation homeostasis, particularly of Ca^{2+} , through multiple paths leading to toxicity. MeHg could act in CGCs via disruption of the γ -aminobutyric acid receptor A (GABA_AR), a target of MeHg even at low concentrations that can regulate Ca^{2+} signaling in CGCs, particularly during migration. Using confocal microscopy and the fluorophore fluo4, we studied the disruption of internal divalent cation concentrations in slices of neonatal rat cerebellum. Slice preparation allows visualization of developing CGCs in multiple stages of their migration. We treated slices acutely with several concentrations of MeHg to determine Ca^{2+} response. In addition, we used the nonselective GABA_AR agonist muscimol and antagonist bicuculline to test their effects on Ca^{2+} and interactions with MeHg treatment. Acute MeHg concentrations increased fluo4 fluorescence within 40 min of treatment up to 260% of baseline in developing CGCs, but increased values only up to 170% of baseline in mature CGCs, showing a difference in cell response based on developmental stage. MeHg increased the fluorescence of processes in the slice as well, but the associated fluorescence was diffuse and could not be quantified as belonging to a single type of process. Purkinje cells (PCs), which are more resistant to MeHg toxicity, rarely fluoresced in these slices, and so could not be compared to CGCs either. Both muscimol and bicuculline reduced the effects of MeHg over 40 min. These results indicate that immediate disruption of Ca^{2+} homeostasis in CGCs is in part through effects on GABA_ARs .

B) INTRODUCTION

Methylmercury (MeHg) is a widespread environmental neurotoxicant known to affect the cerebellum (Hunter and Russell, 1954, Takeuchi et al., 1962, Bakir et al., 1973). In particular, MeHg is toxic to cerebellar granule cells (CGCs), the smallest and most numerous neurons in the brain. These neurons die in both chronic and acute MeHg poisoning, whereas a higher percentage of neighboring Purkinje cells (PCs) survive (Hunter and Russell, 1954, Sakamoto et al., 1998, Edwards et al., 2005, Yuan and Atchison, 2007).

CGC precursors divide and migrate from the external granule cell layer (EGL) through the maturing PC dendrites in the molecular layer (ML) and mature in the internal granule layer (IGL) (Komuro and Rakic, 1998). Human fetuses exposed to MeHg during CGC migration show the greatest susceptibility to toxicity (Amin-Zaki et al., 1974). Rats and mice are also susceptible to MeHg during a postnatal period of CGC migration, suggesting it is not the time before or after birth that indicates susceptibility, but some mechanism involved in neuronal migration and survival (Rice and Barone, 2000, Sakamoto, 2004).

MeHg interacts with and binds many proteins and small molecules, but circulating MeHg initially encounters cell surface proteins. Electrophysiological studies indicate that MeHg interacts with several types of voltage-gated Ca^{2+} channel (VGCC) (Shafer and Atchison, 1991, Sirois and Atchison, 2000, Peng et al., 2002, Hajela et al., 2003). These VGCCs are involved in the normal function of neurons, and do not typically produce large or lasting changes in internal Ca^{2+} concentrations ($[\text{Ca}^{2+}]_i$). Maintenance of low $[\text{Ca}^{2+}]_i$ is critical for cell viability and signaling, and disruption of intracellular divalent cation homeostasis is a common sign of cellular MeHg toxicity (Hare, et al., 1993, Marty and Atchison, 1998, Edwards, et al., 2005). In CGCs, oscillating $[\text{Ca}^{2+}]_i$ is an important migration signal; disruption of Ca^{2+} oscillation can

accelerate, delay, halt or even reverse CGC migration (Komuro and Kumada, 2005). Continuous MeHg treatment delays CGC migration in all layers, suggesting that disruption of Ca^{2+} oscillations occurs (Mancini et al., 2010).

In addition to Ca^{2+} channels, MeHg interacts with GABA_ARs, ligand-gated Cl^- channels that act as the principal inhibitory receptors in the mammalian adult brain (Yuan and Atchison, 1997; Fonfria et al., 2001; Yuan and Atchison, 2003). Cell surface function and subunit composition of GABA_AR differs between CGCs and PCs, which are more resistant to MeHg, including differences in α subunit stoichiometry. These subunits comprise two of the five subunits of the channel (Nusser et al., 1998, Joyce, 2007). CGCs contain an abundance of extrasynaptic GABA_ARs with $\alpha 6$ subunits while PCs contain only synaptic $\alpha 1$ subunits. GABA_ARs containing $\alpha 1$ produce fast inhibitory postsynaptic currents, whereas $\alpha 6$ -containing GABA_ARs produce a hyperpolarizing current with little inactivation, termed tonic current (Saxena and MacDonald, 1996, Bianchi et al., 2002). Tonic current maintains prolonged inhibition and a low $[\text{Ca}^{2+}]_i$ (Brickley et al., 1996, Brickley et al., 2001). In isolated cells in culture, $\alpha 6$ -containing CGCs and cortical cells containing only $\alpha 1$ GABA_ARs displayed similar current block by MeHg in both cell types (Herden et al., 2008). This suggests either that additional differences between CGCs and other cells occur or interactions among the receptor subunits contribute to susceptibility, possibly including other GABA_AR subunits associated with $\alpha 6$ or conditions unique to slice culture.

In addition to expression differences between CGCs and PCs, GABA_ARs undergo important changes during development. Before migration, GABA_AR activation depolarizes immature CGCs, opening VGCCs and increasing $[\text{Ca}^{2+}]_i$ (Owens et al., 1996). This is due to the accumulation of intracellular chloride via activation of the sodium-potassium-chloride

transporter NKCC1 (Yamada et al., 2004). During CGC migration, GABA_ARs switch from excitatory to inhibitory as expression of the potassium-chloride transporter KCC2 overtakes NKCC1, reducing intracellular chloride concentrations (Zheng et al., 2003, Takayama and Inoue, 2006). During this period, expression of CGC GABA_AR subunits changes, including expression changes among relatively unstudied and transient receptor subtypes, such as $\alpha 2$ (Takayama and Inoue, 2004). These findings suggest that both changes in the Cl⁻ ionic gradient and GABA_AR expression may contribute to the effects of MeHg during cerebellar development.

We sought to test the hypothesis that CGCs at different stages of development react differentially to MeHg by investigating the acute actions of MeHg on developing CGCs. Slices of brain maintained in oxygenated artificial cerebrospinal fluid (ACSF) permit rapid and controlled treatment of cells with toxicant, while retaining much of their structure and function. Because CGCs at different stages of development appear to have differential sensitivities to MeHg, we wanted to determine if there is a difference in acutely applied MeHg-dependent disruption of [Ca²⁺]_i. We used the fluorescent indicator fluo4, which labels free divalent cations, to indicate relative changes in [Ca²⁺]_i. In addition, we tested the involvement of GABA_ARs with the non-specific GABA_AR agonist and antagonist muscimol and bicuculline, respectively. While the mechanisms of cerebellar toxicity appear similar between acute and chronic MeHg exposure, the insight gained from these acute studies would require further study in chronic exposures to be certain of their similarity.

C) MATERIALS AND METHODS

a. Chemicals and solutions

Methylmercuric (II) chloride was obtained from Aldrich Chemical (Milwaukee, WI). Fluo4 (NW, no wash), ethidium homodimer-1 (ethD-1) and probenecid were obtained from Invitrogen Molecular Probes (Eugene, OR). Muscimol hydrobromide and bicuculline methobromide were obtained from Sigma Chemical Co. (St. Louis, MO).

Tissue dissections were carried out in a solution containing (in mM): 222.5, sucrose; 2.5, KCl; 4, MgCl₂; 1.25, KH₂PO₄; 26, NaHCO₃; 1, CaCl₂; and 25, D-glucose (pH 7.3-7.5 when oxygenated) at room temperature of 23-25 °C. These low [Na⁺], low [Ca²⁺] high [Mg²⁺] slicing solutions were used to reduce cellular damage during slicing. Slices were kept in this solution for no longer than 15 min. Further incubations were performed in ACSF containing (in mM): 125, NaCl; 2.5, KCl; 1, MgCl₂; 1.25, KH₂PO₄; 26, NaHCO₃; 2, CaCl₂; and 20, D-glucose (pH 7.3-7.5 when oxygenated). ACSF was supplemented with MeHg from a 10 mM stock solution in double-distilled H₂O for treatments. All working solutions were prepared within 48 h of use and oxygenated with 95/5% O₂/CO₂ at room temperature during treatments. 2x stock of fluo4 was prepared according to the supplier's instructions and diluted to a final concentration of 4 μM in ACSF supplemented with 2.5 μM probenecid to facilitate fluorophore loading (Mehlin et al., 2003). Stock solutions of 100 mM muscimol and 10 mM bicuculline were prepared in double-distilled H₂O and stored at -20°C until use. Choice of concentrations of bicuculline and muscimol were based on previous electrophysiological experiments showing bath application of 100 μM muscimol and 10 μM bicuculline depolarize and block, respectively, cells in various brain slices (Yuan and Atchison 1997, 2003), and optimizations showing a temporary increase in [Ca²⁺]_i from bath application of 100 μM muscimol in slices.

b. Acute slice preparation

All animal procedures are in accordance with NIH guidelines for experimental animal use and were approved by the Michigan State University Institutional Animal Care and Use Committee. Timed-pregnant, female Sprague-Dawley rats were obtained from Charles River Laboratories (Cambridge, MA). Pregnant and nursing dams were fed high-fat diets (Purina 7024, Land O Lakes Purina, Richmond, IN) to improve litter size. All rats were given doubly-distilled water to drink *ad libitum*.

Male and female rat pups (M=24, F=14, postnatal days 8-12) were euthanized by rapid decapitation. Their brains were rapidly removed. Cerebella were maintained in ice-cold, oxygenated solution during slicing. Sagittal slices 250 μm thick were cut using a Leica VT100S vibratome (Leica Microsystems Inc., Bannockburn, IL). After slicing, slices were incubated in oxygenated ACSF at room temperature for 1 h.

Incubations in ACSF alone were followed by incubations in fluorophores in ACSF, either for cytotoxicity assays or for time course studies. A live/dead assay using fluo4/ethD-1 was used to determine if the concentrations of MeHg used in time course studies were lethal to cells in slices during the imaging period. Slices were incubated in ACSF with stock fluo4 and 4 μM ethD-1 for 2 h (post-incubation control), for 3 h (+1 h ACSF) or for 3 h supplemented with 20 μM MeHg during the final h (+1 h MeHg). Due to time-constraints in imaging, these were not matched to the 40min MeHg treatments of the time courses, but were kept to 60min treatment and the highest concentration used in time course assays, 20 μM MeHg, to represent the harshest treatment tested. All other treatments incubated slices in ACSF with 1X fluo4 from 2-8 h as needed. In some cases, multiple slices from the same animal were used on a treatment day, but no slices from individual animals or animals in the same litter were given the same treatment.

c. Confocal microscopy

For each treatment, a cerebellar slice was removed from fluorophore incubation and anchored in a microscope perfusion chamber with gravity-fed oxygenated ACSF flowing at 2-3 ml/min at room temperature, 23-25°C. Slices were visualized under 10x and 40x water immersion objectives (NA 0.3 and 0.8, respectively) fitted to an upright Leica TSL confocal scanning microscope (Leica Microsystems Inc., Bannockburn, IL). Magnified regions of the slices were examined using an argon laser at 488 nm excitation. To reduce the incidence of photobleaching, laser power was set at less than 30% of maximum. To maximize the number of cells available for analysis, 40x magnified regions were chosen that contained fluorescent cells in all cerebellar layers, based on initial visualization at 10x magnification.

Slices incubated for the cytotoxicity assays were sequentially scanned for fluo4 and ethD-1. Imaging was performed at 488 and 543 nm laser excitation with emission filters for fluo4 (500-535 nm) and ethD-1 (556-700 nm). For single-label experiments, a wider fluo4 emission could be traced, so an emission filter of 500-700 nm was used. Imaging parameters for both fluorophores were scaled manually to the maximum and minimum saturation limits for pixel values before taking scans. Images were taken at a 512x512 pixel resolution representing a $(300 \mu\text{m})^2$ field of view. The full thickness of each slice, typically 100-160 μm , was scanned as a z-series of images representing an image stack. Between-image depth was set at 3-5 μm to decrease imaging time and minimize photobleaching while still taking multiple images of each cell. Imaging of cytotoxicity assays included two regions of each slice, taken at 10x and 40x magnification. For time course experiments, one region of the slice was selected. To maintain visualization of the same cells through the experiment, framing of the image was manually reset between time points if the slice shifted visibly.

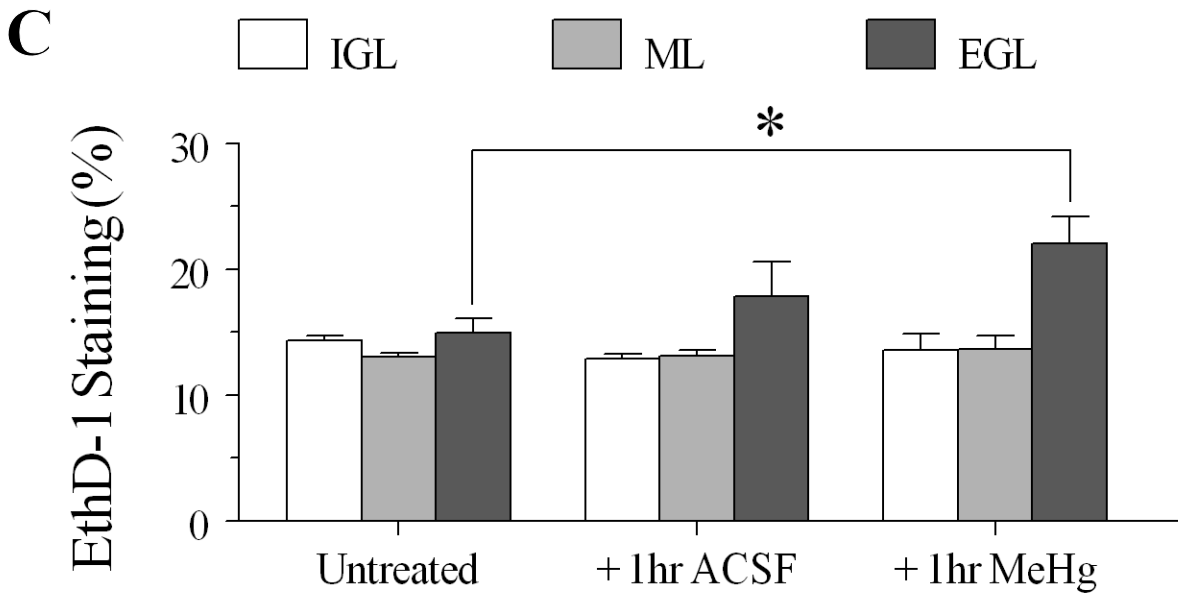
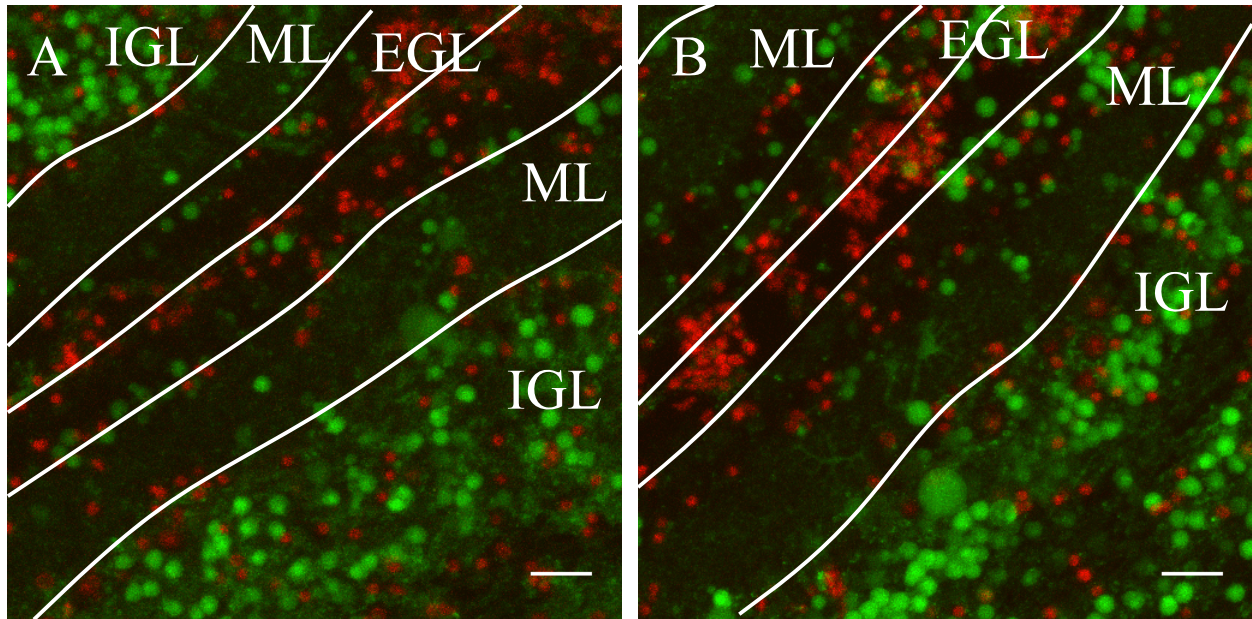


Figure 2.1. **A** A representative pseudocolor fluorescent image of an acutely-isolated cerebellar slice from PND9 rat showing modified fluo4/ethD-1 live/dead cytotoxicity assay, post-incubation control. Images are from internal folds of the developing cerebellum. Images show maximum fluo4 and ethD-1 fluorescence values by pixel. Approximate pial surface of an inner fold is indicated by a white line and other boundaries are indicated by dashed lines. EthD-1 (red), an indicator of dead cells, and Fluo4AM (green), an indicator of relative intracellular calcium concentration, do not colocalize. Scale bar represents 30 μ m.

Figure 2.1 (cont'd). **B** Representative image from separate slice from the same cerebellum after one additional h in ACSF supplemented with 20 μ M MeHg. **C** EthD-1 mean pixel staining (% pixels \pm SEM) comparison of layers post-incubation in fluo4 and ethD-1 (n=5), with an additional 1 h incubation in ACSF (n=3) or with an additional 1 h incubation in 20 μ M MeHg ACSF (n=3). Abbreviations: EGL, external granule layer; ML, molecular layer; IGL, internal granule layer.

Several concentrations of MeHg were tested for effects on $[Ca^{2+}]_i$. In these time course treatments, two pretreatment time points (-10 and -5 min) established a baseline fluo4 signal, followed by 40 min of continuous perfusion with a single concentration of either 1, 5, 10 or 20 μ M MeHg starting at 0 min. These concentrations are higher than those used for isolated cells in culture due to enhanced non-specific binding of MeHg in tissue. They fall between 1 μ M MeHg concentrations shown to allow cell survival and migration in rat cerebellar slice culture for several days (Mancini et al., 2009) and blood concentrations calculated in acute human exposures in Iraq, up to 19.5 μ M (Bakir et al., 1973). Untreated control slices were used to monitor photobleaching with no MeHg treatment over the same time period. For all treatments, image stacks were collected every 5 min.

GABA_AR function and divalent cation regulation was compared in the presence and absence of MeHg using muscimol and bicuculline, a nonspecific GABA_AR agonist and antagonist, respectively. As in treatments with MeHg alone, images were collected at two pretreatment points, -10 and -5 min, and images were collected every 5 min thereafter for 40 min. For combination treatments, continuous perfusion with 20 μ M MeHg started at t=0 min and slices were treated with four 60 sec pulses of either 100 μ M muscimol or 10 μ M bicuculline in ACSF. These treatments repeated addition of the same agent 30 sec before the 10, 20, 30 and 40 min time points to allow the perfusate to reach the slice in time for imaging. Bicuculline and muscimol controls were performed in which these agents were pulsed in the absence of MeHg. The 20 μ M concentration of MeHg was used in combination treatments to allow for treatment comparison to an increase in $[Ca^{2+}]_i$ in all layers.

d. Image analysis and statistics

Cytotoxicity assay images were processed using Leica Confocal Software Lite (ver. 2.61, Leica Microsystems Heidelberg, GmbH). Histological layers were visualized and categorized into EGL, ML or IGL based on fluo4 staining of CGCs (Figure 2.1A). CGCs were identified as spherical cells up to 10 μm in diameter. The EGL, 10 to 30 μm thick, extended from the pial edges of the slice to the origin of dendritic processes (Figures 2.1, 2.2). The ML, 60 to 80 μm thick, contained diffuse fluo4-stained PC dendrites and linear glial processes. CGCs along the EGL/ML line were considered EGL cells. A single layer of PCs divides the ML and IGL, but since PCs in this treatment do not typically appear to fluoresce with fluo4 treatment, the ML/IGL boundary was defined as the end of dendrite staining and the start of densely-packed fluorescent cells. Cells falling on the ML/IGL boundary were excluded from analysis because Purkinje cell processes and other fluorescent processes frequently overlapped with CGCs there. The IGL extended 60 to 80 μm from this line before an observable drop in fluo4 staining occurred, consistent with the edge of cerebellar white matter.

For cytotoxicity assays, regions of interest were made around each visible layer in 40x magnification image stacks, divided by visible boundaries described above (Figure 2.1). Histograms were taken for each layer region of interest, with the threshold for positive staining set at 10% of maximum pixel intensity. From each histogram, the sum of all pixels positive for ethD-1 was divided by the layer's total pixel area to produce ethD-1 pixel intensities, expressed as a percent. Each layer's pixel intensities from two 40x image stacks per slice were averaged to produce mean pixel intensities per animal, and then averaged per treatment. With only one confocal platform to image slices, the +1 h MeHg-treated slices and the +1 h ACSF-treated slices had to come from different animals, so an n of 1 represents all treatments from the same litter.

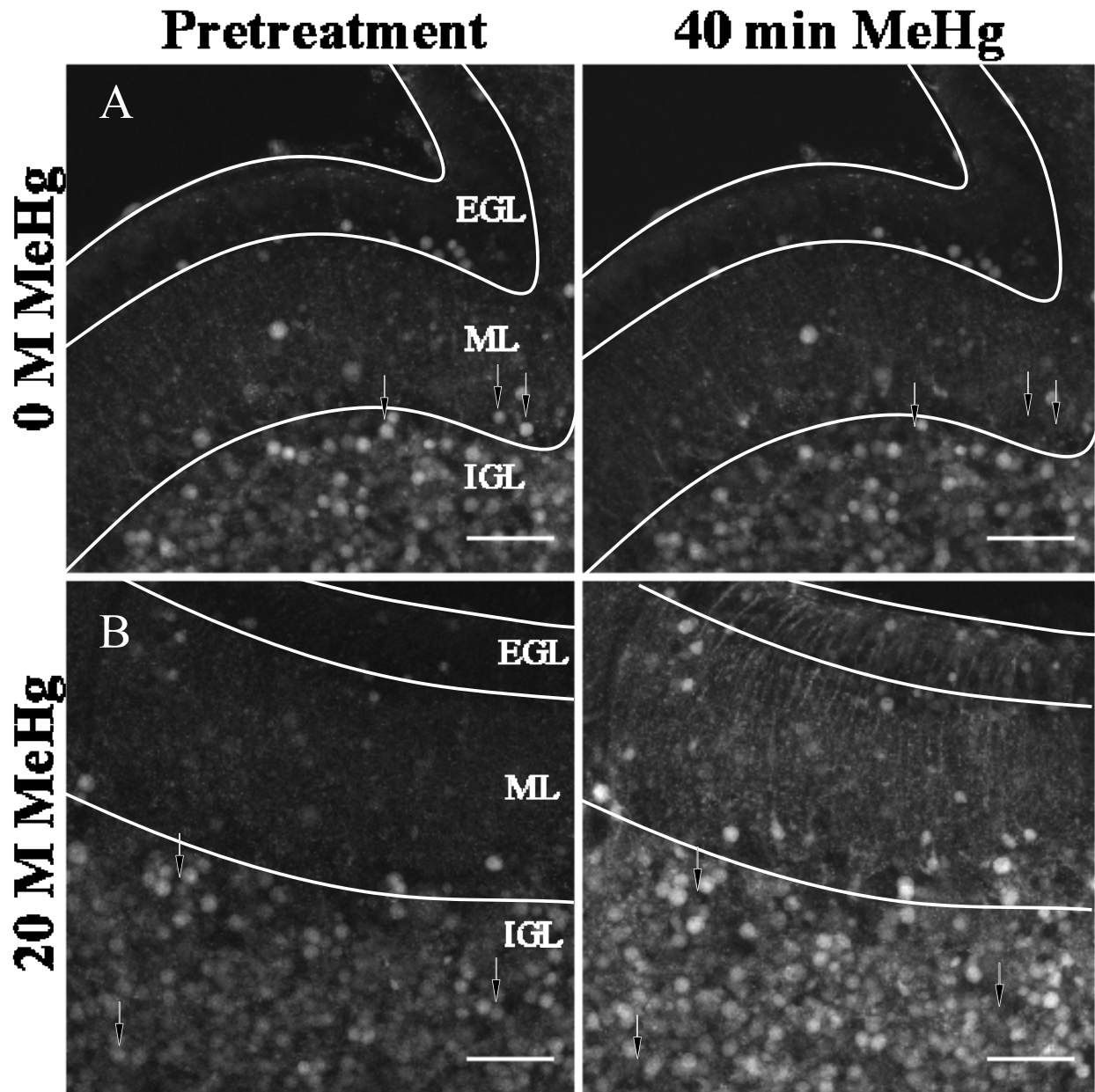


Figure 2.2. 40x grayscale examples of cerebellar slices before (-10) and after (40 min) treatment with MeHg. Images show projection of maximum fluo4 fluorescence by pixel. **A** Fluorescence does not change over the course of imaging in control slices. **B** MeHg increased fluorescence in all layers, with the signal from many cells saturating the detector. Scale bars are 60 μm in all images. Surfaces and boundaries are indicated as with Figure 2.1. White arrows indicate examples of cells with extinguished fluorescence by the end of treatment.

For time courses, image stacks were processed using ImageJ (Rasband, 2011, imagej.nih.gov/ij/). Background was subtracted from each image using the subtract background tool with a 50 pixel rolling-ball radius. Resulting images were divided into time points and projected to two dimensional images by summing the pixels in the z-dimension. These summed image series were aligned over time using the “StackReg” plugin (Thévenaz et al., 1998) and cropped to eliminate unused space, typically removing 10-12 pixels in each dimension. CGCs were chosen from all three layers, using the elliptical brush tool to select approximately 10 μm circles around distinguishable CGCs. Mean pixel intensities (F_t) from these CGCs as circular regions of interest were collected using the “Multi Measure” plugin (Rasband et al., 2006). Cells were classified into two categories. Cells that visibly lysed, visibly detached from the tissue, or lost fluo4 fluorescence between time points and did not recover were tallied as extinguished, as they either lost cell membrane integrity or detached from the tissue between time points. Significant fluorescence loss typical for extinguishing events was determined by finding negative change in fluorescence between time points (ΔF) significantly greater than the mean change of the cells in the same layer ($P < 0.05$). Typical extinguishing events displayed $>10\%$ fluorescence loss, and were checked visually in the original images before discarding. All non-extinguishing mean pixel intensities were tracked for the time course. Pixel intensities were normalized to the average of two pretreatment intensities (F/F_0). Cell density (cells/ $(100 \mu\text{m})^2$) was determined from total cell counts, live and extinguished, corrected for layer areas using additional polygonal regions of interest in ImageJ. Tallies for extinguished cells were compared to total cells counted in each layer.

For cytotoxicity assays, cell densities and extinguished cell counts, paired mean comparisons were made in GraphPad Prism (v4.03, GraphPad Software, Inc., La Jolla, CA). For

Ca²⁺ time course experiments, overall effects and interactions were determined using IBM SPSS Statistics (SPSS) (IBM, Somers, NY). Assays were analyzed using repeated measures ANOVA with layers and time as within-subjects factors (Steel and Torrie, 1960). Because of different numbers of replicates in different groups (n=3 to 6), adjusted means were used for statistical comparisons. No treatment group included enough separate replicates of males and females to compare the two groups. Additionally, each treatment group was assessed separately for significant changes in F/F_0 over time and between layers. *Post-hoc* comparisons were made in SPSS for time and layer comparisons and GraphPad Prism for treatment comparisons. Bonferroni corrections were used for multiple treatment comparisons. All effects, interactions and comparisons were considered significant for $P < 0.05$.

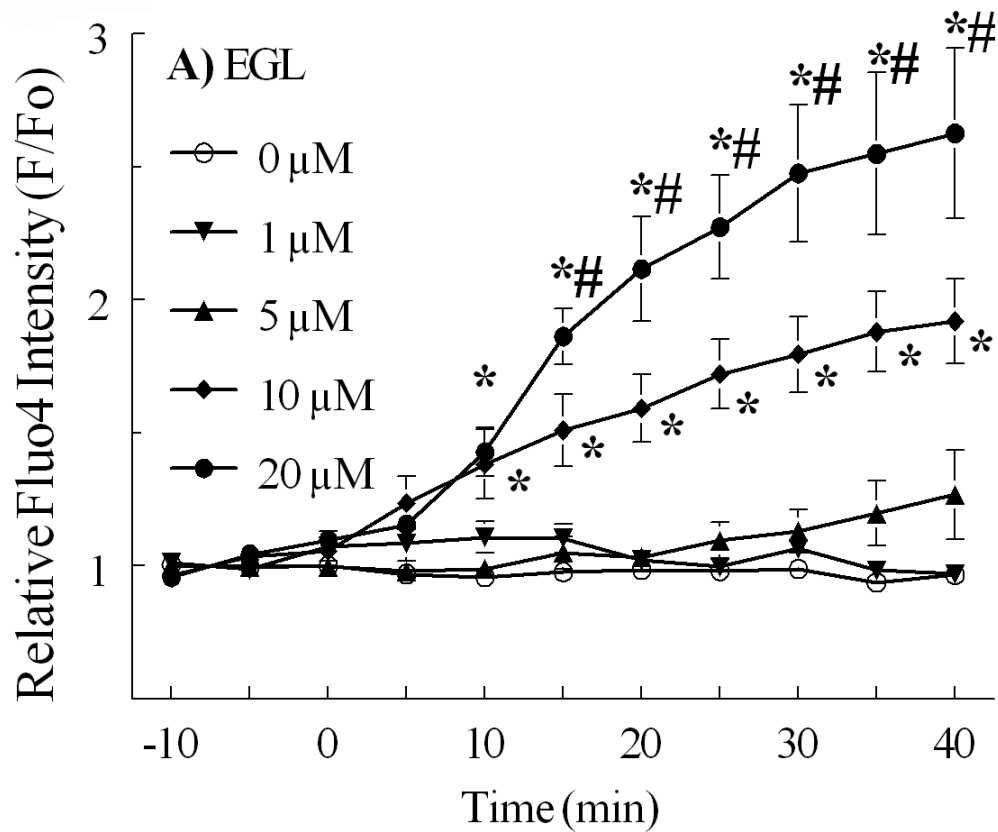
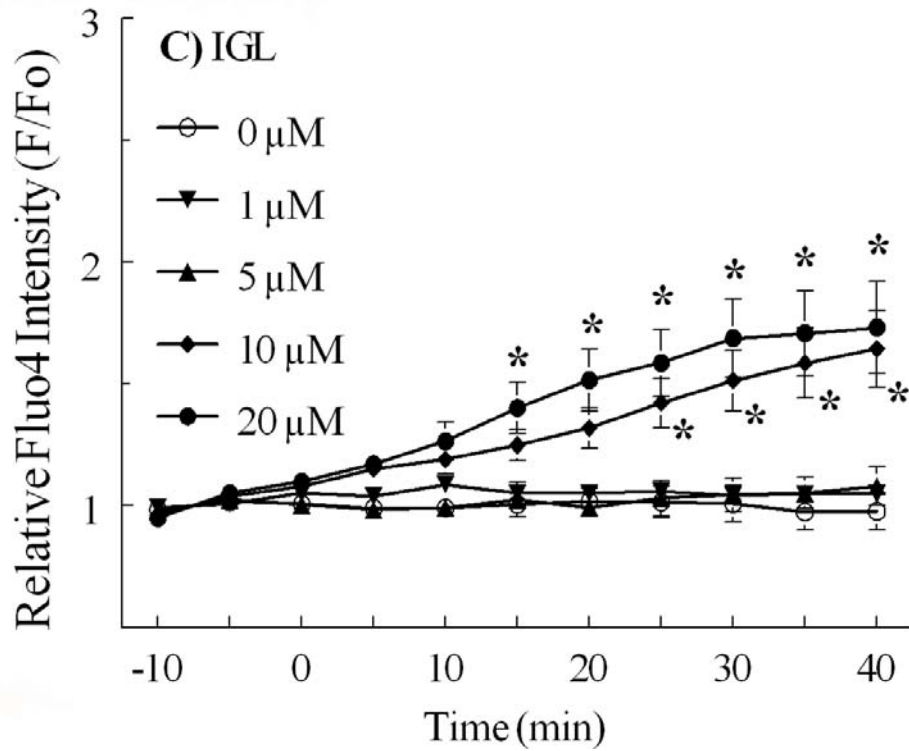
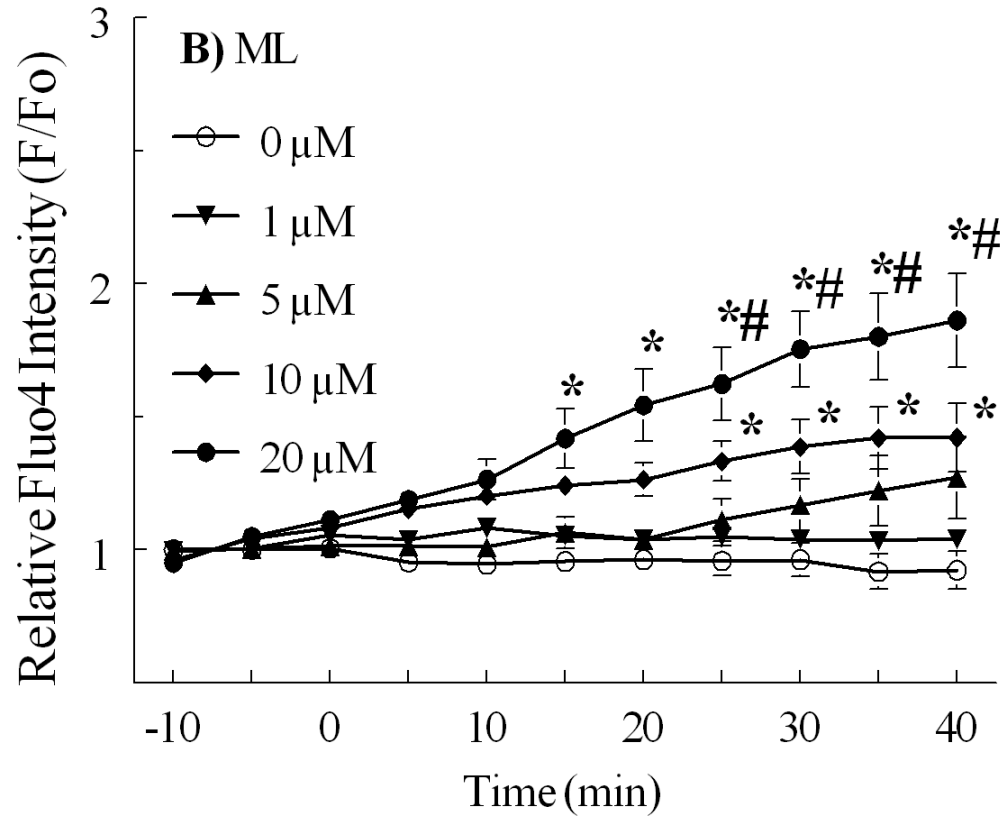


Figure 2.3. Relative fluo4 fluorescence intensity (F/F_0) in CGCs by histological layer in slices from neonatal rat cerebellum exposed to concentrations of MeHg continuously for 30 min. Control MeHg concentrations did not change fluorescence significantly. Continuous perfusion of ACSF with 0 μM (\circ , $n=5$), 1 μM (\blacktriangledown , $n=3$), 5 μM (\blacktriangle , $n=5$), 10 μM (\blacklozenge , $n=6$) or 20 μM MeHg (\bullet , $n=4$) were compared in **A**, the EGL, **B**, the ML, and **C**, the IGL. Significant differences are indicated from untreated control (*) and between 20 μM and 10 μM treatments (#) at the same time point. Intensity values are expressed in arbitrary units (mean \pm SEM).

Figure 2.3 (cont'd)



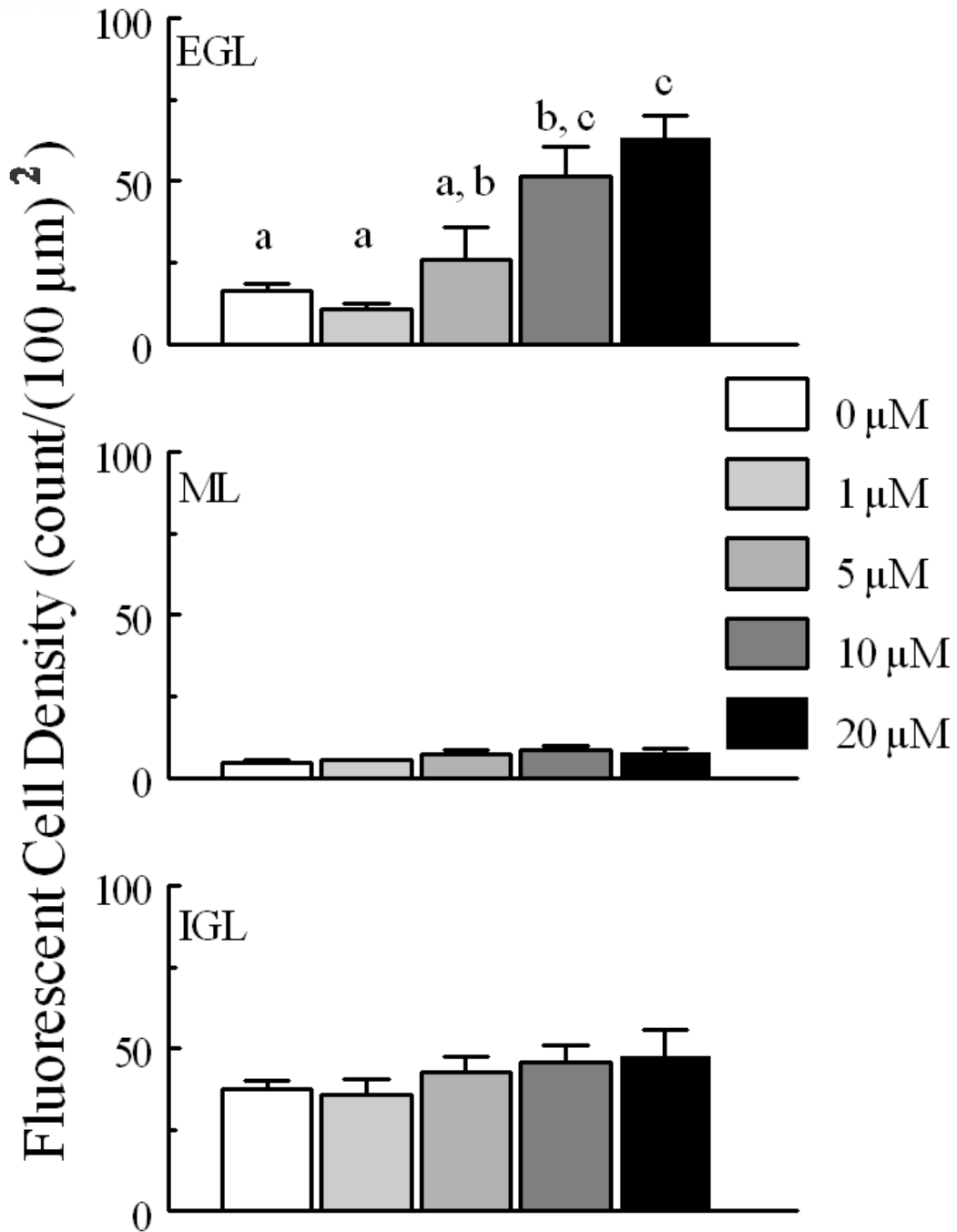


Figure 2.4. Cell density per $(100 \mu\text{m})^2$ for CGCs monitored for fluo4 fluorescence intensity, in each layer (EGL, ML and IGL), for tissue treated with different concentrations of MeHg. Fluorescent CGCs were more dense in the EGL and IGL layers than in the ML. At higher MeHg concentrations, fluorescent CGCs in the EGL were more dense than in IGL, but at lower concentrations, density was higher in the IGL.

Figure 2.4 (cont'd) Within the EGL, fluorescent cell density increased significantly with greater concentrations of continuous MeHg treatment, non-overlapping letters are significantly different comparisons ($P < 0.05$). Paired comparisons were made between each concentration of MeHg by layer. Significantly different pairs within each layer are indicated by different letters ($P < 0.05$). *n* for each treatment is the same as in Figure 2.3.

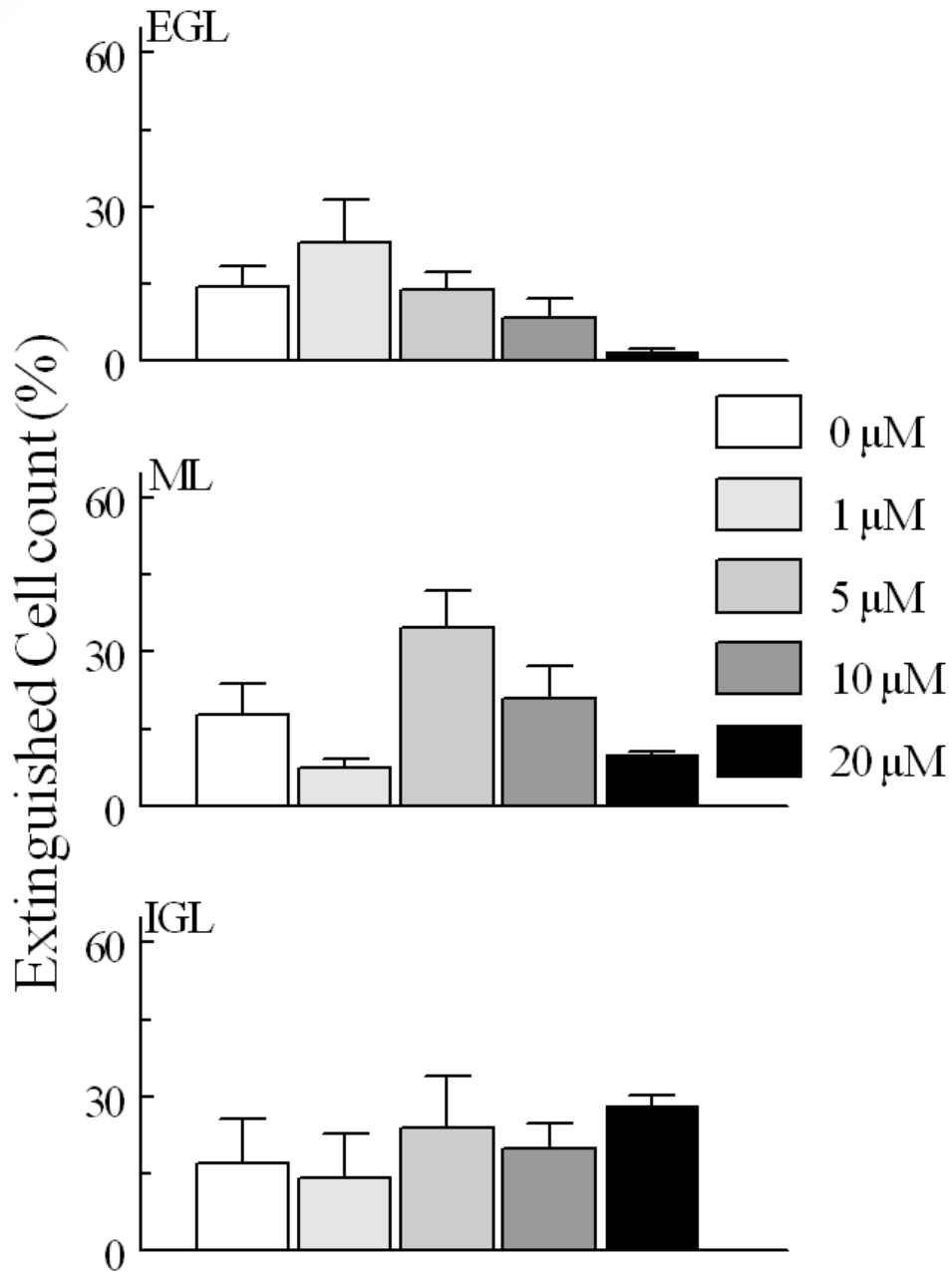


Figure 2.5. Fluorescent cell loss “extinguished” counts from slices during treatment with several concentrations of MeHg over 30 min. Cells extinguished when they lost significant fluo4 fluorescence between time points. Fluo4 fluorescence loss was occasionally associated with visible lysis of cells, so presumably all fluorescence loss is associated with cell death. Comparisons were made between each concentration of MeHg and untreated control, no comparisons were significantly different ($P>0.05$).

D) RESULTS

a. Visualization of layers and cytotoxicity

Fluo4 labeled mainly small (5-10 μm diameter), round somata matching the size and shape of CGCs (Figures 2.1, 2.2). Larger cells were not typically labeled visibly with fluo4, similar to what was seen previously (Yuan and Atchison, 2007). Some processes were visible and were used to delineate boundaries of the ML (Figure 2.1A). These processes include linear structures consistent with Bergmann glia and branching structures consistent with PC dendrites. Occasionally, cells visible at the boundary between the IGL and ML reacted fluorescently during treatment, usually around the addition of MeHg. These cells may be Bergmann glia or other interneurons present in this region that can be loaded with application of fluo4 (Hoogland et al., 2011). They were sufficiently different in shape and size so as not to be confused with CGCs. Fluo4-labeled CGCs were located in all three layers of the cerebellum. In the EGL, CGCs were concentrated at the pial surface and inner folds of lobes, but additional CGCs were located at the boundary between the EGL and ML. Most fluo4-labeled CGCs were situated in the IGL, evenly distributed throughout the slice thickness (Figure 2.1). Comparatively few fluo4-labeled CGCs were located in the ML.

EthD-1 did not stain any fluo4-labeled cells, indicating that only viable cells accumulated the Ca^{2+} indicator fluo4 (Figure 2.1A). In the absence of MeHg, EthD-1 intensity was 15.8% in the IGL, 13.8% in the ML and 16.1% in the EGL at the post-incubation time point matching the start of time course imaging, so ethidium staining was similar in all three layers (Figure 2.1B). This presumably reflects cell damage due to slicing and the incubation process. Slices imaged after one additional h of untreated incubation, corresponding to the end of a time course treatment, were not different in ethD-1 mean pixel intensity, indicating there is not a significant

change in slice viability within the time frame used. In slices incubated for 3 h in fluorophore plus 20 μM MeHg for 1 h, roughly corresponding to slices incubated in MeHg for a time course series, there was an increase in ethD-1 staining in the EGL when compared to untreated slices after 3 h of incubation, but it was not different from ethD-1 staining with one additional h of fluorophore incubation. Thus MeHg appears to exacerbate cell death induced by slicing in the EGL.

b. Acute MeHg slice treatment

Relative pixel fluo4 fluorescence intensity (F/F_0), a measure of changes to $[\text{Ca}^{2+}]_i$, was unaltered over 40 min in slices in the absence MeHg treatment. Changes in mean F/F_0 in cells did not exceed 5% between any two consecutive time points. Thus, none of the observed effects were due to photobleaching of fluo4 during confocal imaging (Figures 2.2, 2.3).

Effects of MeHg on $[\text{Ca}^{2+}]_i$ in CGCs were dependent upon concentration and differed by histological layer. In all treatments with MeHg, the greatest effect on fluorescence occurred in the EGL, and decreased in magnitude in the deeper layers (Figure 2.4). In slices treated with MeHg, all regions appeared to increase in fluorescence over the treatment period, including the processes distributed through the ML (Figure 2.2).

After a 40 min exposure to 20 μM MeHg, fluo4 F/F_0 was significantly increased in CGCs in all three layers, with a significantly larger effect in the EGL compared to deeper laminae (Figures 2.2, 2.3). This MeHg concentration increased mean F/F_0 up to 263% of baseline in the EGL, 186% in the ML and 173% in the IGL. At 10 μM MeHg, CGC F/F_0 increased to 192% baseline in the EGL, 142% in the ML and 164% in the IGL. In the EGL and ML, 20 μM MeHg increased F/F_0 significantly more than 10 μM MeHg. Perfusion with 1 or 5 μM MeHg produced no changes compared to untreated control in any layer over this interval of recording. Changes in

fluorescence were not linear in this time period. The largest changes in fluorescence occurred before the 20 min time point. These changes included a 43% increase in fluorescence relative to F_0 in the EGL between 10 and 15 min time points when treated with 20 μM MeHg.

Fluorescent changes rely heavily on the number of cells being tracked, and it appeared that MeHg treatment increased the number of cells that were visible during treatment. This was reflected in the density of cells that could be counted in layers. In untreated slices, 37 ± 2 CGCs per $(100 \mu\text{m})^2$ were visualized in the IGL over the full course of treatment, 5 ± 1 in the ML and 16 ± 2 in the EGL (Figure 2.4). Cells in the IGL were more densely distributed than in the other two histological layers. There was an increase in the density of CGCs visible in slices treated with 10 or 20 μM MeHg, most notably in the EGL, where visible CGCs increased to a density of up to 63 ± 7 per $(100 \mu\text{m})^2$ (Figure 2.4). Many of the cells tracked in these MeHg treatments were not readily visible at pretreatment time points, but could be tracked due to the registration of images. While increased cell count in MeHg treatments meant comparative difficulty tracking of CGCs in low and no-MeHg treatments with low baseline fluorescence, with the careful setup of the slices there were always enough visible CGCs for tracking in all slices and layers.

Some CGCs appeared to extinguish fluorescence during 50 min of imaging. These CGCs lost fluorescence at a rate that was an outlier to other cells in their layer and were thus excluded from fluorescence intensity measurements made up $17 \pm 7\%$ of total CGCs (Figure 2.5). These extinguished cells were occasionally accompanied by visible lysis or detachment from surrounding tissue, but evidence of these mechanisms is lost between imaging time points for most of the extinguished cells. Because there was no change in percent of dead cells in control treatments in the previous cytotoxicity assay, this percent of cell loss indicates a baseline loss of cells during experiments due to imaging and perfusion.

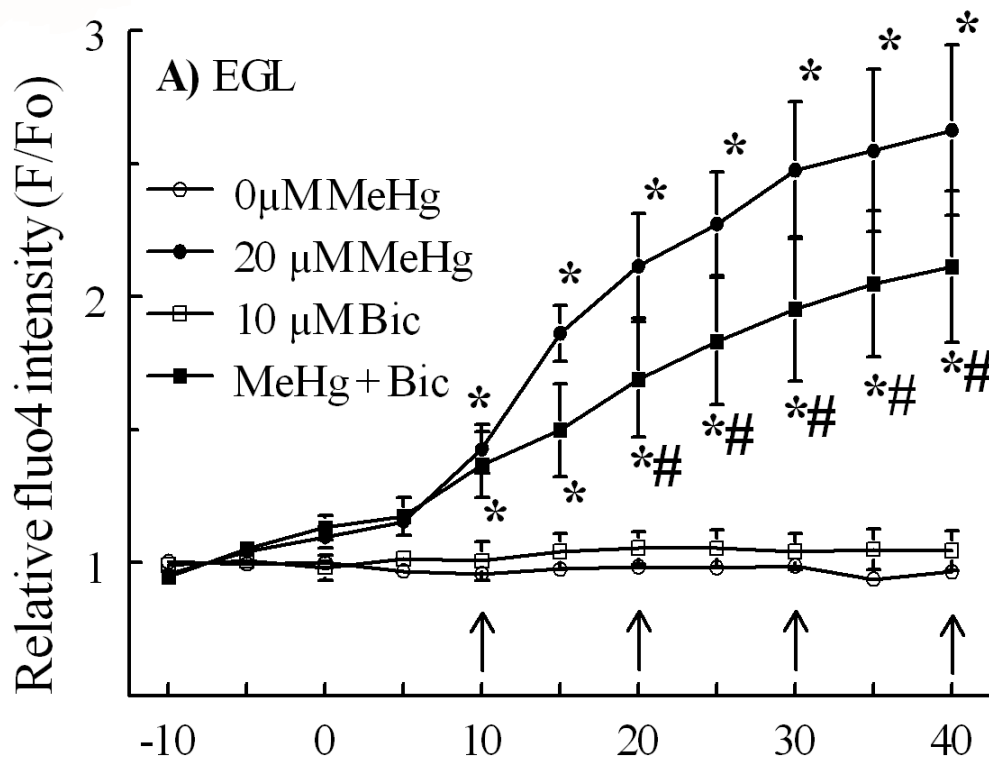
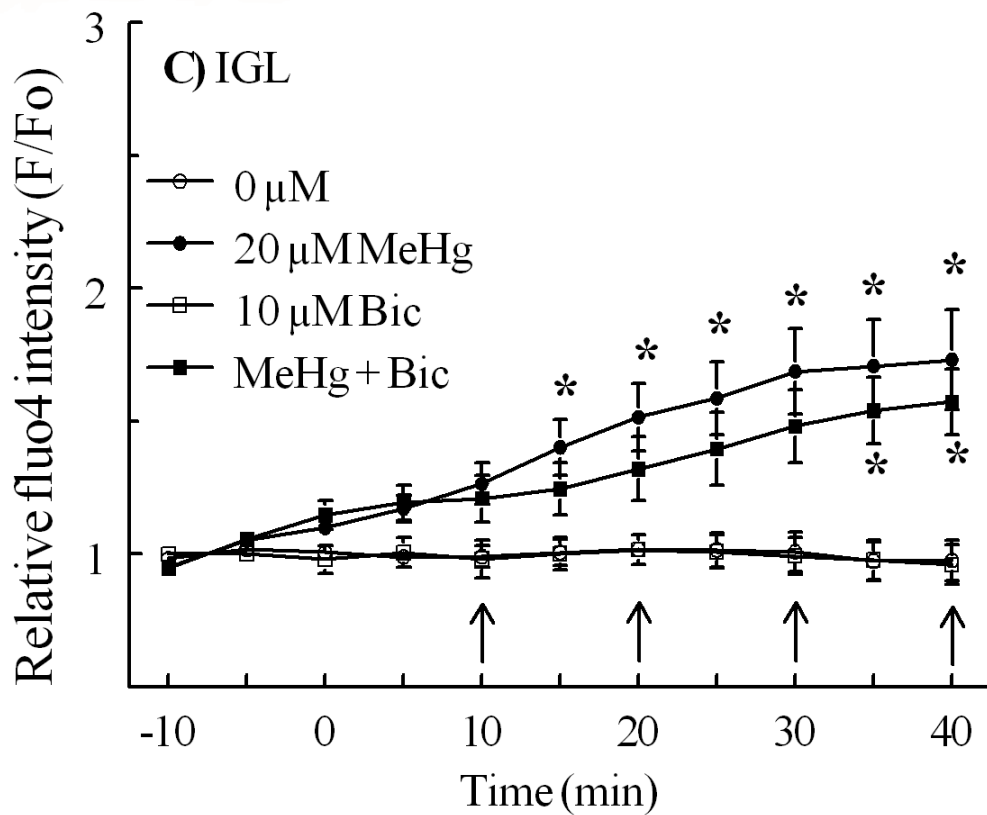
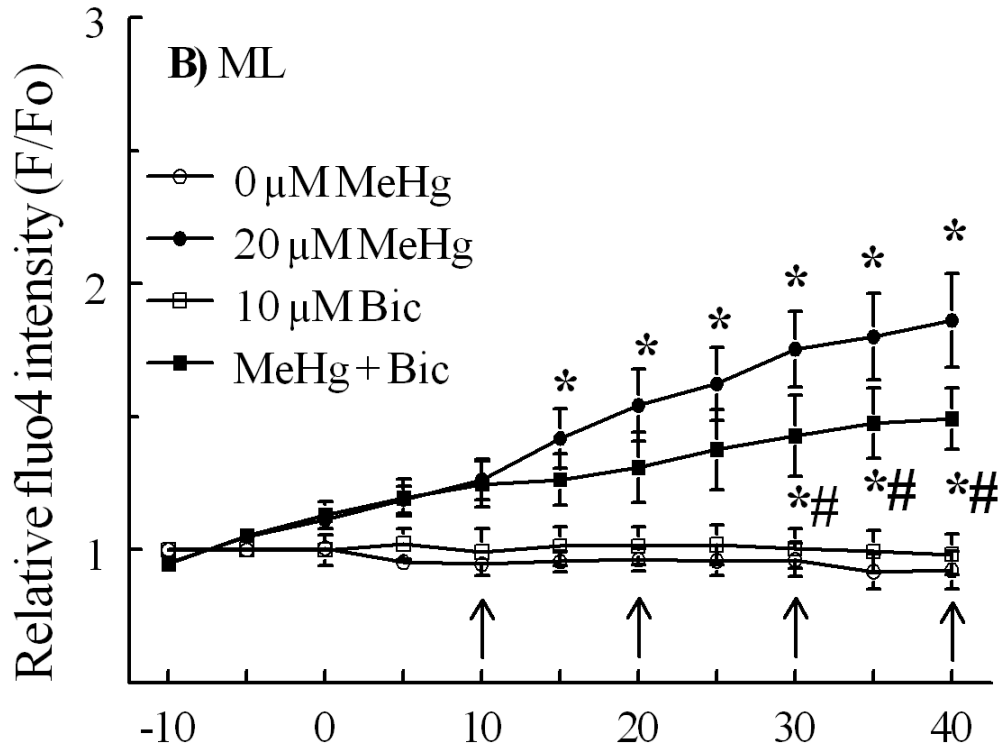


Figure 2.6. Effect of bicuculline and MeHg on relative fluo4 fluorescence intensity (F/F_0) of CGCs by histological layer. Untreated controls (○, $n=5$) and 20 μ M MeHg alone (●, $n=5$) are the same as in Figure 3. Bicuculline pulses (arrows, 10 μ M) with 20 μ M MeHg (■, $n=4$) were compared to bicuculline alone (◻, $n=3$) and MeHg alone. Significant difference are indicated from bicuculline control (*) and from MeHg alone (#) at that time point, $P<0.05$. Intensity values are expressed in arbitrary units (mean \pm SEM).

Figure 2.6 (cont'd)



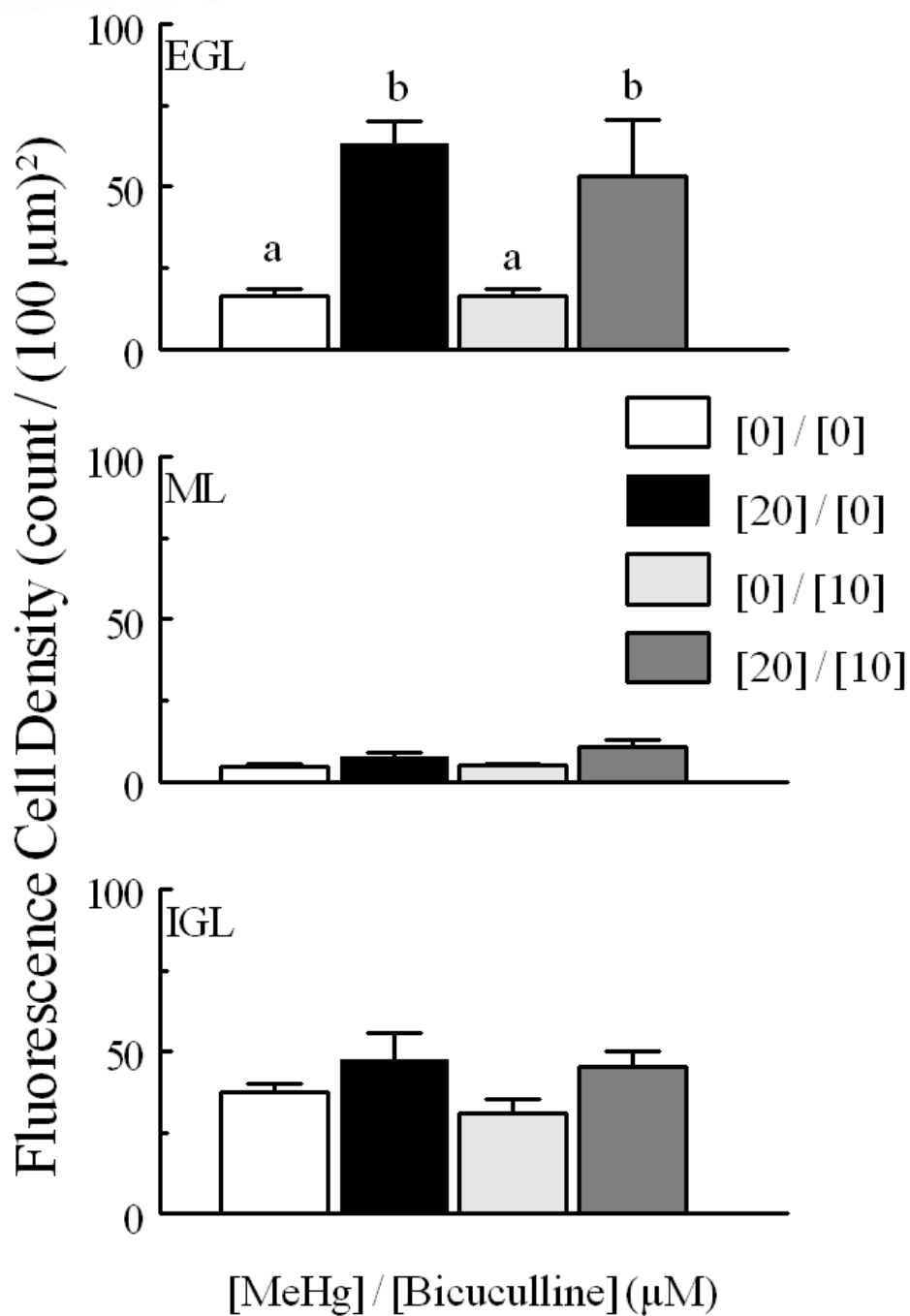


Figure 2.7. Cell density (per $(100 \mu\text{m})^2$) for CGCs monitored for fluo4 fluorescence intensity, in each layer (EGL, ML and IGL) and density for the total tissue, for tissue treated with two concentrations of MeHg (0 and 20 μM) and two concentrations of bicuculline (0 and 10 μM). CGCs were more densely distributed in the EGL and IGL layers than in the ML. Paired comparisons were made between each concentration of MeHg by layer. Significantly different pairs within each layer are indicated by different letters ($P < 0.05$). Values are mean \pm SEM, for the same n as described in Figure 2.6.

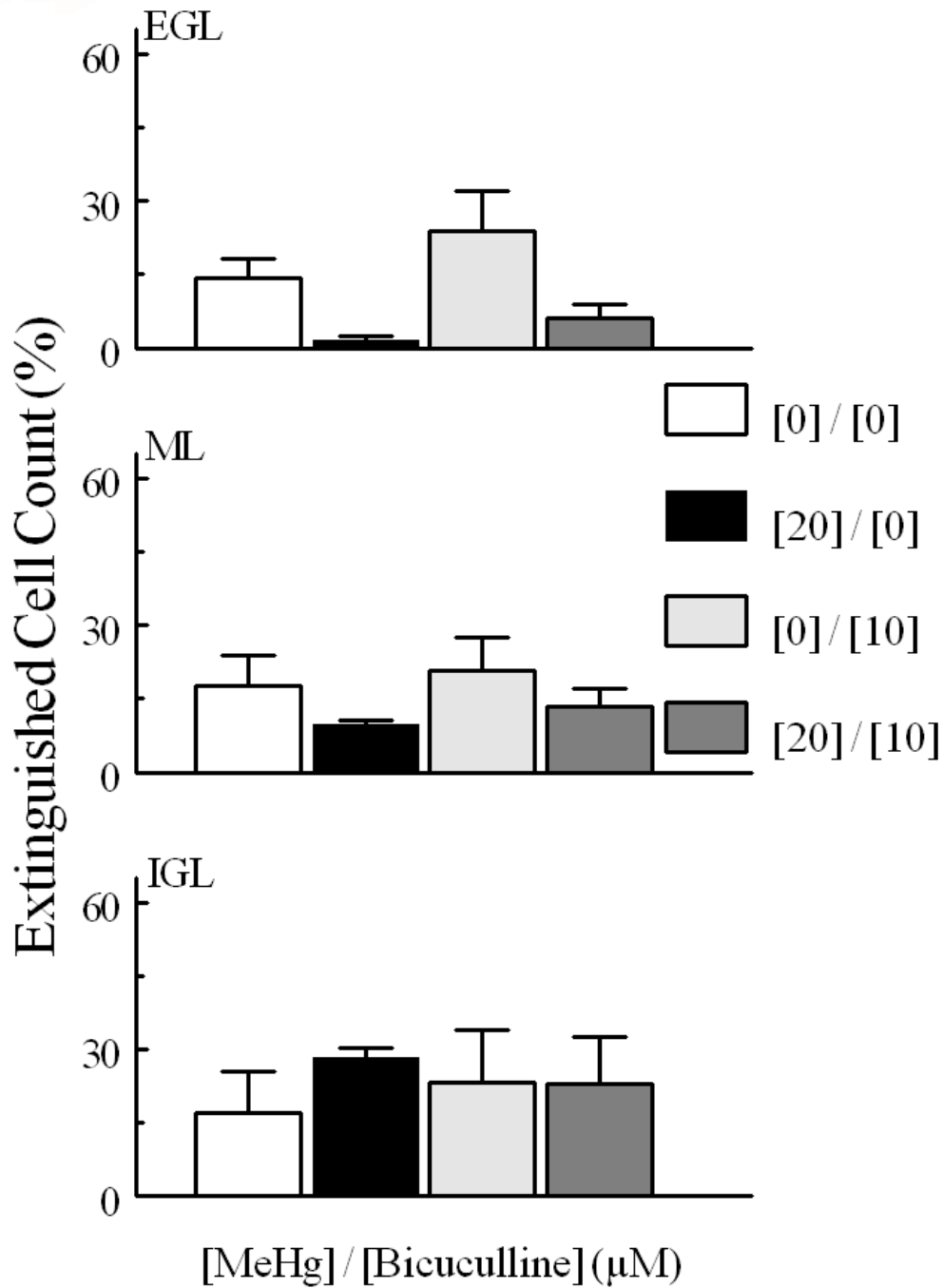


Figure 2.8. Percentage of “extinguished” cells in experiments comparing MeHg and bicuculline treatment. Comparisons were made between 20 and 0 μM MeHg treatments, between bicuculline alone and 0 μM MeHg, between bicuculline alone and bicuculline combined with 20 μM MeHg, and between bicuculline combined with MeHg and 20 μM alone. Significantly different pairs within each layer are indicated by different letters ($P < 0.05$). Values are mean \pm SEM, for the same n as described in Figure 2.6.

c. Muscimol and bicuculline treatment with MeHg

Both the GABA_AR agonist muscimol (100 μM) and the antagonist bicuculline (10 μM) partially decreased the increase in fluo4 fluorescence caused by MeHg on CGCs over time, with similar effects from both agents. Repeated pulses of muscimol or bicuculline alone did not significantly alter F/F₀ in any layer (Figures 2.6, 2.9). Muscimol pulses combined with MeHg treatment increased F/F₀ up to 208% of baseline in the EGL, 148% of baseline in the ML and 141% of baseline in the IGL, but this effect size was significantly less than that caused by MeHg treatment alone in each layer by the end of treatment (Figure 2.6). Bicuculline pulses combined with MeHg increased F/F₀ to 211% of baseline in the EGL, 149% of baseline in the ML, and 157% of baseline in the IGL; these were significantly less than MeHg alone in the EGL and ML (Figure 2.9). In the IGL, where the effect of MeHg alone was smaller than in the other layers, Bicuculline was not significantly effective in reducing the increase in F/F₀ caused MeHg, but delayed the onset of significant fluorescence increase from 15 to 35 min of MeHg treatment, similar to its effect in other layers.

As was seen with the MeHg treatments alone, MeHg treatments in combination with either muscimol or bicuculline also had larger fluorescent cell density, particularly in the EGL, but neither agent on its own increased these counts (Figures 2.7, 2.10). Bicuculline in combination with MeHg was indistinguishable from MeHg alone in terms of fluorescent cell density. Muscimol in combination with MeHg increased the density of trackable fluorescent cells in the EGL when compared to controls, but decreased the density when compared to MeHg alone. In addition the combination increased fluorescent cell density in the IGL enough to be different from untreated tissue, but not from either MeHg or muscimol treatment alone. Bicuculline did not change extinguished cell counts from controls (Figure 2.8). While muscimol

alone did not change extinguished cell counts, pulses of muscimol in combination with 20 μ M MeHg increased extinguished cell counts compared to both control and muscimol alone, but only in the ML and IGL layers (Figure 2.11).

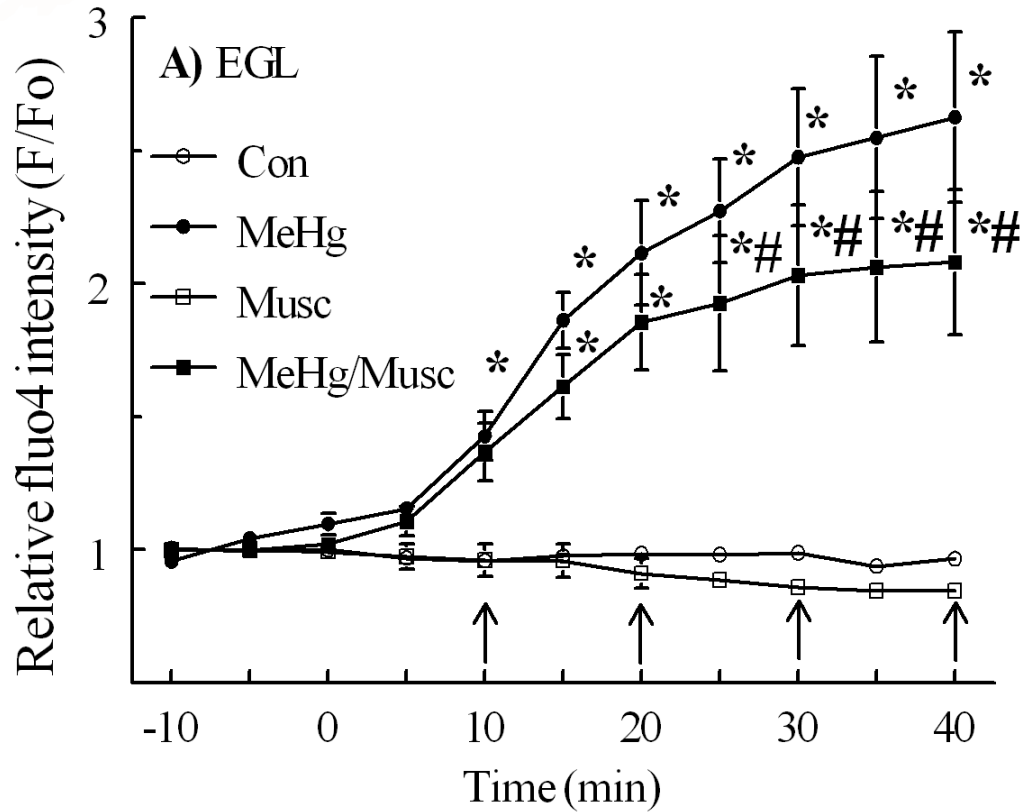
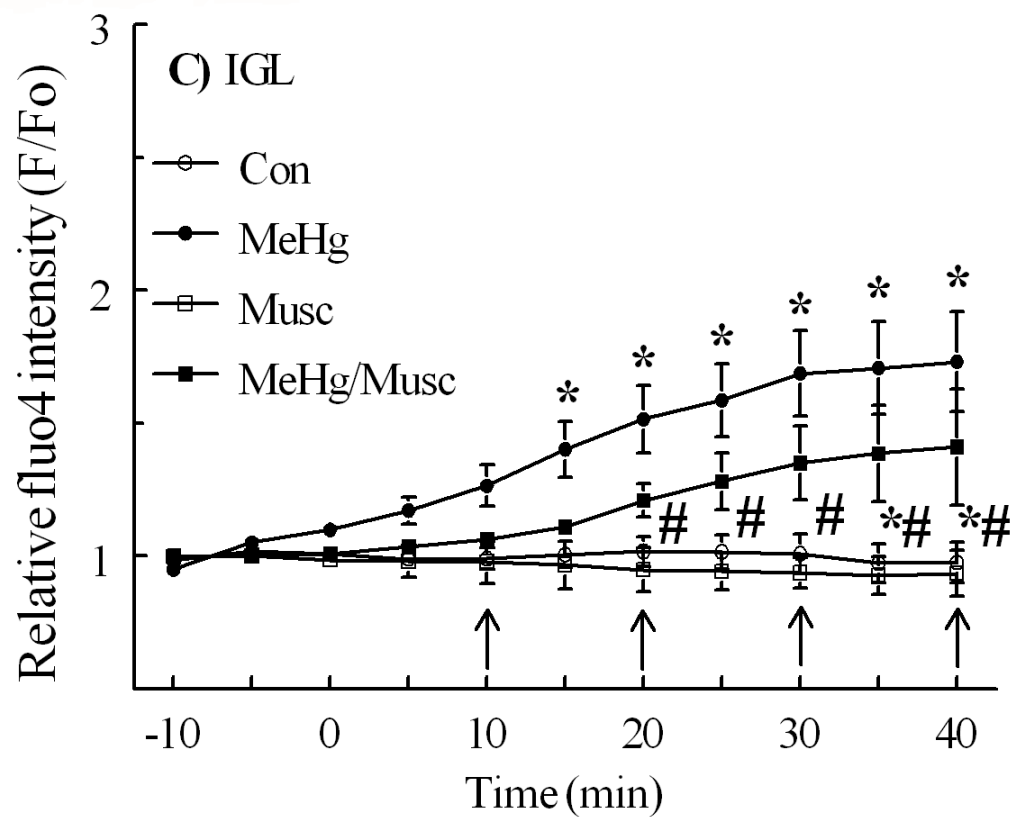
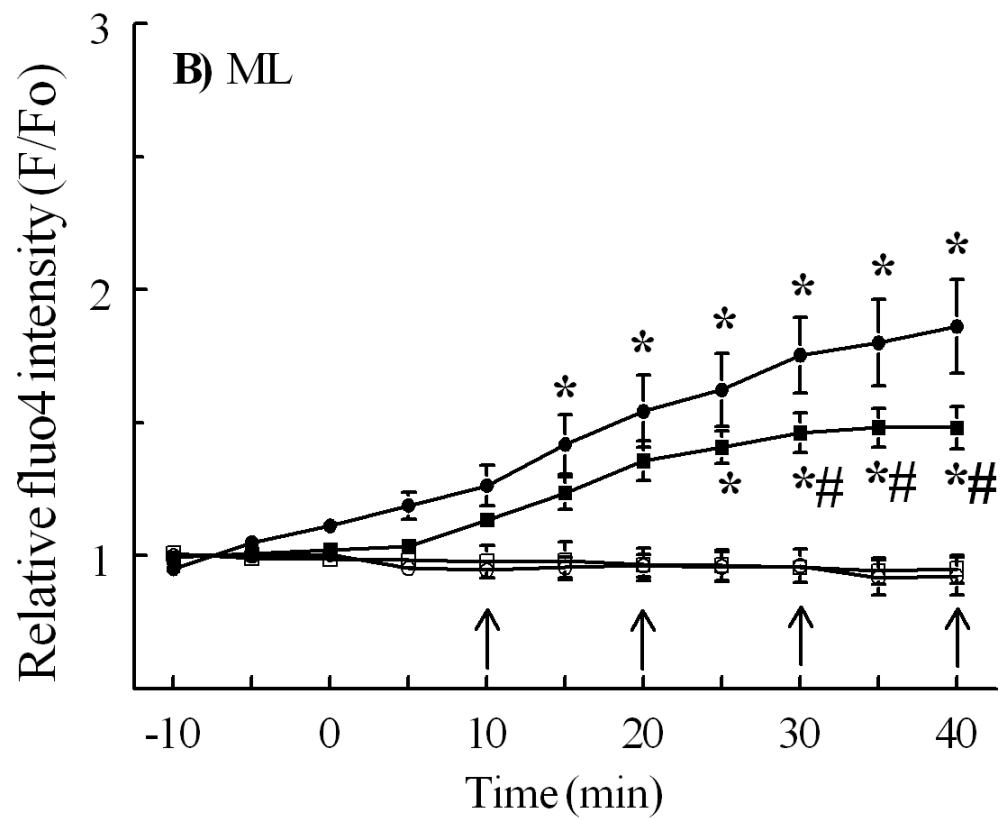


Figure 2.9. Effect of muscimol and MeHg on relative fluo4 fluorescence intensity (F/F_0) of CGCs by histological layer. Untreated controls (\circ , $n=5$) and $20 \mu\text{M}$ MeHg alone (\bullet , $n=5$) are the same as in Figure 3. Muscimol pulses (arrows, $100 \mu\text{M}$) with $20 \mu\text{M}$ MeHg (\blacksquare , $n=4$) were compared to muscimol alone (\square , $n=3$) and MeHg alone. Significant difference are indicated from muscimol control (*) and from MeHg alone (#) at that time point, $P<0.05$. Intensity values are expressed in arbitrary units.

Figure 2.9 (cont'd)



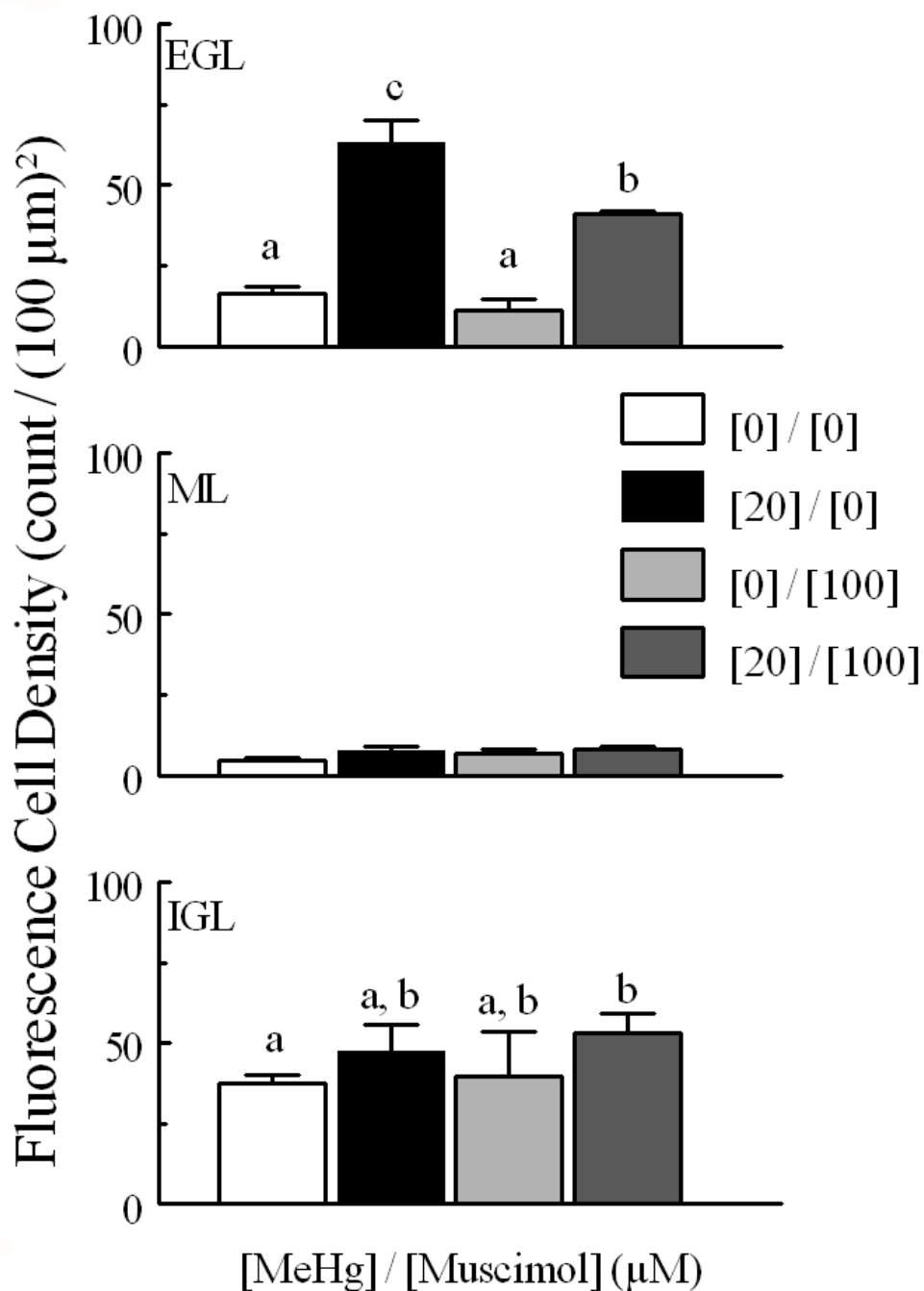


Figure 2.10. Cell density (per $(100 \mu\text{m})^2$) for CGCs monitored for fluo4 fluorescence intensity, in each layer (EGL, ML and IGL) and density for the total tissue, for tissue treated with two concentrations of MeHg (0 and 20 μM) and two concentrations of muscimol (0 and 100 μM). CGCs were more densely distributed in the EGL and IGL layers than in the ML. Paired comparisons were made between each concentration of MeHg by layer. Significantly different pairs within each layer are indicated by different letters ($P < 0.05$). Values are mean \pm SEM with n the same as described in Figure 2.9.

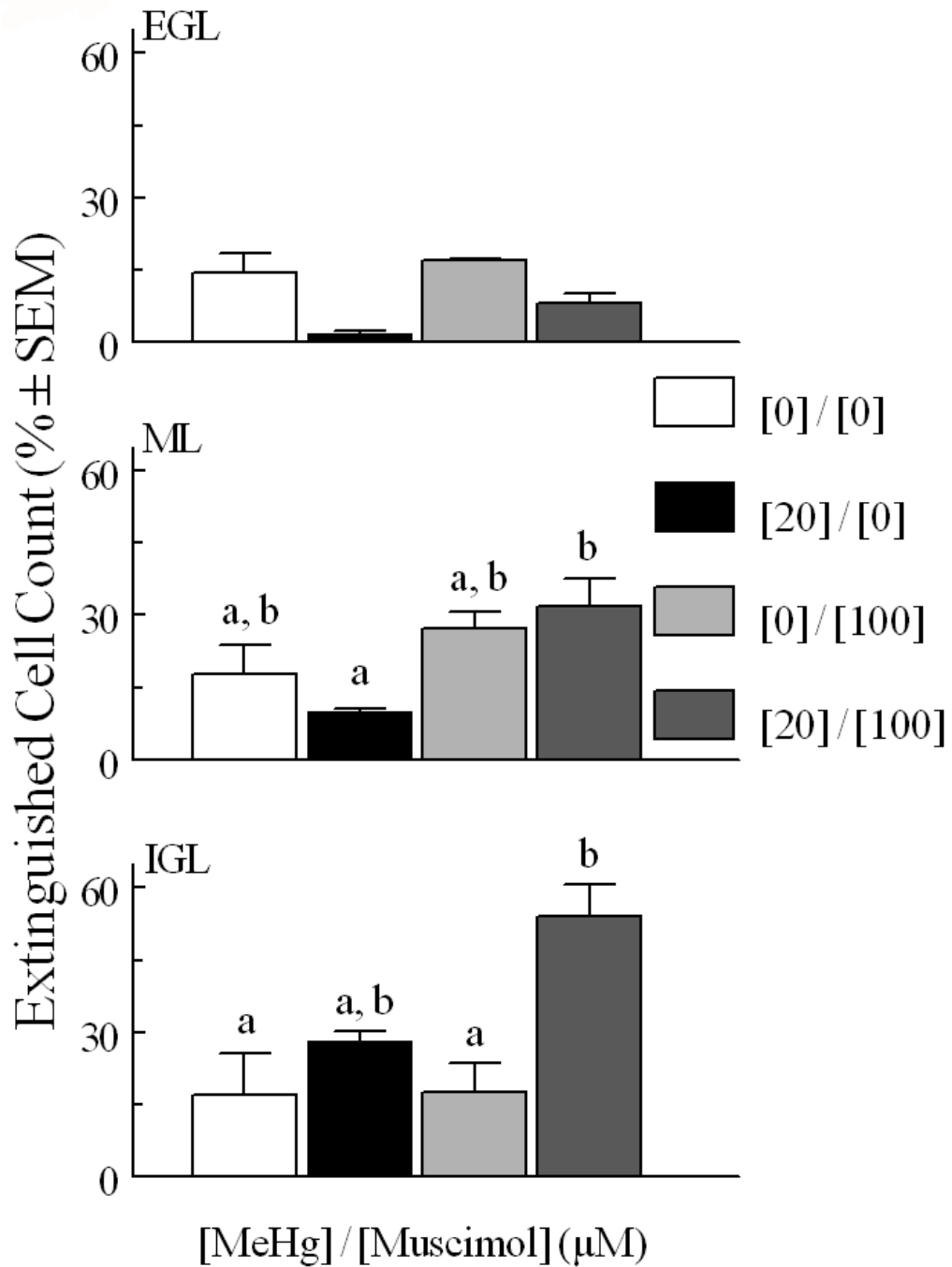


Figure 2.11. Percentage of “extinguished” cells in experiments comparing MeHg and muscimol treatment. Comparisons were made between 20 and 0 μM MeHg treatments, between muscimol alone and 0 μM MeHg, between muscimol alone and muscimol combined with 20 μM MeHg, and between muscimol combined with MeHg and 20 μM alone. Significantly different pairs within each layer are indicated by non-overlapping letters ($P < 0.05$). Values are mean \pm SEM with n the same as described in Figure 2.9.

E) DISCUSSION

The results show that 1) MeHg application triggers rapid and sustained increases in CGC $[Ca^{2+}]_i$; 2) these changes are variable based on the developmental context of the CGCs in slices, and 3) the disruption of $[Ca^{2+}]_i$ is regulated in part by activity of GABA_ARs. The concentrations of MeHg used did not decrease cell viability during the time of exposure compared to slicing alone, as indicated by the cytotoxicity assay, though the large increases in $[Ca^{2+}]_i$ could affect future viability. Slice culture allowed for conditions similar to cell culture and a basic concentration/response assessment for this tissue and treatment. Both 10 and 20 μ M MeHg caused intense increases in fluorescence while 5 and 1 μ M did not in the time course studied. Importantly, we showed differences in response between CGCs at different developmental stages of migration. The basic disruption of $[Ca^{2+}]_i$ shown here is consistent with previous measurements showing these increases are an initial mechanism of MeHg toxicity in CGCs (Marty and Atchison, 1998, Limke et al., 2003, Edwards et al., 2005). We further showed that modulators of GABA_ARs are capable of altering increases in $[Ca^{2+}]_i$ rapidly as well, effectively decreasing and delaying the MeHg-induced increases.

The effects of MeHg on CGCs during migration can clearly be attenuated by GABA_AR modulation, indicating that the receptor can be affected in any stage of development, and supporting a role for GABA_ARs in immediate mechanisms of MeHg toxicity. GABA_AR modulation by either agent does not abolish the effects of MeHg, indicating there are likely other mechanisms occurring simultaneously. This is not surprising as other effects, such as those on VGCCs and muscarinic receptors, are also likely to occur rapidly (Sirois and Atchison, 2000; Limke et al., 2004). Moreover, muscimol appears to be acting similarly to bicuculline over the longer time courses, in that both reduce the effect of MeHg on $[Ca^{2+}]_i$.

There are multiple possible mechanisms by which we could see similar actions of muscimol and bicuculline. If both are acting as competitive antagonists to MeHg, then both would appear to decrease the effect of MeHg, but the two agents act at slightly different sites and the muscimol site activates even if MeHg is bound (Fonfria et al., 2001). Those binding studies assumed an incubation with the agents first. In this study MeHg is applied first, so competition might be different. The reduction in effect by both an agonist and an antagonist could also be due to the nature of most agonists, in that the initial pulse increases conductance transiently, but is followed by lingering desensitization, so we only observe the effects of overall antagonism. Whatever the mechanism, there are a few subtle differences in this study between bicuculline and muscimol. First, the combination of bicuculline and MeHg was indistinguishable from MeHg alone in causing changes in visible density of fluorescent cells, whereas the combination with muscimol decreased this density in the EGL but increased it in the IGL. Second, the combination of MeHg and muscimol pulses increased cytotoxicity as measured by extinguished cells in this study where bicuculline did not. If muscimol transiently increases $[Ca^{2+}]_i$ that is not detectable by these imaging parameters, it is possible that it contributes to MeHg cytotoxicity despite lowering the observed overall $[Ca^{2+}]_i$ in most cells.

There are not big enough differences in effects between the different layers with muscimol or bicuculline treatments as compared to MeHg to suggest that one type of agent is more effective in one layer than another. As the surface expression of receptor subunits such as $\alpha 6$ changes over development, the agents either function similarly regardless of the expression profiles of the CGCs, or specific reactions are lost in the variability of the populations. It would be possible to treat slices with more specific GABA_AR modulators, such as those targeting the

$\alpha 6$ subunit, but the variability of the receptors and the population of CGCs would complicate further results.

A tightly regulated amount of free $[Ca^{2+}]_i$ is critical to driving migration and maturation of CGCs (Komuro and Rakic, 1992, Kumada and Komuro, 2004). As with all neurons, a sustained increase or inability to buffer $[Ca^{2+}]_i$ can lead to activation of cell death pathways, including caspase activation, cytoskeletal breakdown and opening of the mitochondrial transition pore (Fonfria et al., 2002, Limke and Atchison, 2002, Limke et al., 2003, Roda et al., 2008). Critical cycling of increased $[Ca^{2+}]_i$ in CGC migration is another potential susceptibility to MeHg. Continuous increases in $[Ca^{2+}]_i$ from the addition of caffeine or thimerosal, another mercury-based compound, disrupt migration of CGCs (Kumada and Komuro 2004, Komuro and Kumada 2005). Normal physiological changes in $[Ca^{2+}]_i$, as would be seen using electrophysiological current recordings are small, transient, and occur too rapidly to be captured by this confocal microscopy setup. Even a temporary increase in $[Ca^{2+}]_i$ could have profound effects on cell survival.

In these MeHg treatments, the $[Ca^{2+}]_i$ levels in CGCs increased dramatically, but $[Ca^{2+}]_i$ in PCs and other cells present in the slices did not label to any significant degree. This difference in cell body labeling reflects cell susceptibility and underscores the importance of $[Ca^{2+}]_i$ in studying MeHg toxicity. Since the largest $[Ca^{2+}]_i$ changes in CGCs for many treatments were at the end of recording, the concentration may continue to rise and may eventually fall before cell death, as has been seen in previous studies (Yukun and Atchison 2007). This may occur even for those levels of MeHg which did not reach significance in these experiments. Extending the treatment and monitoring might allow such increases to be seen, but could be complicated by the slow export of fluo4 or the continued extinguishing of fluorescence by dead or dying cells.

Clinical manifestations of MeHg poisoning and the susceptibility of human fetuses point strongly to the migration of CGCs in the cerebellum as being a particularly sensitive target for MeHg toxicity. We categorized CGCs into those that were still dividing, those that were migrating and those that had reached their destination based on their location within the cerebellum. In MeHg treatments, fluorescence changes were distinct in the different layers; the more mature CGCs in the ML and IGL reacted less to MeHg than did migrating CGCs as indicated by changes in their F/F_0 . Regardless of the mechanisms, this indicates that immature CGCs experience a larger sustained increase in $[Ca^{2+}]_i$ as an early exposure event than more mature cells.

Even if early free Ca^{2+} is sequestered, lasting disruption of cell signaling is possible. Precise signaling is particularly important for the migration of CGCs; fewer CGCs reaching their target layer and maturing means fewer circuits made. The CGC and PC circuit is the major internal cerebellar neuronal circuit; since many CGCs normally synapse on PCs, their signal can be integrated over a population of the cells. If the population of CGCs is reduced, there is both a larger load placed on any individual CGC as well as poorer integration of signal. This can have lasting consequences long after the initial exposure, including motor coordination and motor memory deficits related to the overall function of the cerebellum. Since MeHg is persistent in brain tissue, if it is present in the brain during development it may continue to be toxic beyond the most susceptible developmental period.

While some exploration of the mechanisms of acute MeHg toxicity focuses on various VGCCs or reactive oxygen species production, the results presented here indicate additional acute effects via $GABA_A$ Rs on $[Ca^{2+}]_i$. GABA is the major inhibitory neurotransmitter in the central nervous system, and has several roles in cerebellar circuitry, so evidence of the

involvement of GABA_ARs in the toxicity of MeHg must be taken into account in the study of the toxicant. The results presented here support initial electrophysiological findings (Yuan and Atchison, 2003, 2007), binding studies (Corda, et al., 1981, Fonfría, et al., 2001), and other toxicological studies (Basu, et al., 2010) in indicating a role here for GABA_ARs and might explain known cellular and developmental susceptibilities to MeHg. Though this work focuses on only acute effects over less than 1 h of MeHg treatment, GABA_ARs respond to stressors with changes in surface expression, indicating that acute effects could trigger longer-term effects as well. Whether the effects of MeHg on GABA_ARs are acute or chronic, the sensitive migration and maturation of CGCs is affected, contributing to the susceptibility of these cells at a crucial point in development.

CHAPTER THREE

**ACUTE METHYLMERCURY TREATMENT INCREASES FLUO4 FLUORESCENCE
IN NEONATAL MOUSE CEREBELLAR SLICES AND IS DEPENDENT ON GABA_AR
 α 6 SUBUNIT EXPRESSION, MIGRATIONAL STAGE AND GABA_AR MODULATION**

A) ABSTRACT

Developing CGC migration is a primary target of MeHg neurotoxicity.. GABA_AR subunit composition may contribute to cell-specific and developmental susceptibilities to MeHg. We examined acute effects of MeHg on cerebellar slices from mice lacking the $\alpha 6$ GABA_AR subunit. This subunit exists exclusively in mature CGCs and regulates their tonic inhibition. It coexists in CGCs with the abundant $\alpha 1$ subunit, which is not involved in tonic inhibition, nor expressed only in CGCs. Changes in fluo4 fluorescence induced by MeHg were compared in acutely prepared slices from PND 8-12 knockout (-/-) and wild type (+/+) mice using fluorescent confocal microscopy. Migrating CGCs were imaged in developmental layers (EGL and ML), along with post-migratory CGCs in the IGL. MeHg (20 μ M) increased CGC fluorescence over time in the EGL and ML. In (-/-) cerebellar slices, MeHg increased fluorescence significantly at 15 min and continued up to 201% over baseline in the EGL at 55 min, the end of treatment. Significant fluorescent changes were delayed and decreased in the IGL, reaching significance at 25 min and continuing up to 145% over baseline. Though MeHg treatment appeared to increase fluorescence in (+/+) slices, the effect was only significant in the EGL within 55 min. Pulses of the GABA_AR agonist muscimol (100 μ M) to tissue perfused with MeHg reduced fluorescence changes by 75% compared to MeHg alone in the IGL of (-/-) mice and delayed the onset of significant increases. The GABA_AR antagonist bicuculline (10 μ M) also reduced and delayed the effect of MeHg. While the $\alpha 6$ subunit is not expressed fully in CGCs until maturation, there still is a pronounced effect of MeHg on $[Ca^{2+}]_i$ in immature CGCs of (-/-) mice. Thus $\alpha 6$ expression may establish inhibition in developing CGCs, perhaps by controlling

neurotransmission or expression of another subunit which contributes to regulation of $[Ca^{2+}]_i$ in migrating CGCs.

B) INTRODUCTION

MeHg is a neurotoxicant that targets the cerebellum, and more specifically the CGCs in the cerebellar cortex. In Chapter Two, we demonstrated that MeHg disruption of $[Ca^{2+}]_i$ was dependent on CGC development, and that alterations of GABA_ARs by the agonist muscimol and antagonist bicuculline reduced this disruption in $[Ca^{2+}]_i$. Further characterization was needed, particularly to model gene-environment interactions in the toxicology of MeHg.

There are several potentially important differences in gene expression that could contribute to the susceptibility of CGCs to MeHg. Many of these differences relate to $[Ca^{2+}]_i$ signaling and have been determined by comparison to the relatively resistant PCs in the cerebellum onto which CGCs synapse. Differences in expression of intracellular Ca^{2+} binding proteins such as calretinin, calbindin and parvalbumin lead to differences in function and excitability (Gall, et al., 2003, Bearzatto, et al., 2006, Bornschein, et al., 2013). Similarly, CGCs and PCs have differences in Ca^{2+} channels and receptors, such as VGCCs, AMPA receptors and others (Chung, et al., 2000, Huang, et al., 2007, Shevtsova and Leitch, 2012).

One receptor expression difference is perhaps most notable of all and that is the difference in GABA_ARs. Mature CGCs express mostly GABA_ARs containing $\alpha 6$ subunits, whereas PCs express $\alpha 1$ exclusively (Nusser, et al., 1995). The two receptors are functionally distinct, with $\alpha 1$ -containing receptors functioning as typical inhibitory synaptic receptors while $\alpha 6$ -containing receptors reside extrasynaptically and respond to ambient GABA. GABA_AR gene interactions are particularly important in development, during which CGCs go through several stages of expression before maturation. GABA_AR subunit expression goes through several stages

as well during development in CGCs. The $\alpha 6$ subunit is not expressed until maturation in CGCs, and is dependent on the change in chloride gradient (Ortinski, et al., 2004, Takayama and Inoue, 2004, Bortone and Polleux, 2009). Interestingly, differences in subunit expression appear to lead to differences in response to MeHg, both functionally and in cell viability (Yuan and Atchison, 2003, 2007; Herden, et al., 2008) These individual differences indicate larger functional differences based on a single variable in gene expression, so it makes GABA_ARs a strong candidate to explore through gene knockout.

The GABA_AR $\alpha 6$ knockout (-/-) mouse was developed alongside other subunit knockouts as a potential model for epilepsy, but was found to not have a distinct epilepsy phenotype; in fact it had no apparent phenotype apart from alterations to pharmacological stimuli associated with the $\alpha 6$ subunit (Homanics, et al., 1997, Makela, et al., 1997, Nusser, et al., 1999). With no defects in normal function, it appears that GABA_AR activity is compensated, most likely by a change in potassium current (Brickley, et al., 2001). This potassium “leak” current is able to maintain CGCs in a less excited state, similar to the hyperpolarized state of normal CGCs, but is relatively depolarized compared to normal CGCs, and may require more ATP production to maintain. Motor coordination in these mice can be disrupted treatment with diazepam, which indicates an important role for remaining $\alpha 1$ and γ subunits, even if there is no indication that their expression is changed (Korpi, et al., 1999). Despite the lack of an epileptic or otherwise dysfunctional phenotype, this knockout could provide answers as to whether GABA_AR $\alpha 6$ expression contributes to MeHg toxicity or if it is protective.

The slice model for cerebellum has proven valuable in determining the $[Ca^{2+}]_i$ changes induced by MeHg application in developing rat, and has already indicated some involvement of

GABA_ARs, so it is the approach used here with developing mice. GABA_AR $\alpha 6$ (-/-) and (+/+) mice are used from the same colony to determine the effect of genotype, and the GABA_AR agonist muscimol and antagonist bicuculline are used once again to determine the action of GABA_AR signaling within the context of MeHg treatment. These experiments will determine effects of GABA_AR expression and signaling to the toxicity of MeHg in developing mice, and in combination with other sections of this dissertation, will contribute to an overall characterization of GABA_ARs, $[Ca^{2+}]_i$, and MeHg in multiple susceptible developmental stages.

C) MATERIALS AND METHODS

a. Chemicals and solutions

Materials and solutions for slicing of cerebella and Ca^{2+} imaging with fluo4 are described in Chapter Two. Unless otherwise stated, methods for isolating and imaging cells in slice were identical for mouse brains as for those used for rat brains.

b. Animal care and genotyping of transgenic animals

Animal care was performed according to NIH guidelines for experimental use and was approved in advance by the Michigan State University Institutional Animal Care and Use Committee. $\text{GABA}_A\text{R } \alpha 6$ (-/-) mice (B6;129-*Gabra6*^{tm1Geh}/J, strain #002710) and the background strain (+/+) (B6:129/J) were originally obtained from Jackson Laboratories (Bar Harbor, ME). Mice were maintained in a breeding colony at MSU, and fed, housed and enriched normally according to MSU IACUC guidelines. Breeding pairs were co-housed serially over multiple litters when needed. Multiple breeding strategies were tried at various times depending on needed genotypes, including (-/-) x (-/-) for producing all (-/-) litters, (+/-) x (+/-) for producing maximally mixed litters, and (-/-) x (+/-) or (-/-) x (+/+) for producing needed breeders for successive generations. Every three generations, male (-/-) mice were back-crossed with (+/+) background strain females obtained directly from Jackson Laboratories.

Genotyping was performed according to the developer of the strain (Homanics, et al., 1997), with some changes to accommodate the use of neonates. Genotyping was performed between PND5 and PND21, depending on need for experiments, as mouse pups of this age have

less innervation of the tail. Pups were temporarily, individually removed from the box and sterile 2% (w/v) lidocaine hydrochloride jelly (Akorn, Inc., Lake Forest, IL) was applied to the tip of the tail to anesthetize the area. Tails were disinfected with a 1:100 dilution of Nolvasan (Zoetis, Florham Park, NJ). Less than 2 mm of the end of the tail was removed and immediately placed in 200 μ l of lysis buffer solution containing 10 mM Tris, 50 mM NaCl, 25 mM EDTA, 0.5% SDS and 5 μ M Proteinase K (Sigma-Aldrich, Milwaukee, WI) in 1 ml tubes, labeled and kept on ice while all tissue was collected. Mouse pups younger than PND18 were coded using colored non-toxic permanent markers on skin of the stomach, feet and base of tail, and color was reapplied as needed until PND18. Pups PND18 or older were coded by ear punch. Immediately after tissue collection and coding, the remaining tail was dipped in styptic powder (Kwik-Stop, ARC Laboratories, Atlanta, GA) to stop bleeding, and the pup was returned to the litter.

Genotyping tissue was kept in lysis buffer overnight in a 50°C dry heating block. Dissolved tissue was precipitated in a solution of 3 M potassium acetate and 2 M acetic acid, vortexed and centrifuged (16 g, 10 min) to form a pellet and supernatant containing DNA. Supernatant was transferred to matching labeled tubes containing 200 μ l isopropyl alcohol (F.T. Baker) and mixed once by inversion. These tubes were centrifuged for 15 min (16 g) to form another pellet containing the DNA. The supernatant was removed carefully and replaced with a wash of -20°C 100% ethanol. These tubes were centrifuged for 25 min (16 g). Supernatant wash was removed and tubes were allowed to dry. Pellets were dissolved in the tubes using 50 μ l of diethylpyrocarbonate (DEPC)-treated water to eliminate RNase activity (Life Technologies).

Isolated DNA was amplified by polymerase chain reaction (PCR). PCR reagents were mixed according to manufacturers specifications, such as with RedTaq polymerase (Sigma-

Aldrich), including concentrations of primers, deoxyribonucleotide triphosphate (dNTP) monomers and aliquots of DNA and PCR buffer. Forward and reverse primers for the transgenic neomycin insert and GABA_AR α6 subunit gene were obtained according to Jackson lab protocols (neomycin generic primers, 5'-CTTGGGTGGAGAGGCTATTC-3' and 5'-AGGTGAGATGACAGGAGATC-3', GABA_AR α6 subunit primers, 5'-GACCACCTTAAGCATCAG-3' and 5'-TTTGACTTTGCCACAGGG-3') and diluted to 1/50 of the original concentration before mixing. Additional MgCl₂ was added to the PCR mixture to bring it to a final concentration of 25 mM, even though many PCR buffers contained a lower concentration already. PCR was run on a GeneAmpPCR 9700 96-well PCR machine (Perkin-Elmer, Waltham, MA) using settings according to the PCR buffer manufacturers specifications for denaturation, amplification, and annealing steps. An initial 1 min denaturation step at 94°C was added if not included.

Amplified bands of neomycin and GABA_AR α6 subunit were resolved by gel electrophoresis. PCR product was dyed with <1 μl xylene cyanol dye and placed in wells of a 1.5% agarose Tris-acetic acid-EDTA (TAE) gel. Neomycin, indicating presence of at least one allele containing the neomycin cassette interrupting GABA_AR α6, resolved at 280 bp, while uninterrupted GABA_AR α6 resolved at 240 bp. Heterozygote (+/-) appeared as two bands. Genotypes for initial experiments, those comparing (-/-) and (+/+) littermates for reaction to MeHg treatment in slices, were blinded from ABB by others in the laboratory, by labeling the final results as (+/-), “group 1” or “group 2”, with no indication as to whether group 1 or 2 was (-/-). The initial coding of groups was maintained through the blinding period. (+/-) animals were not coded as they were not used in initial experiments, but were a natural result of (+/-) crosses.

Group coding results were decoded after initial graphical results were obtained, and were not performed on further experiments.

c. Acute slice preparation

Slices were prepared as in Chapter Two, with the following changes. Male and female mouse pups (M= 12, F= 14, PND 8-12) were euthanized by rapid decapitation to provide brains. After slicing in ice cold slicing solution, slices were incubated in ACSF warmed to 37°C for the first 30 min, followed by 30 min at room temperature (23-25°C) before fluorophore incubation and for the remainder of incubations. As both rat and mouse cerebellum appeared to have sufficient rates of uptake of fluorophores for imaging, concentrations used and periods of incubation were identical. If possible based on genotyping, matching treatments were performed on one (-/-) and one (+/+) mouse from the same litter within 24 h.

d. Confocal microscopy

Slice imaging was performed as described in Chapter Two, with some changes for efficiency. As cells in mouse cerebellum looked identical to cells from rat cerebellum and had similar fluorescence, laser power and acquisition was kept the same. Fluo4 fluorescence was always collected at 500-535 nm, the setting used previously for fluo4/ethD-1 experiments in rats. Between-image depth was set to exactly 3 µm for all image stacks to maintain resolution in the Z-dimension. Imaging timing was automated and extended, so that two pretreatment imaging scans were taken and two sets of 5 images collected automatically during treatment at 5 min intervals unless interrupted by obvious X, Y or Z shifts in the slice. This allowed for a longer treatment time, extending to 50 min of treatment compared to 40 min shown in Chapter Two.

Only four treatments of the type used in Chapter Two were continued in these experiments. Two to three of these treatments were applied, in random order on the same day, to slices from the same brain, so maintain closer consistency between slices. Continuous 20 μM MeHg and no MeHg controls were compared in both (-/-) and (+/+) cerebellar slices. Additionally, 100 μM muscimol pulses and 10 μM bicuculline pulses were also studied in combination with 20 μM MeHg, and compared to continuous MeHg alone, in both (-/-) and (+/+) slices. Because of the extended treatment time, one additional muscimol or bicuculline pulse was used, as compared to rat treatments, at the 50 min time point.

Image analysis and statistics

All image processing was performed in ImageJ (v 1.45s, imagej.nih.gov/ij/). A scale factor of 300 μm / 512 pixels was applied to all images imported from Leica Confocal Software. CGCs and histological layers were otherwise identified exactly as in Leica software, as mouse CGCs and layers were highly similar to those in rat cerebella. Image stacks, imported as separate image series, were concatenated to form a single image series. Backgrounds were subtracted and image stacks summed and registered to maintain cell position as described in Chapter Two. Histological layers were drawn with the ImageJ polygon brush tool and cells were highlighted using the elliptical brush set as a 10 μm circle. Multiple regions of interest, either the histological layers or multiple cells, were tracked using the ROI manager tool. Cells with extinguished fluorescence were tallied and excluded as in Chapter Two.

Overall statistical comparisons were performed in SPSS statistics (v 20.0.0, IBM, Armonk, NY) while paired comparisons were made in GraphPad Prism (v 4.03, La Jolla, CA).

For extinguished cell counts, within-subject t-tests were performed in Prism between MeHg-treated and untreated slices, and separated by layer and genotype. For time courses, the factors considered for ANOVA analysis were genotype ((-/-) versus (+/+)), treatment, with two treatments in each analysis (control/MeHg, MeHg/muscimol combination or MeHg/bicuculline combination), layers (EGL, ML and IGL), and time (13 time points). Because of the paired nature of the experiments, the treatment measure was considered a within subjects repeated measure, as was time. Paired comparisons were made between MeHg-treated and untreated slices from the same animal, as well as between muscimol or bicuculline combination treatments and their MeHg-only counterparts. Paired comparisons were also made between genotypes within each layer and treatment. Each genotype*treatment*layer mean was compared to pretreatment time points by repeated measures ANOVA to determine change over time. All comparisons were considered significant for $P < 0.05$, with Bonferroni corrections as applied in Prism for multiple comparisons.

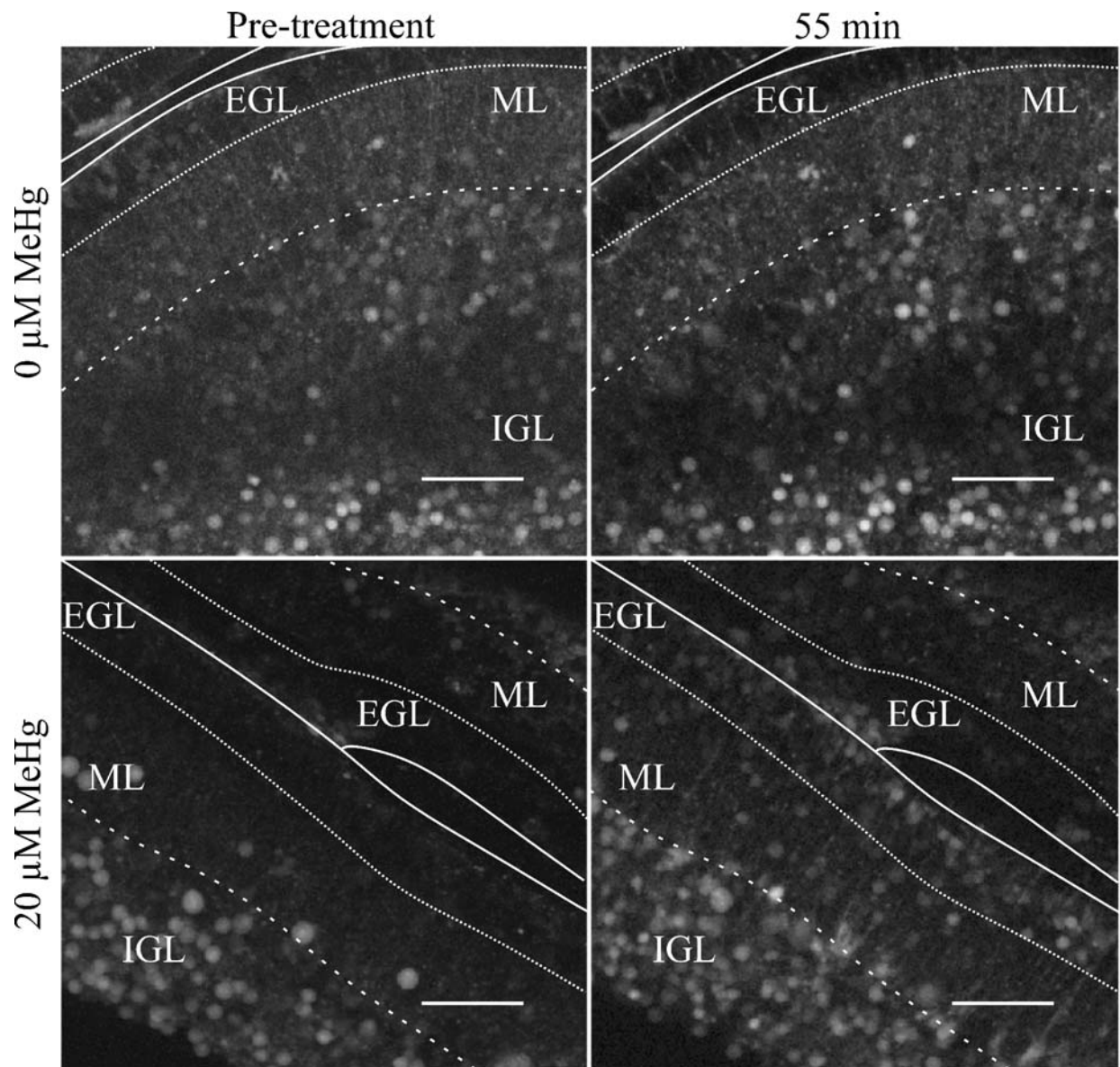


Figure 3.1. Representative images of frames of interest and labeled layers from (-/-) mouse cerebellar slices. Images are from two slices; both slices are from the same (-/-) mouse. Detailed description of assigning boundaries is discussed in Chapter Two materials and methods. Layers and boundaries from surface of cerebellum (solid line) include the external granule layer (EGL), the EGL-ML interface (dotted line), the molecular layer (ML), the Purkinje layer (dashed line) and the internal granule layer (IGL). The left images are prior to administration of MeHg, and right images are the last image taken from respective series. The top slice was treated with only ACSF (0 μ M MeHg, untreated control) for 55 min, the bottom slice was treated to 20 μ M MeHg in ACSF for 55 min.

Figure 3.1 (cont'd). Untreated control had little change to fluorescence, but 20 μM treatment increased fluorescence ~ 2 -fold in the EGL in this example, with smaller increases in the ML and IGL. Scale bar is equal to 50 μm . Images are summary projections of ~ 30 scans through the depth of the slice, intensity values are adjusted to the value histogram of the first image. Images are cropped to remove blank space around edges from image registration.

D) RESULTS

a. Visualization of layers

As with the acutely prepared rat cerebellar slices collected in Chapter Two, in mouse cerebellar slices fluo4 labeled mostly round somata matching the characteristics of CGCs (Figure 3.1). Fluo4-fluorescent soma were from 5-10 μm in diameter, and the remainder of the fluorescent material in the images was diffuse staining in an area matching the description of the ML, based on distance from the pial surface. PCs were not frequently visibly fluorescent lining the boundary between fluorescent CGCs in the IGL and the diffuse ML staining, but this lack of PC fluorescence has been noted before in Chapter Two and in previous experiments (Yuan and Atchison, 2007).

Many of the characteristics of neonatal mouse cerebellar slices appeared similar to rat slices. The EGL was 10 to 40 μm thick and contained a high density of CGC precursors at the pial surface and lining the boundary with the ML, while the ML was 60-100 μm thick and contained relatively few CGCs. CGCs packed the IGL densely in all dimensions. At the slice thickness used, very few fluorescent CGCs overlapped within the same space in projections along the Z axis. In all treatments, the visible area contained 38 ± 4 CGCs in IGL, 11 ± 1 in the ML, and 14 ± 2 in the EGL, fluorescent CGC counts did not differ between MeHg treatment and untreated controls ($P > 0.05$). Also, fluorescent cell counts did not differ between (+/+) and (-/-) genotypes.

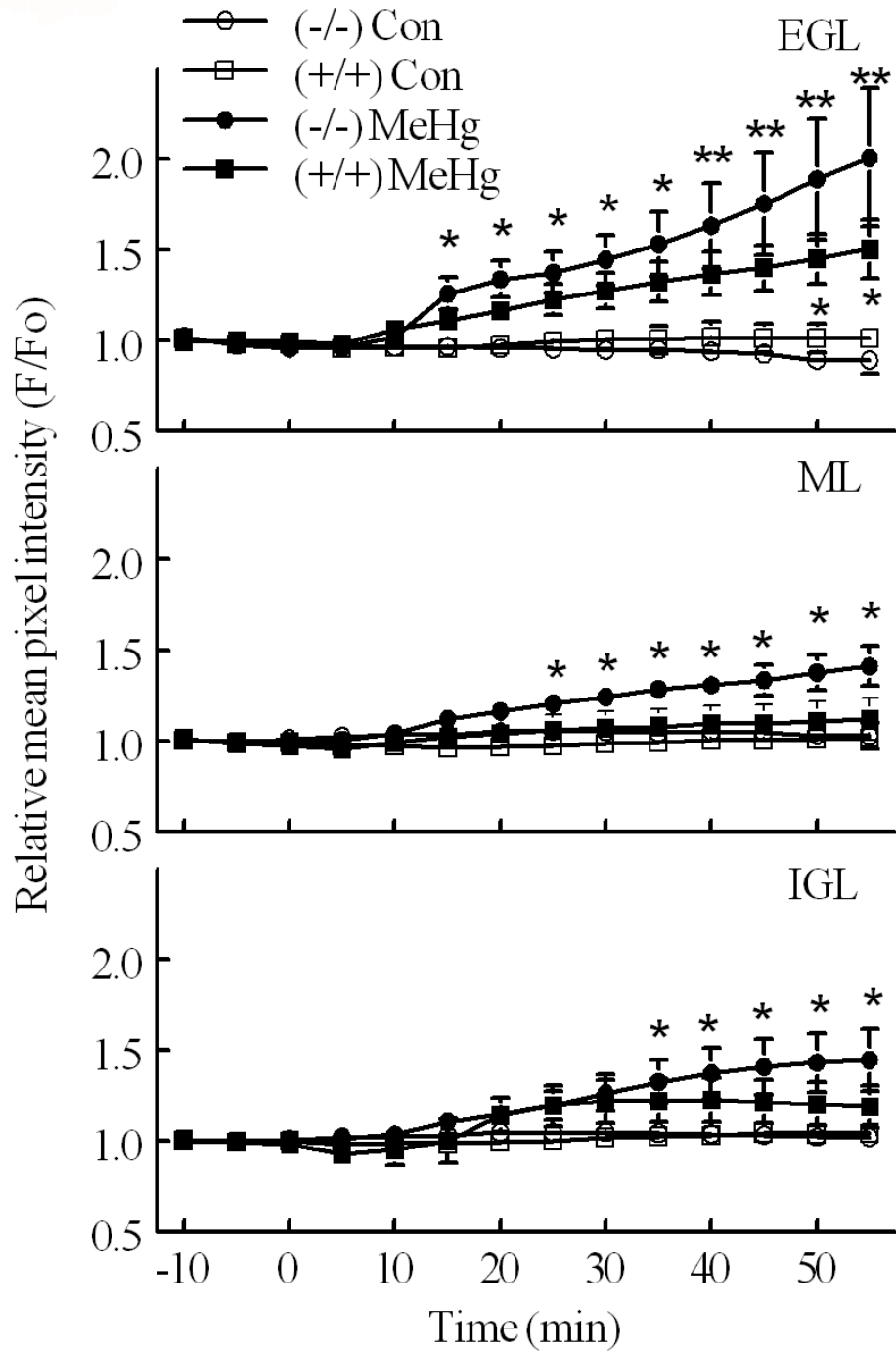


Figure 3.2. Time course of effects of MeHg on fluo4 fluorescence in cerebellar slices from neonatal $\alpha 6$ (+/+) and (-/-) mice. Mean fluo4 fluorescence intensity was compared between 0 (untreated control, Con) and 20 μM MeHg (MeHg) in (-/-) (circles, $n=5$) and (+/+) (squares, $n=6$) mice over 55 min of treatment. Each of the three developmental layers are shown separately. MeHg is applied continuously for the duration of the experiment starting at $t=0$ (20 μM , black; 0 μM , white).

Figure 3.2 (cont'd). MeHg treatment causes a rapid increase in fluo4 fluorescence in all layers and genotypes, with the largest change in the (-/-) EGL. * represents time points that are significantly greater than pretreatment ($P < 0.05$) and ** represents time points that are significantly greater than pretreatment as well as greater than the paired, untreated time point ($P < 0.05$).

b. Acute MeHg paired treatment in (+/+) and (-/-) mice

As a measure of photobleaching, relative fluo4 fluorescence (F/F_0) based on mean pixel intensities of selected cells did not change from pretreatment time points when slices from both genotypes were treated with ACSF alone (untreated control) (Figure 3.2). Relative fluorescence in these slices, when corrected as described for extinguishing cells, did not change by more than 5% between adjacent time points, indicating no positive or negative change in F/F_0 from imaging at the settings used. Overall changes in untreated controls over 55 min were at most down 10 ± 7 % in the EGL of (-/-) slices and up 4 ± 1 % in the IGL of (+/+) slices.

Overall, MeHg caused an increase in F/F_0 over time, but was dependent on both genotype and layer (Figure 3.2). In (-/-) mouse cerebellar slices, MeHg treatment increased F/F_0 up to 201% of baseline in the EGL, 141% in the ML and 145% in the IGL. When comparing to initial untreated time points, these results were significant in the EGL from 15 min on, in the ML from 25 min on and in the IGL from 35 min on. When comparing MeHg treatment to time-matched points from untreated slices from the same animals, MeHg induced significantly greater fluorescence from 35 min on in the EGL, and 50 min on in the ML. This comparison was not significant in the IGL, despite the differences from pretreatment time points. In (+/+) littermates, MeHg treatment increased F/F_0 significantly compared to pretreatment only in the EGL, where it increased the F/F_0 up to 150% baseline, and was significantly elevated from time matched untreated control at 50 min on.

As with rat treatments, the change in F/F_0 was not linear with MeHg treatment. Large

Figure 3.3

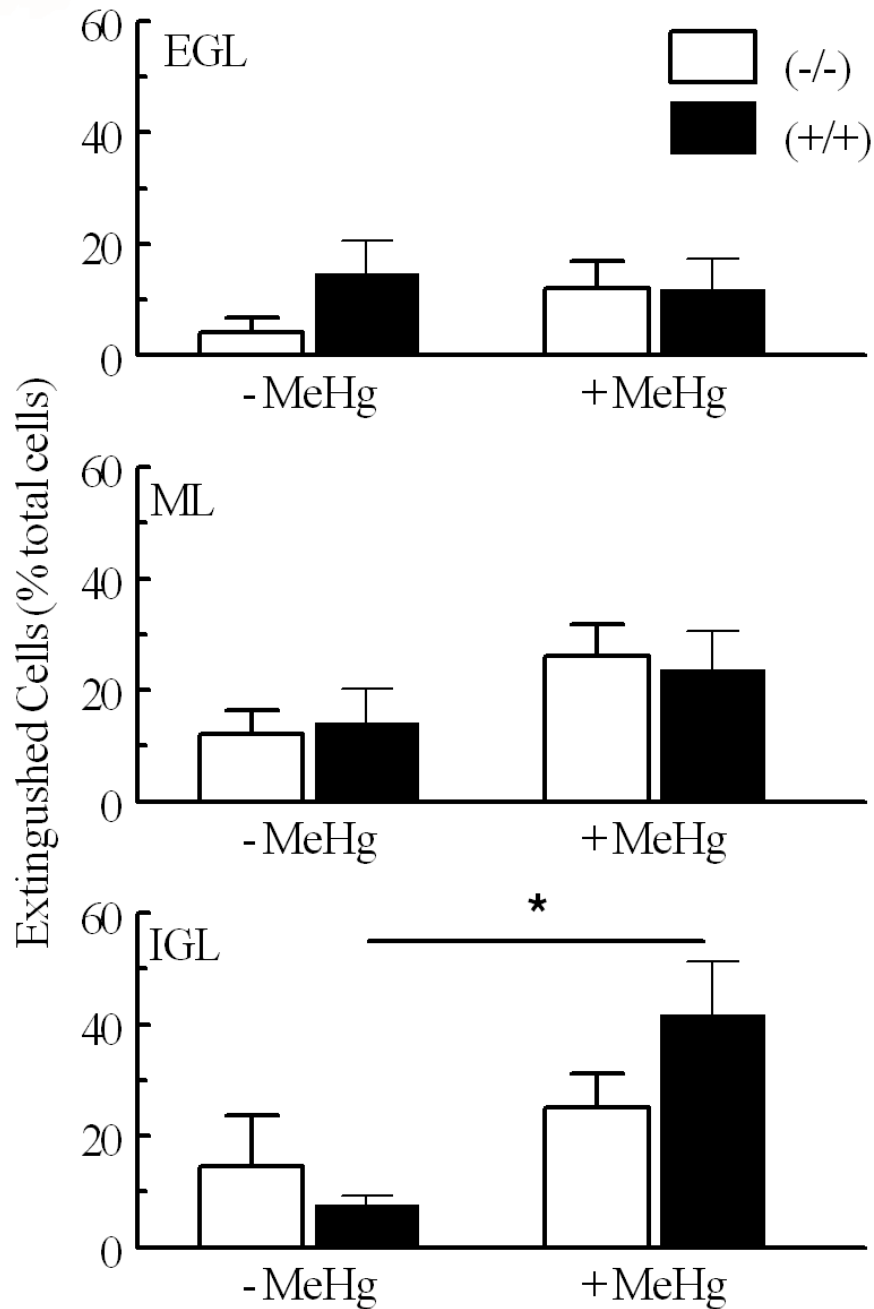


Figure 3.3. Extinguished cell percentages as found in paired mouse cerebellar slices treated with 0 (ACSF) and 20 μ M MeHg (MeHg) from (-/-) (white bars) and (+/+) (black bars) mice. Extinguished cells are cells that rapidly and significantly lose fluo4 fluorescence intensity as compared to the normal variation during treatment. These cells are removed from time course intensity traces and tallied. In these MeHg treatments, only the CGCs in (+/+) IGL significantly extinguish as compared to their untreated paired slices (*, $P < 0.05$)

increases in fluorescence occurred between 5 and 20 min time points, but continued to steadily increase in all MeHg treatments and layers except the (+/+) IGL, where it began to decrease towards the end of treatment, after 35 min.

All treatment groups had some CGCs that showed extinguishing fluorescence, a rapid decline of F/F_0 associated with loss of cell integrity and viability that was significantly greater than expected by the variance of the cells (Figure 3.3). This loss of cells was generally less than 20% of CGCs found. While there was a general increase in this loss in the different cell layers with MeHg treatment, the change was not significant except in the IGL of (+/+) slices. Despite this interaction specific to the (+/+) IGL, there was no significant difference between collective genotypes or layers.

c. Muscimol and bicuculline paired treatments with MeHg

As with results in Chapter Two in rats, pulses of both muscimol (100 μ M) and bicuculline (10 μ M) decreased the effects of MeHg on fluo4 fluorescence, but in this case effects were heavily dependent on layer. These experiments were performed on a different set of animals than the ACSF and MeHg treatment pairings, with a different set of 20 μ M MeHg treatment used as a baseline. The effect of MeHg in the two experiments was not significantly different. In these paired (-/-) mice, MeHg treatment caused a significant elevation in F/F_0 compared to pretreatment as of 10 min in the EGL, ML and IGL layers and remained elevated. In the corresponding (+/+) mice, MeHg treatment reached F/F_0 significance at 30 min in the EGL, 25 min in the IGL, where F/F_0 remained elevated, while in the ML, the only significant

point was 35 min. Neither muscimol nor bicuculline treatments significantly affected fluorescent cell count or extinguishing cell counts (data not shown).

Muscimol pulses decreased the response to MeHg treatment in all layers and both genotypes (Figures 3.4, 3.5). In all cases but one, muscimol treatment maintained F/F_0 close to baseline, similar to ACSF treatment alone. In IGL of (+/+) mice, F/F_0 does eventually increase significantly, but only at the 50 min time point. In direct comparisons between the muscimol and MeHg treatments at corresponding time points, there is no significant difference.

As with muscimol, bicuculline dramatically reduced the effect of MeHg, this reduction was dependent on layer and genotype. In (-/-) slices, bicuculline eliminated the effect of MeHg in the IGL, and reduced the effect in the EGL and ML to the point where significant effects were delayed until 35 and 40 min respectively. In (+/+) slices, bicuculline eliminated the effect of MeHg in the ML, but had no significant effect in the EGL and IGL, where it was only able to delay significant changes in F/F_0 by 5 min.

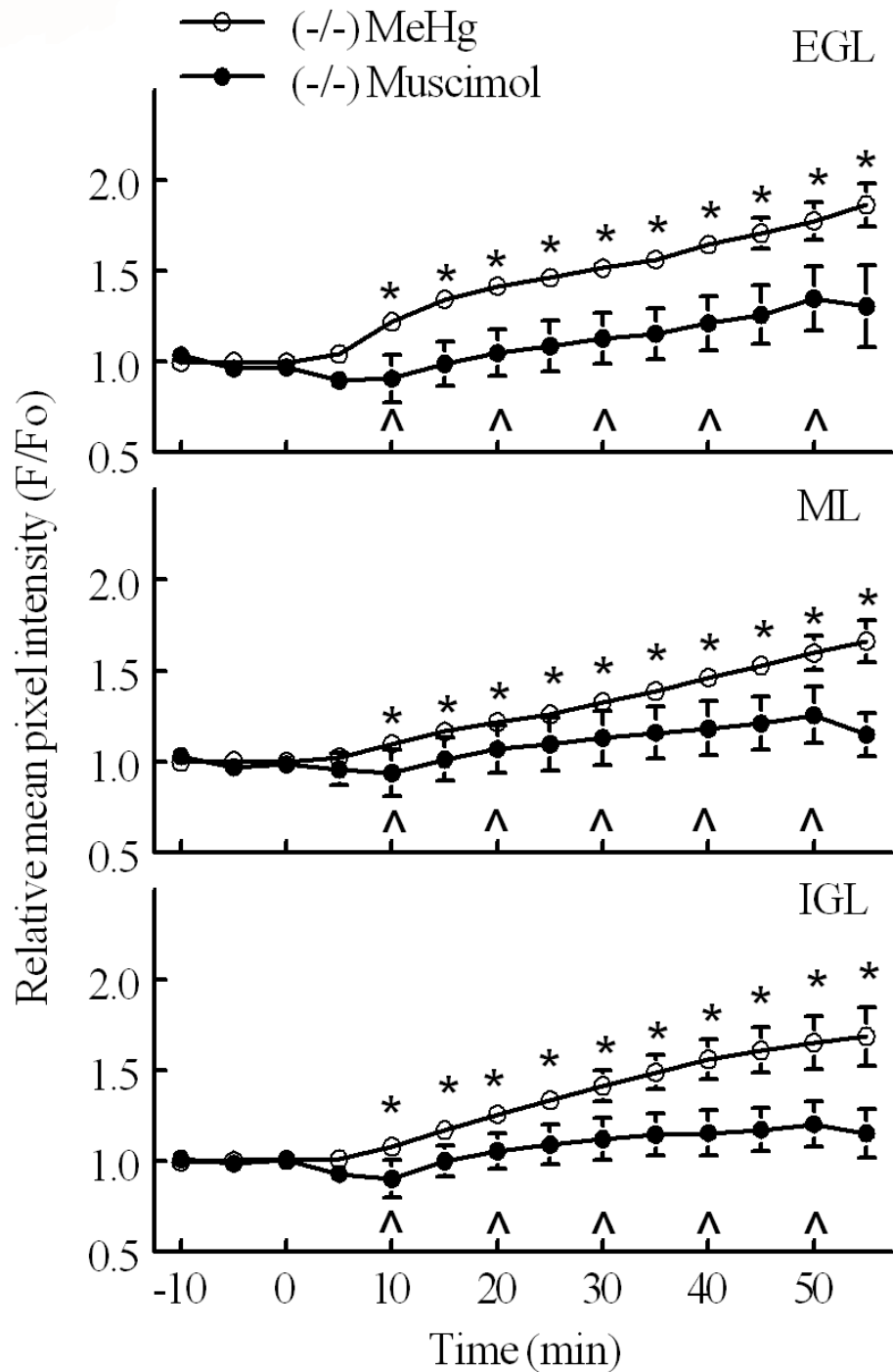


Figure 3.4. Time course of effects of MeHg and muscimol on fluo4 fluorescence in cerebellar slices from neonatal $\alpha 6$ (-/-) mice. Mean fluo4 fluorescence intensity was compared between 20 μM MeHg (MeHg, white circles) and 20 μM MeHg with 100 μM muscimol pulses (Muscimol, black circles) in (-/-) mice over 55 min of treatment (\pm SEM, $n=5$). Each of the three developmental layers are shown separately. MeHg is applied continuously for the duration of the experiment starting at $t=0$ and muscimol is pulsed into the feed for 60 s at 9.5, 19.5, 29.5, 39.5 and 49.5 min (arrows).

Figure 3.4 (cont'd). Time course of effects of MeHg and muscimol on fluo4 fluorescence in cerebellar slices from neonatal $\alpha 6$ (-/-) mice. Mean fluo4 fluorescence intensity was compared between 20 μ M MeHg (MeHg, white circles) and 20 μ M MeHg with 100 μ M muscimol pulses (Muscimol, black circles) in (-/-) mice over 55 min of treatment (\pm SEM, n=5). Each of the three developmental layers are shown separately. MeHg is applied continuously for the duration of the experiment starting at t=0 and muscimol is pulsed into the feed for 60 s at 9.5, 19.5, 29.5, 39.5 and 49.5 min (arrows).

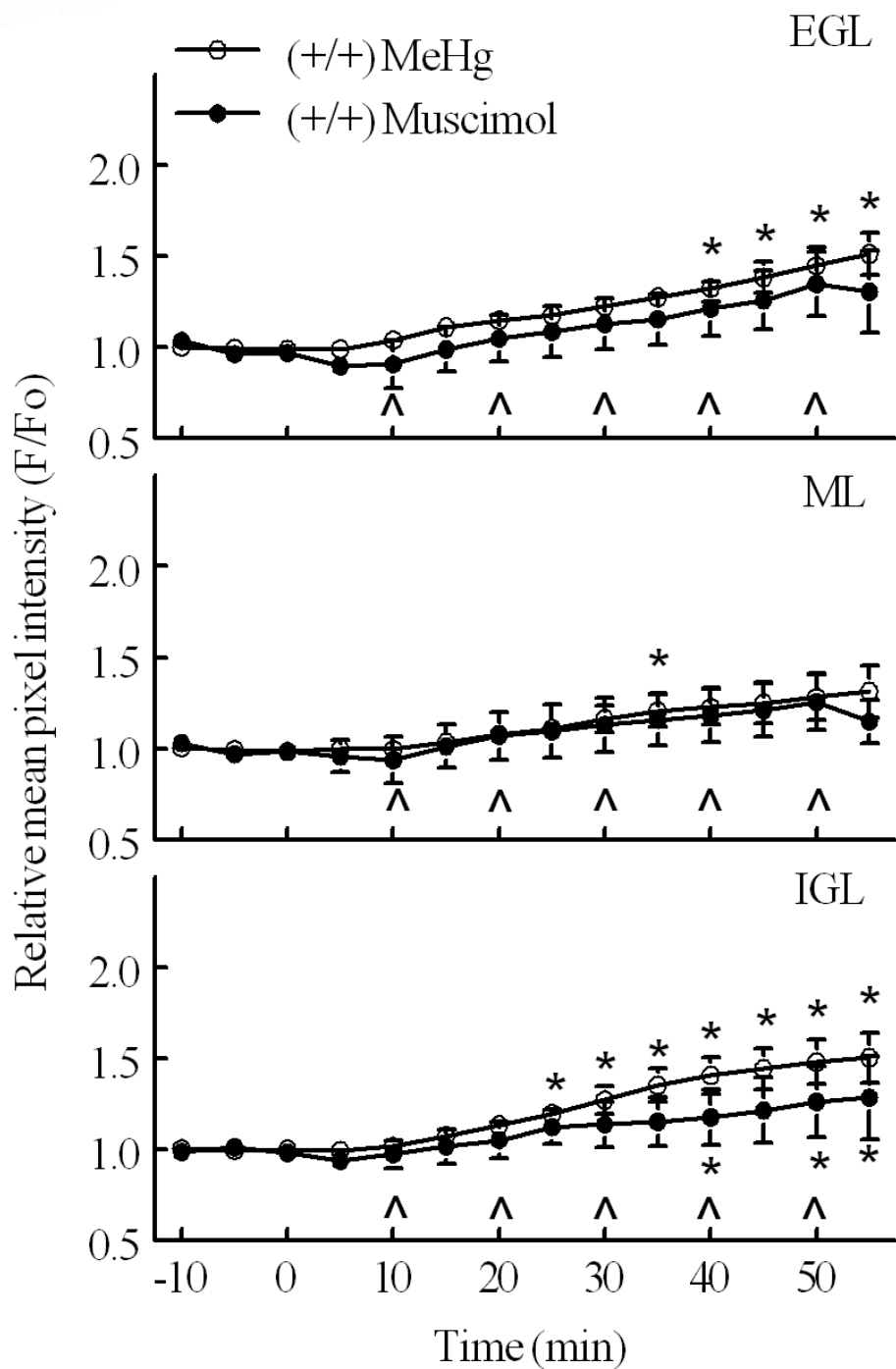


Figure 3.5. Time course of effects of MeHg and muscimol on fluo4 fluorescence in cerebellar slices from neonatal $\alpha 6$ (+/+) mice. Mean fluo4 fluorescence intensity was compared between 20 μ M MeHg (MeHg, white circles) and 20 μ M MeHg with 100 μ M muscimol pulses (Muscimol, black circles) in (+/+) mice over 55 min of treatment (\pm SEM, n=5). Each of the three developmental layers are shown separately. MeHg is applied continuously for the duration of the experiment starting at t=0 and muscimol is pulsed into the feed for 60 s at 9.5, 19.5, 29.5, 39.5 and 49.5 min (arrows).

Figure 3.5 (cont'd) MeHg alone causes a rapid increase in fluo4 fluorescence in all layers in a manner similar to previous paired experiments in (+/+) mice. Muscimol pulses reduced this effect in all layers and kept fluo4 fluorescence near baseline for the duration of experiments in the EGL and ML. * represents time points that are significantly greater than pretreatment ($P < 0.05$).

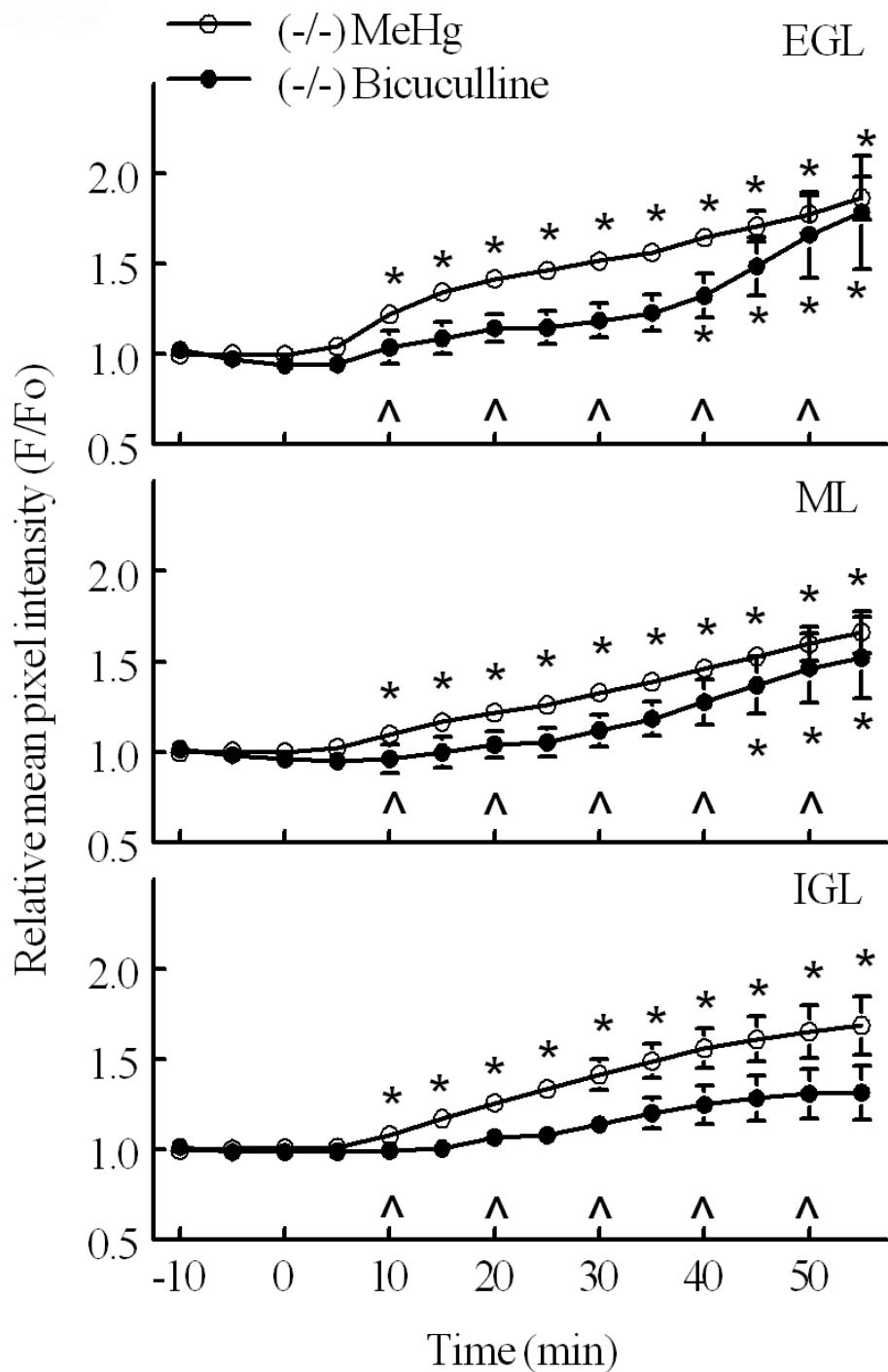


Figure 3.6. Time course of effects of MeHg and bicuculline on fluo4 fluorescence in cerebellar slices from neonatal $\alpha 6$ (-/-) mice. Mean fluo4 fluorescence intensity was compared between 20 μ M MeHg (MeHg, white circles) and 20 μ M MeHg with 10 μ M bicuculline pulses (Bicuculline, black circles) in (-/-) mice over 55 min of treatment (\pm SEM, n=5). Each of the three developmental layers are shown separately. MeHg is applied continuously for the duration of the experiment starting at t=0 and bicuculline is pulsed into the feed for 60 s at 9.5, 19.5, 29.5, 39.5 and 49.5 min (arrows).

Figure 3.6 (cont'd). MeHg alone causes a rapid increase in fluo4 fluorescence in all layers in a manner similar to previous paired experiments in (-/-) mice. Bicuculline pulses reduced this effect immediately and kept fluo4 fluorescence near baseline for the duration of experiments in the IGL. * represents time points that are significantly greater than pretreatment ($P < 0.05$).

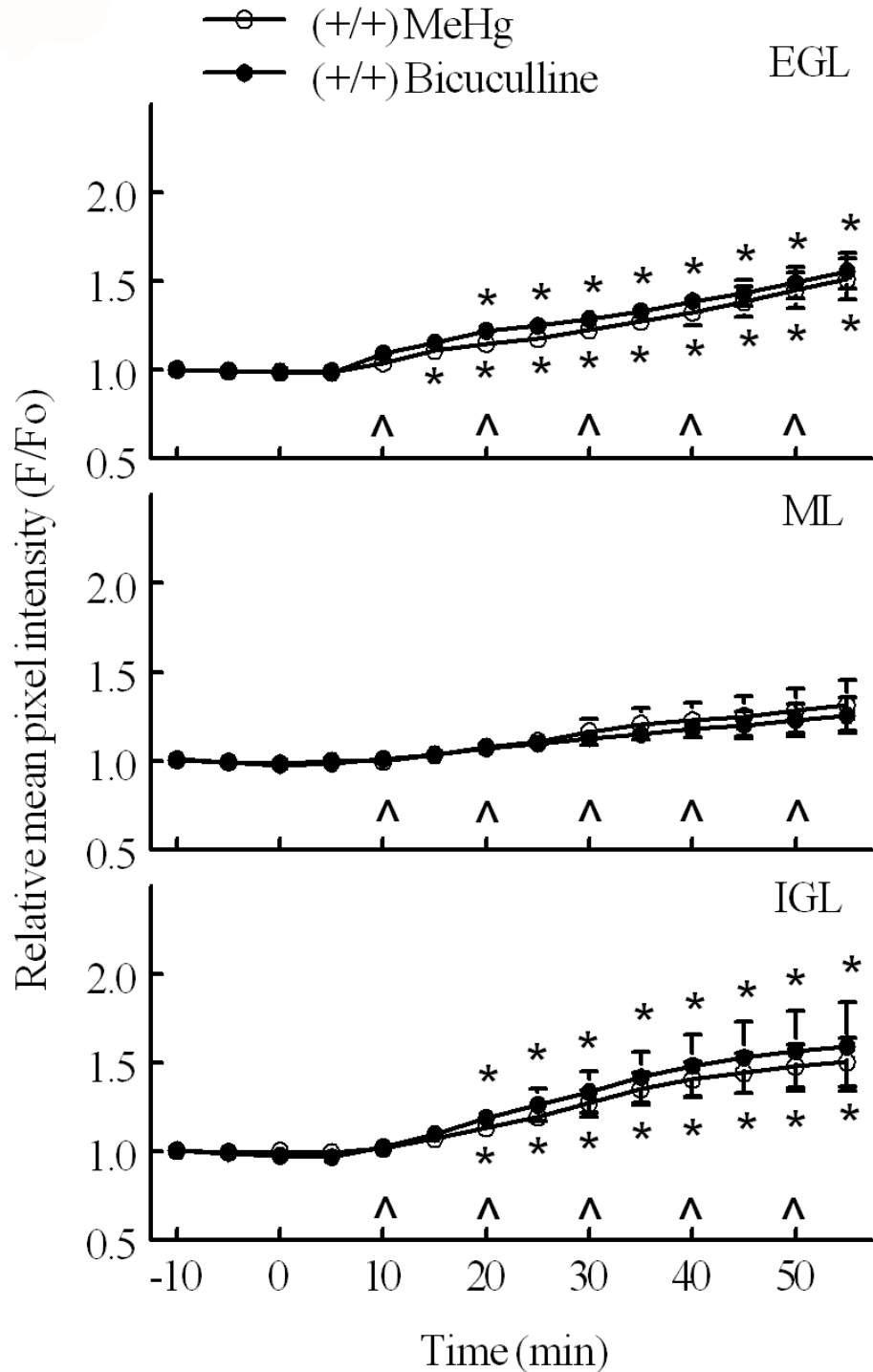


Figure 3.7. Time course of effects of MeHg and bicuculline on fluo4 fluorescence in cerebellar slices from neonatal $\alpha 6$ (+/+) mice. Mean fluo4 fluorescence intensity was compared between 20 μM MeHg (MeHg, white circles) and 20 μM MeHg with 10 μM bicuculline pulses (Bicuculline, black circles) in (+/+) mice over 55 min of treatment (\pm SEM, $n=6$). Each of the three developmental layers are shown separately. MeHg is applied continuously for the duration of the experiment starting at $t=0$ and bicuculline is pulsed into the feed for 60 s at 9.5, 19.5, 29.5, 39.5 and 49.5 min (arrows).

Figure 3.7 (cont'd). MeHg alone causes an increase in fluo4 fluorescence in all layers in a manner similar to previous paired experiments in (+/+) mice. Bicuculline did not reduce the effect in any layers, but also did not increase fluo4 fluorescence in the ML compared to pretreatment. * represents time points that are significantly greater than pretreatment ($P < 0.05$).

E) DISCUSSION

Results here further support a role for GABA_ARs in MeHg-induced increases in $[Ca^{2+}]_i$ in developing CGCs. This occurs both through the differences apparent with the knockout of one of the receptor subunits and through the actions of a GABA_AR agonist and antagonist. MeHg causes rapid increases in $[Ca^{2+}]_i$ that reach significance in these slices at concentrations that match estimated acute blood concentrations in the Iraq exposure event for ataxia (Bakir, et al., 1974). Permanent genetic knockout of the GABA_AR $\alpha 6$ subunit, the major subunit expressed in adult CGCs, enhanced $[Ca^{2+}]_i$ responses in these slices. Intriguingly, this occurred in the layers that should not express the subunit normally. Muscimol and bicuculline each decrease this CGC response to MeHg, consistent with rat neonatal slices, with some important differences between their responses dependent on development of the CGCs and genotype. This approach works with minimal changes to the protocol from rat slice preparation, and allows for extended imaging of the slices. Some direct comparisons between treatments are difficult to make with the large variability of relative fluorescent responses in these mouse CGC populations, but by pairing treatments on slices from the same brain many important comparisons could still be made.

The effects of 20 μ M MeHg on relative fluo4 fluorescence intensity in mouse cerebellar slices, while perhaps not as large as those seen in rat cerebellar slices for the same concentration, was still enough to cause significant increases within 50 min. Changes in intensity were greater in the EGL than other layers, consistent with previous findings, while in the ML of (+/+) mice MeHg barely registered any changes. With further time points analyzed than in previous experiments, it is still clear that the changes in $[Ca^{2+}]_i$ are maintained, as long as CGCs are divided into those that are alive and those that have lost integrity and thus fluorescence, which

after 65 min of continuous recording under the microscope only appears to be about 20% of visible CGCs. Live cell monitoring could be extended with this protocol in mind, but it is not clear how many more cells could be lost without losing the integrity of the overall signal. Extinguished cells have not been correlated conclusively with cell death in these experiments, but like the rat CGCs in Chapter Two, extinguished fluorescent was occasionally recorded with visible lysis of CGCs.

Notably, MeHg effects were genotype-dependent. In all three layers of (-/-) mice, MeHg almost immediately increased fluo4 fluorescence in the whole population. Though variability was enough to make the responses statistically similar, in (-/-) cerebellum MeHg caused an additional 30% increase in fluo4 fluorescence in CGCs in the EGL compared to (+/+). This clearly indicates a role for the $\alpha 6$ subunit in protecting CGCs at all stages of development. The actual mechanisms for this are not clear from these experiments. The inhibitory action of $\alpha 6$ -containing GABA_AR activation could conceivably contribute to protection in the mature CGCs of the IGL and possibly those CGCs migrating in the ML. In those layers, knockout of $\alpha 6$ produces less inhibition and thus less protection, but this does not explain the larger effect size in the EGL, where CGCs have been shown not to express the subunit yet. Expression profiles of normal developing CGCs clearly show a change in $\alpha 6$ subunit expression at the cell surface as well as other subunit expression over the course of CGC migration (Gault and Siegel, 1997, Takayama and Inoue, 2004). This switch to $\alpha 6$ subunit is prominent in the IGL, not the EGL or ML. If $\alpha 6$ expression alone is responsible for protection of CGCs and neither (+/+) nor (-/-) mice express detectable $\alpha 6$ in CGCs migrating through the EGL and ML, then the response to MeHg should not be expected to be different in these populations, yet they are in the EGL.

Absent some role for undetectable minor amounts of $\alpha 6$ expression in migrating and maturing normal CGCs, the enhanced fluorescence intensity increase in developing CGCs visualized here indicates an indirect mechanism for the loss of protection in (-/-) CGCs. Other neurons and cells in the cerebellum do not express $\alpha 6$, so they presumably would not be directly affected by the change in genotype either. The most direct connection between mature CGCs expressing $\alpha 6$ in the IGL and the developing CGCs in the EGL is through the parallel fiber axons projecting from mature CGCs through the ML. These fibers would be found near the pial surface where immature CGCs are present. It is possible that some signaling goes on between mature CGC axons and the immature CGCs at the surface. This is an intriguing proposal, in that it also suggests that toxic signaling, such as excessive release of glutamate from MeHg-exposed axon terminals, could contribute just as much to the $[Ca^{2+}]_i$ increases in immature CGCs as direct actions. This glutamate neurotransmission-dependent mechanism could be explored further in this model. If maturing CGCs are able to release neurotransmitter or otherwise signal immature CGCs, it is possible altered signaling from mature (-/-) CGCs would result in loss of protective mechanisms or enhanced toxicity pathways. Conceivably, some difference in normal signaling could alter receptor expression patterns of the immature CGCs, such as VGCC or GABA_AR subunit expression, and thus their reaction to new signals. Alterations in migrating cells' reaction to signals and movement is critical for migration, such as GABA signaling from interneurons (Farrant and Brickley, 2003). MeHg-induced effects on CGC migration also suggest changes in gene expression and signal response could be involved here (Mancini, et al., 2011, Fahrion, et al., 2012). Even though gene expression changes are relatively long-term changes and would not be noticed in acute MeHg application, the long-term status of a knockout could prime the cells for MeHg susceptibility. A surface expression approach could be performed in these cells to

determine changes in expression of receptors such as GABA_ARs and VGCCs. Gene expression profiling would require selection of populations from the different stages of development, which would be difficult but not impossible with currently available approaches.

Muscimol and bicuculline application with MeHg further indicate subtle differences in the genotype. As with application in rat cerebellum slices, both the agonist and the antagonist of GABA_ARs cause overall decreases in the [Ca²⁺]_i changes induced by MeHg. Comparisons between the treatments, layers and genotypes are complicated by several interactions. With the additional time points, it appears that the reductions in MeHg response from these GABA_AR agents may be delays instead, both muscimol and bicuculline produced effects that eventually reached the same significance above baseline as their MeHg only pairings. This is an expected result; MeHg increases [Ca²⁺]_i through many different mechanisms. Hence, blocking one pathway can at best delay changes. While many of the genotype, layer and treatment effects are complicated by interactions, it appears that muscimol and bicuculline treatment may be more effective in (-/-) mice than in (+/+), in that muscimol is only ineffective in IGL of (+/+) and bicuculline decreases or delays the response to MeHg in all three layers in (-/-). Previous characterization of GABA_AR α6 (-/-) mice indicates a 50% decrease in GABA_ARs at the cell surface with no compensation from other subunit types (Jones, et al., 1997, Nusser, et al., 1999). Our results indicate GABA_AR activation is more effective in (-/-) slices. Muscimol and bicuculline could be more effective because of the elimination of a large population of their targets. In GABA_AR α6 (-/-) mice, increases in the effects of BZs, which normally target α1 receptors with γ subunits, have been attributed to elimination of the populations of α6γ receptors (Korpi, et al., 1999). This also indicates that better knowledge of the surface expression and

subunit composition of GABA_ARs would be useful for further exploration of modulator effects. With some further knowledge of the GABA_AR subunit expression profiles present in slices, agents tailored to development stage-specific targets could be used, rather than the agonist and antagonist used here. Subunit-specific GABA_AR modulators, including neurosteroids, are being characterized that could provide approaches to further explore these differences within this model (Mennerick, et al., 2005, Simeone, et al., 2006, Khom, et al., 2010). It is possible that both changes to GABA_AR expression or function in immature CGCs as well as some change to the excitotoxic potential of mature CGCs could be important here in combination, so it is worth considering both in further study.

These experiments further characterized the populations of neurons most susceptible to MeHg toxicity. They include mature, relatively resistant CGCs and susceptible, developing CGCs in the same frame, along with PCs and other cells that did not visibly respond to MeHg. These experiments also characterized GABA_AR involvement in the mechanisms of MeHg toxicity through the knockout of an important subunit and the application of GABA_AR agonist and antagonist. These characterizations support results of previous live cell Ca²⁺ imaging and electrophysiology experiments in showing that GABA_AR involvement has a variable effect on MeHg toxicity that occurs through changes in [Ca²⁺]_i (Yuan and Atchison, 2007, Herden, et al., 2008). Further characterization is possible and needed to determine how much MeHg toxicity is direct on CGCs versus a larger, circuit-dependent disruption as may be the case with glutamate excitotoxicity or expression changes between (+/+) and (-/-) mice.

CHAPTER FOUR

COMPARATIVE Ca^{2+} EFFECTS OF CHRONIC EXPOSURE OF ADULT MICE TO MeHg OR ISRADIPINE

A) ABSTRACT

Studies on the effects of MeHg on animals have focused on developmental exposures, with few examining the effects of chronic adult exposures, despite the potential of lifetime exposure for exacerbating genetic conditions or the declines of aging. As part of a comprehensive study of molecular, behavioral, and pathological effects of chronic MeHg exposure in adult BalbC mice, as well as the effects of a L-type VGCC blocker isradipine, we imaged $[Ca^{2+}]_i$ dynamics in cerebellar slices. We sought to determine if chronic MeHg or isradipine treatment altered Ca^{2+} -dependent mechanisms, and whether they interact chronically, as acutely isradipine and other VGCC blockers reduce the effects of MeHg. Two imaging approaches were used, confocal imaging of fluo4-loaded slices to examine acute application of MeHg and test for changes to sensitivity, and high-speed epifluorescence microscopy of fura-2-loaded slices to test for changes in Ca^{2+} signaling pathways and receptors through applications of AMPA, NMDA and depolarization by high $[KCl]$ ACSF. In slices from 6 month mice, MeHg application caused a rapid and significant ($P < 0.05$) increase in $[Ca^{2+}]_i$, up to 2-fold compared to baseline. No differences were noted between chronic treatment groups. In slices from the same animals, AMPA caused significant, greater than 2-fold increases in relative fura-2 signal, and thus $[Ca^{2+}]_i$ in chronic control mice. Other chronic treatment groups had similar responses at this age, though the combination MeHg and isradipine treatment returned to baseline quickly after the pulse. NMDA was not able to alter $[Ca^{2+}]_i$ in CGCs as a population at 6 months, and KCl treatment was only able to increase $[Ca^{2+}]_i$ significantly and temporarily in the control group. At 12 months, slices responded similarly to MeHg, but due to the addition of a paired, acute ACSF (0 MeHg) treatment, there was a subtle, but significant, decrease in the effect in chronic

isradipine-treated groups. In slices from this age group, AMPA induced larger and more permanent increases in $[Ca^{2+}]_i$ and all groups had significant increases from KCl treatment as well, but NMDA responses were small and variable among cells, so there was no concerted change. Additional treatments were added at 12 months, including no change in perfusion from ACSF wash, which surprisingly still caused individual and population-wide depolarization. These additional treatments also included muscimol, which increased $[Ca^{2+}]_i$, but only in mice treated chronically with MeHg, and bicuculline, which did not induce any population-wide changes. Together these results indicate widespread changes in Ca^{2+} -dependent mechanisms induced by chronic MeHg and isradipine treatment in mice, and will be integrated with many other results from this project.

B) INTRODUCTION

As established in previous chapters, MeHg is a neurotoxicant of special concern to developing cerebellum. What has not been emphasized so far is that lifetime exposure to MeHg and the possible interaction of aging with the toxicant are also concerns. Because of the long latency periods of MeHg toxicity and because of its low clearance from the body, it is clear that even if people are able to avoid MeHg during development and childhood, many populations maintain long, low concentrations of MeHg in their CNS as adults. The actions of MeHg have mostly been studied in high exposure conditions, such as after the Japan and Iraq exposures, not chronic exposures.

While developmental exposure is of the utmost concern for neurotoxicology, MeHg exposure occurs at low levels over a lifetime, as indicated by the frequent metrics of hair and blood total Hg concentration used in epidemiological and experimental studies (Myers, et al., 2009, Yaginuma-Sakirai, et al., 2012, Bellanger, et al., 2013). As with several other similar low-consumption, persistent, ubiquitous neurotoxicants, MeHg has been hypothesized as a risk factor for neurodegenerative diseases such as Parkinson's Disease or psychiatric disorders (Uchino, et al., 1995, Weiss, et al., 2002, Petersen, et al., 2008, Weiss, 2010, Yorifuji, et al., 2011). It is unclear if the increased risk is due to lifetime exposure or exposure during another susceptible period, such as development (Fox et al., 2012). Even leaving out a potential for developmental sources for neurodegenerative disorders in aging, aging brains may be susceptible on their own. As discussed in Chapter One, the susceptibility of aging brains may be due to an increased level of baseline $[Ca^{2+}]_i$ in aging neurons which is functionally relevant to normal declines in aging,

but also poses a susceptible set of mechanisms on which MeHg can act (Toescu and Vreugdenhil, 2010).

Since we have already seen that MeHg rapidly increases $[Ca^{2+}]_i$ in susceptible neonatal neurons, it was clear that aged animals represented another susceptible population in which the effects of acute MeHg exposure might be seen. Experimental results using models treated over a lifetime have been scarce, particularly postnatal exposures, and have shown divergent results. Some indicate few or no neurological results (Yasutake, et al., 1997). Some indicate moderate increases in dysfunction in geriatric rodents compared to adults (Paletz, et al., 2007, Vitalone, et al., 2010). Finally, some indicate robust differences in neurological decline, particularly if lifetime exposure includes some perinatal exposure (Stern, et al., 2001, Weiss et al., 2005, Heath, et al., 2010). These results emphasize the need for comprehensive study of lifetime exposure to MeHg, including adult-only exposure regimens, to determine if adult and aging brains are themselves vulnerable to chronic MeHg.

A chronic study also provides the opportunity to examine potentially protective interventions. Ca^{2+} blockers reduce and delay the effects of MeHg both *in vitro* and *in vivo* (Sakamoto, et al., 1996, Sirois and Atchison, 2000, Peng, et al., 2002). One Ca^{2+} blocker, isradipine, is a selective antagonist for $Ca_v1.3$ (L-type) VGCCs and is typically used chronically to treat hypertension and angina, but also has protective effects against stroke-induced neurodegeneration in the brain (Rüegg and Nelson, 1989, Sauter and Rudin, 1990, 1991; Campbell, et al., 1997). Changes to L-type VGCC expression in the hippocampus are associated with aging as well as neurodegenerative diseases such as Alzheimer's Disease (Coon, et al., 1999, Veng, et al., 2003, Brewer, et al., 2007). In the cerebellum, L-type VGCCs are associated

with PCs, and could alter expression during aging as well (Araki, et al., 1993, Chung, et al., 2001). Isradipine has not been examined for interactions with MeHg in chronic treatments, but could be protective in several brain regions.

As part of a comprehensive, highly-collaborative project to study the cellular basis for MeHg neurotoxicity and isradipine intervention in adult and chronic exposures, we used our established slice imaging protocols to characterize $[Ca^{2+}]_i$ responses in chronically-treated mice. This includes confocal imaging of acute MeHg exposure, both to establish a baseline to compare to neonatal susceptible populations and to determine if there are sufficient chronic effects on the mechanisms to produce a different response entirely, positive or negative. Treatments also include high-speed imaging of responses to various $[Ca^{2+}]_i$ stimuli to test other baselines of aging and effects of chronic treatments. High-speed imaging was chosen for many of these treatments because of the better temporal resolution for effects and the ability to use UV-based ratiometric fluorophores. Unlike MeHg, with its continual increases in $[Ca^{2+}]_i$ over hours, the effects of most agents occur on the order of seconds, so better temporal resolution was needed.

AMPA facilitates a fast $[Ca^{2+}]_i$ response through the AMPA receptors, a typical receptor important for Ca^{2+} influx for signaling or for reestablishing $[Ca^{2+}]$ in organelles. AMPA receptors are also highly regulated, typically by internalization when overly active, so chronic treatments could conceivably regulate their expression. NMDA activates the NMDA receptor, an ionotropic and voltage-dependent Ca^{2+} channel that is normally responsive to glutamate. NMDA receptors could be involved in MeHg toxicity through glutamate release, and could also be involved with changes in aging (Glazner and Mattson, 2000, Faro, et al., 2002, Fang, et al., 2005, Petroni, et al., 2011). Interestingly, chronic MeHg exposure is also associated with NMDA

expression (Basu, et al., 2007). NMDA responses are generally slower, in part due to voltage sensitive block of the pore by a Mg^{2+} ion. High [KCl] solutions are able to depolarize excitable cells. That depolarization induces Ca^{2+} influx through VGCCs, so this treatment can be used to characterize both excitability of cells and the function of their VGCCs. The effects of $GABA_A$ R modulation were suggested for these experiments as well, but due to constraints on the use of slices, these treatments were only able to be performed in the 12 month chronically-treated groups. Muscimol and bicuculline were used in experiments that also tested baseline activity of these slices through treatment with the ACSF that is used throughout incubations and washes.

C) MATERIALS AND METHODS

a. Chemicals and solutions

Chemicals and solutions described in Chapter Two were also used in these experiments as formulated previously, including ACSF, MeHgCl, sucrose slicing solution, and fluo4. Some handling of these solutions were changed and those changes are described fully here, along with alternate solutions and additions. For incubation and treatment solutions, Fura-2 AM, TPEN, AMPA, NMDA, pluronic acid, muscimol and bicuculline methobromide were obtained from Sigma-Aldrich (Milwaukee, WI). Probenecid was obtained from Molecular Probes (Eugene, OR). All incubation solution chemicals were aliquoted in double-distilled H₂O or DMSO according to manufacturer instructions and stored at -20 °C.

Sucrose slicing solution was made as described previously. Stock (5X) solutions of slicing solution minus MgCl₂ and CaCl₂ were kept at 4 °C, and then diluted to 1X with MgCl₂ and CaCl₂ added within 48 h of use. About 25% of this prepared solution was frozen in cubes at least 8 h at -20 °C, while the remainder was stored at 4 °C. 8 cubes, approximately 200 ml, were crushed in a blender just before animal dissection, and supplemented with 200 ml 4 °C solution. This solution was immediately oxygenated by bubbling a 95%/5% O₂/CO₂ gas mixture through it. All oxygenated solutions were bubbled with this gas mixture. ACSF and Mg²⁺-free ACSF were kept at room temperature (23-25 °C) for at least an hour prior to dissection on the day of treatments to avoid temperature changes during imaging.

In order for the NMDA receptor to respond to NMDA application alone, slices for microfluorimetry needed to incubate in Mg^{2+} -free ACSF. This ACSF was made simply by not adding $MgCl_2$ when mixing the solution, the difference in osmolarity and pH was not significant. 10 ml solutions each of 25 μ M AMPA, 50 μ M NMDA plus 10 μ M glycine, 100 μ M muscimol and 10 μ M bicuculline, were made in Mg^{2+} -free ACSF on the day of each relevant experiment. Additionally, 40 mM KCl ACSF (containing 87.5 mM NaCl; 40 mM KCl; 1.25 mM KH_2PO_4 ; 26 mM $NaHCO_3$; 25 mM D-glucose; 1 mM $MgCl_2$; and 2 mM $CaCl_2$), was prepared weekly.

b. Animal care and treatments

All animal use and care was based on NIH laboratory animal use guidelines and was approved by the MSU Institutional Animal Care and Use Committee. Male BalbC mice were obtained from Harlan (Frederick, MD) at approximately three weeks of age, housed in pairs with standard feed (Teklad 18% Protein Global Rodent Diet) obtained from Harlan, water and accommodations and given hard plastic houses and nesting material for enrichment. Isradipine was obtained from VWR (Chicago, IL) and sent directly to Harlan. Isradipine was mixed into standard feed at 2 ppm to make a custom diet, and an inert yellow dye was added to the isradipine diet to distinguish it from the control diet. Sixteen batches of eight mice each were obtained in a staggered configuration to allow for weekly sets of several different experimental approaches. These mice were acclimated until three months of age, when they were divided into four treatment pairs and coded by ear punch. The first pair received standard feed and water. The second pair received standard feed and water supplemented with 6.25 ppm MeHg. The third pair received isradipine-supplemented feed and standard water. The fourth pair received both the MeHg-supplemented water and the isradipine-supplemented feed. One animal from each pair

was chosen randomly for 6 month collection, while the other was retained for 12 month collection. Animals were coded by numbers and colors, to allow for treatment blinding from those working on the tissue and behavioral tests.

All animals were monitored daily for any health problems. Animals were weighed and checked for hind-limb crossing caused by weakness and paralysis, three times a week (M, W, F). Additionally, for one week of training and acclimation and again three times every other week (T, W, Th), animals were given balance testing on a variable-speed rotating cylinder (IITC, Inc., Woodland Hills, CA) to test cerebellar function. All bedding, waste and food was handled as potential hazardous waste due to the presence of MeHg.

c. Tissue collection

Each week one animal from each of the four treatment groups was selected for dissection and tissue collection. Because of the time required for incubations and experiments performed on the same day, no more than 2 animals were used on a given day. One mouse was removed and sealed in a transparent glass container with 2 ml of 99% isoflurane (Abbott laboratories, Chicago, IL) absorbed into a cotton swab as anesthetic until righting reflex was lost and breathing slowed. The mouse was removed and secured to a cold dissecting platform, with additional isoflurane applied over the nose to maintain unconsciousness. Secured mice were checked for blink reflex, without which they were determined sufficiently unconscious for cardiac perfusion. The chest cavity was opened and the heart pierced in the left ventricle with a 27 gauge needle attached to a 50 ml syringe loaded with blended frozen slicing solution. The right atrium was cut, and resulting blood collected from the chest cavity by pipette, placed in a

labeled tube and frozen in liquid nitrogen to be removed to -80 °C for storage. The entire 50 ml blended slicing solution was pumped through the left ventricle to replace blood throughout the body. This was immediately followed by removal of the head. Cardiac perfusion and decapitation were considered to be time of death.

Various tissues, including spinal cord, liver, kidneys, and EDL muscle were taken as needed for other studies and are not included in this section. The head was removed to a bath of blended slicing solution, and allowed at least 1 min to cool. The head was removed from the bath, the skin was removed and the skull removed as described in Chapter Two, with special attention added to removing the forebrain and brainstem without damage. Forebrain was given to another researcher for other studies. Brainstem and trimmed excess hemisphere tissue from cerebellum was frozen in liquid nitrogen and stored at -80°C. Sagittal slices of 180 µm thickness were taken from the cerebellum in a bath of blended slicing solution. This thickness was chosen because it is a size preferable for electrophysiological studies, which were performed in addition to the imaging studies described here. Slices were immediately removed to a mesh surface in a container of oxygenated ACSF at 37°C. These slices were incubated at this warm temperature for 30 min from the last addition of a slice, and then the container was removed to room temperature for further incubations. The time between animal death and heated slice incubations was kept minimal, and generally did not exceed 10 min.

Immediately upon completion of 37°C incubation, one slice was chosen for either high-speed or confocal imaging. When possible, imaging platform use was staggered in order to complete more treatments before starting a new animal. Because time between slicing and use

could potentially lead to degradation, slicing times and start times for imaging were tracked to compare to markers of slice quality taken from images and notes.

d. High-speed imaging

A slice was transferred to an opaque 35mm petri dish containing a solution of 2 mL ACSF supplemented with 5 μ M fura-2 AM, 2.5 mM probenecid, 5 μ M TPEN, and 0.002% (w/v) pluronic acid. Pluronic acid and probenecid were used in order to facilitate uptake and inhibit expulsion of fluorophore, respectively. TPEN is a selective intracellular Zn^{2+} chelator which eliminates any Zn^{2+} -dependent components of fluorescence. This solution was prepared during 37 °C incubation. This incubation bath was transported to a 5% CO_2 , 37 °C incubator for 45 min. This is the only step in which ACSF is not oxygenated, to reduce the production of insensitive fura-2 intermediates.

During incubation, the slice imaging chamber on an inverted Nikon Eclipse TE 2000-U microscope was perfused with oxygenated Mg^{2+} -free ACSF with a tissue anchor in the chamber. This was to prepare the chamber and soak the anchor so there was less movement during treatment. After incubation, the slice was placed in the chamber and the anchor was laid on top to secure it. Fresh Mg^{2+} -free ACSF was perfused across the chamber via a perfusion pump running at about 2 mL/min. The slice was allowed at least 10 min to wash. During this time a frame of interest was visualized using the microscope. The frame was selected by finding a region with a reasonable number (>20) of CGCs, recognizable by size and shape, fluorescent and in focus at this excitation line, and no obvious tears or other damage. Light from a Polychrome V light source (Till Photonics) was shone through a custom fura-2 dichroic mirror (Chroma,

71000A Fura2 C59742) and a 40x oil immersion objective (Nikon S Fluor 40x/1.3 oil DIC H/N2) onto the slice from below. A special low fluorescence oil was used for contact between the objective and chamber (FF, Cargill, Cedar Grove, NJ). For frame acquisition, a 380 nm excitation line was used.

Frame of interest acquisition was handled through software when possible to limit continuous illumination of the slice. Image acquisition was performed using TillVision control software (v 4.0). Live acquisition of the frame of interest was tested using live acquisition grab settings, set to 380 nm and 500 ms intervals. This briefly switches on the Polychrome V light source, and opens the high-speed electron-multiplying CCD camera (Ixon EM+, Andor, South Windsor, CT) to reduce illumination on the cells compared to eyepiece illumination. Fura-2 is a ratiometric fluorophore, with the value of emission at 500-540 nm based on the excitation at 340 nm for Ca^{2+} -bound fluorophore, and 380 nm for Ca^{2+} -free fluorophore. As $[\text{Ca}^{2+}]_i$ increases, the value from 340 nm increases and the value from 380 nm decreases. For the start of experiments, illumination time was adjusted at 380 nm to about 75% of maximum, to allow for decreases at this wavelength with stimulus. This illumination time was checked at 340 nm as well, which generally started at a much lower fluorescence emission and could be adjusted further. Initial frame snapshots were saved for both of these wavelengths.

Illumination time was adjusted in a template protocol in TillVision. Briefly, this template kept the settings between treatments the same, apart from this adjustment to illumination time, and automated the collection of images. This protocol specified three treatment periods, each consisting of a set of 300 images taken at 2 s intervals (10 min total) with each time point

imaging twice with a rapid switch between 340 and 380 nm illuminations. A user-terminated pause was set between each treatment period to allow for extra wash times or other adjustments.

Once the initial 10 min wash and the frame of interest and illumination was set, treatment was started. Concentrations of AMPA, NMDA and KCl were selected based on previous Ca^{2+} recordings from brainstem slices (Johnson, et al., 2011). These concentrations were optimized in cerebellar slices from up to 18 month mice before the experiments performed here. The perfusion buffer was switched to 25 μM AMPA in Mg^{2+} -free ACSF for 2 min and the start of imaging. Once two minutes passed with the AMPA stimulus treatment, perfusion was switched back to Mg^{2+} -free ACSF for the remaining 8 min of imaging as well as at least 2 min more of wash. The second treatment was performed exactly as the first, but used 50 μM NMDA + 10 μM glycine as treatment. The third treatment in this series was performed exactly as the first two, but used 40mM ACSF.

In the 12 month treated animals, an additional set of slices from the same animals as the first was taken, and an additional series was added. The concentrations of muscimol and bicuculline used were based on concentrations that induced or blocked depolarization in cerebellar slices, respectively (Yuan and Atchison, 1997, 2003). In this treatment series, the first treatment consisted of continuing Mg^{2+} -free ACSF (i.e. no treatment), the second treatment consisted of 100 μM muscimol, and the third 10 μM bicuculline.

Image series were exported from TillVision as tagged image files (.tif). In Image J (v 1.45s, imagej.nih.gov/ij/). Background was subtracted by a 50 pixel rolling ball subtraction and images were registered to lessen movement between time frames. Because of the time this

algorithm takes to process these steps in 300 images, background subtraction and registration were performed automatically by batch processing. Images from 6 month-old animals were processed manually using the “region of interest (ROI) manager” tool collecting circles with 14-18 pixel diameters. Using the “multi” tool in the ROI manager, mean intensity values for both 340 and 380 nm excitations from these ROIs were exported in spreadsheets. In contrast, because of an increase in number of treatments and total experiments, 12 month images were processed by an automated method. In this automated approach, registered image stacks for 380 nm were opened for further processing. From the first 380 nm image, a granulometric filter (circle, 7 pixel radius, 2 pixel step) was run to remove non-cellular fluorescence and highlight circular cells between 7 and 9 pixels, representing CGCs (Prodanov, et al., 2006). This filter tags points (“granules”) in the image that represent uniformly fluorescent circles of the selected size. It produces a new image with the selected size circles added to these points with a value of 1, several of these circles can overlap around the center of mass of a cell. More clustered points represent more confidence a cell has been found of the correct size. CGCs typically have 5 or more of these points in the center of mass, so a binary filter was added wherein all areas in this filter with >5 points were considered positive (1) and all <5 points negative (0). Since some CGCs touched or were even collected in clusters, binary watershed filtering was applied to this image to insert borders between uniformly sized sections of clustered cells. The “analyze particles” tool was used to define the cells in this image and export them to the “ROI manager” tool. Once these cells were defined in ROI manager, the defined cells were applied to the original image stack. Just as with manual tracking of ROIs, the “multi” tool was used to determine mean intensity values from these ROIs and means were exported in spreadsheets. The locations of all ROIs used were saved for reference.

Spreadsheets were imported into Excel® (Microsoft, Redmond, WA), from which ratiometric values (R) were produced from the individual 340 and 380 nm traces. Of these traces, only those that started with a 380 nm value greater than 340 nm were used, as a reversed 340 to 380 ratio indicates a damaged cell. Additionally, some traces displayed a sudden extinguishing of 340 and 380 fluorescence. This was indicated by a significantly outlying negative change in fluorescence at both wavelengths. Since this loss of fluorescence represents a burst or detached cell similar to the loss of fluo4 fluorescence described in Chapters Two and Three, these cells were excluded from time course analyses. Counts of reversed ratio cells and counts of extinguished cells were compared to other potential markers of slice quality, such as time from slicing by linear regression and chronic treatment group by ANOVA.

e. Confocal microscopy

A slice was transferred to an opaque chamber consisting of a mesh bed in a well of a 12-well culture plate containing oxygenated 1x fluo4NW + probenecid as described in Chapter 3, with the addition of 5 μ M TPEN to eliminate the contribution of Zn^{2+} to fluorescence in these experiments. This incubation lasted 40 min at room temperature (25-27°C). While this incubation ran, the imaging chamber on the microscope used in Chapter Three was prepared, with ACSF flowing at about 1.5 mL/min via a gravity feed.

Imaging on confocal was performed as described in Chapter Three, with a few changes described here. Briefly, only one pretreatment image scan was taken, the remainder images were taken exactly as described in Chapter Three, with two blocks of five automated imaging scans

with a break in between to check for slice movement. Emission range was reset to settings described in Chapter Two for fluo4 alone.

Due to time constraints, only 20 μM MeHg treatment was performed on the confocal imaging platform for 6 month treated mice. An additional control, 0 μM MeHg in ACSF, was deemed necessary partway through 12 month experiments, and performed on the last 5-7 mice from each treatment group. These concentrations are based on the experiments conducted in Chapters Two and Three in which MeHg treatment caused a several fold, significant increase in fluo4 fluorescence within 50 minutes in cerebellar slices.

Image series were imported into ImageJ and concatenated into raw image series. A 50-pixel rolling ball radius was used to remove background from these series. These images were grouped and converted into sum projections. CGCs were manually drawn as 15 pixel diameter circles and tracked using the ROI manager tool. Once ROIs were defined, the ROI manager multi tool was used to produce a spreadsheet of the means over 11 time points.

f. Statistics

Spreadsheets were imported into Excel® to check traces. Extinguished cells were determined by determining negative outliers for changes in fluorescence. These cells were tallied and removed from the population of traces. Remaining traces were collected and averaged for treatment groups. Count, standard deviations and standard errors were collected. Means for each animal were exported to SPSS (IBM, Somers, NY) and overall statistics were calculated by multifactorial, repeated measures ANOVA. All traces were normalized to the initial time point.

For high-speed imaging, no statistical software appears to be able to handle all the factors used (300 time points, 4 chronic treatments, 6 acute treatments, 2 age groups) when determining overall statistics, so only every tenth time point was used for calculating these statistics. Within-subject repeated measures included time (30 time points) and acute treatment (3 levels in order, as part of either AMPA/NMDA/KCl or ACSF/muscimol/bicuculline). Between subjects factors included chronic MeHg treatment (control or 6.25 ppm), chronic isradipine treatment (control or 2 ppm), and treatment series (AMPA/NMDA/KCl or ACSF/muscimol/bicuculline). To reduce error caused by differences in initial R, statistics were performed with traces that were normalized to their initial value (R/R_0). Based on significant effects and interactions, normalized treatment traces were compared to the second time point used in statistics (20 s) to determine if a significant change in fluorescence occurred and when.

For confocal imaging, within-subject factors included time (11 time points) and acute treatment (20 μ M MeHg or control). Between subject factors included chronic MeHg treatment (control or 6.25 ppm) and chronic isradipine treatment (control or 2 ppm). Based on significant effects and interactions, traces were compared to the initial time point to determine if a significant change in fluorescence occurred and when. Paired time points, focusing at the end of treatment, were compared between each treatment group.

A

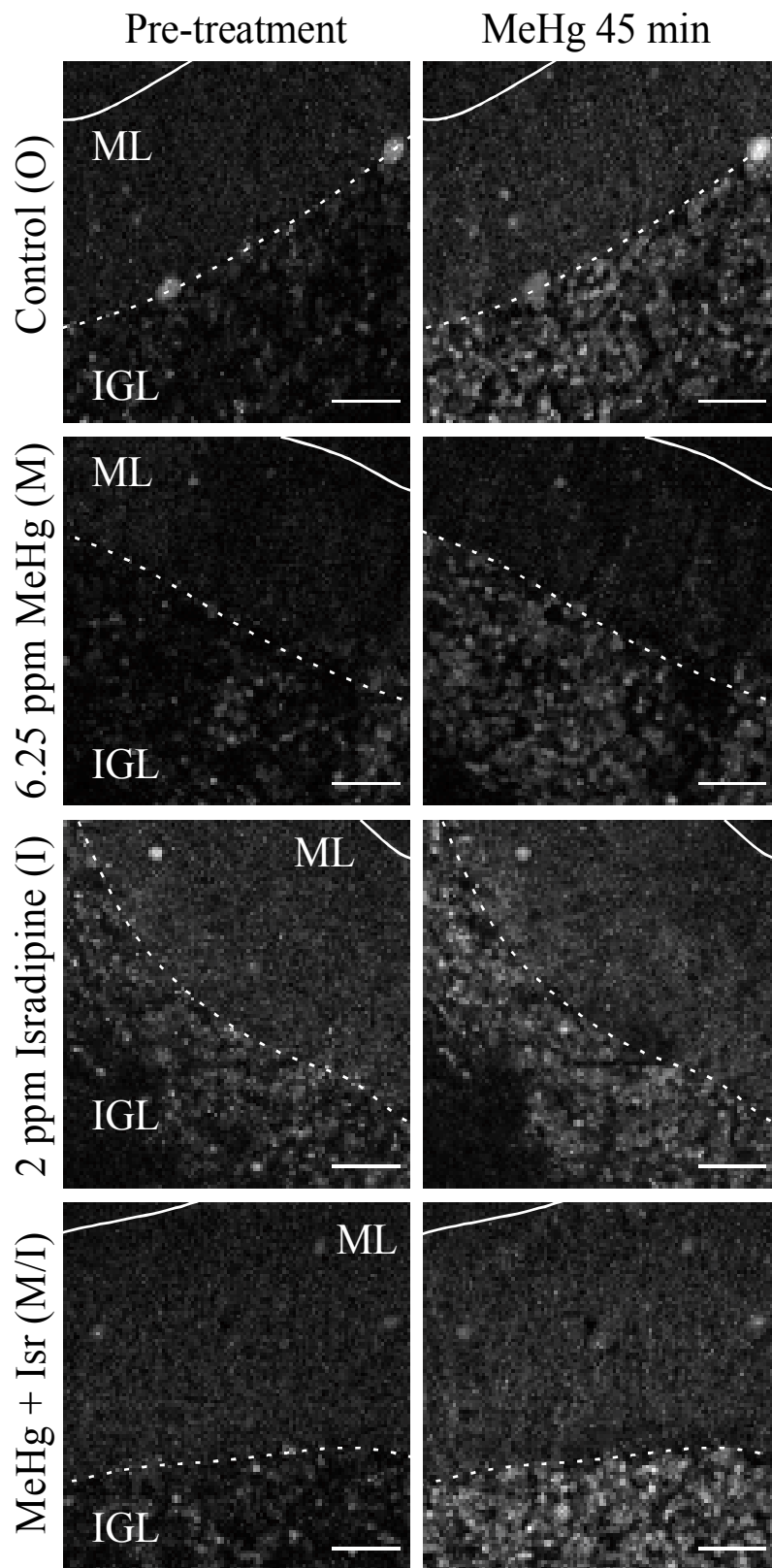


Figure 4.1. Example frames of interest from confocal fluo4 time course imaging.

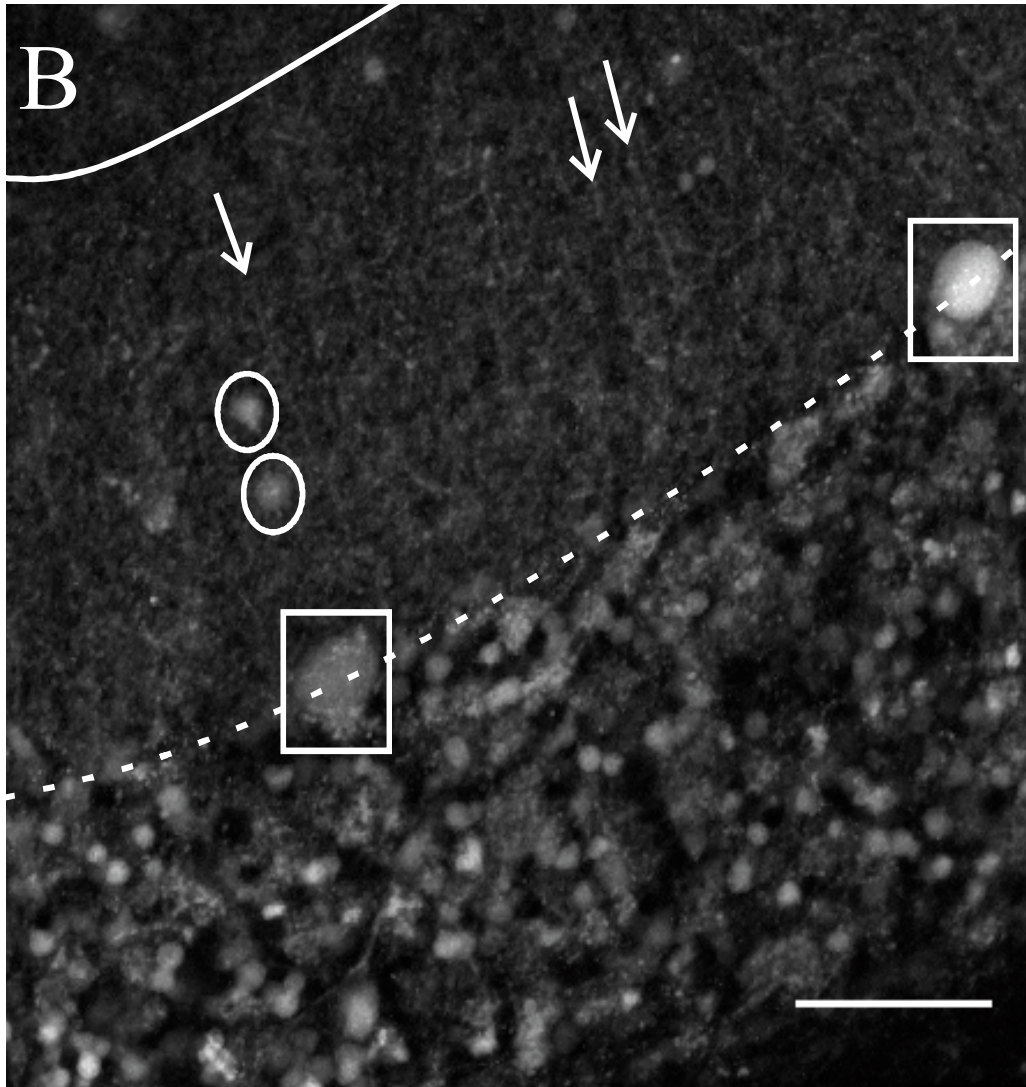


Figure 4.1 (cont'd). Slices were imaged through 45 min of continuous perfusion with 20 μ M MeHg in 6 month chronically-treated mice. All images are from the same batch of animals. Images are registered, rotated and cropped for clarity; scale bar equals 50 μ m. **A.** Slices of cerebellum are from four 9 month old animals treated chronically for 6 months with, in order, standard food and water (O), 6.25 ppm MeHg in drinking water (M) with standard food, 2 ppm isradipine in food (I) with standard water, and the combination of MeHg in water and isradipine in food (M/I). MeHg application over 45 min increases relative fluo4 fluorescence in CGCs in the IGL by about 2-fold within 45 min, the duration of observation, in all 4 chronic treatment groups. **B.** Expanded frame of interest from group O after 45 min of continuous MeHg perfusion. Image highlights processes in the ML that become apparent with MeHg treatment (arrows), infrequent PC fluorescence (boxes), and non CGC cells in the ML (circles).

RESULTS

a. Confocal Ca^{2+} imaging

Acute treatments of 20 μ M MeHg were applied to slices from four sets of chronically treated animals in order to assess functional differences in Ca^{2+} -dependent mechanisms that could come about by long-term exposure to MeHg and isradipine. Differences between CGCs could come about from changes in receptor expression, trafficking or recycling, and other long-term differences in signaling, such as changes in baseline $[Ca^{2+}]_i$. Animals collected at 6 month time points only received acute MeHg treatments, so could only be compared to pretreatment baselines, while 12 month time had two treatments where possible, one slice received MeHg while another received only ACSF. Unlike in neonatal rodents as described in previous chapters, CGCs were located only in the IGL (Figure 4.1 B). Many processes in the ML were visible, but diffusely stained and difficult to distinguish (Figure 4.1 B). PCs rarely fluoresced as efficiently as CGCs, but could be seen in some slices from all age and treatment groups. Some additional interneurons or glia were evident in the ML or other positions, but could be distinguished from CGCs by shape (larger than CGCs, not always circular) and position.

Acute MeHg treatment caused rapid increases in relative fluo4 fluorescence in CGCs tracked in both 6 month and twelve month treatment groups and in all chronic treatments used. In 6 month control animals (0 MeHg, 0 isradipine, designated O), acute MeHg increased relative fluo4 fluorescence, up to $203 \pm 13\%$ of baseline (Figures 4.1, 4.2). In 6-month chronically MeHg-treated mice (6.25 ppm MeHg, 0 isradipine, designated M), acute MeHg application

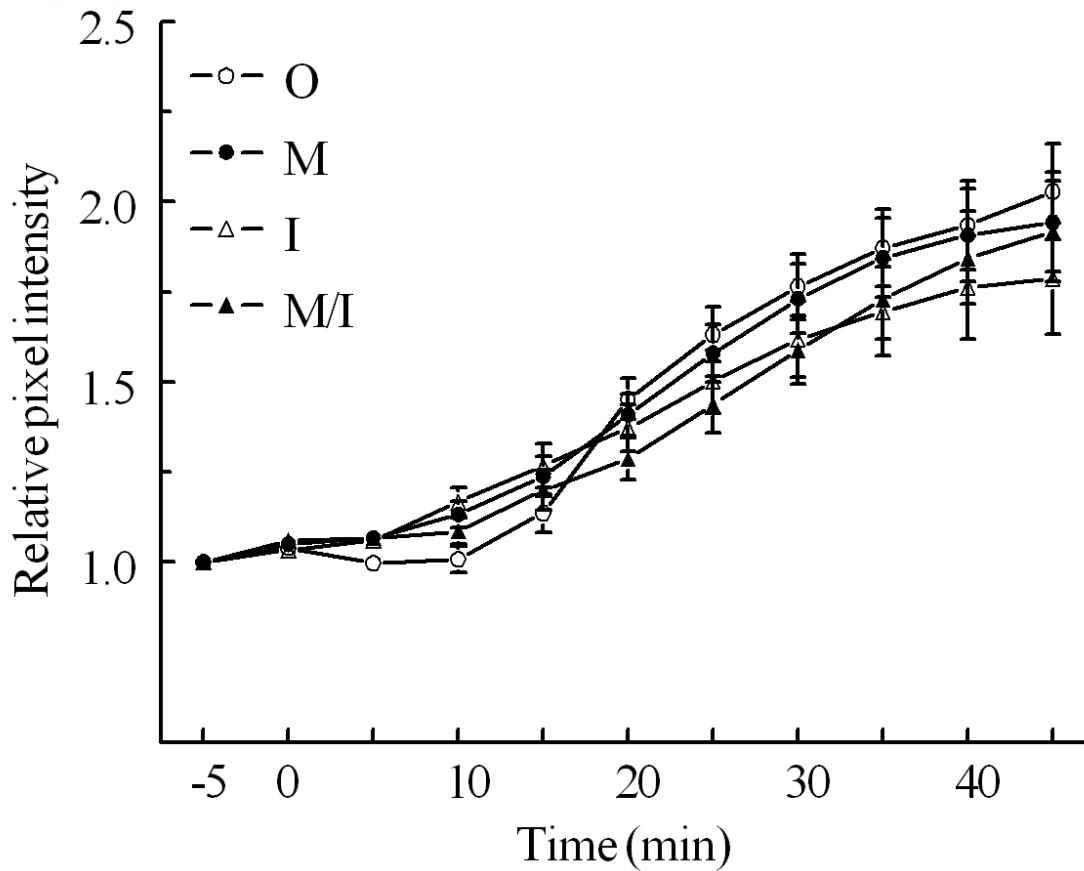


Figure 4.2. Mean relative fluo4 fluorescence intensities as measured from confocal time course image series of cerebellum slices from 6 month chronically-treated mice. Slices from untreated control (O, n=11, white circles), MeHg-treated (M, n=11, black circles), isradipine-treated (I, n=9, white triangles), and combination MeHg- and isradipine-treated (M/I, n=11, black triangles) were imaged at 5 min intervals for 50 min with one pretreatment scan and 10 images with 20 μ M MeHg flowing over the slices. All acute MeHg treatments caused about a 2-fold increase in relative fluo4 fluorescence in CGCs (\pm SEM) and reached significance compared to pretreatment by 20 min of imaging ($P < 0.05$), but were not significantly different from one another ($P > 0.05$).

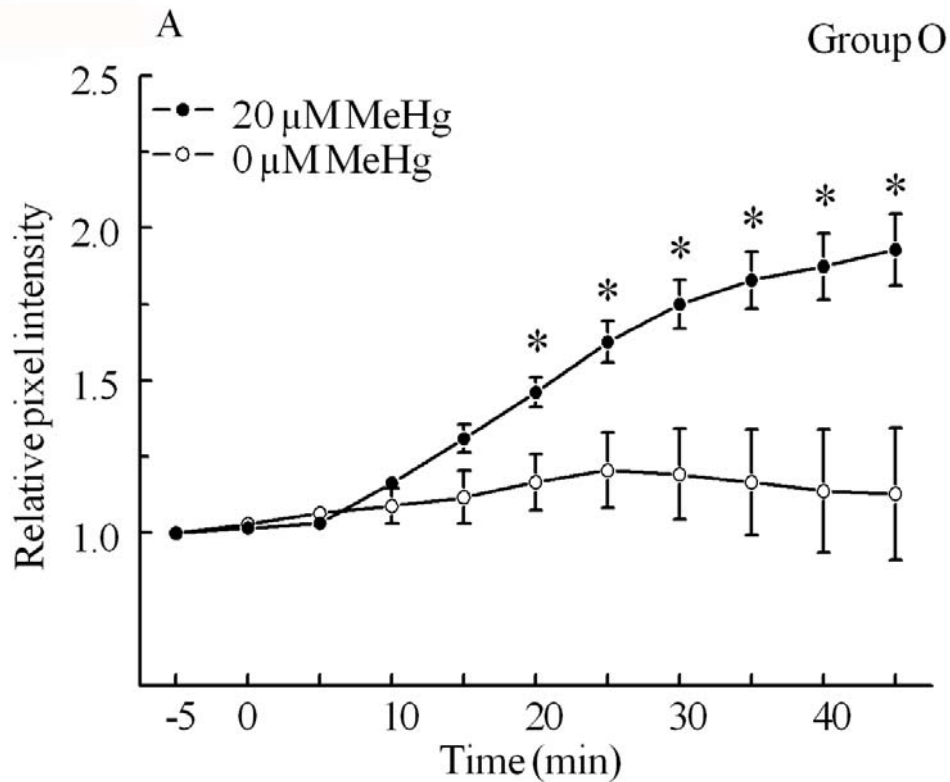


Figure 4.3. Mean relative fluo4 fluorescence intensities of CGCs in slice during 20 μ M MeHg exposure over 45 min from 12 month chronically-treated mice. Traces are from acute treatments of 0 μ M MeHg (untreated controls, white circles) and 20 μ M MeHg (black circles) applied in the bath ACSF solution to cerebellum from 15 month old mice chronically treated for 12 months. Paired comparisons were made between matching time points (*, $P < 0.05$). **A.** Acute treatments of mice receiving no chronic MeHg or isradipine (Group O). Acute MeHg treatment ($n=16$) significantly increased fluorescence above no MeHg treatment ($n=5$). **B.** Acute treatments of mice receiving chronic 6.25 ppm MeHg in water and no isradipine (Group M). Acute MeHg treatment ($n=16$) significantly increased fluorescence above no MeHg treatment ($n=7$). **C.** Acute treatments of mice receiving no MeHg and 2 ppm isradipine in diet (Group I). Acute MeHg treatment ($n=13$) increased fluorescence above no MeHg treatment ($n=5$), but only at one intermediate time point. **D.** Acute treatments of mice receiving both 6.25 ppm MeHg in water and 2 ppm isradipine in diet (Group M/I). Acute MeHg treatment ($n=17$) did not significantly increase fluorescence above no MeHg treatment ($n=6$) during observation.

Figure 4.3 (cont'd)

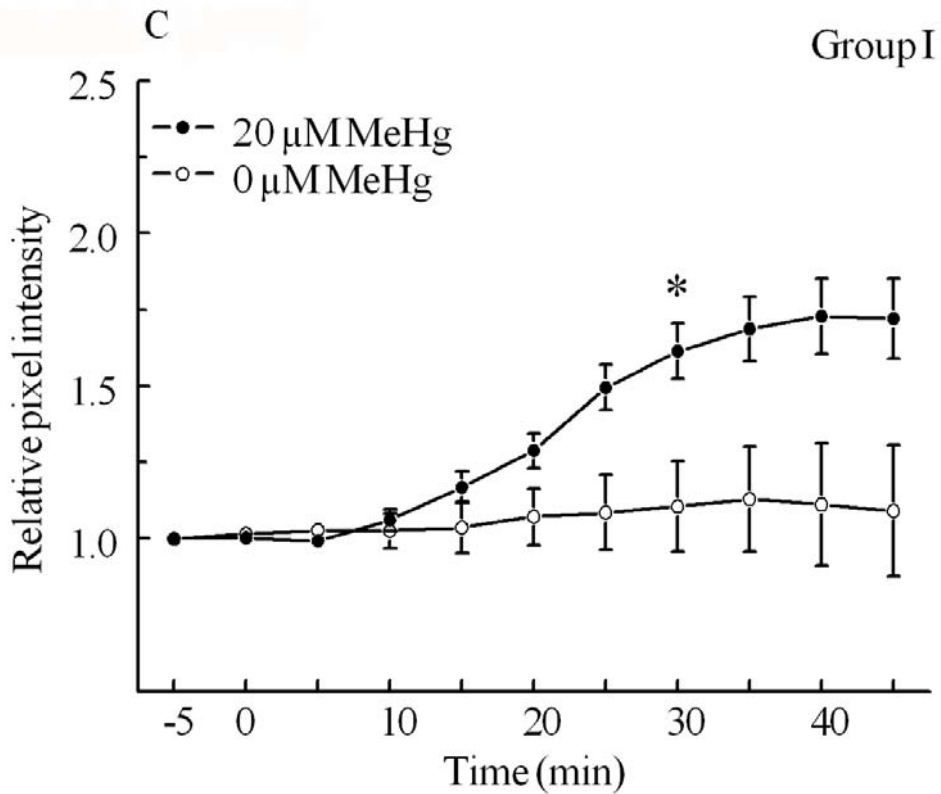
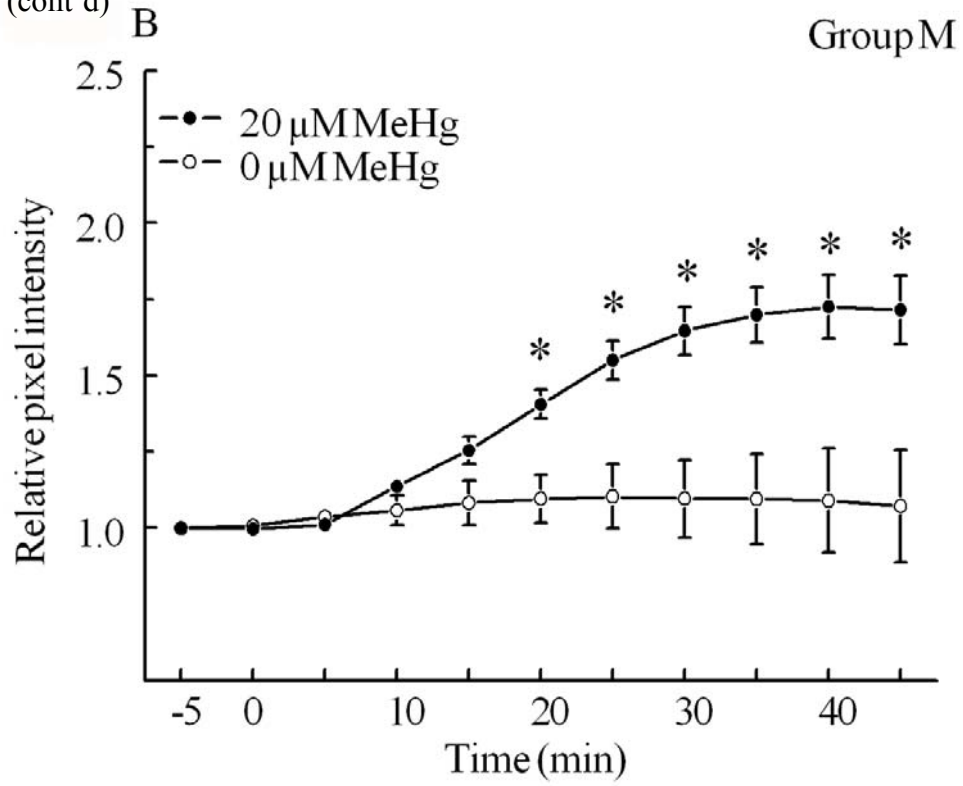
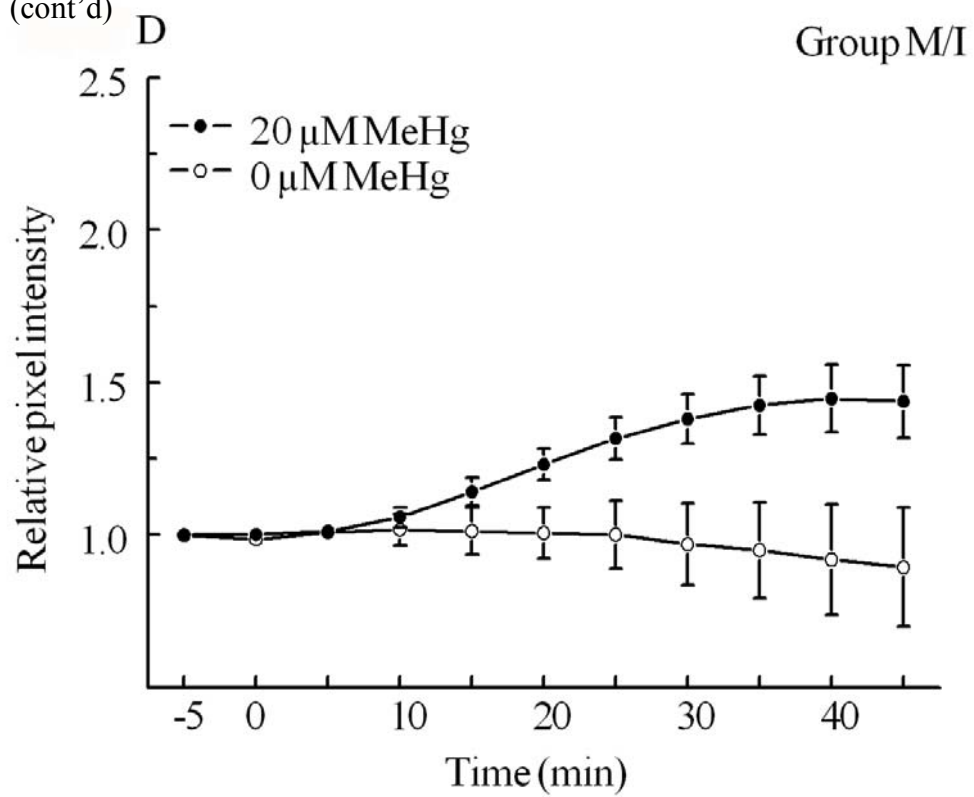


Figure 4.3 (cont'd)



increased relative fluorescence of $194 \pm 14\%$ of baseline. In 6-month chronically isradipine-treated mice (0 MeHg, 2 ppm isradipine, designated I), acute MeHg treatment increased fluorescence $179 \pm 15\%$ over baseline. Finally in 6-month combination treatments (6.25 ppm MeHg, 2 ppm isradipine, designated M/I), acute MeHg caused an increase of $192 \pm 13\%$. All four groups had significantly elevated fluorescence compared to baseline by the end of the experiment. While the two isradipine-treated groups appear to have a smaller increase in fluorescence than the other two groups, this difference was not significant.

Slices from mice treated for 12 months (the last 4-6 from each treatment group) were able to be used for an additional treatment from each subject. This was an untreated control which was continually perfused with ACSF for the imaging period instead of MeHg in ACSF. These treatments indicated that, in all treatment groups, perfusion of ACSF and imaging did not in itself change the relative fluorescence intensities of slices. After 12 months of chronic treatments, acute MeHg treatment increased relative fluorescence $190 \pm 12\%$ in group O (Figure 4.3A), $172 \pm 11\%$ in group M (B), $174 \pm 13\%$ in group I (C), and $148 \pm 12\%$ in group M/I (D). While all these groups displayed smaller increases in fluorescence than their 6 month counterparts, none were sufficiently smaller to indicate significant differences. Where the comparisons do indicate subtle but significant differences between treatments is in time-matched comparisons with the control treatments. Here, slices from the same brain in groups O and M treated with acute MeHg were significantly more intense than ACSF control from 20 minutes onward, while group I was only different at 30 min and group M/I was no different at any time point. This indicates that chronic isradipine treatment subtly reduces the reaction of slices to acute MeHg, regardless of the actions of chronic MeHg.

b. High-speed Ca^{2+} imaging

Slices incubated with fura-2 were given several stimuli meant to evoke Ca^{2+} changes while imaged at high speed to determine detailed time courses of these changes and any differences that might be apparent. Much like the acute MeHg treatment on the confocal platform, changes to the underlying signaling pathways important for each stimuli would be seen under one or more of these treatments. In the 6 month treatment groups, slices were exposed to three stimuli. AMPA, the ligand of fast ligand-gated cation (Ca^{2+} , Na^+ and K^+) channel, was applied to slices first. AMPA binding to AMPA receptors causes Ca^{2+} influx from the extracellular space as well as passing Na^+ and K^+ . The receptor rapidly internalizes or is trafficked to the membrane under various stimuli. NMDA and glycine were applied second in order to activate NMDA receptors, another non-selective cation channel that can pass Ca^{2+} . This step normally requires a voltage change to the membrane to remove Mg^{2+} from the pore, but Mg^{2+} was removed from the treatment solutions to facilitate the ion's removal. Third, slices in this series were forced to depolarize through application of a high $[K^+]$ (40 mM) solution.

The populations of cells chosen for tracking reacted differently to each of these treatments. Even though the use of fura-2 allows for the calculation of precise nanomolar concentrations of $[Ca^{2+}]_i$ when $[Zn^{2+}]_i$ is bound by TPEN, as it is in these treatments, the measurement of maximum fluorescence and minimum fluorescence has not been performed in these cells, so results are provided as relative to the starting ratio of cells.

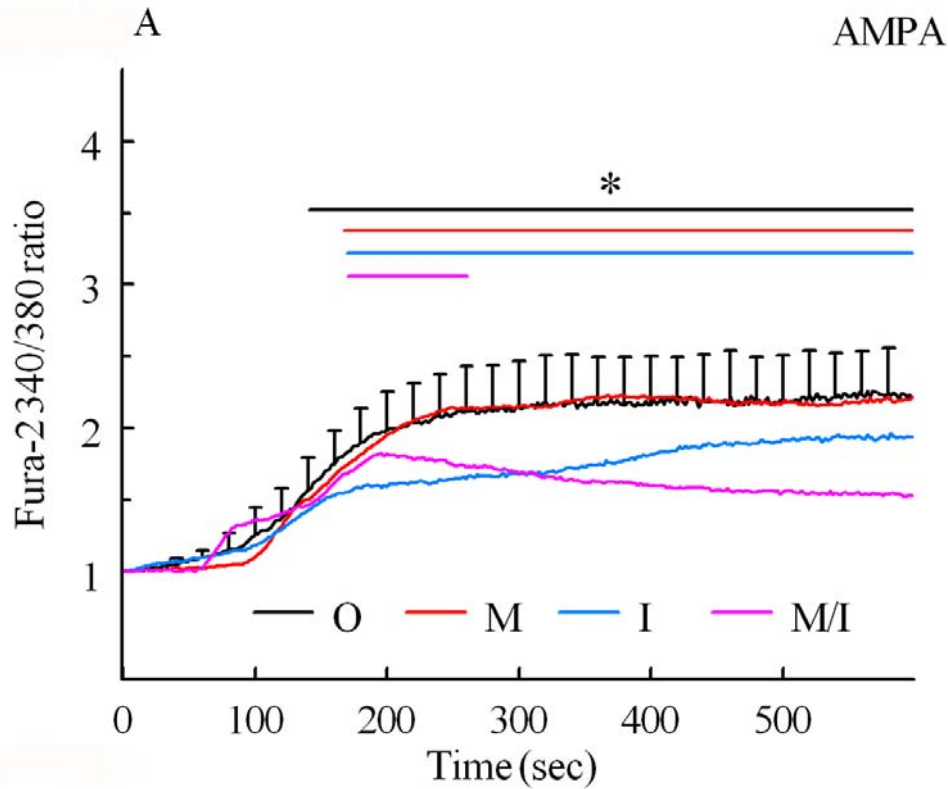
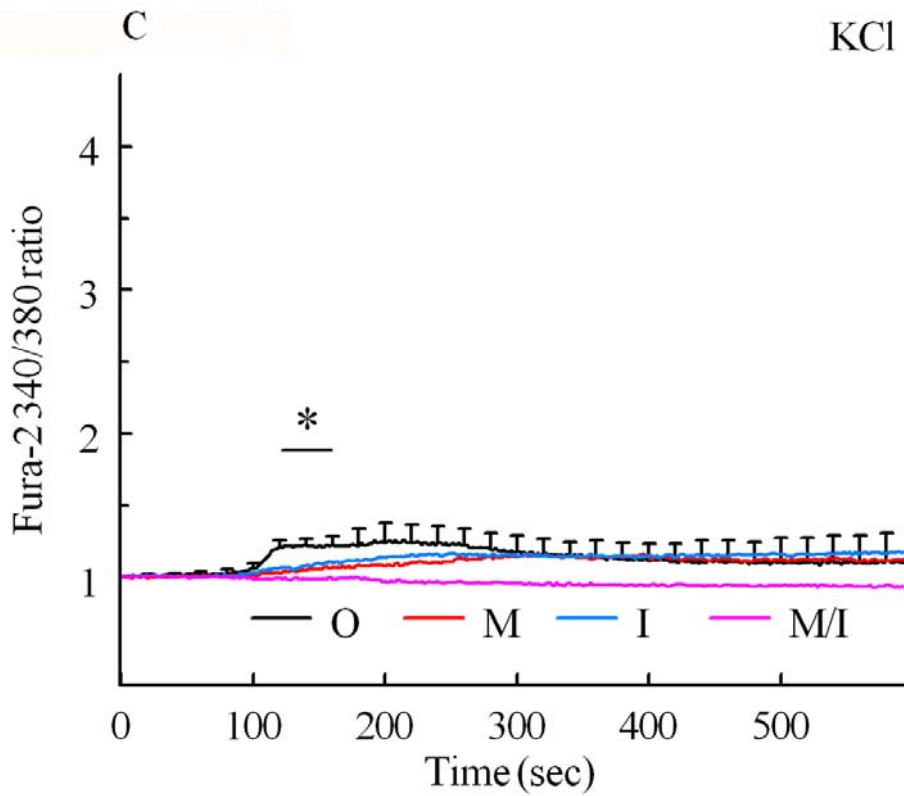
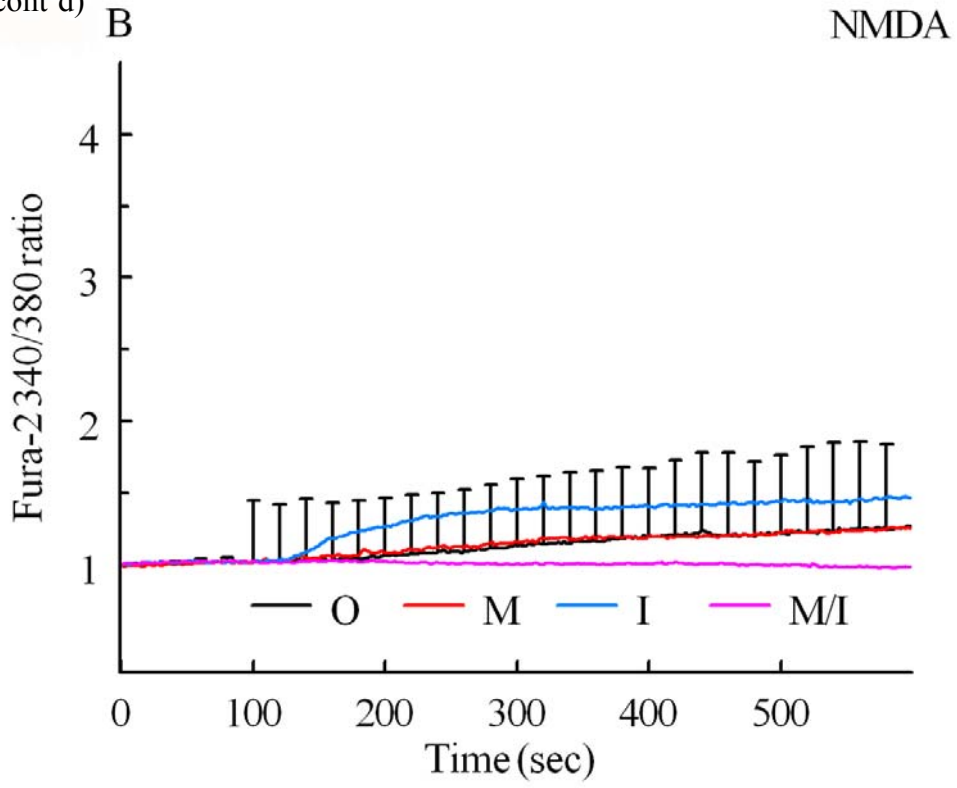


Figure 4.4. Mean relative fura-2 ratio values for acute 25 μ M AMPA, 50 μ M NMDA + 10 μ M glycine and 40 mM KCl applications measured from high-speed (0.5 Hz) time course image series in cerebellar slices from 9 month old mice. Mice were treated chronically for 6 months with MeHg or isradipine. Separate lines represent different chronic treatments, including no MeHg and no isradipine (Group O, black line, n=13, representative +SEM shown), MeHg and no isradipine (Group M, red line, n=11), isradipine and no MeHg (Group I, blue line, n=11), and both MeHg and isradipine (Group M/I, magenta line, n=11). Treatments are in order, and consisted of treatment for 2 min, with approximately 20 s to reach the bath, imaging for an additional 8 min and a 2 min wash between imaging. **A.** AMPA treatment of slices, all four chronic treatment groups responded to the treatment (*, $P < 0.05$ compared to baseline). Several stayed above baseline ratio, while group M/I returned during the imaging period. **B.** NMDA treatment of slices, following AMPA. No population-wide change in fluorescence occurred. **C.** KCl treatment, following NMDA. Only group O showed a significant, population-wide change in fluorescence ratio during treatment.

Figure 4.4 (cont'd)



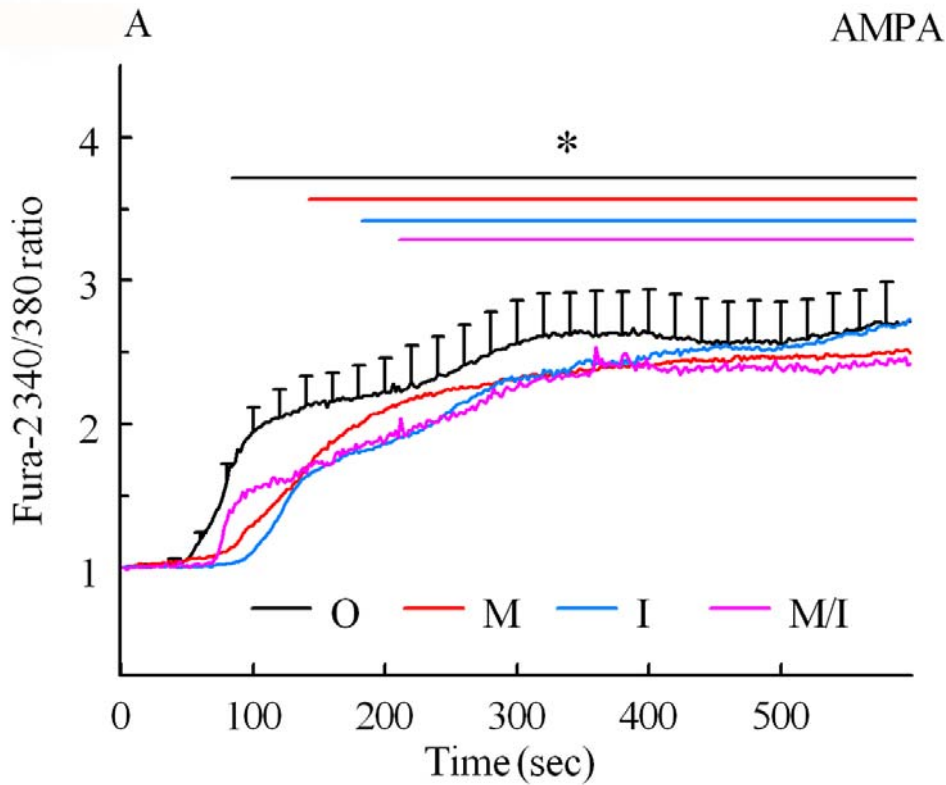
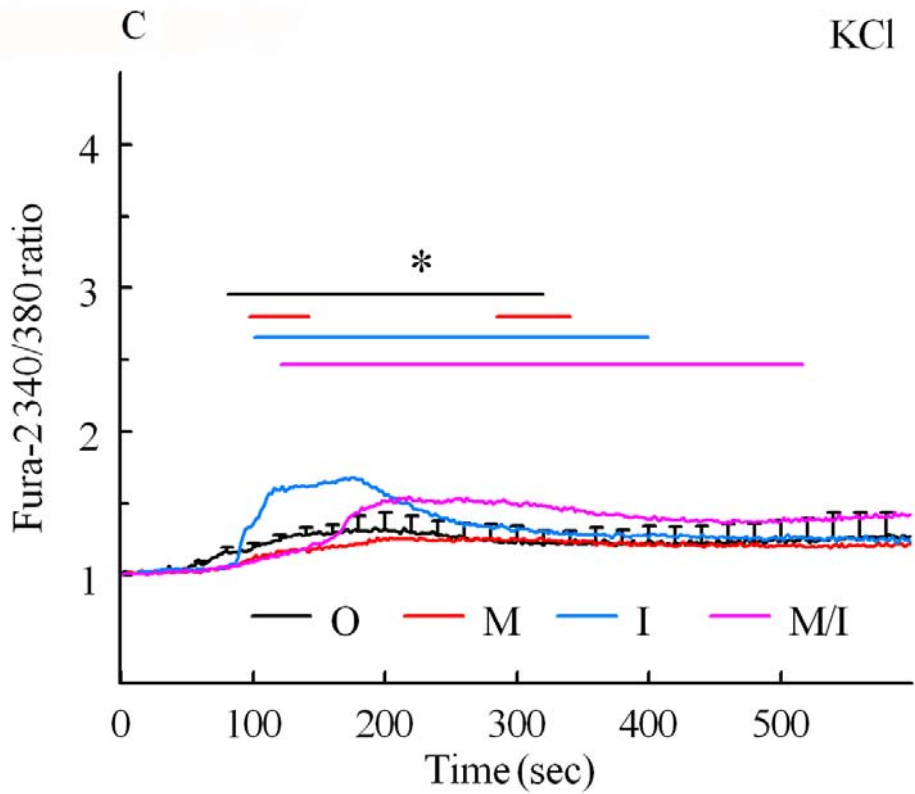
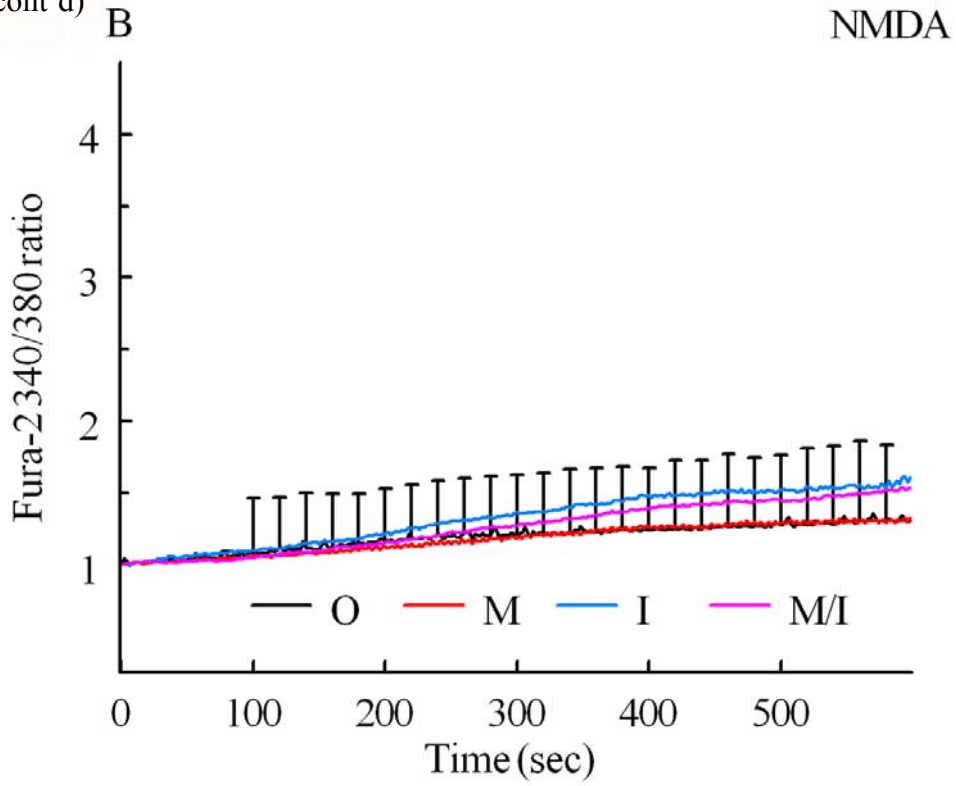


Figure 4.5. Mean relative fura-2 ratio values for acute 25 μ M AMPA, 50 μ M NMDA + 10 μ M glycine and 40 mM KCl applications measured from high-speed (0.5 Hz) time course image series in cerebellar slices from 15 month old mice. Mice were treated chronically for 12 months with MeHg or isradipine. Separate lines represent different chronic treatments, including no MeHg and no isradipine (Group O, black line, n=15 representative +SEM shown), MeHg and no isradipine (Group M, red line, n=17), isradipine and no MeHg (Group I, blue line, n=14), and both MeHg and isradipine (Group M/I, magenta line, n=15). Treatments are in order, and consisted of treatment for 2 min, with approximately 20 s to reach the bath, imaging for an additional 8 min and a 2 min wash between imaging. **A.** AMPA treatment of slices, all four chronic treatment groups responded to the treatment (*, $P < 0.05$ compared to baseline). All stayed above the baseline ratio for the duration of the imaging period. **B.** NMDA treatment of slices, following AMPA. No population-wide change in fluorescence occurred. **C.** KCl treatment, following NMDA. All four chronic treatment groups showed significant responses to treatment, and all were temporary.

Figure 4.5 (cont'd)



AMPA treatment caused the largest and most rapid changes in fluorescence (Figure 4.4A), increasing the relative fluorescence ratio value, R, by up to 226% of baseline in group O. This occurs rapidly, over about 120 s once the agonist reaches the slice. AMPA treatment in the chronic MeHg treatment group M appears almost identical, with a rapid rise and apparent plateau. While not significantly different at any time points from O and M, and despite high variability, the isradipine-treated groups (I and M/I) are closer to baseline at the end of AMPA treatment than the other treatments. Rather than a single phase change as occurred with groups O and M, these groups appear to have multiple phases of $[Ca^{2+}]_i$ increase. Not only that, but where group I shows both phases early, before 200 s, followed by a slow decrease, the traces in M/I are much more protracted. All four treatment groups reach significant increases in their ratios, but again some differences are apparent. Groups O, M and I all reach significance at about 180 s and continue to stay above baseline. Group M/I reaches significance at about 180 s, but due to variability loses such significance by 280 s.

While NMDA treatment, the second in the series, did cause some individual CGCs in slices to react similarly to AMPA treatment, as a whole the CGCs picked out did not react significantly to NMDA, even if they clearly reacted to the previous ligand (Figure 4.4B). Peaks in fluorescence ratio only reached 148% of baseline in group I, while they reached 128% in O, 124% in M and 103% in M/I. R was not different from baseline in any of these treatments, nor were the comparisons between them significant.

KCl depolarized many CGCs across all chronic treatment groups, however due to a high percentage of nonreactive CGCs, overall the population changes in $[Ca^{2+}]_i$ are more subtle (Figure 4.4C). Group O saw a significant increase to 126% of baseline fluorescence as a

population at about 140-180 s, but this was a transient increase. Fluorescence increased steadily as a population in groups I and M, but did not reach significance compared to initial values. Group M/I decreased fluorescence over time, though not significantly from initial time points.

Slices from mice treated at 12 months showed many similar responses to those of the 6 month treatment group. AMPA caused the largest increases, up to 272% in group O, 252% in group M, 273% in group I and 254% in group M/I (Figure 4.5A). While the different chronic treatments did not differ from one another, all were above baseline for most of the imaging acquisition, Group O at about 80 s, Group M at about 140 s, Group I at about 160 s and Group M/I at about 140 s. It appears that some of the treatments may be multiphasic as a population, similar to what happened in some 6 month treated groups.

NMDA treatment at 12 months chronic treatments once again showed no significant changes in overall fura-2 fluorescence in the population of CGCs (Figure 4.5B). As a whole, the 12 month NMDA treatments led to higher fluorescence at the end of imaging than 6 month treatments, including up to 136% baseline in group O, 133% in group M, 161% in group I and 154% in group M/I, but due to variation, the two groups were not different, nor were the treatment groups different from one another.

KCl depolarizations appeared to have a more noticeable effect in 12 month chronic treatment slices, with population-wide transient depolarizations in all 4 chronic treatment groups (Figure 4.5C). Increases occurred between 80-320 s for group O, between 120-340 s for group M, between 120-400 s for group I, and between 140-500 s in group M/I. Due to high variability,

these chronic treatments were not significantly different compared to one another, nor were they different from 6 month treatments.

In the last 5-7 batches of the 12 month treated mice, an additional acute treatment series was added. The first treatment of this series was continuous Mg^{2+} -free ACSF, the starting buffer for all other treatments, to try to establish a baseline for activity. Even without a stimulus treatment, individual, transient fluorescence increases were observed in some cells in slices. In addition to these spontaneous transients, some slices experienced population-wide depolarization despite the lack of a stimulus. This occurred frequently enough that ACSF treatments as a whole showed trends toward increases in the fluorescence ratio. This increase was significant in MeHg treatments, where group M increased at 220 s onward to up to 247% baseline and group M/I increased from 440 s onward to up to 274% baseline (Figure 4.6A). These results indicate that, at least in 12 month chronic MeHg treatment, a change in Ca^{2+} dynamics and homeostasis might be occurring even without stimulus.

Following the ACSF control treatments, a treatment containing muscimol was added to the slice. Muscimol activates $GABA_A$ Rs, and is of interest here. $GABA_A$ R activation is coupled to VGCCs, so it could contribute to changes in $[Ca^{2+}]_i$ even in adult CGCs, and may even depolarize some neurons under stress (Eilers, et al., 2001, Chavas, et al., 2004, Galeffi, et al., 2004). MeHg exposure appears to potentiate $GABA_A$ Rs at least temporarily (Arakawa, et al., 1991, Yuan and Atchison, 2003). $GABA_A$ Rs internalize during stress, so differences in response to muscimol could indicate changes to receptor expression and function (Lyons, et al., 2001, Maguire, et al., 2009, Basu, et al., 2011). In fact, both groups M and M/I show significant increases in fluorescence over baseline (Figure 4.6B). Group M increased significantly over

baseline at about 480s onwards and increased to a maximum of 400% of baseline. Group M/I had a significant increase above baseline from 60-100 s, but grew too variable to continue to be significant. As with all other treatments, population variability was too great to compare chronic treatment groups directly.

Finally, bicuculline was used as an antagonist of GABA_ARs to complement treatment with muscimol. Similarly to NMDA treatment, while there was a tendency for fluorescence to increase in several groups, in this case Group O, Group M/I, and particularly in Group M, there was sufficient variability to keep the increases from significance (Figure 4.6C).

Several factors of slice quality were checked in 12 month mouse slices. Up to 99% of CGCs picked up by automatic tracking were unusable because they started at an inverted ratio of 340/380 fluorescence. This was not dependent on chronic treatment. All groups averaged about 35% of cells in this inverted state. Inverted ratios were not significantly related to the time taken from the end of slicing to the start of imaging by linear regression, nor were they associated with the batch (1-16) of the mouse (data not shown). Similarly, “extinguished” cells as tagged by automated algorithms, displayed that about 15% and up to 58% of the remaining cells lost significant total fluorescence during treatment series and imaging. As with inverted fluorescence counts, extinguished cell counts were also not dependent on chronic treatment, acute treatment or time from slicing (data not shown).

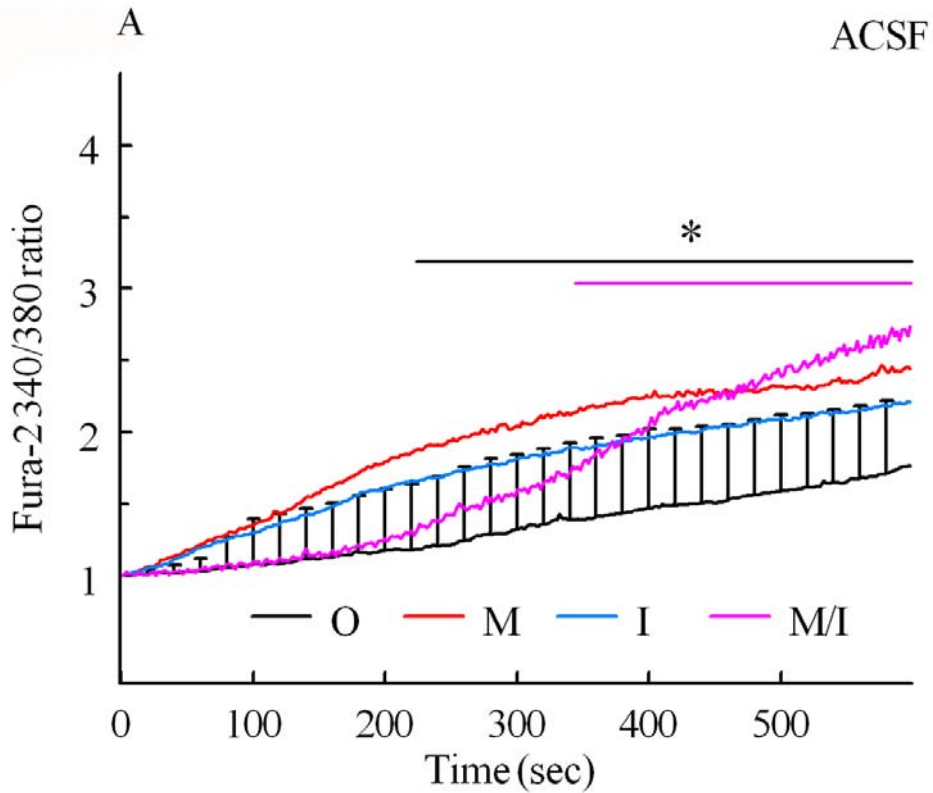


Figure 4.6. Mean relative fura-2 ratio values from acute ACSF control, 100 μ M muscimol and 10 μ M bicuculline applications as measured from high-speed (0.5 Hz) time course image series in cerebellar slices from 15 month old mice. Mice were treated chronically for 12 months with MeHg or isradipine. Separate lines represent different chronic treatments, including no MeHg and no isradipine (Group O, black line, n=5, representative +SEM shown), MeHg and no isradipine (Group M, red line, n=6), isradipine and no MeHg (Group I, blue line, n=4), and both MeHg and isradipine (Group M/I, magenta line, n=6). Treatments are in order, and consisted of treatment for 2 min, with approximately 20 s to reach the bath, imaging for an additional 8 min and a 2 min wash between imaging. **A.** ACSF control treatment (no change from pretreatment) of slices. Both chronically MeHg-treated groups (M and M/I) showed significant responses during this treatment (*, $P < 0.05$ compared to baseline). **B.** Muscimol treatment of slices. Both chronically MeHg-treated groups showed significant increases in fluorescence, including the largest increase of any treatment in Group M. **C.** Bicuculline treatment of slices, showing no significant changes from baseline.

Figure 4.6 (cont'd)

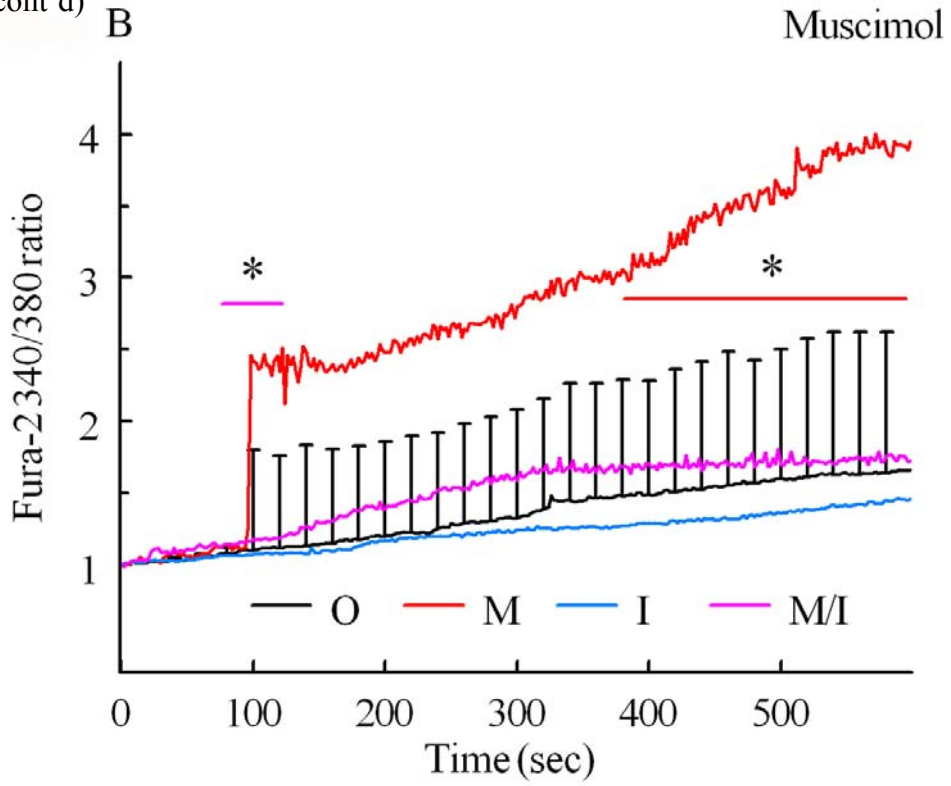
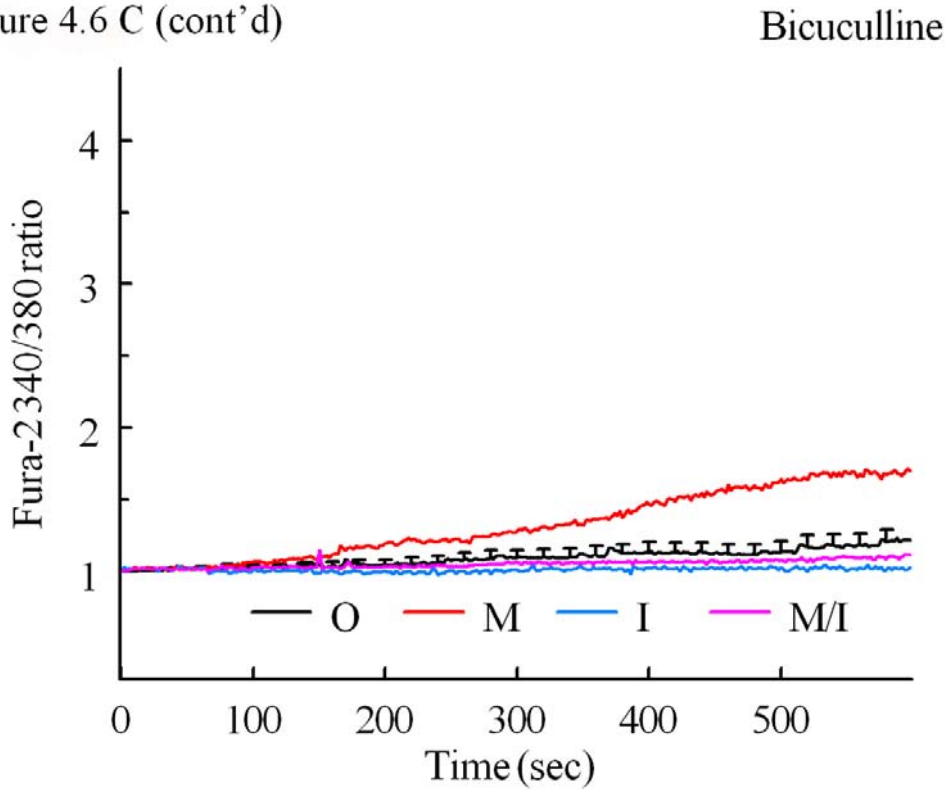


Figure 4.6 C (cont'd)



E) DISCUSSION

Both MeHg and isradipine chronic treatments in adult mice show effects on $[Ca^{2+}]_i$ -dependent mechanisms. None of the chronic treatments substantially protects against acute MeHg disruption of $[Ca^{2+}]_i$, baseline increases in fluorescence all groups at both 9 and 15 months of age are about 2-fold. This response indicates that chronic exposures do not greatly change the response to acute exposures. However, chronic isradipine in diet with or without MeHg subtly reduce acute MeHg disruption of $[Ca^{2+}]_i$, indicating some potential alterations to the underlying mechanisms behind the disruption. At a population-wide level, differences in responses to AMPA, NMDA, KCl depolarization, muscimol and bicuculline are also subtle, but some common differences occur. First, baseline effects at 9 months of age with no chronic treatments appear to be about a 2-fold increase in fluo4 fluorescence in response to AMPA, no population-wide response to NMDA and a transient response to KCl depolarization, the last of which is not seen in other chronic treatments. At 15 months of age, there is a larger increase in fluorescence induced by AMPA, still no population-wide response to NMDA, and a larger response to KCl. Additionally, there is no population-wide response to ACSF, no response to muscimol and no response to bicuculline in this treatment group. Isradipine treatment as a whole appears to reduce both the effects of acute exposure to MeHg and some of the effects of other acute stimuli. Chronic MeHg treatments as a whole appear to enhance both spontaneous depolarization seen in the high-speed imaging of ACSF treatment and the reaction to muscimol.

As for individual treatments, there are subtle differences as well. Acute application of 20 μ M MeHg application on its own does not appear to be much different from results in neonatal mice described in previous chapters, at least as far as fold change in relative fluorescence. 200%

changes to baseline are around the high end for CGCs in the neonatal IGL, but not particularly different, and adult and geriatric mice do not have the more susceptible developing CGCs. There is not a large difference between age groups within this project either. AMPA and KCl treatments display somewhat enhanced $[Ca^{2+}]_i$ responses in the 12 month group, but not remarkably so, and not enough to indicate statistical differences. NMDA application was able to cause responses in some CGCs, but not enough to cause any population-wide increases like other treatments. This may point to the difficulty of requiring Mg^{2+} -free buffer; even though the slices spend over an hour in incubations and baths without Mg^{2+} , endogenous intracellular Mg^{2+} may still be present and may still block many NMDA receptors in the slice. Age effect was not compared in NMDA treatment because of the lack of significant acute population-wide effects. Age effects also were not compared in ACSF, muscimol and bicuculline treatments because they were not used in the 6 month experiments.

Along with mostly subtle effects, some unexpected results complicate the conclusions that could be taken from these sets of experiments. Control treatments were suggested early for slices on the confocal and high-speed imaging platforms, but slices and time were limited, so they were not incorporated until the 12 month treatment period. These control treatments were helpful in finding subtle differences in the confocal results, and allowed for some characterization of $[Ca^{2+}]_i$ -based $GABA_A$ R response in the slices, but the untreated controls produced a surprising result. Many untreated slices depolarized with no stimulus. It is unclear what might have caused such a depolarization, it is possible the change from incubation in a 5% CO_2 incubator to perfusion with 95/5% O_2/CO_2 ACSF buffer could disturb the neurons enough to depolarize. Even with a 10 min wash before imaging, this depolarization happened frequently

enough during the ACSF control treatment that the overall fluorescence means increased in some treatment groups. The significant changes in fluorescence shown during the ACSF treatment of slices are particularly problematic to the other results, because it indicates that at least in the older mice that individual cells and even the whole slice can depolarize at any time, meaning that at least some of the depolarization noted in other treatments may not be due to treatment. It is particularly confusing when compared to NMDA and bicuculline responses, which both had small, mostly linear responses over time. As a population, those responses might now be considered to be lower than no treatment, as they don't cause any mean increases in $[Ca^{2+}]_i$. It might be possible to further characterize this issue, but it would require more adult mice and possibly more chronically-treated mice. An ACSF treatment like this could at least be used as a baseline for comparisons to the AMPA treatments from the same animals, as they were both the first in a series. This could be performed similar to paired comparisons in Chapter Three and to some extent in the second set of confocal results in this chapter. Spontaneous depolarization may also contribute to the apparent multiphase traces of some AMPA depolarizations. Some of the issues in comparing populations of CGCs in these experiments may also be solved by comparing individual traces instead of population means.

Few chronic treatment studies have directly characterized Ca^{2+} -dependent biochemical mechanisms. This is in part because many characterizations, including the Ca^{2+} imaging presented here, require euthanasia of the animal. Most rely on behavioral monitoring followed by pathology or other fixed tissue or homogenized end-points, such as total neurotransmitter or ROS concentration, instead of live or *ex vivo* experiments on tissue (Heath et al., 2010, Bourdineaud, et al., 2012). In one experiment that isolated and plated live CGCs, these

dissociated CGCs from aged mice treated acutely with MeHg showed no difference in basal $[Ca^{2+}]_i$ levels (Bellum, et al., 2012). This is not surprising as this basal $[Ca^{2+}]_i$ at the time collected could easily be based more on the age of the animal than an acute dose of toxicant. The differences in ROS and mitochondrial depolarization detected in that same set of experiments indicates that Ca^{2+} -dependent mechanisms are still involved in acute toxicity. Here we demonstrate changes to Ca^{2+} dynamics imaged live in slices as opposed to single measurements in dissociated CGCs. Results here of course are part of a larger project, and the results from approaches such as electrophysiology, ATP production, gene expression, histology, and behavior have not yet come together. Behavioral approaches in this collaboration are also coming together, indicating that another Ca^{2+} blocker, nimodipine, is able to reduce or eliminate behavioral deficits in memory acquisition and performance caused by MeHg (Bailey, et al., 2013). These comparisons are needed for this project to piece together many conclusions; changes determined in other approaches will complement results here and these results will complement the other approaches. For instance, we show here several differences in responses to receptor agonists. If gene expression or immunohistochemistry results indicate a difference in $GABA_A$ R expression with chronic MeHg treatment, then the differences in fura-2 response in the muscimol results presented here could be interpreted as due to expression. Gene expression may in fact be the keystone to this project, as chronic exposures, particularly those that don't cause overt effects, may still alter gene expression, signaling pathways and susceptibility to other treatments. This collaboration of biochemical, behavioral and pathological approaches to studying the toxicity of MeHg may redefine the level of complexity that can be assessed and integrated in toxicological studies.

CHAPTER FIVE

HIGH-SPEED Ca^{2+} IMAGING REVEALS SPONTANEOUS Ca^{2+} TRANSIENTS IN CEREBELLAR SLICES FROM YOUNG AND OLD MICE

A) ABSTRACT

Spontaneous neuronal and glial activity is a hallmark of many normal functions of the central nervous system. Loss of this activity can have profound effects, such as those associated with neurodegenerative diseases. In experiments meant to optimize imaging of small, transient calcium responses in cerebellar slice preparations to depolarization, agonists and the neurotoxicant methylmercury, we regularly visualized unexpected spontaneous increases in fluorescence in some cells. We imaged fluo4 fluorescence, an indicator of internal Ca^{2+} concentration, in slices of mouse cerebellum with a high-speed CCD camera and epifluorescence microscope. Images were acquired at 2 Hz and 60x magnification and focused on cells from the internal granule cell layer. Groups included young (PND 8-14) (+/+) and $\text{GABA}_A\text{R } \alpha 6$ (-/-) mice and 22 month-old (+/+) mice. The knockout line lacks tonic inhibition in mature cerebellar granule cells and displayed increased calcium responses to MeHg exposure in previous experiments. Older animals may also display differences in calcium homeostasis, contributing to susceptibility to toxicity and neurodegeneration. Previous experiments determined that stimuli such as NMDA receptor activation induce Ca^{2+} transients and activity in cells, but stimulus-free activity has not been detailed previously in cerebellar slices. During pre-treatment imaging in all cases, spontaneous increases in fluorescence occurred in 4 - 33% of visible cells. Events were rapid; typically within 2.5 seconds they increased fluorescence 50-300% compared to the mean of the whole trace. Fluorescence returned to a steady baseline near the pre-event intensity over 2-12 seconds in young mouse cerebella. There was no significant difference between young (+/+) and (-/-) number or intensity of spontaneous activity, suggesting these events are not in general related to $\alpha 6$ -containing GABA_ARs in of granule cell neurons. However, young (-/-) mice had a

larger number of shorter duration transients in their distribution than their (+/+) counterparts, suggesting there might be different forms of these transient in the distribution. In slices from older mice, it appears that there is no rapid return to baseline; spontaneous events remained near their peak for several minutes of imaging, and the slices contained more long events than short. In all groups, events were smaller, shorter and occurred in fewer cells than fluorescence increases associated with depolarization of the whole slice. Among spontaneous events, cells showed a variety of responses, including synchrony and repetition, unrelated to imaging conditions. The identity of cells involved in these events is not certain, but based on location, shape and relative abundance they could be glial cells or processes such as basket cell terminals rather than neurons. These unexpected results show clearly that it is possible to regularly image spontaneous live activity in slices of cerebellum in a relatively simple setup.

B) INTRODUCTION

As introduced in previous chapters, MeHg is a neurotoxicant that targets the cerebellum, particularly developing CGCs. Molecular targets include GABA_ARs and several other regulators of cellular Ca²⁺ homeostasis. We have utilized multiple techniques for recording MeHg effects on molecular targets, including electrophysiology and cell viability assays, and this dissertation has already shown several approaches using cerebellar slices and Ca²⁺ imaging. Chapters Two through Four all indicate that MeHg and other agents alter [Ca²⁺]_i in young and old animals. Both Chapters Two and Three indicate subtle effects of GABA_AR modulators in attenuating the effects of MeHg on [Ca²⁺]_i. Additionally, Chapter Three indicates that knockout of the α6 subunit of the GABA_AR in mice makes immature CGCs more susceptible to [Ca²⁺]_i increases induced by MeHg.

Despite the multiple results indicating GABA_ARs and Ca²⁺ signaling as important components of MeHg toxicity, confocal imaging approaches do not offer optimal temporal resolution for these events. This is particularly noticeable in the response of cerebellar slices to muscimol versus bicuculline. In order for an agonist to desensitize a receptor, as has been suggested for the reason muscimol appears to antagonize GABA_AR_s in confocal images of Chapters Two and Three, it must first activate the receptor. In this case GABA_AR activation by muscimol is expected to temporarily increase [Ca²⁺]_i before desensitizing the receptor, preventing some of the potentiation associated with MeHg. This connection between GABA_AR activation and an increase in [Ca²⁺]_i has been established in several models (Eilers, et al., 2001, Brodinsky et al., 2003) and has even been shown in previous imaging experiments in our lab

(Limke, dissertation observation). Despite this, confocal results in Chapters Two and Three do not indicate the presence of a transient increase in $[Ca^{2+}]_i$.

With the possibility that confocal imaging is missing subtle alterations in Ca^{2+} dynamics, we sought to visualize $[Ca^{2+}]_i$ in a system that acquires images rapidly. Ideally this approach could still sample from a large population of cells in slice and utilize protocols already established, such as the use of the bath-applied fluorophore fluo4. In addition, we sought to measure $[Ca^{2+}]_i$ activity in slices from multiple groups for comparison, including those in developing mice, where CGCs are still migrating, in adult and geriatric mice and in a mouse line lacking the $GABA_A R \alpha 6$ subunit. Because higher temporal resolution requires larger imaging data sets, we sought to automate the selection of cell regions of interest (ROIs) and analysis of $[Ca^{2+}]_i$ activity where possible. These are the first steps to optimizing a new approach where we could compare the Ca^{2+} dynamics involved in MeHg and test hypotheses generated by other experiments, such as whether or not there is a transient Ca^{2+} influx in slices treated with muscimol. The results here were surprising, in that we uncovered Ca^{2+} activity that could be measured without providing a stimulus. These experiments did not achieve the intended outcomes and optimizations, such as a collection of depolarizations and MeHg treatments in slices, but are presented primarily as a baseline for future experiments.

C) MATERIALS AND METHODS

a. Chemicals and solutions

Chemicals and solutions used for these experiments have been described previously in Chapters Two and Four. These include ACSF, sucrose slicing solution, fluo4 and ACSF with 40 mM KCl. Where handling is any different, the methods are described here in full. All solutions were continuously bubbled with 95%/5% O₂/CO₂ during all experiments.

b. Animal care and use

All animal use was in accordance with NIH guidelines for laboratory animals and all procedures were approved by the MSU Institutional Animal Care and Use Committee. As this was primarily an attempt to develop protocols for use of a high-speed epifluorescence microscope platform for use in the experiments described in Chapter Four, these experiments included tissue from multiple sources. Tissue included cerebella from post-natal day (PND) 7-14 GABA_AR $\alpha 6$ (-/-) and (+/+) mice included in the experiments of Chapter Two. Additionally, one 3 month (+/+) mouse from the same colony, and two 22 month IRC mice (Harlan, Frederick, MD) from a separate experiment not described in this dissertation were used. The 3 month mouse was grouped with the 22 month mice for the purposes of having two groups, and did overlap with the young mice in any measures taken.

Collection of cerebella was described previously in Chapters Three and Four. For young mice, cerebella were collected as in Chapter Three, with rapid decapitation and slicing in ice-cold slicing solution. For adult mice, collection was performed as described in Chapter Four,

with cardiac perfusion of near-frozen blended slicing solution, decapitation and slicing in blended slicing solution. Slice incubations were similar, acclimation in ACSF contained in a heated water bath at 37°C for 30 min, followed by 30 min at room temperature (23-25°C) and 1 h in an opaque container for fluo4 incubation before use. Multiple slices from the same animal were used if possible.

c. Image acquisition and treatment

Slices were moved from incubation to a chamber on an inverse epifluorescence microscope (Nikon Eclipse TE2000-U) and anchored in a bath of ACSF perfusing at about 2 mL/min. Slices were illuminated using a fast switching polychromatic light source (Polychrome V, Till Photonics, GmbH), set at 488 nm excitation and 512 emission, through a custom dichroic filter (Chroma 71000A Fura2 C59742), a 40x oil objective and either a 1x or 1.5x mirror. A low fluorescence oil (FF, Cargill, Cedar Grove, NJ) was used for the oil immersion beneath the chamber. Illumination time was minimized by switching to live software imaging (Till Vision, Till Photonics) when possible rather than constant illumination through the eyepiece. Images were captured using an electron-multiplying CCD camera (iXon EM+, Andor, South Windsor, CT)

Regions of the slice were chosen that contained at least several dozen visible and clear CGCs and no visible tissue damage or scarring. Exposure time was adjusted so that the bulk of visible cells was at about 25% of the camera's available maximum, to allow for optimum dynamic range. Once a frame of interest was ready, 512 x 512 images were taken in series at 2-4 Hz for 150-600 s, depending on treatment. Some slices received treatment after 150 seconds,

consisting of 40 or 80 μM KCl ACSF, 20 or 100 μM MeHg. Since none of these treatments were repeated sufficiently often for quantitative comparisons, only the initial 150 s before treatment were compared from these slices, and treatments are only noted as qualitative comparisons.

Image series were exported from TillVision software as tagged image files (.tif) and imported into ImageJ. Image series were trimmed if they contained treatments and backgrounds were subtracted using a 50 pixel rolling ball radius method. These processed files were moved into a folder for batch processing by the LC_Pro plugin, which is designed to find intensity transients in large populations of cells based only on the size of the cell (Francis, et al., 2012). The total count of cells determined by the algorithm was obtained while the algorithm ran; it is not present in the output. These cell counts also do not account for regional differences, such as the EGL present in young mice, so they are not compared to framed region areas, as previous experiments. Outputs from the algorithm include number, repetition, significant traces, and location of each of the significant events. Means of several parameters, including number of total cells, percent active cells, intensity of events and frequency of events was calculated for each of the three groups and compared using T-tests. Duration of transients was plotted as a cumulative % histogram and maximum distance (maxD) was calculated and compared to the critical difference (critD). To calculate critD, the standard deviation ($\sigma = 1.36$ for $\alpha=0.05$) was multiplied by the square root of the sum of counts to be compared divided by the product of the counts to be compared ($\sigma * \sqrt{(\text{sum of counts} / \text{product of counts})}$). For comparing young (+/+) (n=47 events) and young (-/-) (n=416 events), critD was 16%. Comparing young (+/+) and old (+/+) (n=26 events), critD was 30%

D) RESULTS

a. Visualization of CGCs

CGCs labeled with fluo4 were characterized as small round somata clustered in the IGL, and in young slices also in the EGL. A frame of interest contained these CGCs in at least 25% of the frame. Pixel size of CGCs was dependent on magnification (40x or 60x), but equaled 5-10 μm , with the larger CGCs situated in the IGL compared to the precursors in the EGL. Unlike confocal recording, the entire slice thickness could not be scanned, so some of the CGCs remained out of focus. Slightly out of focus cells were still trackable. Slices of cerebellum from young mice had characteristic layers as described in Chapter Three, with CGCs in the EGL, IGL, and sometimes migrating through the ML, though without scanning of the slice these ML CGCs were not always present.

b. Spontaneous Ca^{2+} transients

Spontaneous flashes of fluo4 from some cells were noted even while acquiring a frame of interest for treatments. These were concentrated in cells, with the brightness of the flash often extending throughout the frame due to reflectivity. Some transients occurred in cell soma in focus, presumably CGCs because of the size, shape and positions, while other flashes were out of focus or out of the frame. These events were visible, but were shorter and less intense than those caused by stimuli such as depolarization (Figure 5.1).

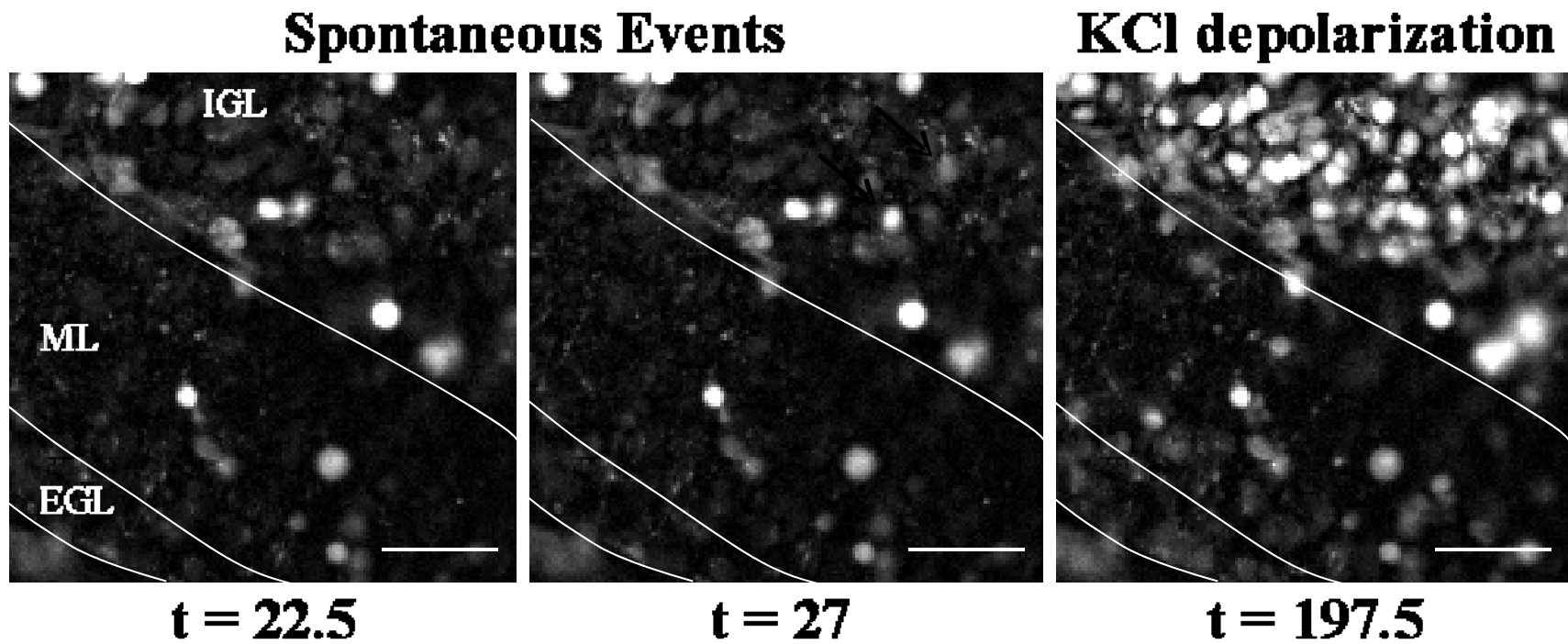


Figure 5.1. Example of two spontaneous events and KCl depolarization from a young (+/+) mouse cerebellar slice loaded with fluo4-AM. Images are registered, cropped and contrast enhanced for clarity. Images were captured at 60x magnification; the scale bar equals 100 μm . Two nearly simultaneous events in the IGL are depicted in the first two images. The first image is just before the events and the second at the peak intensity. Arrows indicate the two cells showing the events. This slice was later treated with high [KCl] ACSF for the purposes of depolarizing the slice. Peak depolarization is depicted in the third image. The two cells that displayed spontaneous transients were depolarized by this treatment, as were most cells in the slice.

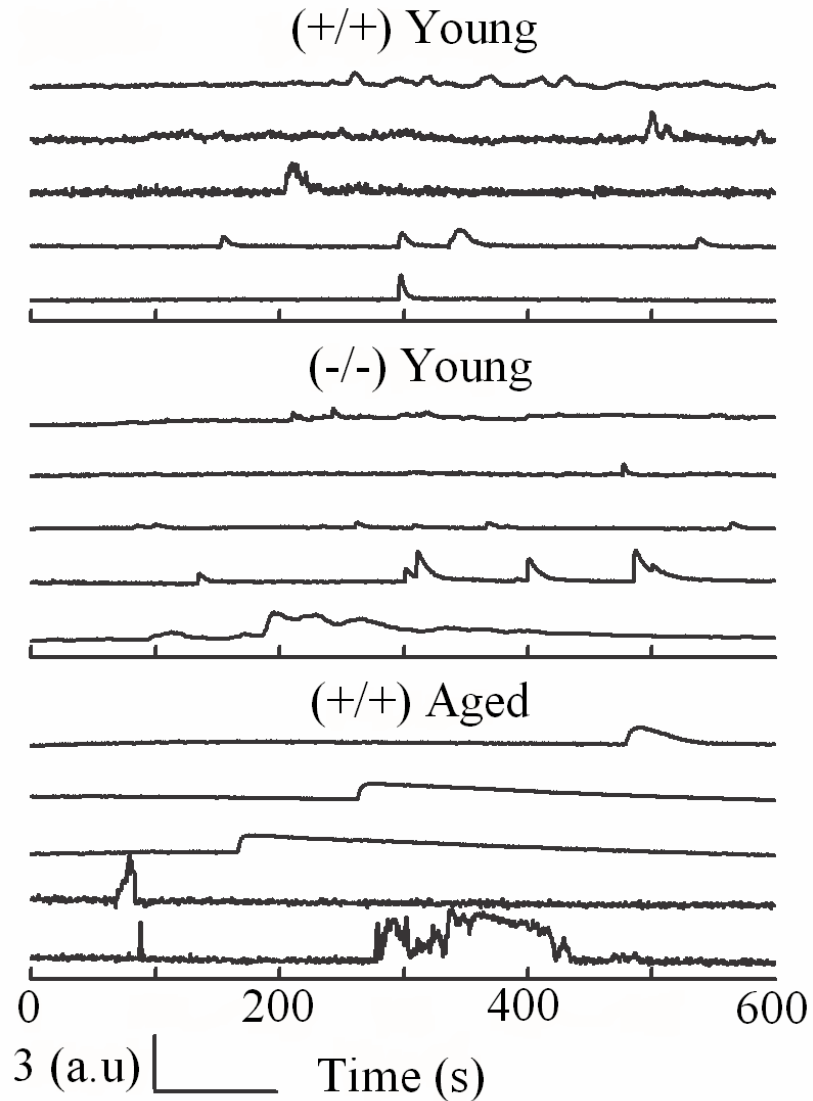


Figure 5.2. Representative fluo4 intensity traces from cells in three groups. Each trace is normalized to the mean intensity value of the individual trace, so units are relative. The first group is traces from young (PND 4-14) $\text{GABA}_A \alpha 6$ $(+/+)$ mice while the second is traces from young $(-/-)$ mice. The third set includes traces from older mice (22 months) from a separate line, so they are considered $(+/+)$ for the purposes of these results. Some qualities of the traces can be seen from these examples. Note that several spontaneous events are repeated in young animals and the fluo4 events in aged animals were much more protracted..

An ImageJ plugin, LC_Pro, was used to assess these flashes. From an image series with background subtracted and images registered to avoid movement, LC_Pro took image series and determined the presence of cells then proceeded to tally and characterize any significant increases in live cell fluorescence, in this case fluo4.

Subjects were originally intended to be divided into 3 age groups, young, adult and geriatric, however not enough adult and geriatric mice could be gathered in the available time frame and hence the two groups were combined. The adult (3 mo) mouse and the geriatric (22 mo) mice had enough repetitions each to determine that the groups were not significantly different in number of cells counted, % of active cells, and peak intensities. Mice were subsequently divided into age and genotype groups, including (+/+) young ((+/+) Y), (-/-) young ((-/-) Y) and (+/+) aged ((+/+) A).

LC_Pro returned 482 events from frames of interest across a total of 23 slices used (Figure 5.2). These events occurred in 389 unique ROIs out of a total of 1615 ROIs. Once stratified into age and genotype groups, the groups did not differ in number of cells counted in frames of interest (Figure 5.3), or intensity of events (Figure 5.4), (+/+) A mice had significantly fewer active cells producing transients as a percent of total cells, ($4 \pm 3\%$) compared to (+/+) Y ($19 \pm 4\%$) and (-/-) Y mice ($27 \pm 6\%$) (Figure 5.5).

Additionally, the duration of these transients appears to differ by group. Because of the wide distribution and variability of events, even though the mean duration of events in aged mice was over 20-fold longer than in young mice, the comparison could not be made from mean values, but had to be calculated from cumulative distribution plots. (+/+) A mice have a longer

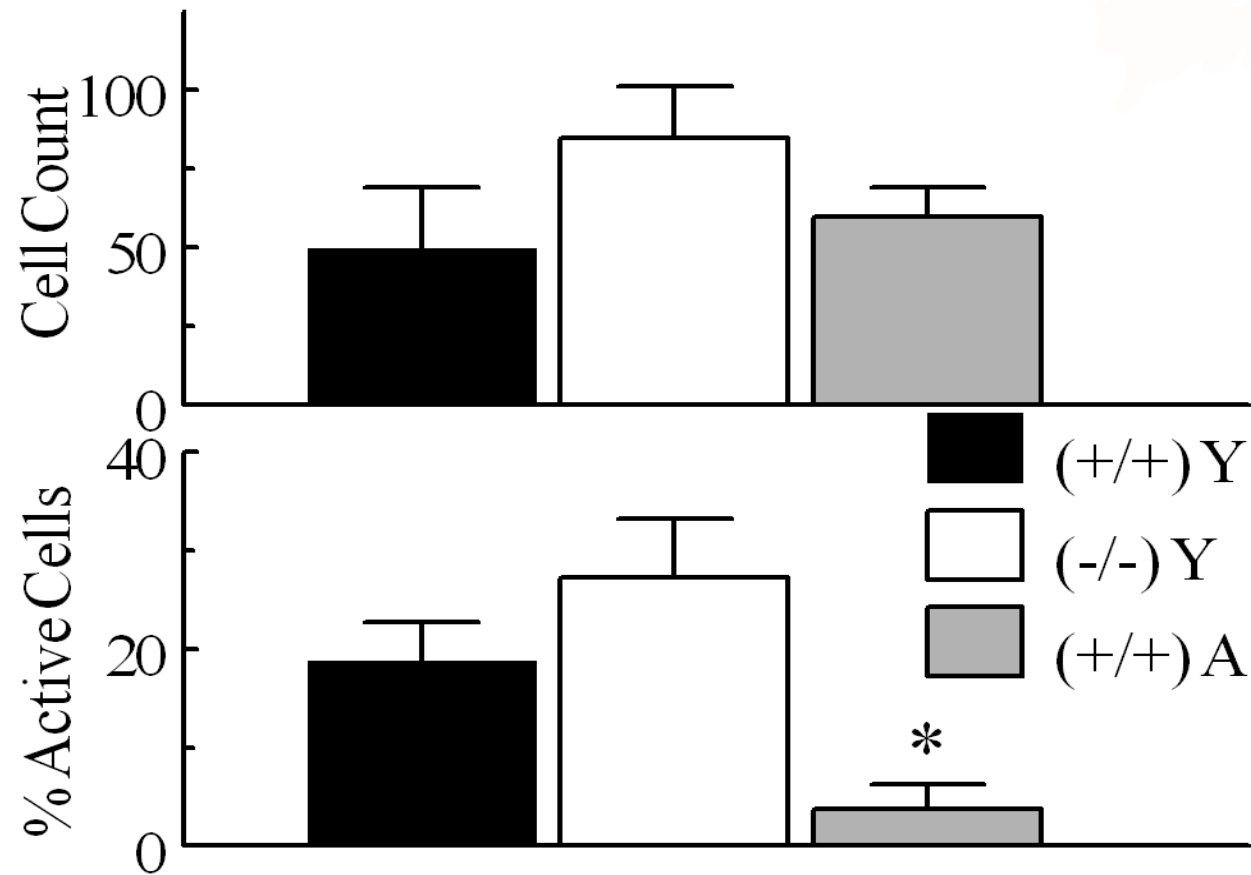


Figure 5.3. Slice characteristics from total cell and active cell regions of interest (ROI). Parameters from the automated event counter included cell counts and unique event ROIs, allowing a count of total cells as well as active cells. Because of the differences between layers in young (Y) and aged (A) mice, these counts are not divided into layers or corrected to calculate cell density as has been performed in previous experiments in this dissertation. No significant differences were found in comparisons of total cell count. Young $\alpha 6$ (+/+) and (-/-) slices showed 13-33% active cells while aged slices only showed about 4% compared to total fluorescent cells, which is significantly fewer ($P < 0.05$).

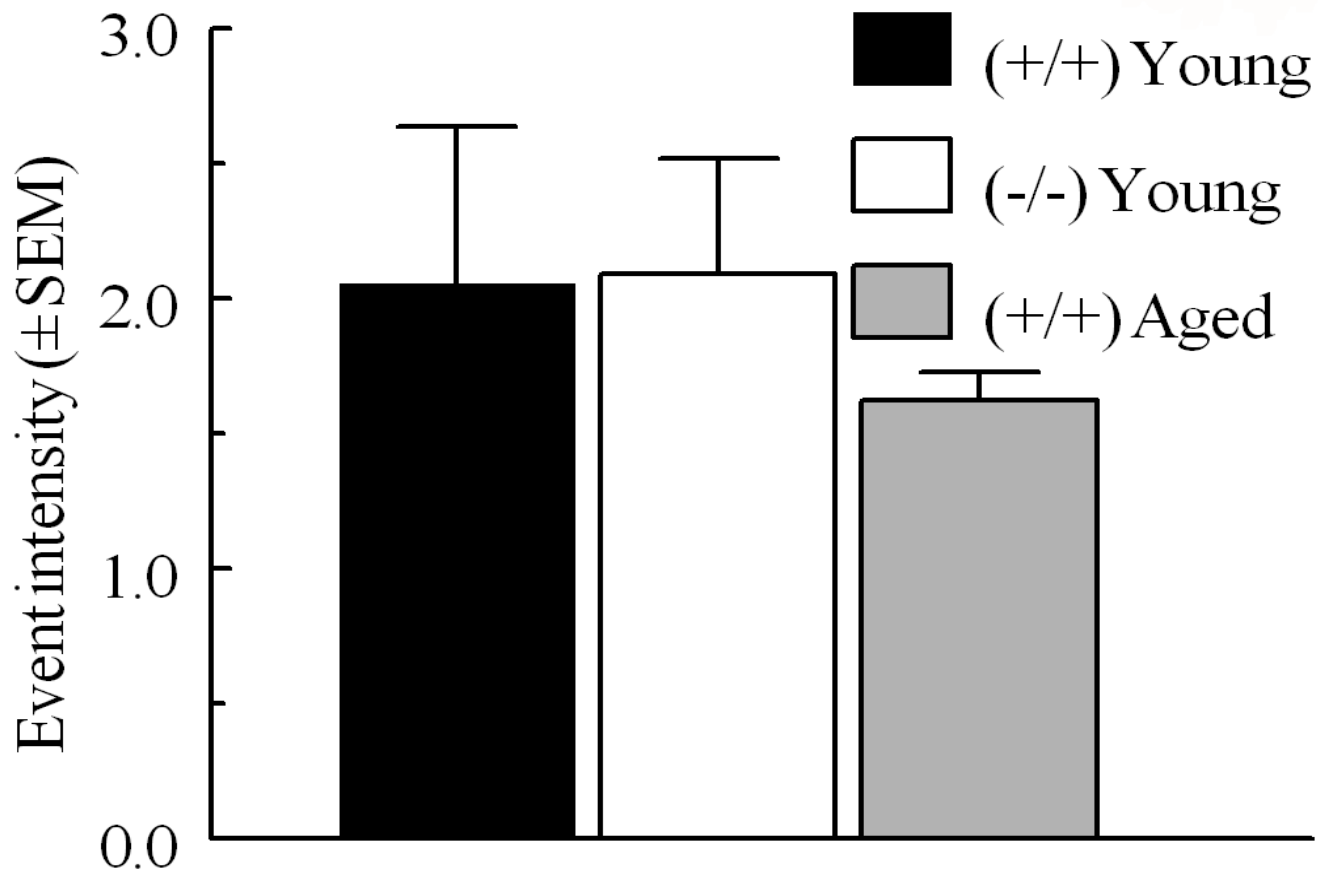


Figure 5.4. Mean fluo4 intensity of events within frames of interest in slices from $\alpha 6$ (+/+) and (-/-) genotypes and young and old age groups. Event parameters were calculated relative to the mean value of an ROI over all time points, so values are relative. Even though it appeared that (+/+) A had lower overall intensity, there were no significant differences.

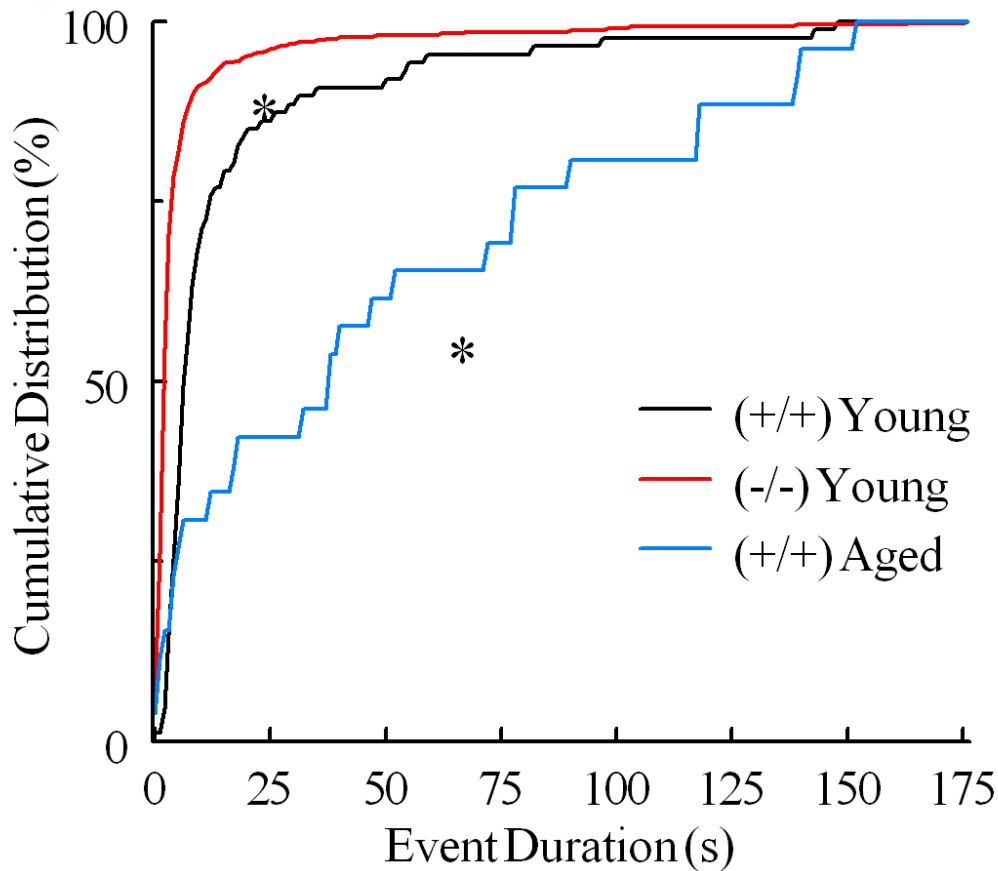


Figure 5.5. Cumulative distribution of event durations in slices from $\alpha 6$ (+/+) and (-/-) genotypes and young and old age groups. Events were distributed into 1 sec bins and plotted cumulatively up to 100% and out to the longest duration of 174 sec. Because of the relative differences in number of total events, young mice have a smoother distribution. Statistics were run comparing the largest % difference between distributions and comparing to the critical difference (D) calculated from event counts and standard deviation (σ). Slices from young (-/-) mice had significantly more short duration events than (+/+) mice, while slices from aged (+/+) mice had significantly more long duration events.

distribution than (+/+) Y, meaning that more of their transients last longer. At the maximum difference, 97% of transients in (+/+) Y are less than 33 s long, while only 42% of (+/+) are less than 33 s. In contrast, (-/-) Y mice have a shorter distribution compared to (+/+) Y. 70% of (-/-) Y transients are less than 5 s long, while only 15% of (+/+) are that short. While this could have been due to frequent repetition in (-/-), it does not appear that transients repeat significantly more in (-/-) Y compared to (+/+) Y, while (+/+) A mice have almost no repetition of transients (Figure 5.6).

Overall this indicates that older mice have fewer, but longer Ca^{2+} transients, many of which appear to be due to long tails. Additionally, while the $\text{GABA}_A\text{R } \alpha 6$ (-/-) do not have a phenotype, and do not differ from (+/+) in percent of active cells or frequency of repeated firing, they do appear to differ in spontaneous activity, with more short duration events. The frequency of events in (-/-) young, which would reflect an increase in repetition of the transients, is several fold greater by mean, 0.23 Hz, than (+/+) young at 0.04 Hz, but is not significantly different.

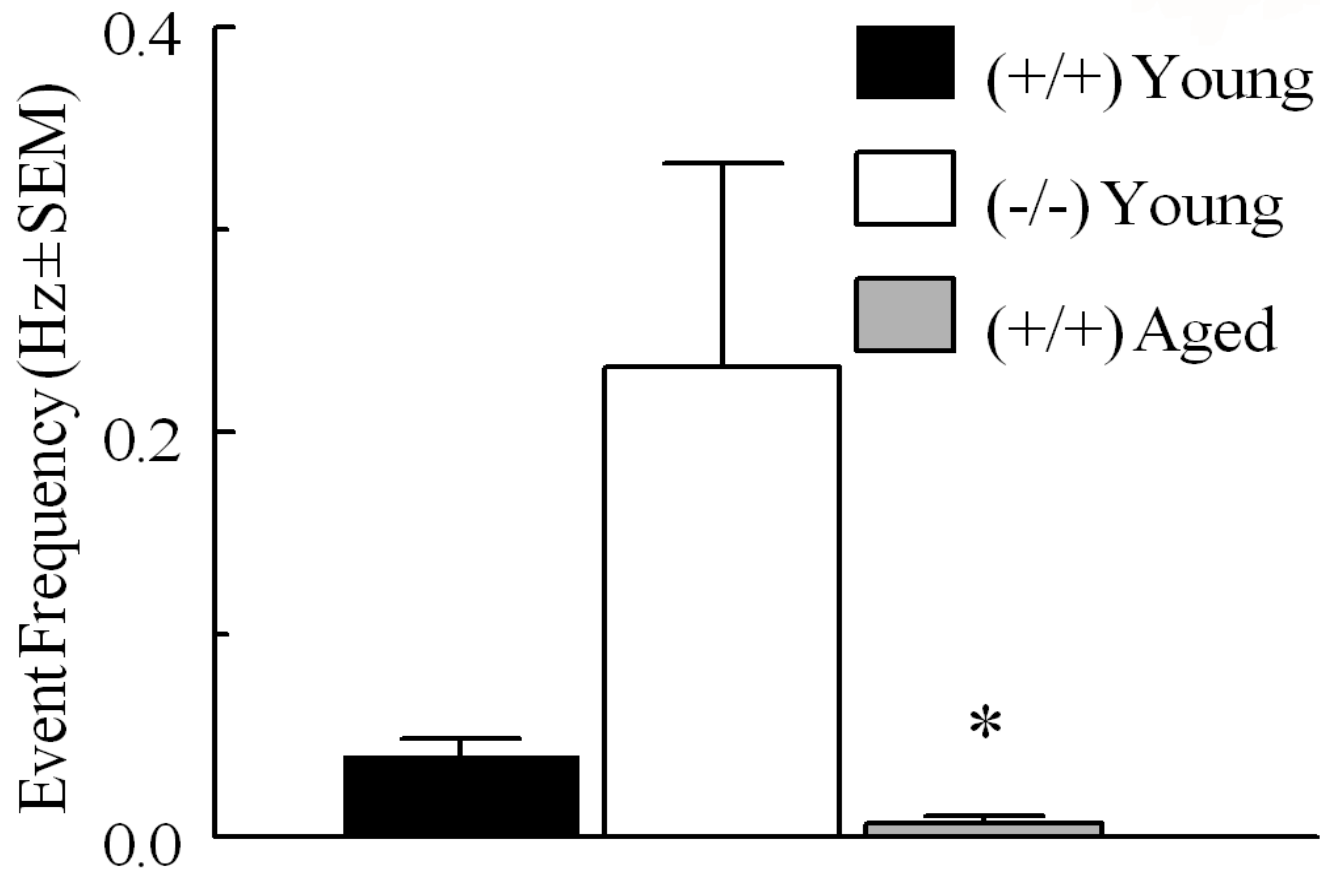


Figure 5.6. Mean frequency of events in slices from $\alpha 6$ (+/+) and (-/-) genotypes and young and old age groups. Frequency was calculated from the total events over total time, with some total times reduced to just pretreatment time to focus on the spontaneous events. All slices had at least one significant event. Events occur about every 20 s in young (+/+) slices, about every 4 s in young (-/-) slices and about every 150 s in (+/+) aged slices.

E) DISCUSSION

The presence of spontaneous transient Ca^{2+} events in slices came as a surprise, while electrophysiological monitoring of neurons and interneurons in slices frequently show spontaneous activity, Ca^{2+} transients without stimulation have not been characterized visually with epifluorescence microscopy. In confocal imaging used in Chapters Two through Four, because of the long time between image captures, the fine planar focus and linear scanning of the slice, these events were not generally visible, though presumably they were occurring. With the same fluorophore loading protocols in the same type of cerebellar slice, using epifluorescence microscopy we observed Ca^{2+} transients even through the microscope eyepieces. Here we show some simple grouping of initial results and characterize several significant differences. The most obvious is the differences in the overall activity of neurons in older slices compared to younger slices, but we also demonstrate a difference in transient duration between genotypes.

In older mice, the lower percent active cells and frequency of events are likely related, as fewer active cells means fewer overall events and less chance of more than one event occurring, resulting in a frequency of 0. This does not appear to be a result of a higher baseline of fluorescent cells, which could contribute to fewer significant events, nor do the slices from aged mice appear to contain fewer overall cell counts due to death or dysfunction. It is possible that fewer events occur because cells require more time to recover. This may be, but some events appear to have multiple peaks during recovery, such as the final trace in young (-/-) mice in Figure 5.2, as opposed to the long linear recovery of several of peaks from aged mice. Alternatively, it is possible that cells in slices from the young mice are more active, as opposed to those from the older mice being less so. Indeed, we would expect any CGCs that are still

migrating to express Ca^{2+} oscillations critical for migration similar to what has been characterized in CGC cell cultures (Komuro and Rakic, 1992, Komuro and Rakic, 1993, Komuro and Kamada, 2005). It is possible that these oscillations make up the majority of the transient events demonstrated here in acute slices. Even CGCs embedded in the IGL might still exhibit these frequent oscillations if they haven't matured to the point at which this mechanism stops. Migratory transients do not explain the events visualized here in the adult and aged mice, though. The protocols for young mice and old mice are sufficiently different, because of the need for more preservative steps in collection and use of tissue, that the protocol or buffers used could reduce the activity of slices from aged mice. Further characterization is necessary here, both to establish the adult mouse brain as a baseline compared to young mice and aged mice, and to determine any differences that protocols and buffers contribute to activity. These would be valid approaches and optimizations, necessary even before testing the effects of stimuli such as MeHg and depolarization.

The source of the difference in transient durations between young (-/-) and (+/+) is less clear than are the reasons for the differences in the young versus aged animals. Without tonic inhibition provided by extrasynaptic GABA_A Rs in mature CGCs, those neurons could conceivably be more active and display more events. This agrees with both research into the molecular mechanisms of GABA_A R $\alpha 6$ knockout mice (Brickley et al., 2001) and in the pharmacology of the whole animal, in which potentiation of remaining GABA_A Rs induces dysfunction (Korpi, et al., 1998). Alternatively, less direct mechanisms could contribute to the observations made. It is possible that altered signaling mechanisms from mature CGCs lacking the GABA_A R $\alpha 6$ subunit change the state of immature CGCs in the EGL, contributing to more events from dividing or migrating CGC precursors in the the EGL or ML. The locations of ROIs

provided by the algorithm do not appear to indicate that this is the case, as (-/-) do not appear to have increased numbers of ROIs in the EGL and ML. Even so, it is unclear if some of the active cells in the IGL are still migrating, versus maturing and putting out axons. It would be valuable to characterize the individual cells that have been highlighted for events further, and to characterize the different layers in young slices, but this will require many more repetitions of these experiments to optimize.

One of the drawbacks of automating the tracing of these cells is that it could conceivably pick up events that are not based in CGCs. While the locations of the events have been traced back to the original images and many are clearly CGC neurons, it is not always clear the type of cell that was visualized. In some cases cells overlap or are out of focus or do not appear to be quite the normal size or shape of CGCs. It is possible that other cell types contribute to the spontaneous transients. Golgi interneurons are frequently firing action potentials during development while making inhibitory synapses (Farrant and Brickley, 2003), and though larger and more branched than CGCs, might be captured by the algorithm. Basket cell termini, located in the PC layer, could also be dense enough to be confused for a cell body, and have been shown to have spontaneous activity in intact two-photon imaging of cerebellum (Conti, et al., 2004). Because not all of the ROIs associated with events can conclusively be ascribed to CGCs, they are here referred to as cells.

There are a few potential solutions to determine the cell populations that are contributing to spontaneous events, and to further characterize these transients. First, CGC-specific labels would be an ideal solution, particularly if those labels can be associated with the live transients. This could be achieved in a few ways, most notably by other live imaging methods. The

genetically-encoded calcium indicator GCaMP could be used with specific promoters instead of the bath fluorophore fluo4 to indicate Ca^{2+} dynamics in cell populations at any level of specificity, from neurons versus glia, to CGCs, and perhaps even specific developmental stages of CGCs. Alternatively, live cell fluorescent glucose analogues and live measurements of NADH in neurons can also distinguish between neurons and glia, and would have the added benefit of producing measures of energy metabolism associated with transient activity (Pancani, et al., 2011). Fixation and immunohistochemistry of cells post-recording could also be used to determine surface expression of receptors and other relevant factors. If the location imaged can then be traced back from IHC, the specific cells could be associated with transient activity, not just generalized. This might be accomplished with rapid fixation while the slice is still on the microscope, but would have to be optimized.

Coupling of electrophysiology and Ca^{2+} imaging is another potential approach. Patching of neurons in slice is possible, and with up to 33% of neurons displaying fluorescent transients in only a few minutes of recording, many cells could be recorded by both techniques. Readings from an electrode could immediately determine if these transients are associated with action potentials, and would characterize the events well. It is clear that these types of transients are not all the same, electrophysiology would further characterize them. Some of the transients might be migrational Ca^{2+} oscillations, in which case there would not be action potentials, while signals from glia or basket cell termini might be associated with characteristic neurotransmitter release. Some of the fluorescent transients might be other signals entirely. Electrophysiology setups also allow for other valuable tools, such as puff application of stimulants directly onto a neuron of interest or even injection of labels. This high-speed imaging approach on its own has much

potential, but coupling high-speed imaging with electrophysiology would provide an excellent direction to further experiments.

CHAPTER SIX

SUMMARY AND CONCLUSIONS

SUMMARY AND CONCLUSIONS

This dissertation presents several projects designed to relate MeHg toxicity, $[Ca^{2+}]_i$ homeostasis and the GABA_A receptor. These projects build on the correlation we have established between MeHg toxicity and increases in $[Ca^{2+}]_i$ by demonstrating that the same signaling mechanisms which occur in cultured neurons occur in functionally intact slices under a variety of conditions, from developing rats and mice to chronically-treated aged mice. Treatments focus on a receptor that is susceptible to MeHg but that has not been fully characterized in the mechanisms of MeHg toxicity.

The results presented in this dissertation support the hypothesis that MeHg disrupts $[Ca^{2+}]_i$ partially through the actions of GABA_AR signaling and that forcing block of GABA_AR signaling can interfere with the actions of MeHg on $[Ca^{2+}]_i$ (Figure 6.1). MeHg acts on CGCs to increase $[Ca^{2+}]_i$ and CGCs show developmental and aging susceptibility. In developing CGCs in both rats and mice, where GABA_AR activation would be depolarizing, increases in $[Ca^{2+}]_i$ are enhanced compared to mature CGCs. In mature CGCs, where GABA_AR activation would be hyperpolarizing, GABA_AR modulators reduce, but do not eliminate the immediate effects of MeHg on $[Ca^{2+}]_i$ and they act at all developmental stages, indicating that GABA_ARs are coupled to $[Ca^{2+}]_i$ even in mature, hyperpolarized CGCs. While there is an increase in $[Ca^{2+}]_i$ by muscimol alone, this effect is only temporary. This dissertation also offers a few intriguing results that indicate that interactions between the effects of MeHg and GABA_A receptors may be more complex, based on the subtype of GABA_ARs involved and the duration of MeHg treatment. Knockout of the GABA_AR $\alpha 6$ subunit does not alter the effects of MeHg in the IGL, where $\alpha 6$ is prominent in (+/+) but absent in (-/-), and not compensated by change in expression

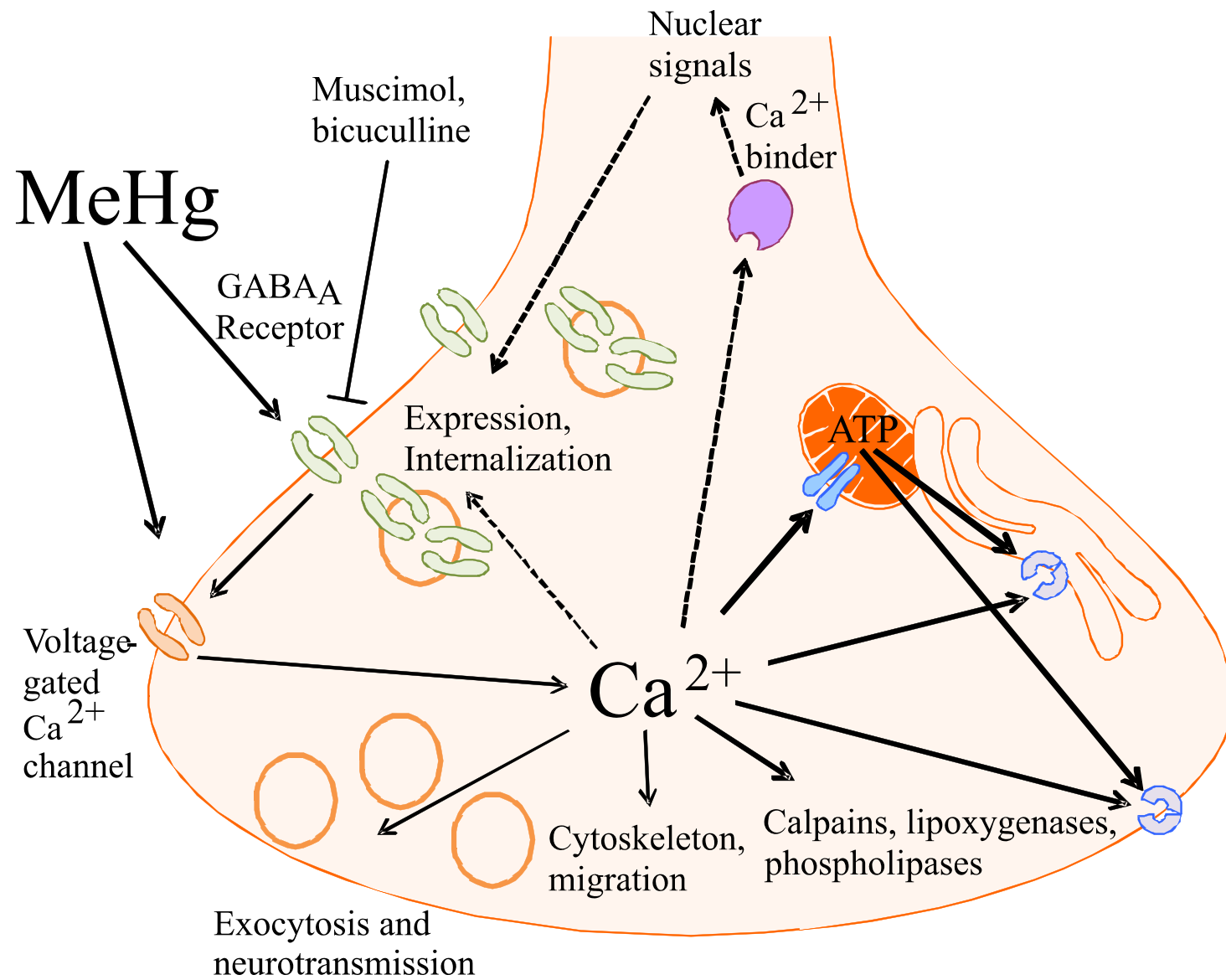


Figure 6.1. Cartoon depiction of GABA_A R and MeHg interactions with $[\text{Ca}^{2+}]_i$ as highlighted by results of this dissertation.

Figure 6.1 (cont'd) MeHg acts through GABA_ARs in part to increase [Ca²⁺]_i in all CGCs and all developmental stages. Both muscimol and bicuculline reduce MeHg effects on [Ca²⁺]_i through GABA_ARs, apparently by desensitization in the case of muscimol and direct inhibition by bicuculline. Loss of α6 subunits is disruptive to developing granule cells, possibly through increased neurotransmission associated with mature CGCs with local synapses or possibly through alterations in GABA_AR expression. [Ca²⁺]_i-dependent cell death, through enzyme activation, rundown of ATP and aberrant nuclear signaling, is present, but not significant compared to regular handling. Chronic MeHg appears to alter responses to muscimol, indicating a role for changes in GABA_AR surface expression, such as through internalization, as well as possible changes in gene expression of GABA_AR subunits (dashed arrows).

of other subunits (Jones, et al., 1997, Nusser et al., 1999). Knockout enhances the effect in developing CGCs. These CGC neuronal precursors in $\alpha 6$ (-/-) mice would not be expected to be any different from (+/+) because $\alpha 2$ is expressed in development. This unexpected result indicates secondary effects of GABA_AR expression and/or MeHg toxicity. Developing (-/-) CGCs also demonstrate an increase in short spontaneous $[Ca^{2+}]_i$ transients as shown by high-speed imaging. Alterations in the normal function of this critical mechanism could indicate another susceptible target of MeHg toxicity in (-/-) mice. Finally, chronic MeHg treatment appears to unmask a large increase in the effectiveness of muscimol to increase $[Ca^{2+}]_i$. These results leave open several areas of potential further inquiry, both to build the characterizations of GABA_AR and MeHg signaling, and to use the techniques and optimizations established here to probe additional interesting interactions.

In the initial set of experiments using rat cerebellar slices as the model, we first characterized the concentration-response to MeHg in slices, as well as the viability of CGCs in these slices. These experiments are the foundation for all the others used in this dissertation. In studying the cellular and molecular toxicity of MeHg, it is extremely important to find balanced concentrations to use that do not induce immediate cell death, but that can induce other non-lethal effects over the time period being observed, otherwise experiments lose relevance to actual exposures. In time course experiments in rat neonatal slices, we determined that 20 μ M MeHg is a valid concentration to use because it induces large increases in $[Ca^{2+}]_i$ -dependent fluo4 fluorescence, does not induce neuronal cell death more than trauma from slicing and time alone do, and clearly displays developmental specificity, generating a larger increase in fluorescence in developing CGCs in the EGL than in any other population. In other studies, concentrations of 0.2 to 5 μ M MeHg have been used in neuronal culture treatments, including on cultured CGCs, and

induce a high incidence of cell death within a few hours (Marty and Atchison, 1998, Limke, et al., 2004, Edwards, et al., 2005). This relative difference in MeHg concentration response indicates that acute slice treatment may be more relevant to acute toxicity because the associated tissue present buffers some of the MeHg compared to dissociated neurons. This is also an interesting concentration to find because it falls within estimated blood MeHg concentrations seen in the Iraq poisoning associated with acute adult toxicity (Bakir, et al., 1973).

In addition to the 20 μM MeHg concentration used in many parts of this dissertation, several MeHg concentrations were added to this characterization of rat slice culture response, and it is likely that even 5 or 1 μM MeHg could have interesting $[\text{Ca}^{2+}]_i$ responses in slices with extension of the experiments. Along that line, it appeared that monitoring of slices could easily continue much farther than the extensions performed over the course of this dissertation. Slice viability and maintenance of function is continually improving in slice culture protocols, such as with the use of low $[\text{Ca}^{2+}]_i$, high $[\text{Mg}^{2+}]_i$ sucrose solutions during slicing and bath recovery methods used in this dissertation, but could be improved in further experiments through methods such as supplementation with n-methyl-d-glucamine in adult slicing solutions (Tanaka, et al., 2008, Peca, et al., 2011) With the development and optimization of ACSF solutions and slice protocols that went into this dissertation, as well as the automation of imaging at the microscope, slice imaging could potentially extend to several hours, bridging the gap between acute slice protocols and organotypic slice culturing.

The initial use of muscimol and bicuculline in Chapter One introduced one of the most intriguing results of this dissertation, that an agonist and an antagonist of the same receptor could both reduce the effect of MeHg. This was later confirmed in the experiments described in

Chapter Two. Previous experiments in the laboratory had demonstrated the expected opposite effects of muscimol and bicuculline on electrophysiological spikes in hippocampal neurons (Yuan and Atchison, 1997) and on $[Ca^{2+}]_i$ in some cerebellar slices during optimization of the bath application used in this dissertation (Mancini, unpublished dissertation report). It led to an interesting internal hypothesis, that muscimol was desensitizing the receptor after an initial activation and thus appearing to act as an antagonist in displaying no change at imaging time points. This hypothesis led to many attempts to work out the timing of muscimol activation and attempts to capture an increase in $[Ca^{2+}]_i$ induced by muscimol on slices imaged with confocal microscopy. Eventually, it led to using the high-speed imaging system for any attempts to find such potentially transient responses. Because none of these attempts were successful or repeatable, none of these experiments have been included in this dissertation. This agonist appearance as antagonist mechanism still is not certain, and probably cannot be confirmed by Ca^{2+} imaging alone. Future work on this mechanism could include coupling imaging with electrophysiology, either directly as with patch clamp studies or by monitoring network activity using multi-electrode arrays. In the case of the former, it is much clearer to add a pulse of muscimol directly onto a neuron and monitor Ca^{2+} signaling along with electrophysiology, but with the latter it would also be interesting to monitor the response as muscimol diffuses across a bath.

In Chapter Two we switched models from rats to mice in order to add genotype as a factor, since knockout mice had been established well as models compared to rats. Switching models always has the potential to complicate protocols, but it appeared that for the most part there was no change in responses. Slices from mice appear to have a somewhat smaller response to acute MeHg, displaying up to about a 2-fold $[Ca^{2+}]_i$ increase in CGC populations whereas rats

displayed up to 3-fold increases, but mouse cerebellar slices still respond significantly compared to control. It was because of this smaller response, and inspired by seeing electrophysiological and other biochemical recordings from two complementary phrenic nerves from lung diaphragm, that it was determined that experiments on cerebellar slices should be paired whenever possible.

The GABA_AR $\alpha 6$ (-/-) mouse model requires more characterization to fully understand the results presented in this dissertation. Going into this with the MeHg model of preferential block of $\alpha 6$ -containing GABA_ARs, and with the previous results showing block by muscimol and bicuculline in the presence of MeHg as protective, the expected result would have been protection in adult CGCs in IGL. It is in the IGL where $\alpha 6$ is prominently expressed (Takayama and Inoue, 2004), but the biggest differences in the results here were within EGL, where $\alpha 6$ would not normally be expressed. Since those precursor cells in the EGL have not yet normally developed expression of $\alpha 6$, the (-/-) model would not be hypothesized to show any difference between those and the (+/+). We need to characterize what is happening in the (-/-) EGL beyond the changes in $[Ca^{2+}]_i$ before this project can really be complete. Several approaches could be used. In the discussion of Chapter Three, it was suggested that the increase in $[Ca^{2+}]_i$ in EGL CGCs might in part be due to enhanced excitotoxic release of glutamate from (-/-) GCG axons. It would be possible to probe this hypothesis using pharmacological or toxic agents that block neurotransmission without interfering with other mechanisms of MeHg toxicity. Other released factors might also be measured in the bath solution or blocked as well. If the susceptibility of developing (-/-) neurons is not based on neurotransmission, then it may be based on gene expression alterations. Even if $\alpha 6$ is not yet expressed, the expression profiles of developing (+/+) and (-/-) CGCs may still be different.

In Chapter Four, the hypotheses that changes to $[Ca^{2+}]_i$ homeostasis in aged animals contributes to susceptibility was tested by bringing the principles established in previous chapters to mice chronically-treated as adults. Some of these experiments used a different $[Ca^{2+}]_i$ -dependent fluorophore, fura-2, which is ratiometric, but the same principles apply to Ca^{2+} imaging as with fluo4. The results of fura-2 Ca^{2+} imaging in cerebellum slices from these mice indicate that baseline $[Ca^{2+}]_i$ is very similar between 6 month and 12 month chronic treatment groups, but that responses to stimuli such as AMPA and KCl are slightly enhanced. Because many MeHg response pathways, including $GABA_A$ Rs, might have been altered with chronic MeHg exposure, Ca^{2+} channel blockers, or with aging when compared to other groups such as the neonatal mice characterized in Chapter Three, this project also explored acute MeHg treatment in these slices using fluo4 and confocal imaging. MeHg-induced $[Ca^{2+}]_i$ response in these aged slices was greater than responses in IGL in neonatal mice, about 2-fold increase in aged while neonatal slices only display about 1.5-fold increases. A direct comparison is more complex because these are not the same mouse lines nor did they receive the same treatments throughout life. Chronic treatments only slightly altered MeHg-induced $[Ca^{2+}]_i$ responses, but were enough to push responses above or below significance. For example, all chronic treatment group slices displayed a lack of concerted depolarization, as would be indicated by a transient $[Ca^{2+}]_i$ increase, when treated with bath application of high [KCl] as compared to the control aged mice. In 12 month treatment groups, treatment responses were enhanced slightly, but enough that all groups remained above baseline with AMPA treatment and all groups displayed significant increases during KCl depolarization. These readings may be complicated because additional experiments performed indicated that a large enough portion of CGCs in at least two treatment groups (M and M/I) depolarize spontaneously during imaging that this response may

boost the readings from other treatments. This issue was discussed in Chapter Four, and it may require further analysis on the data to determine if and how results need to be corrected.

Chapter Four also includes results suggesting a role for GABA_ARs in mechanisms of susceptibility to MeHg in aged mice, but only in the 12 month treatment groups. Because the temporal resolution has been improved, these results show an effect of muscimol on $[Ca^{2+}]_i$, both at the individual cellular level and at the population level as indicated by the means used in Figure 4.6 B. Muscimol increases $[Ca^{2+}]_i$ in these slices, particularly in chronic MeHg treatment groups (M and M/I). This muscimol application in MeHg-treated mice, while highly variable, was the largest mean increase in fura-2 fluorescence ratio of any treatment, up to about a 4-fold increase. Bicuculline, applied shortly after muscimol, did not significantly change fluorescence. Of all the muscimol results in this dissertation, this was the largest effect by the agent, and clearly points to a change in chronically MeHg-treated mice. These mice have some alteration that effectively potentiates GABA_ARs, making activation much more effective. These results suggest widespread changes in chronic MeHg treatment and will be useful in strengthening arguments in the literature against conclusions that adult exposure to MeHg displays no functional change (Bellum, et al., 2012). It will take additional characterizations to determine the source of this difference rather than speculate, and these characterizations may come from additional approaches used within the framework of the group project.

The group project of which Chapter Four was a part is a massive undertaking and results from many researchers involved in the four major parts, biochemical, behavioral, electrophysiological, and pathological, are still being processed. Ca^{2+} imaging was part of the biochemical approach to this project, and results from other approaches within this laboratory,

including gene expression, immunohistochemical, electrophysiological, and metabolic assays and analyses are of particular interest to the conclusions presented here, and will contribute to an overall integration of results. As of now, the results presented in this dissertation must stand independently, but some general conclusions can be applied, and several other 6 month results from the study are available from within this lab. For instance, chronic treatments did not display detectable differences in rota-rod motor performance or general health and weight, but MeHg treatment did increase partial weakness in the hind limbs as indicated by the hind-limb cross test, so the collaboration with a behavioral monitoring lab may have interesting behavioral phenotypes to add soon. ATP-level assays indicated that the combination of chronic MeHg and isradipine increase maximum ATP production in striatal neurons (unpublished observation). If this metabolic change is also present in CGCs, then it would suggest the extra ATP capacity is needed to counteract toxicity brought about by large increases in $[Ca^{2+}]_i$ observed in this dissertation. Many more connections between the approaches will be made as results become available.

Chapter Five addresses some issues and hypotheses that came up during confocal imaging studies. While the intent of the high-speed imaging approach was to determine if muscimol increased $[Ca^{2+}]_i$ in a way that was missed in the low temporal resolution of confocal imaging, the opportunity to test muscimol in this imaging approach did not occur until the experiments described in Chapter Four. Even so, the collection of results showed an interesting reaction in slices, spontaneous $[Ca^{2+}]_i$ transients, which have been shown in advanced microscopy approaches such as two-photon microscopy, but have not been characterized in epifluorescent microscopy of slices (Conti, et al., 2004). By dividing into age groups, these results were enough to determine some interesting interactions between $GABA_A$ Rs and $[Ca^{2+}]_i$

transients in slices. Neonatal GABA_AR α6 (-/-) mice, as used in Chapter Three, while otherwise similar to matched (+/+) mice when measuring transients, had a distribution of events that had many more short events. The significance of these shorter events is unclear, but as with the results of Chapter Three, if genotype alters the activity of mature CGCs and thus neurotransmission, then a response in developing CGCs to that activity could have altered the signaling that regulates spontaneous events.

Together, the results from Chapter Five and the spontaneous response in slices from aged animals in Chapter Four to extended untreated imaging indicate a need to characterize spontaneous events in these slices further. The discussion in Chapter Five mentioned several approaches that could be used to improve characterization of each experiment performed on the high-speed imaging system, including coupling imaging to electrophysiology, adding other live fluorescent probes, or fixation of slices post experiment to determine expression profiles and other characteristics. It would be useful to consider these approaches if the types of experiment performed in Chapters Four and Five are continued, because spontaneous activity could continue to affect results. As for directions this type of project could go in the future, the groups used in Chapter Five could be expanded to include neonatal, young, adult and geriatric mice to determine the baseline characteristics of spontaneous events in far more detail than has already been shown in these results. As GABA_AR α6 (-/-) mice have already been shown here to be significantly different at a neonatal age, it would be particularly useful to continue using this genotype model in further age groups. Further research could extend this into other mouse lines with aberrant Ca²⁺ dynamics in the cerebellum, including the natural Ca²⁺ channel mutation lines *lethargic*, *tottering*, or *stargazer*, or other GABA_AR subunit knockouts. From Chapter Four, an interesting future direction would be to continue characterizing MeHg treatment and

other chronic and acute treatments. Where MeHg acute treatment increases $[Ca^{2+}]_i$ on its own, perhaps lower concentrations and longer treatment times would affect the spontaneous transients clearly. Slice culture and high-speed imaging are powerful tools, and with continued optimization and exploration, the possibilities to characterize the mechanism of spontaneous events and how they relate to MeHg toxicity and GABA_AR are unlimited.

The mechanisms of action summarized in Figure 6.1 (and 1.1) indicate that $[Ca^{2+}]_i$ is a central feature of MeHg toxicity, but non- Ca^{2+} -dependent effects may also be critical. For example, MeHg treatment also increases $[Zn^{2+}]_i$ in synaptosomes, (Denny, et al., 1993, Denny and Atchison, 1994), neuronal cell lines (Hare, et al., 1993, Marty and Atchison, 1997) and cultured CGCs (Edwards, et al., 2005). In these cultured CGCs, the use of the Zn^{2+} -specific chelator TPEN diminished the first phases of fura-2 fluorescence increases during MeHg treatment, but did not alter other effects of MeHg. Within this dissertation, experiments presented in Chapters Two and Three did not use TPEN in order to examine all possible effects of MeHg, while 4 and 5 used TPEN in order to examine Ca^{2+} -dependent effects. ROS are also produced excessively in the cerebellum by MeHg treatment, likely through the actions of excess $[Ca^{2+}]_i$ on mitochondria, and may contribute to toxicity (Yee and Choi, 1994, Yee and Choi, 1996, Bellum, et al., 2007). This ROS production and MeHg toxicity can be reduced by antioxidants such as probucol and vitamin E in some neuronal models (Gassó, et al., 2001, Usuki, et al., 2001), but not others (Sarafian and Verity, 1991, Ou, et al., 1999, Edwards, et al., 2005), suggesting that ROS production is not a critical factor in all neuron types. Interestingly, a recent study of a fungal neurotoxin Penitrem A indicates toxicity in CGCs through GABA_ARs and ROS production, possibly through a $[Ca^{2+}]_i$ -dependent mechanism (Berntsen, et al., 2013). While the interaction between GABA_ARs and $[Ca^{2+}]_i$ is still not clear, this supports the

conclusions of this dissertation in demonstrating that GABA_ARs are coupled to Ca²⁺ signaling at least in CGCs.

There are certainly many more components of the relationships between MeHg, [Ca²⁺]_i and GABA_ARs that may be characterized. In several discussion sections, expression is mentioned as an important component of this characterization, and this dissertation has only touched on expression, both at the genetic level and at the surface of neurons, as it relates to the ongoing project associated with Chapter Four. An interesting potential project here would be characterizing surface expression of GABA_ARs as they relate to MeHg-induced stress. As mentioned in the introduction, GABA_ARs can be internalized during stress, and these changes can be seen through impermeable labeling of GABA_ARs as compared to permeable labels (Maguire, et al., 2009, Poulter, et al., 2009). Alterations in surface expression like this might be behind the change in muscimol response in chronically MeHg-treated mice. Muscimol and bicuculline are certainly useful tools in probing GABA_AR effects on [Ca²⁺]_i and MeHg toxicity, but in order to fully characterize these mechanisms and determine the specific subunits involved, more specific GABA_AR modulators should be used, and many are now just available for research. GABA_ARs are receiving more attention for potential involvement in many neurological disorders as finely tuned pharmacological targets. As the GABA_AR structure, dynamics and interactions are explored, the potential for more specific drugs and interactions with MeHg will become available. Unlike muscimol, which is psychoactive and sedative, and bicuculline, which can induce epilepsy, these new drugs may be used in future therapies for many disorders. As described in Chapter One, GABA_AR signaling disorders include epilepsy and anxiety, but may be important in disorders such as schizophrenia, Alzheimer's disease and Parkinson's disease. Due to the many additional mechanisms of MeHg toxicity, such as through M3 receptors,

VGCCs and mitochondria (Figure 1.1), at best the therapeutic potential of GABA_AR modulators for MeHg poisoning would be partial, much like Ca²⁺ channel blockers such as nifedipine (Sakamoto, et al., 1996, Marty and Atchison, 1998).

In conclusion, this dissertation shows that MeHg rapidly increases [Ca²⁺]_i in CGCs in a way that is dependent in part on GABA_AR signaling. This disruption is dependent on the development of CGCs, and is enhanced in migrating CGCs, where migration is critically [Ca²⁺]_i-dependent. GABA_AR block by bicuculline and desensitization by muscimol both delay the immediate actions of MeHg, much as Ca²⁺ channel blockers are demonstrated to do. Genetic knockout of the prominent $\alpha 6$ subunit of GABA_ARs in mature CGCs enhances the effect of MeHg in immature CGCs, indicating an uncharacterized interaction between CGC axons and immature CGCs. Finally, chronic MeHg treatment is shown to greatly enhance the effectiveness of muscimol in producing [Ca²⁺]_i transients on aged cerebellar slices. Along with MeHg actions on VGCCs, muscarinic receptors and mitochondria, the actions on and through the GABA_AR contribute to [Ca²⁺]_i-dependent toxicity of MeHg.

REFERENCES

REFERENCES

- Abdalla, F.H., Bellé, L.P., Bitencourt, P.E.R., da Silva, J.E., Roman, S., da Rosa, C., Schetinger, M.R., and Moretto, M.B. (2012). Methylmercury-induced changes in target organs of suckling rat pups. *Exp. Toxicol. Path.* **64**, 605-609.
- Abramian, A.M., Comenencia-Ortiz, E., Vithlani, M., Verena Tretter, E., Sieghart, W., Davies P.A., and Moss, S.J. (2010). Protein Kinase C phosphorylation regulates membrane insertion of GABA_A receptor subtypes that mediate tonic inhibition. *J. Biol. Chem.* **285**, 41795-41805.
- Akagi, H., Grandjean, P., Takizawa, Y., and Weihe, P. (1998). Methylmercury Dose Estimation from Umbilical Cord Concentrations in Patients with Minamata Disease. *Environ. Res., Sect. A* **77**, 98-103.
- Amico-Ruvio, S.A., Murthy, S.E., Smith, T.P., Popescu, G.K. (2011). Zinc effects on NMDA receptor gating kinetics. *Biophys. J.* **100**, 1910-1918.
- Amin-Zaki, L., Elhassani, S., Majeed, M.A., Clarkson, T.W., Doherty, R.A., and Greenwood, M. (1974). Intra-uterine methylmercury poisoning in Iraq. *Pediatrics* **54**, 587-595.
- Arakawa, O., Nakahiro, M., and Narahashi, T. (1991). Mercury modulation of GABA-activated chloride channels and non-specific cation channels in rat dorsal root ganglion neurons. *Brain Res.* **551**, 58-63.
- Araki, T., Kanai, Y., Kato, H., Kogure, K., Shuto, K., and Ishida, Y. (1993). Effect of vinconate against regional age-related changes in the gerbil brain. *Pharmacol. Biochem. Behav.* **44**, 17-25.
- Aremu, D.A., Madejczyk, M.S., and Ballatori, N. (2008) N-acetylcysteine as a potential antidote and biomonitoring agent of methylmercury exposure. *Environ Health Perspect.* **116**, 26-31.
- Aschner, M., and Aschner, J.L. (1990) Mercury neurotoxicity: mechanisms of blood-brain barrier transport. *Neurosci Biobehav Rev.* **14**, 169-76.
- Aschner, M., Conklin, D.R., Yao, C.P., Allen, J.W., Tan, K.H. (1998). Induction of astrocyte metallothioneins (MTs) by zinc confers resistance against the acute cytotoxic effects of methylmercury on cell swelling, Na⁺ uptake, and K⁺ release. *Brain Res.* **813**, 254-261.

- Aschner, M., Eberle, N.B., Miller, K., and Kimelberg, H.K. (1990). Interactions of methylmercury with rat primary astrocyte cultures: inhibition of rubidium and glutamate uptake and induction of swelling. *Brain Res.* **530**, 245-250.
- Aschner, M., Mullaney, K.J., Wagoner, D.E. Jr., Lash, L.H., and Kimelberg, H.K. (1995). Adenosine modulates methylmercuric chloride (MeHgCl)-induced D-aspartate release from neonatal rat primary astrocyte cultures. *Brain Res.* **689**, 1-8.
- Atchison, W.D. (1986). Extracellular calcium-dependent and -independent effects of methylmercury on spontaneous and potassium-evoked release of acetylcholine at the neuromuscular junction. *JPET* **237**, 672-680.
- Atchison, W.D. (1987). Effects of activation of sodium and calcium entry on spontaneous release of acetylcholine induced by methylmercury. *J Pharmacol Exp Ther.* **241**, 131-9.
- Atchison, W.D. (2005) Is chemical neurotransmission altered specifically during methylmercury-induced cerebellar dysfunction. *TRENDS in Pharmacol. Sci.* **26**, 549-557.
- Atchison, W.D., and Hare, M.F. (1994). Mechanisms of methylmercury-induced neurotoxicity. *FASEB J.* **8**, 622-9.
- Atlas, D., Wiser, O., and Trus, M. (2001). The voltage-gated Ca²⁺ channel is the Ca²⁺ sensor of fast neurotransmitter release. *Cell. Mol. Neurobiol.* **21**, 717-731.
- Augustine, G.J., Charlton, M.P., and Smith, S.J. (1985). Calcium entry and transmitter release at voltage-clamped nerve terminals of squid. *J. Physiol.* **367**, 163-181.
- Babot, Z., Teresa Vilaró, M., and Suñol, C. (2007). Long-term exposure to dieldrin reduces γ -aminobutyric acid type A and N-methyl-D-aspartate receptor function in primary cultures of mouse cerebellar granule cells. *J. Neurosci. Res.* **85**, 3687-3695.
- Bailey, J.M., Hutsell, B.A., and Newland, M.C. (2013). Dietary nimodipine delays the onset of methylmercury neurotoxicity in mice. *Neurotoxicology* **37**, 108-117.
- Bakir, F., Damluji, S.F., Amin-Zaki, L., Murtadha, M., Khalidi, A., Al-Rawi, N.Y., Tikriti, S., Dhahir, H.I., Clarkson, T.W., Smith, J.C., and Doherty, R.A. (1973). Methylmercury poisoning in Iraq. *Science* **181**, 230-241.
- Basu, N., Scheuhammer, A.M., Rouvinen-Watt, K., Grochowina, N., Evans, R.D., O'Brien, M., and Chan, H.M. (2007) Decreased N-methyl-D-aspartic acid (NMDA) receptor levels are associated with mercury exposure in wild and captive mink. *NeuroToxicology*, **28**, 587-93
- Basu, N., Scheuhammer, A.M., Rouvinen-Watt, K., Evans, R.D., Trudeau, V.L., and Chan, L.H.M. (2010). *In vitro* and whole animal evidence that methylmercury disrupts

- GABAergic systems in discrete brain regions in captive mink. *Comp. Biochem. and Physiol., part C*. **151**, 379-385.
- Baumgartner, H.K., Gerasimenko, J.V., Thorne, C., Ferdek, P., Pozzan, T., Tepikin, A.V., Petersen, O.H., Sutton, R., Watson, A.J., Gerasimenko, O.V. (2009). Calcium elevation in mitochondria is the main Ca²⁺ requirement for mitochondrial permeability transition pore (mPTP) opening. *J. Biol. Chem.* **284**, 20796-20803.
- Baur, R., Simmen, U., Senn, M., Séquin, U., and Sigel, E. (2005). Novel plant substances acting as beta subunit isoform-selective positive allosteric modulators of GABA_A receptors. *Mol. Pharmacol.* **68**, 787-792.
- Bearzatto, B., Servais, L., Roussel, C., Gall, D., Baba-Aïssa, F., Schurmans, S., de Kerchove d'Exaerde, A., Cheron, G., and Schiffmann, S.N. (2006). Targeted calretinin expression in granule cells of calretinin-null mice restores normal cerebellar functions. *FASEB J.* **20**, 380-382.
- Belelli, D., Harrison, N.L., Maguire, J., Macdonald, R.J., Walker, M.C., and Cope, D.W. (2009). Extrasynaptic GABA_A Receptors: Form, Pharmacology, and Function. *J. Neurosci.* **29**, 12757-12763.
- Bellanger, M., Pichery, C., Aerts, D., Berglund, M., Castaño, A., Cejchanová, M., Crettaz, P., Davidson, F., Esteban, M., Fischer, M.E., Gurzau, A.E., Halzlova, K., Katsonouri, A., Knudsen, L.E., Kolossa-Gehring, M., Koppen, G., Ligočka, D., Miklavčič, A., Reis, M.F., Rudnai, P., Tratnik, J.S., Weihe, P., Budtz-Jørgensen, E., Grandjean, P.; DEMO/COPHES. (2013). Economic benefits of methylmercury exposure control in Europe: monetary value of neurotoxicity prevention. *Environ. Health* **12**, 3.
- Bellum, S., Bawa, B., Thuett, K.A., Stoica, G., Abbott, L.C. (2007). Changes in biochemical processes in cerebellar granule cells of mice exposed to methylmercury. *Int. J. Toxicol.* **26**, 261-269.
- Bellum, S., Thuett, K.A., Bawa, B., and Abbott, L.C. (2012). The effect of methylmercury exposure on behavior and cerebellar granule cell physiology in aged mice. *J. Appl. Toxicol.* Advanced access published August 10, 2012. doi:10.1002/jat.2786.
- Ben-Ari, Y., Woodin, M.A., Sernagor, E., Cancedda, L., Vinay, L., Rivera, C., Legendre, P., Luhmann, H.K., Bordey, A., Wenner, P., Fukuda, A., van den Pol, A.N., Gaiarsa, J., and Cherubini, E. (2012). Refuting the challenges of the developmental shift of polarity of GABA actions: GABA more exciting than ever! *Frontiers in Cell. Neurosci.* **6.35**, 1-18.
- Berends, M., Maex, R., De Schutter, E. (2004). A detailed three-dimensional model of the cerebellar granule cell layer. *Neurocomputing.* **58-60**, 587-592.

- Berntsen, H.F., Wigestrand, M.B., Bogen, I.L., Fonnum, F., Walaas, S.I., and Moldes-Anaya, A. (2013). Mechanisms of penitrem-induced cerebellar granule neuron death in vitro: possible involvement of GABAA receptors and oxidative processes. *Neurotoxicology* **35**, 129-136.
- Bianchi, M.T., Haas, K.F., and Macdonald, R.L. (2002). $\alpha 1$ and $\alpha 6$ subunits specify distinct desensitization, deactivation and neurosteroid modulation of GABA_A receptors containing the δ subunit. *Neuropharmacology* **43**, 492-502.
- Bornschein, G., Arendt, O., Hallermann, S., Brachtendorf, S., Eilers, J., and Schmidt, H. (2013). Paired-pulse facilitation at recurrent Purkinje neuron synapses is independent of calbindin and parvalbumin during high-frequency activation. *J. Physiol.* **591**, 3355-3370.
- Bortone, D., and Polleux, F. (2009). KCC2 expression promotes the termination of cortical interneuron migration in a voltage-sensitive calcium-dependent manner. *Neuron* **62**, 53-71.
- Bracamontes, J., McCollum, M., Esch, C., Li, P., Ann J., Steinbach, J.H., and Akk, G. (2011). Occupation of either site for the neurosteroid allopregnanolone potentiates the opening of the GABAA receptor induced from either transmitter binding site. *Mol Pharmacol.* **80**, 79-86.
- Bregetovski, P., and Bernard, C. (2012). Excitatory GABA: how a correct observation may turn out to be an experimental artifact. *Front. Pharmacol.* **3**, 65.
- Brewer, L.D., Thibault, O., Staton, J., Thibault, V., Rogers, J.T., Garcia-Ramos, G., Kraner, S., Landfield, P.W., Porter, N.M. (2007). Increased vulnerability of hippocampal neurons with age in culture: temporal association with increases in NMDA receptor current, NR2A subunit expression and recruitment of L-type calcium channels. *Brain Res.* **1151**, 20-31.
- Brickley, S.G., Cull-Candy, S.G., and Farrant, M. (1996). Development of a tonic form of synaptic inhibition in rat cerebellar granule cells resulting from activation of GABAA receptors. *J. Physiol.* **497.3**, 753-759.
- Brickley, S.G., Farrant, M., Swanson, G.T., and Cull-Candy, S.G. (2001). CNQX increases GABA-mediated synaptic transmission in the cerebellum by an AMPA/kainite receptor independent mechanism. *Neuropharmacology.* **41**, 730-736.
- Brickley, S.G., Revilla, V., Cull-Candy, S.G., Wisden, W., and Farrant, M. (2001). Adaptive regulation of neuronal excitability by a voltage-independent potassium conductance. *Nature* **409**, 88-92.

- Brickley, S.G., and Mody, I. (2011). Extrasynaptic GABA_A receptors: their function in the CNS and implications for disease. *Neuron*. **73**, 23-34.
- Bright, D.P. and Brickley, S.G. (2008). Acting locally but sensing globally: impact of GABAergic synaptic plasticity on phasic and tonic inhibition in the thalamus. *J. Physiol.* **586.21**, 5091-5099.
- Bright, D.P., Renzi, M., Bartram, J., McGee, T.P., MacKenzie, G., Hosie, A.M., Farrant, M., and Brickley, S.G. (2011). Profound desensitization by ambient GABA limits activation of δ -containing GABA_A receptors during spillover. *J. Neurosci.* **31**, 753-763.
- Briz, V., Parkash, J., Sánchez-Redondo, S., Prevot, V., and Suñol, C. (2012). Allopregnanolone prevents Dioldrin-induced NMDA receptor internalization and neurotoxicity by preserving GABA_A receptor function. *Endocrinology*. **153**, 847-860.
- Brodinsky, L.N., O'Leary, D., Neale, J.H., Vicini, S., Coso, O.A., and Fiszman, M.L. (2003). GABA-induced neurite outgrowth of cerebellar granule cells is mediated by GABAA receptor activation, calcium influx and CaMKII and erk1/2 pathways. *J. Neurochem.* **84**, 1411-1420.
- Cace, I.B., Milardovic, A., Prpic, I., Krajina, R., Petrovic, O., Vukelic, P., Spiric, Z., Horvat, M., Mazej, D., and Snoj, J. (2011). Relationship between the prenatal exposure to low-level of mercury and the size of a newborn's cerebellum. *Med. Hypotheses*. **76**, 514-516.
- Campbell, C.A., Mackay, K.B., Patel, S., King, P.D., Stretton, J.L., Hadingham, S.J., and Hamilton, T.C. (1997). Effects of isradipine, an L-type calcium channel blocker on permanent and transient focal cerebral ischemia in spontaneously hypertensive rats. *Exp. Neurol.* **148**, 45-50.
- Cannell, M.B., and Cody, S.H. (2006). Fluorescent ion measurement. In Handbook of Biological Confocal Microscopy (J.B. Pawley, ed.), 3rd ed., pp.736-745. Springer Science+Business Media, New York, NY.
- Castejón, O.J., Fuller, L., and Dailey, M.E. (2004). Localization of synapsin-I and PSD-95 in developing postnatal rat cerebellar cortex. *Brain Res Dev Brain Res.* **151**, 25-32.
- Castoldi, A.F., Barni, S., Turin, I., Gandini, C., and Manzo, L. (2000) Early acute necrosis, delayed apoptosis and cytoskeletal breakdown in cultured cerebellar granule neurons exposed to methylmercury. *J. Neurosci. Res.* **59**, 775-787.
- Castoldi, A.F., Johansson, C., Onishchenko, N., Coccini, T., Roda, E., Vahter, M., Ceccatelli, S., Manzo, L. (2008). Human developmental neurotoxicity of methylmercury: impact of variables and risk modifiers. *Regul Toxicol Pharmacol* **51**, 201-14.

- Catterall, W.A. and Few, A.P. (2008). Calcium channel regulation and presynaptic plasticity. *Neuron* **59**, 882-901.
- Catterall, W.A., Perez-Reyes, E., Snutch, T.P., and Striessnig, J. (2005). International Union of Pharmacology. XLVII. Nomenclature and structure-function relationships of Voltage-gated Calcium channels. *Pharmacol. Rev.* **57**, 411-425.
- Cerella, C., Diederich, M., and Ghibelli, L. (2010). The dual role of Calcium as messenger and stressor in cell damage, death, and survival. *Int. J. Cell Biol.* Article 546163.
- Chad, J.E., and Eckert, R. (1984). Calcium domains associated with individual channels can account for anomalous voltage relations of CA-dependent responses. *Biophys. J.* **45**, 993-999.
- Chan, S.L., and Mattson, M.P. (1999) Caspase and calpain substrates: roles in synaptic plasticity and cell death. *J. Neurosci. Res.* **58**, 168-190.
- Chandra, D., Halonen, L.M., Linden, A.M., Procaccini, C., Hellsten, K., Homanics, G.E., and Korpi, E.R. (2010). Prototypic GABA(A) receptor agonist muscimol acts preferentially through forebrain high-affinity binding sites. *Neuropsychopharmacology* **35**, 999-1007.
- Chapman, E.R. (2008). How does synaptotagmin trigger neurotransmitter release? *Annu. Rev. Biochem.* **77**, 615-41.
- Chavas, J., Forero, M.E., Collin, T., Llano, I., and Marty, A. (2004). Osmotic tension as a possible link between GABAA receptor activation and intracellular calcium elevation. *Neuron*, **44**, 701-713.
- Cheng, A., Gonçalves, J.T., Golshani, P., Arisaka, K., and Portera-Cailliau, C. (2011). Simultaneous two-photon calcium imaging at different depths with spatiotemporal multiplexing. *Nature Methods.* **8**, 139-142.
- Cherubini, E. (2012). Refuting the challenges of the developmental shift of polarity of GABA actions: GABA more exciting than ever! *Frontiers in Cell. Neurosci.* **6.35**, 1-18.
- Chiu, C., Brickley, S., Jensen, K., Southwell, A., Mckinney, S., Cull-Candy, S., Mody, I., and Lester, H.A. (2005). GABA transporter deficiency causes tremor, ataxia, nervousness, and increased GABA-induced tonic conductance in cerebellum. *J. Neurosci.* **25**, 3234-3245.
- Choe, M., Ortiz-Mantilla, S., Makris, N., Gregas, M., Bacic, J., Haehn, D., Kennedy, D., Pienaar, R., Caviness, Jr., V.S., Benasich, A.A., and Grant, P.E. (2012). Regional infant brain development: an MRI-based morphometric analysis in 3 to 13 month olds. *Cerebral Cortex*. Advanced access published September 6, 2012. doi:10.1093/cercor/bhs197.

- Choi, B.H., Yee, S., and Robles, M. (1996). The effects of glutathione glycoside in methyl mercury poisoning. *Toxicol Appl Pharmacol.* **141**,357-64.
- Chung, Y.H., Shin, C.M., Kim, M.J., Shin, D.H., Yoo, Y.B., and Cha, C.I. (2001). Differential alterations in the distribution of voltage-gated calcium channels in aged rat cerebellum. *Brain Res.* **903**, 247-252.
- Chung, Y.H., Shin, C., Park, K.H., and Cha, C.I. (2000). Immunohistochemical study on the distribution of neuronal voltage-gated calcium channels in the rat cerebellum. *Brain Res.* **865**, 278-282.
- Clancy, B., Darlington, R.B., and Finlay, B.L. Translating developmental time across mammalian species. *Neuroscience* **105**, 7-17.
- Coccini, T., Roda, E., Castoldi, A.F., Poli, D., Goldoni, M., Vettori, M.V., Mutti, A., and Manzo, L. (2011). Developmental exposure to methylmercury and 2,2',4,4',5,5'-hexachlorobiphenyl (PCB153) affects cerebral dopamine D1-like and D2-like receptors of weanling and pubertal rats. *Arch. Toxicol.* **85**, 1281-1294.
- Conti, R., Tan, Y.P., and Llano, I. (2004). Action potential-evoked and ryanodine-sensitive spontaneous Ca²⁺ transients at the presynaptic terminal of a developing CNS inhibitory synapse. *J. Neurosci.* **24**, 6946-6957.
- Coon, A.L., Wallace, D.R., Mactutus, C.F., and Booze, R.M. (1999). L-type calcium channels in the hippocampus and cerebellum of Alzheimer's disease brain tissue. *Neurobiol. Aging* **20**, 597-603.
- Concha, M.G., Concas, A., Rossetti, Z., Guarneri, P., Corongiu, F.P., and Biggio, G. (1981). Methyl mercury enhances [3H]diazepam binding in different areas of the rat brain. *Brain Res.* **229**, 264-269.
- Csordás, G., Thomas, A.P., Hajnóczky, G. (1999). Quasi-synaptic calcium signal transmission between endoplasmic reticulum and mitochondria. *EMBO J.* **18**, 96-108.
- Davidson, P.W., Sloane-Reeves, J., Myers, G.J., Hansen, O.N., Huang, L., Georger, L.A., Cox, C., Thurston, S.W., Shamlaye, C.F., and Clarkson, T.W. (1998). Association between prenatal exposure to methylmercury and visuospatial ability at 10.7 years in the seychelles child development study. *NeuroToxicology* **29**, 453-459.
- Dahlem, Y.A., Wolf, G., Siemen, D., and Horn, T.F. (2004). Combined modulation of the mitochondrial ATP-dependent potassium channel and the permeability transition pore causes prolongation of the biphasic calcium dynamics. *Cell Calcium* **39**, 387-400.

- De Schutter, E. (2002). Cerebellar cortex: computation by extrasynaptic inhibition? *Curr. Biol.* **12**, R363-365.
- De Zeeuw, C.I., Hoebeek, F.E., Bosman, L.W.J., Schonewille, M., Witter, L., and Koekkoek, S.K. (2011). Spatiotemporal firing patterns in the cerebellum. *Nat. Rev. Neurosci.* **12**, 327-344.
- Debes, F., Budtz-Jørgensen, E., Weihe, P., White, R.F., Grandjean, P. (2006). Impact of prenatal methylmercury exposure on neurobehavioral function at age 14 years. *Neurotox. and Teratol.* **28**, 363-375.
- Demarchi, F., and Schneider, C. (2007). The calpain system as a modulator of stress/damage response. *Cell Cycle* **6**, 136-138.
- Deniaud, A., Sharaf el dein, O., Maillier, E., Poncet, D., Kroemer, G., Lemaire, C., and Brenner, C. (2008). Endoplasmic reticulum stress induces calcium-dependent permeability transition, mitochondrial outer membrane permeabilization and apoptosis. *Oncogene* **27**, 285-299.
- Denny, M.F., and Atchison, W.D. Methylmercury-induced elevations in intrasynaptosomal zinc concentrations: an 19F-NMR study. *J. Neurochem.* **63**, 383-386.
- Denny, M.F., Hare, M.F., and Atchison, W.D. (1993). Methylmercury alters intrasynaptosomal concentrations of endogenous polyvalent cations. *Toxicol. Appl. Pharmacol.* **122**, 222-232.
- D'hulst, C., Atack, J.R., and Kooy, R.F. (2009). The complexity of the GABAA receptor shapes unique pharmacological profiles. *Drug Discovery Today* **14**, 866-875.
- Ding, J., Zhang, L., Qu, F., Ren, X., Zhao, X., and Liu, Q. (2011). Cell activity analysis by capillary zone electrophoresis combined with specific cell staining. *Electrophoresis.* **32**, 455-463.
- Doherty, D. (2009) Joubert syndrome: insights into brain development, cilium biology, and complex disease. *Semin. Pediatr. Neurol.* **16**, 143-154.
- Doroshenko, P.A., Woppmann, A., Miljanich, G., and Augustine, G.J. (1997). Pharmacologically distinct presynaptic calcium channels in cerebellar excitatory and inhibitory synapses. *Neuropharmacology* **36**, 865-872.
- Drexler, B., Jurd, R., Rudolph, U., Antkowiak, B. (2009). Distinct actions of etomidate and propofol at beta3-containing gamma-aminobutyric acid type A receptors. *Neuropharmacology* **57**, 446-455.

- Earl, D.E. and Tietz, E.I. (2011). Inhibition of recombinant L-type voltage-gated calcium channels by positive allosteric modulators of GABAA receptors. *JPET*. **337**, 301-311.
- Eccles, J.C., Ito, M., Szenta'gothai, J. (1967). The cerebellum as a neuronal machine. Springer-Verlag, Berlin.
- Edwards, J.R., Marty, M.S., and Atchison, W.D. (2005). Comparative sensitivity of rat cerebellar neurons to dysregulation of divalent cation homeostasis and cytotoxicity caused by methylmercury. *Toxicol Appl Pharmacol* **208**, 222-232.
- Egawa, K., Kitagawa, K., Inoue, K., Takayama, M., Takayama, C., Saitoh, S., Kishino, T., Kitagawa, M., and Fukuda, A. (2012). Decreased tonic inhibition in cerebellar granule cells causes motor dysfunction in a mouse model of Angelman Syndrome. *Science Trans. Med.* **4**, 163ra157.
- Eilers, J., Plant, T.D., Marandi, N., and Konnerth, A. (2001). GABA-mediated Ca²⁺ signalling in developing rat cerebellar Purkinje neurones. *J. Physiol.* **536.2**, 429-437.
- Eimerl, S., and Schramm, M. (1991). Acute glutamate toxicity in cultured cerebellar granule cells: agonist potency, effects of pH, Zn²⁺ and the potentiation by serum albumin. *Brain Res.* **560**, 282-290.
- Engel, G.L., Delwig, A., and Rand, M.D. (2012). The effects of methylmercury on Notch signaling during embryonic neural development in *Drosophila melanogaster*. *Toxicol. in Vitro.* **26**, 485-492.
- Engelman, H.S., and MacDermott, A.B. (2004) Presynaptic ionotropic receptors and control of transmitter release. *Nat. Rev. Neurosci.* **5**, 135-145.
- Erceg, S., Ronaghi, M., Zipancic, I., Lainez, S., Roselló, M.G., Xiong, C., Moreno-Manzano, V., Rodríguez-Jiménez, F.J., Planells, R., Alvarez-Dolado, M., Bhattacharya, S.S., and Stojkovic, M. (2010). Efficient differentiation of human embryonic stem cells into functional cerebellar-like cells. *Stem Cells and Dev.* **19**, 1745-1756.
- Erreger, K., Traynelis, S.F. (2008). Zinc inhibition of rat NR1/NR2A N-methyl-D-aspartate receptors. *J. Physiol.* **586**, 763-778.
- Exton, J.H. (1990). Signaling through phosphatidylcholine breakdown. *J. Biol. Chem.* **265**, 1-4.
- Fahrion, J.K., Komuro, Y., Li, Y., Ohno, N., Littner, Y., Raoult, E., Galas, L., Vaudry, D., and Komuro, H. (2012). Rescue of neuronal migration deficits in a mouse model of fetal Minamata disease by increasing neuronal Ca²⁺ spike frequency. *PNAS.* **109**, 5057-5062.

- Fang, M., Li, J., Tiu, S.C., Zhang, L., Wang, M., Yew, D.T. (2005). N-methyl-D-aspartate receptor and apoptosis in Alzheimer's disease and multiinfarct dementia. *J. Neurosci. Res.* **81**, 269-274.
- Faro, L.R., do Nascimento, J.L., Alfonso, M., and Durán, R. (2002). Protection of methylmercury effects on the in vivo dopamine release by NMDA receptor antagonists and nitric oxide synthase inhibitors. *Neuropharmacology* **42**, 612-618.
- Farrant, M., and Brickley, S.G. (2003). Properties of GABA_A receptor-mediated transmission at newly formed Golgi-granule cell synapses in the cerebellum. *Neuropharmacology.* **44**, 181-189.
- Feng, H., Kao, C., Gallagher, M.J., Jansen, E.D., Mahadevan-Jansen, A., Konrad, P.E., and Macdonald, R.L. (2010). Alteration of GABAergic neurotransmission by pulsed infrared laser stimulation. *J Neurosci. Methods.* **30**, 110-114.
- Findeisen, F., and Minor, Jr., D.L. (2009). Disruption of the IS6-AID linker affects voltage-gated Calcium channel inactivation and facilitation. *J. Gen. Physiol.* **133**, 327-343.
- Fogelson, A.L., and Zucker, R.S. (1985). Presynaptic calcium diffusion from various arrays of single channels. Implications for transmitter release and synaptic facilitation. *Biophys. J.* **48**, 1003-1017.
- Fonfría, E., Rodríguez-Farré, E., and Suñol, C. (2001). Mercury interaction with the GABA_A receptor modulates the benzodiazepine binding site in primary cultures of mouse cerebellar granule cells. *Neuropharmacology.* **41**, 819-833.
- Fonfría, E., Dare, E., Benelli, M. Suñol, C., and Ceccatelli, S. (2002). Translocation of apoptosis-inducing factor in cerebellar granule cells exposed to neurotoxic agents inducing oxidative stress. *Eur J Neurosci* **16**, 2013-2016.
- Fox, D.A., Grandjean, P., de Groot, D., and Paule, M.G. (2012). Developmental origins of adult diseases and neurotoxicity: epidemiological and experimental studies. *Neurotoxicology* **33**, 810-816.
- Gall, D., Roussel, C., Susa, I., D'Angelo, E., Rossi, P., Bearzatto, B., Galas, M.C., Blum, D., Schurmans, S., and Schiffmann, S.N. (2003). Altered neuronal excitability in cerebellar granule cells of mice lacking calretinin. *J. Neurosci.* **23**, 9320-9327.
- Gall, D., Roussel, C., Nieuw, T., Cheron, G., Servais, L., D'Angelo, E., and Schiffmann, S.N. (2005). Role of calcium binding proteins in the control of cerebellar granule cell neuronal excitability: experimental and modeling studies. *Prog Brain Res.* **148**, 321-8.

- Galeffi, F., Sah, R., Pond, B.B., George, A., and Schwartz-Bloom, R.D. (2004). Changes in intracellular chloride after oxygen-glucose deprivation of the adult hippocampal slice: effect of diazepam. *J. Neurosci.* **24**, 4478-4488.
- Galofré, M., Babot, Z., García, D.A., Iraola, S., Rodríguez-Farré, E., Forsby, A., and Suñol, C. (2010). GABA_A receptor and cell membrane potential as functional endpoints in cultured neurons to evaluate chemicals for human acute toxicology. *Neurotoxicol. Teratol.* **32**, 52-61.
- Gault, L.M., and Siegel, R.E. (1997). Expression of the GABA_A receptor δ subunit is selectively modulated by depolarization in cultured rat cerebellar granule neurons. *J. Neurosci.* **17**, 2391-2399.
- Gassó, S., Cristòfol, R.M., Selema, G., Rosa, R., Rodríguez-Farré, E., and Sanfeliu, C. (2001). Antioxidant compounds and Ca²⁺ pathway blockers differentially protect against methylmercury and mercuric chloride neurotoxicity. *J. Neurosci. Res.* **66**, 135-145.
- Geppert, M., Goda, Y., Hammer, R.E., Li, C., Rosahl, T.W., Stevens, C.F., and Sudhof T.C. (1994). Synaptotagmin I: a major Ca²⁺ sensor for transmitter release at a central synapse. *Cell* **79**, 717-727.
- Gibon, J., Tu, P., Frazzini, V., Sensi, S.L., and Bouron, A. (2010). The thiol-modifying agent N-ethylmaleimide elevates the cytosolic concentration of free Zn(2+) but not of Ca(2+) in murine cortical neurons. *Cell Calcium* **48**, 37-43.
- Glazner, G.W., and Mattson, M.P. (2000). Differential effects of BDNF, ADNF9, and TNF α on levels of NMDA receptor subunits, calcium homeostasis, and neuronal vulnerability to excitotoxicity. *Exp. Neurol.* **161**, 442-452.
- Gleichmann, M., and Mattson, M.P. (2011). Neuronal calcium homeostasis and dysregulation. *Antioxid. Redox Signal.* **14**, 1261-73.
- Grabrucker, A.M., Knight, M.J., Proepper, C., Bockmann, J., Joubert, M., Rowan, M., Nienhaus, G.U., Garner, C.C., Bowie, J.U., Kreutz, M.R., Gundelfinger, E.D., and Boeckers, T.M. (2011). Concerted action of zinc and ProSAP/Shank in synaptogenesis and synapse maturation. *EMBO J.* **30**, 569-581.
- Grishin, A., Li, H., Levitan, E.S., and Zaks-Makhina, (2006). Identification of γ -aminobutyric acid receptor-interacting factor 1 (TRAK2) as a trafficking factor for the K⁺ channel Kir2.1. *J. Biol. Chem.* **281**, 30104-30111.
- Hajela, R.K., Peng, S.Q., and Atchison, W.D. (2003). Comparative effects of methylmercury and Hg²⁺ on human neuronal N- and R- type high-voltage activated calcium channels

- transiently expressed in Human Embryonic Kidney 293 cells. *J Pharmacol Exp Ther* **306**, 1129-1136.
- Haller, V.L., Bernstein, M.A., and Welch, S.P. (2005). Chronic morphine treatment decreases the CaV1.3 subunit of the L-type calcium channel. *Eur. J. Pharmacol.* **578**, 101-107.
- Harada, M. (1978). Congenital Minamata disease: intrauterine methylmercury poisoning. *Teratology.* **18**, 285-288.
- Hare, M.F., McGinnis, K.M., and Atchison, W.D. (1993). Methylmercury increases intracellular concentrations of Ca⁺⁺ and heavy metals in NG108-15 cells. *J. Pharmacol. Exp. Ther.* **266**, 1626-1635.
- Hashimoto, M., and Hiri, M. (2012). Development and evolution of cerebellar neural circuits. *Develop. Growth Differ.* **54**, 373-389.
- Heath, J.C., Banna, K.M., Reed, M.N., Pesek, E.F., Cole, N., Li, J., and Newland, M.C. (2010). Dietary selenium protects against selected signs of aging and methylmercury exposure. *Neurotoxicology* **31**, 169-179.
- Helmcke, K.J., Aschner, M. (2010). Hormetic effect of methylmercury on *Caenorhabditis elegans*. *Toxicol. Appl. Pharmacol.* **248**, 156-164.
- Herden, C.J., Pardo, N.E., Hajela, R.K., Yuan, Y., and Atchison, W.D. (2008). Differential effects of methylmercury on γ -aminobutyric acid type A receptor currents in rat cerebellar granule and cerebral cortical neurons in culture. *J Pharmacol Exp Ther* **324**, 517-528.
- Homanics, G.E., Ferguson, C., Quinlan, J.J., Daggett, J., Snyder, K., Lagenaur, C., Mi, Z.P., Wang, X.H., Grayson, D.R., Firestone, L.L. (1997) Gene knockout of the $\alpha 6$ subunit of the gamma-aminobutyric acid type A receptor: lack of effect on responses to ethanol, pentobarbital, and general anesthetics. *Mol. Pharmacol.* **51**, 588-596.
- Hoogland, T.M., Kuhn, B., and Wang, S.S.-H. (2011). Preferential loading of Bergmann glia with synthetic acetoxymethyl calcium dyes. *Cold Spring Harb. Protoc.* **2011**, 1228-1231.
- Houston, C.M., McGee, T.P., MacKenzie, G., Troyano-Cuturi, K., Mateos Rodriguez, P., Kutsarova, E., Diamanti, E., Hosie, A.M., Franks, N.P., and Brickley, S.G. (2012). Are extrasynaptic GABAA receptors important targets for sedative/hypnotic drugs? *J. Neurosci.* **32**, 3887-3897.
- Huang, C., Liu, S., Hsu, C., Lin-and Shiau, S. (2011). Neurotoxicological effects of low-dose methylmercury and mercuric chloride in developing offspring mice. *Toxicol. Lett.* **201**, 196-204.

- Huang, W.C., Young, J.S., and Glitsch, M.D. (2007). Changes in TRPC channel expression during postnatal development of cerebellar neurons. *Cell Calcium* **42**, 1-10.
- Hunter, D., and Russell, D.S. (1954). Focal cerebral and cerebellar atrophy in a human subject due to organic mercury compounds. *J Neurol Neurosurg Psychiat* **17**, 235-241.
- Inada, H., Watanabe, M., Uchida, T., Ishibashi, H., Wake, H., Nemoto, T., Yanagawa, Y., Fukuda, A., and Nabekura, J. (2011). GABA regulates the multidirectional tangential migration of GABAergic interneurons in living neonatal mice. *PLoS One*. **6**, e27048.
- Inoue, T., and Bryant, B.P. (2005). Multiple types of sensory neurons respond to irritating volatile organic compounds (VOCs): Calcium fluorimetry of trigeminal ganglion neurons.
- Isaev, N.K., Lozier, E.R., Novikova, S.V., Silachev, D.N., Zorov, D.B., and Stelmashook, E.V. (2012). Glucose starvation stimulates Zn²⁺ toxicity in cultures of cerebellar granule neurons. *Brain Res. Bull.* **87**, 80-84.
- Ito, M. (2006). Cerebellar circuitry as a neuronal machine. *Prog. In Neurobiol.* **78**, 272-303.
- Ito, M. (2008). Control of mental activities by internal models in the cerebellum. *Nat. Rev. Neurosci.* **9**, 304-313.
- Jacob, T.C., Moss, S.J., and Jurd, R. (2008). GABA(A) receptor trafficking and its role in the dynamic modulation of neuronal inhibition. *Nat. Rev. Neurosci.* **9**, 331-43.
- Jiang, D., Sullivan, P.G., Sensi, S.L., Steward, O., Weiss, J.H. (2001). Zn(2+) induces permeability transition pore opening and release of pro-apoptotic peptides from neuronal mitochondria. *J. Biol. Chem.* **276**, 47524-47529.
- Johnson, F.O., Yuan, Y., Hajela, R.K., Chitrakar, A., Parsell, D.M., and Atchison, W.D. (2011). Exposure to an environmental neurotoxicant hastens the onset of amyotrophic lateral sclerosis-like phenotype in human Cu²⁺/Zn²⁺ superoxide dismutase 1 G93A mice: glutamate-mediated excitotoxicity. *J. Pharmacol. Exp. Ther.* **338**, 518-527.
- Joksimović, S., Varagic, Z., Kovačević, J., Van Linn, M., Milić, M., Rallapalli, S., Timić, T., Sieghart, W., Cook, J.M., and Savić, M.M. (2013). Insights into functional pharmacology of $\alpha 1$ GABAA receptors: how much does partial activation at the benzodiazepine site matter? *Psychopharmacology*. Advanced Access published May 18, 2013. doi:10.1007/s00213-013-3143-4.
- Jones, R.S., and Heinemann, U.H. (1987). Differential effects of calcium entry blockers on pre- and postsynaptic influx of calcium in the rat hippocampus in vitro. *Brain Res.* **416**, 257-266.

- Jones, A., Korpi, E.R., McKernan, R.M., Pelz, R., Nusser, Z., Mäkelä, R., Mellor, J.R., Pollard, S., Bahn, S., Stephenson, F.A., Randall, A.D., Sieghart, W., Somogyi, P., Smith, A.J.H., and Wisden, W. (1997). Ligand-gated ion channel subunit partnerships: GABA_A receptor $\alpha 6$ subunit gene inactivation inhibits δ subunit expression. *J. Neurosci.* **17**, 1350-1362.
- Joyce, C.J. (2007). In silico comparative genomic analysis of GABA_A receptor transcriptional dynamics. *BMC Genomics* **8**, 203.
- Juárez, B.I., Portillo-Salazar, H., González-Amaro, R., Mandeville, P., Aguirre, J.R., and Jiménez, M.E. (2005). Participation of N-methyl-D-aspartate receptors on methylmercury-induced DNA damage in rat frontal cortex. *Toxicology* **207**, 223-9.
- Kass, G.E., and Orrenius, S. (1999). Calcium signaling and cytotoxicity. *Environ. Health Perspect.* **107**, 25-35.
- Kasischke, K., Büchner, M., Ludolph, A.C., and Riepe, M.W. (2001). Nuclear shrinkage in live mouse hippocampal slices. *Acta Neuropathol.* **101**, 483-490.
- Kerper, L.E., Ballatori, N., and Clarkson, T.W..(1992) Methylmercury transport across the blood-brain barrier by an amino acid carrier. *Am. J. Physiol.* **262**, R761-765.
- Khom, S., Strommer, B., Ramharter, J., Schwarz, T., Schwarzer, C., Erker, T., Ecker, G.F., Mulzer, J., and Hering, S. (2010). Valerenic acid derivatives as novel subunit-selective GABA_A receptor ligands - in vitro and in vivo characterization. *Br. J. Pharmacol.* **161**, 65-78.
- Knight, M.M., Roberts, S.R., Lee, D.A., and Bader, D.L. (2003). Live cell imaging using confocal microscopy induces intracellular calcium transients and cell death. *Am J Physiol Cell Physiol* **284**, C1083–C1089.
- Komuro, H., and Kumada, T. (2005). Ca²⁺ transients control CNS neuronal migration. *Cell Calcium* **37**, 387-393.
- Komuro, H., and Rakic, P. (1992). Selective role of N-type calcium channels in neuronal migration. *Science* **257**, 806-809.
- Komuro, H., and Rakic, P. (1993). Modulation of neuronal migration by NMDA receptors. *Science* **260**, 95-97.
- Komuro, H., and Rakic, P. (1998). Distinct modes of neuronal migration in different domains of developing cerebellar cortex. *J Neurosci* **18**,1478-1490.

- Korpi, E.R., Koikkalainen, P., Vekovischeva, O.Y., Mäkelä, R., Kleinz, R., Uusi-Oukari, M., and Wisden, W. (1999). Cerebellar granule-cell-specific GABAA receptors attenuate benzodiazepine-induced ataxia: evidence from alpha 6-subunit-deficient mice. *Eur. J. Neurosci.* **11**, 233-240.
- Kuhn, B., Hoogland, T.M., and Wang, S.S.-H. (2011). Cerebellar craniotomy for in vivo calcium imaging of astrocytes. *Cold Spring Harb. Protoc.* **2011**, 1224-1227.
- Kukulski, W., Schorb, M., Welsch, S., Picco, A., Kaksonen, M., and Briggs, J.A.G. (2011). Correlated fluorescence and 3D electron microscopy with high sensitivity and special precision. *J. Cell Biol.* **192**, 111-119.
- Kullman, D.M., Ruiz, A., Rusakov, D.M., Scott, R., Semyanov, A., and Walker, M.C. (2005). Presynaptic, extrasynaptic and axonal GABAA receptors in the CNS: where and why? *Prog. Biophys. Mol. Bio.* **87**, 33-46.
- Kumada, T., and Komuro, H. (2004). Completion of neuronal migration regulated by loss of calcium transients. *PNAS* **101**, 8479-8484.
- Kumada, T., Komuro, Y., Li, Y., Hu, T., Wang, Z., Littner, Y., and Komuro, H. (2010). Inhibition of cerebellar granule cell turning by alcohol. *Neuroscience* **170**, 1328-1344.
- Laha, K.T., and Wagner, D.A. (2011). A state-dependent salt-bridge interaction exists across the β/α inter-subunit interface of the GABAA receptor. *Mol. Pharmacol.* **79**, 662-671.
- Landfield, P.W., Pitler, T.A. (1984). Prolonged Ca²⁺-dependent afterhyperpolarizations in hippocampal neurons of aged rats. *Science* **226**, 1089-1092.
- Laure-Kamionowska, M., and Maślińska, D. (2011). Cerebellar cortical neurons misplaced in the white matter due to disturbed migration during development of human brain. *Folia Neuropathol.* **49**, 282-294.
- Leclerc, C., Néant, I., and Moreau, M. (2011). Early neural development in vertebrates is also a matter of calcium. *Biochimie* **93**, 2102-2111.
- Lee, H.H.C., Walker, J.A., Williams, J.R., Goodier, R.J., Payne, J.A., and Moss, S.J. (2007). Direct protein kinase C-dependent phosphorylation regulates the cell surface stability and activity of the potassium chloride cotransporter KCC2. *J. Biol. Chem.* **282**, 29777-29784.
- Lehoullier, P.F., and Ticku, M.K. (1989). The pharmacological properties of GABA receptor-coupled chloride channels using ³⁶Cl-influx in cultured spinal cord neurons. *Brain Res.* **487**, 205-214.

- Letts, V.A., Felix, R., Biddlecome, G.H., Arikath, J., Mahaffey, C.L., Valenzuela, A., Bartlett, F.S. 2nd., Mori, Y., Campbell, K.P., and Frankel, W.N. (1998). The mouse stargazer gene encodes a neuronal Ca²⁺-channel gamma subunit. *Nat. Genet.* **19**, 340-347.
- Levesque, P.C., and Atchison, W.D. (1987). Interactions of mitochondrial inhibitors with methylmercury on spontaneous quantal release of acetylcholine. *Toxicol. Appl. Pharmacol.* **87**, 315-324.
- Limke, T.L., Bearss, J.J., and Atchison, W.D. (2004). Acute exposure to methylmercury causes Ca²⁺ dysregulation and neuronal cell death in rat cerebellar granule cells through an M₃ muscarinic receptor-linked pathway. *Toxicol Sci* **80**, 60-68.
- Limke, T.L., and Atchison, W.D. (2002). Acute exposure to methylmercury opens the mitochondrial permeability transition pore in rat cerebellar granule cells. *Toxicol Appl Pharmacol* **178**, 52-61.
- Limke, T.L., Otero-Montañez, J.K., and Atchison, W.D. (2003). Evidence for interactions between intracellular calcium stores during methylmercury-induced intracellular calcium dysregulation in rat cerebellar granule cells. *J Pharmacol Exp Ther* **304**, 949-958.
- Lo, W., Lagrange, A.H., Hernandez, C.C., Harrison, R., Dell, A., Haslam, S.M., Sheehan, J.H., and Macdonald, R.L. (2010). Glycosylation of $\beta 2$ subunits regulates GABAA receptor biogenesis and channel gating. *J. Biol. Chem.* **285**, 31348-31361.
- Long, P., Mercer, A., Begum, R., Stephens, G.J., Sihra, T.S., and Jovanovic, J.N. (2009). Nerve terminal GABAA receptors activate Ca²⁺/Calmodulin-dependent signaling to inhibit voltage-gated Ca²⁺ influx and glutamate release. *J. Biol. Chem.* **284**, 8726-8737.
- Lyons, H.R., Land, M.B., Gibbs, T.T., and Farb, D.H. (2001). Distinct signal transduction pathways for GABA-induced GABAA receptor down-regulation and uncoupling in neuronal culture: a role for voltage-gated calcium channels. *J. Neurochem.* **78**, 1114-1125.
- MacDermott, A.B., Role, L.W., and Siegelbaum, S.A. (1999). Presynaptic ionotropic receptors and the control of transmitter release. *Annu. Rev. Neurosci.* **22**, 443-485.
- Macdonald, R.L., Kang, J., and Gallagher, M.J. (2010). Mutations in GABAA receptor subunits associated with genetic epilepsies. *J Physiol.* **588.11**, 1861-1869.
- Magos, L., and Clarkson, T.W. (2006) Overview of the clinical toxicity of mercury. *Ann Clin Biochem.* **43**, 257-68.
- Maguire, J., Ferando, I., Simonsen, C., and Mody, I. (2009) Excitability changes related to GABAA receptor plasticity during pregnancy. *J. Neurosci.* **29**, 9592-601.

- Mahapatra, C.T., Bond, J., Rand, D.M., and Rand, M.D. (2010). Identification of methylmercury tolerance gene candidates in *Drosophila*. *Toxicol. Sci.* **116**, 225-238.
- Mäkelä, R., Uusi-Oukari, M., Homanics, G.E., Quinlan, J.J., Firestone, L.L., Wisden, W., and Korpi, E.R. (1997). Cerebellar gamma-aminobutyric acid type A receptors: pharmacological subtypes revealed by mutant mouse lines. *Mol. Pharmacol.* **52**, 380-388.
- Mancini, J.D., Autio, D.M., and Atchison, W.D. (2009). Continuous exposure to low concentrations of methylmercury impairs cerebellar granule cell migration in organotypic slice culture. *NeuroToxicology* **30**, 203-208.
- Manev, H., Kharlamov, E., Uz, T., Mason, R.P., Cagnoli, C.M. (1997). Characterization of zinc-induced neuronal death in primary cultures of rat cerebellar granule cells. *Exp. Neurol.* **146**, 171-178.
- Mao, X., Ma, P., Cao, D., Sun, C., Ji, Z., Min, D., Sun, H., Xie, N., Cai, J., and Cao, Y. (2011). Altered expression of GABAA receptors ($\alpha 4$, $\gamma 2$ subunit), potassium chloride cotransporter 2 and astrogliosis in tremor rat hippocampus. *Brain Res. Bull.* **25**, 373-379.
- Marchionni, I., Kasap, Z., Mozrzymas, J.W., Sieghart, W., Cherubini, E., and Zacchi, P. (2009). New insights on the role of gephyrin in regulating both phasic and tonic GABAergic inhibition in rat hippocampal neurons in culture. *Neuroscience.* **164**, 552-562.
- Marczynski, T.J. (1998). GABAergic deafferentation hypothesis of brain aging and Alzheimer's disease revisited. *Brain Res. Bull* **45**, 341-379.
- Marty, M.S., and Atchison, W.D. (1997). Pathways mediating Ca^{2+} entry in rat cerebellar granule cells following in vitro exposure to methyl mercury. *Toxicol Appl Pharmacol.* **147**, 319-30.
- Marty, M.S., and Atchison, W.D. (1998). Elevations of Ca^{2+} as a probable contributor to decreased viability in cerebellar granule cells following acute exposure to methylmercury. *Toxicol Appl Pharmacol* **150**, 98-105.
- Mehlin, C., Crittenden, C., and Andreyka, J. (2003). No-wash dyes for calcium flux measurement. *BioTechniques* **34**, 164-166.
- Mennerick, S., He, Y., Jiang, X., Manion, B.D., Wang, M., Shute, A., Benz, A., Evers, A.S., Covey, D.F., Zorumski, C.F. (2005). Selective antagonism of 5 α -reduced neurosteroid effects at GABA(A) receptors. *Mol. Pharmacol.* **65**, 1191-1197.
- Métin, C., Vallee, R.B., Rakic, P., and Bhide, P.G. (2008). Modes and mishaps of neuronal migration in the mammalian brain. *J. Neurosci.* **28**, 11746-11752.

- Micheva, K.D., Busse, B., Weiler, N.C., O'Rourke, N., and Smith, S.J. (2010). Single-synapse analysis of a diverse synapse population: proteomic imaging methods and markers. *Neuron*. **68**, 639-653.
- Minnema, D.J., Cooper, G.P., and Greenland, R.D. (1989). Effects of methylmercury on neurotransmitter release from rat brain synaptosomes. *Toxicol. Appl. Pharmacol.* **99**, 510-521.
- Morishima, T., Uematsu, M., Furukawa, T., Yanagawa, Y., Fukuda, A., and Yoshida, S. (2010). GABA imaging in brain slices using immobilized enzyme-linked photoanalysis. *Neurosci. Res.* **67**, 347-353.
- Myers, G.J., Thurston, S.W., Pearson, A.T., Davidson, P.W., Cox, C., Shamlaye, C.F., Cernichiari, E., and Clarkson, T.W. (2009). Postnatal exposure to methyl mercury from fish consumption: a review and new data from the Seychelles Child Development Study. *Neurotoxicology* **30**, 338-349.
- Nusser, Z., Ahmad, Z., Tretter, V., Fuchs, K., Wisden, W., Sieghart, W., and Somogyi, P. (1999). Alterations in the expression of GABAA receptor subunits in cerebellar granule cells after disruption of the $\alpha 6$ subunit gene. *Eur. J. Neurosci.* **11**, 1685-1697.
- Nusser, Z., Roberts, J.D., Baude, A., Richards, J.G., and Somogyi, P. (1995). Relative densities of synaptic and extrasynaptic GABAA receptors on cerebellar granule cells as determined by a quantitative immunogold method. *J. Neurosci.* **15**, 2948-2960.
- Nusser, Z., Sieghart, W., and Somogyi, P. (1998). Segregation of different GABA_A receptors to synaptic and extrasynaptic membranes of cerebellar granule cells. *J Neurosci* **18**, 1693-1703.
- Ohtsuki, G., and Hirano, T. (2008). Bidirectional plasticity at developing climbing fiber-Purkinje neuron synapses. *Eur. J. Neurosci.* **28**, 2393-2400.
- Olsen, R.W., Bureau, M.H., Endo, S., and Smith, G. (1991). The GABAA receptor family in the mammalian brain. *Neurochem. Res.* **16**, 317-325.
- Olsen, R.W., and Sieghart, W. (2009). GABA A receptors: subtypes provide diversity of function and pharmacology. *Neuropharmacology.* **56**,141-8.
- Olsen, R.W., and Tobin, A.J. (1990). Molecular biology of GABAA receptors. *FASEB J.* **4**, 1469-1480.

- Onishchenko, N., Karpova, N., Sabri, F., Castrén, E., and Ceccatelli, S. (2008). Long-lasting depression-like behavior and epigenetic changes of BDNF gene expression induced by perinatal exposure to methylmercury. *J. Neurochem.* **106**, 1378-1387.
- Ophoff, R.A., Terwindt, G.M., Vergouwe, M.N., van Eijk, R., Oefner, P.J., Hoffman, S.M., Lamerdin, J.E., Mhrenweiser, H.W., Bulman, D.E., Ferrari, M., Haan, J., Lindhout, D., van Ommen, G.J., Hofker, M.H., Ferrari, M.D., Frants, R.R. (1996). Familial hemiplegic migraine and episodic ataxia type-2 are caused by mutations in the Ca²⁺ channel gene CACNL1A4. *Cell* **87**, 543-552.
- Ortinski, P.I., Lu, C., Takagaki, K., Fu, Z., and Vicini, S. (2004). Expression of distinct alpha subunits of GABAA receptor regulates inhibitory synaptic strength. *J. Neurophysiol.* **92**, 1718-1727.
- Ou, Y.C., White, C.C., Krejsa, C.M., Ponce, R.A., Kavanagh, T.J., and Faustman, E.M. (1999). The role of intracellular glutathione in methylmercury-induced toxicity in embryonic neuronal cells. *Neurotoxicology* **20**, 793-804.
- Owens, D.F., Boyce, L.H., Davis, M.B.E., and Kriegstein, A.R. (1996). Excitatory GABA responses in embryonic and neonatal cortical slices demonstrated by gramicidin perforated-patch recordings and calcium imaging. *J. Neurosci.* **16**, 6414-6423.
- Paletz, E.M., Day, J.J., Craig-Schmidt, M.C., and Newland, M.C. (2007). Spatial and visual discrimination reversals in adult and geriatric rats exposed during gestation to methylmercury and n-3 polyunsaturated fatty acids. *Neurotoxicology*. **28**, 707-19.
- Pancani, T., Anderson, K.L., Porter, N.M., Thibault, O. (2011). Imaging of a glucose analogue, calcium and NADH in neurons and astrocytes: dynamic responses to depolarization and sensitivity to pioglitazone. *Cell Calcium*. **50**, 548-558.
- Pardo, N.E., Hajela, R.K., and Atchison, W.D. (2006). Acetylcholine release at neuromuscular junctions of adult tottering mice is controlled by N- (Cav2.2) and R-type (Cav2.3) but not L-type (Cav1.2) Ca²⁺ channels. *JPET*. **319**, 1009-1020.
- Payne, H.L., Connelly, W.M., Ives, J.H., Lehner, R., Furtmuller, B., Sieghart, W., Tiwari, P., Lucocq, J.M., Lees, G., and Thompson, C.L. (2007). GABAA $\alpha 6$ -containing receptors are selectively compromised in cerebellar granule cells of the ataxic mouse, Stargazer. *J. Biol. Chem.* **282**, 29130-29143.

- Payne, H.L., Ives, J.H., Sieghart, W., and Thompson, C.L. (2008). AMPA and kainate receptors mediate mutually exclusive effects on GABAA receptor expression in cultured mouse cerebellar granule neurones. *J. Neurochem.* **104**, 173-186.
- Peça, J., Feliciano, C., Ting, J.T., Wang, W., Wells, M.F., Venkatraman, T.N., Lascola, C.D., Fu, Z., Feng, G. (2011). Shank3 mutant mice display autistic-like behaviours and striatal dysfunction. *Nature* **472**, 437-442.
- Pelkey, K.A., Topolnik, L., Lacaille, J.C., and McBain, C.J. (2006). Compartmentalized Ca(2+) channel regulation at divergent mossy-fiber release sites underlies target cell-dependent plasticity. *Neuron* **52**, 497-510.
- Peng, S.Q., Hajela, R.K., and Atchison, W.D. (2002). Effects of methylmercury on human neuronal L-type calcium channels transiently expressed in Human Embryonic Kidney cells (HEK-293). *J Pharmacol Exp Ther* **302**, 424-432.
- Petersen, M.S., Halling, J., Bech, S., Wermuth, L., Weihe, P., Nielsen, F., Jørgensen, P.J., Budtz-Jørgensen, E., and Grandjean, P. (2008). Impact of dietary exposure to food contaminants on the risk of Parkinson's disease. *Neurotoxicology* **29**, 584-590.
- Petroni, D., Tsai, J., Mondal, D., and George, W. (2011). Attenuation of low dose methylmercury and glutamate induced-cytotoxicity and tau phosphorylation by an N-methyl-D-aspartate antagonist in human neuroblastoma (SHSY5Y) cells. *Environ. Toxicol.* Early Access: doi: 10.1002/tox.20765.
- Poulter, M.O., Du, L., Zhurov, V., Merali, Z., and Anisman, H. (2009) Plasticity of the GABA(A) receptor subunit cassette in response to stressors in reactive versus resilient mice. *Neuroscience* **165**, 1039-51.
- Prodanov, D., Heeroma, J., and Marani E. (2006). Automatic morphometry of synaptic boutons of cultured cells using granulometric analysis of digital images. *J. Neurosci. Methods* **151**, 168-177.
- Pugh, J.R., and Jahr, C.E. (2011). Axonal GABAA receptors increase cerebellar granule cell excitability and synaptic activity. *J. Neurosci.* **31**, 565-574.
- Qian, Z., Yakhnitsa, V., and Barmack, N.H. (2011). Climbing fiber-evoked Purkinje cell discharge reduces expression of GABA(A) receptor-associated protein (GABARAP) and decreases its interaction with GABA(A) receptors. *J. Neurochem.* **117**, 197-208.

- Raiteri, L., Schmid, G., Prestipino, S., Ratieri, M., and Bonanno, G. (2001). Activation of $\alpha 6$ GABAA receptors on depolarized cerebellar parallel fibers elicits glutamate release through anion channels. *Neuropharmacology*. **41**, 943-951.
- Rakotomamonjy, J., Levenes, C., Bailieu, E.E., Schumacher, M., and Ghomari, A.M. (2011) Novel protective effect of mifepristone on detrimental GABAA receptor activity in immature Purkinje cells. *FASEB J.* **25**, 3999-4010.
- Rand, M.D. (2010). Drosophotoxicology: the growing potential for Drosophila in neurotoxicology. *Neurotoxicol. Teratol.* **32**, 74.
- Rasband, W.S. "ImageJ", US National Institutes of Health, Bethesda, Maryland, USA, 1997-2011. rsb.info.nih.gov/ij/index.html Accessed 17 April 2012.
- Rasband, W., Dougherty, B., Collins, T., Karperian, A. and Stervbo, U. "Multi-Measure" Optinav, Inc. 2006. www.optinav.com/imagej.html accessed 17 April 2012.
- Rice, D., and Barone, S. Jr. (2000). Critical periods of vulnerability for the developing nervous system: evidence from human and animal models. *Environ Health Perspect* **108**, Suppl:511-533.
- Rizzuto, R., Bastianutto, C., Brini, M., Murgia, M., and Pozzan, T. (1994). Mitochondrial Ca^{2+} homeostasis in intact cells. *J. Cell Biol.* **126**, 1183-1194.
- Roda, E., Coccini, T., Acerbi, D., Castoldi, A., Bernocchi, G., and Manzo, L. (2008). Cerebellum cholinergic muscarinic receptor (subtype-2 and -3) and cytoarchitecture after developmental exposure to methylmercury: an immunohistochemical study in rat. *J Chem Neuroanat* **35**, 285-294.
- Roda, E., Manzo, L., and Coccini, T. (2012) Application of chemical markers for assessing health effects after developmental methylmercury and PCB coexposure. *J. Toxicol.* **2012**, 216032.
- Rüegg, P.C., and Nelson, D.J. (1989). Safety and efficacy of isradipine, alone and in combination, in the treatment of angina pectoris. *Am. J. Med.* **86**, 70-74.
- Ruiz, A., Matute, C., and Alberdi, E. (2009) Endoplasmic reticulum Ca^{2+} release through ryanodine and IP(3) receptors contributes to neuronal excitotoxicity. *Cell Calcium* **46**, 273-281.
- Sabatini, B.L., and Regehr, W.G. (1995). Detecting changes in calcium influx which contribute to synaptic modulation in mammalian brain slice. *Neuropharmacology* **34**, 1453-1467.

- Sainlos, M., Tigaret, C., Poujol, C., Olivier, N.B., Bard, L., Breillat, C., Thiolon, K., Choquet, D., and Imperiali, B. (2010). Biomimetic divalent ligands for the acute disruption of synaptic AMPAR stabilization. *Nature Chem. Biol.* **7**, 81-91.
- Sakamoto, M., Ikegami, N., and Nakano A. (1996). Protective effects of Ca²⁺ channel blockers against methyl mercury toxicity. *Pharmacol. Toxicol.* **78**, 193-199.
- Sakamoto, M., Wakabayashi, K., Kakita, A., Takahashi, H., Adachi, T., and Nakano, A. (1998). Widespread neuronal degeneration in rats following oral administration of methylmercury during the postnatal development stage: a model of fetal-type Minamata disease. *Brain Res* **784**, 351-354.
- Sakamoto, M., Kakita, A., de Oliviera, R.B., Pan, H.S., and Takahashi, H. (2004). Dose-dependent effects of methylmercury administered during neonatal brain spurts in rats. *Dev Brain Res* **152**, 171-176.
- Sanna, E., Mascia, M.P., Klein, R.L., Whiting, P.J., Biggio, G., and Harris, R.A. (1995). Actions of the general anesthetic propofol on recombinant human GABAA receptors: influence of receptor subunits. *JPET* **274**, 353-360.
- Sanna, E., Murgia, A., Casula, A., Usala, M., Maciocco, E., Tuligi, G., and Biggio, G. (1996). Direct activation of GABAA receptors by loreclezole, an anticonvulsant drug with selectivity for the beta-subunit. *Neuropharmacology* **35**, 1753-1760.
- Sarafian, T., and Verity, M.A. (1991). Oxidative mechanisms underlying methyl mercury neurotoxicity. *Int. J. Dev. Neurosci.* **9**, 147-153.
- Sauter, A., and Rudin, M. (1990). Calcium antagonists for reduction of brain damage in stroke. *J. Cardiovasc. Pharmacol.* **15 Suppl. 1**, S43-S47.
- Sauter, A., and Rudin, M. (1991). Prevention of stroke and brain damage with calcium antagonists in animals. *Am. J. Hypertens.* **4**, 121S-127S.
- Saxena, N.C., and Macdonald, R.L. (1996). Properties of putative cerebellar gamma-aminobutyric acid A receptor isoforms. *Mol Pharmacol* **49**, 567-579.
- Schmid, G., Chittolini, R., Raiteri, L., and Bonanno, G. (1999). Differential effects of zinc on native GABA(A) receptor function in rat hippocampus and cerebellum. *Neurochem. Int.* **34**, 399-405.
- Schneggenberger, R., Han, Y., and Kochubey, O. (2012). Ca²⁺ channels and transmitter release at the active zone. *Cell Calcium* **52**, 199-207.

- Schonewille, M., Belmeguenai, A., Koekkoek, S.K., Houtman, S.H., Boele, H.J., van Beugen, B.J., Gao, Z., Badura, A., Ohtsuki, G., Amerika, W.E., Hosal, E., Hoebeek, F.E., Elgersma, Y., Hansel, C., and De Zeeuw, C.I. (2010). Purkinje cell-specific knockout of the protein phosphatase PP2B impairs potentiation and cerebellar motor learning. *Neuron*. **67**, 618-628.
- Scott, J.A., Hamzelou, K.S., Rajagopalan, V., Habas, P.A., Kim, K., Barkovich, A.J., Glenn, O.A., and Studholme, C. (2012). 3D morphometric analysis of human fetal cerebellar development. *Cerebellum*, **11**, 761-770.
- Sensi, S.L., Yin, H.Z., and Weiss, J.H. (2000). AMPA/kainate receptor-triggered Zn²⁺ entry into cortical neurons induces mitochondrial Zn²⁺ uptake and persistent mitochondrial dysfunction. *Eur. J. Neurosci.* **12**, 3813-3818.
- Shafer, T.J., and Atchison, W.D. (1991). Methylmercury blocks N- and L-type Ca⁺⁺ channels in nerve growth factor-differentiated pheochromocytoma (PC12) cells. *JPET* **258**, 149-157.
- Shafer, T.J., Bushnell, P.J., Benignus, V.A., and Woodward, J.J. (2005). Perturbation of voltage-sensitive Ca²⁺ channel function by volatile organic solvents. *JPET*. **315**, 1109-1118.
- Shevtsova, O., and Leitch, B. (2013). Selective loss of AMPA receptor subunits at inhibitory neuron synapses in the cerebellum of the ataxic stargazer mouse. *Brain Res.* **1427**, 54-64.
- Shoshan-Barmatz, V., Zalk, R., Gincel, D., and Vardi, N. (2004). Subcellular localization of VDAC in mitochondria and ER in the cerebellum. *Biochim. Biophys. Acta.* **1657**, 105-114.
- Shrivastava, A.N., Triller, A., and Sieghart, W. (2011). GABA_A receptors: post-synaptic colocalization and cross-talk with other receptors. *Frontiers in Cell. Neurosci.* **5.7**, 1-12.
- Sigel, E., and Baur, R. (2000). Electrophysiological evidence for the coexistence of alpha1 and alpha6 subunits in a single functional GABA(A) receptor. *J. Neurochem.* **74**, 2590-2596.
- Simeone, T.A., Wilcox, K.S., and White, H.S. (2006). Subunit selectivity of topiramate modulation of heteromeric GABA(A) receptors. *Neuropharmacology* **50**, 845-857.
- Sirois, J.E., and Atchison, W.D. (1996) Effects of mercurials on ligand- and voltage-gated ion channels: a review. *NeuroToxicology* **17**, 63-84.
- Sirois, J.E., and Atchison, W.D. (2000). Methylmercury affects multiple subtypes of calcium channels in rat cerebellar granule cells. *Toxicol Appl Pharmacol* **167**, 1-11.

- Smith, A.J., Oxley, B., Malpas, S., Pillai, G.V., and Simpson, P.B. (2004). Compounds exhibiting selective efficacy for different beta subunits of human recombinant gamma-aminobutyric acid A receptors. *JPET* **311**, 601-609.
- Spät, A., Szanda, G., Csordás, G., and Hajnóczky, G. (2008). High- and low-calcium-dependent mechanisms of mitochondrial calcium signalling. *Cell Calcium* **44**, 51-63.
- Spurny, R., Ramerstorfer, J., Price, K., Brams, M., Ernst, M., Nury, H., Verheij, M., Legrand, P., Bertrand, D., Bertrand, S., Dougherty, D.A., de Esch, I.J.P., Corringer, P., Sieghart, W., Lummis, S.C.R., and Ulens, C. (2012). Pentameric ligand-gated ion channel ELIC is activated by GABA and modulated by benzodiazepines. *PNAS*. **109**, E3028-E3034.
- Stanley, E.F. (1993). Single calcium channels and acetylcholine release at a presynaptic nerve terminal. *Neuron* **11**, 1007-1011.
- Steel, R.G.D., and Torrie, J.H. (1960). Principles and procedures of statistics. New York: McGraw.
- Stern, S., Cox, C., Cernichiari, E., Balys, M., and Weiss, B. (2001). Perinatal and lifetime exposure to methylmercury in the mouse: blood and brain concentrations of mercury to 26 months of age. *Neurotoxicology* **22**, 467-477.
- Ström, S., Helmfrid, I., Glynn, A., and Berglund, M. (2011). Nutritional and toxicological aspects of seafood consumption – An integrated exposure and risk assessment of methylmercury and polyunsaturated fatty acids. *Environ. Res.* **111**, 274-280.
- Stutzmann, G.E. (2007). The pathogenesis of Alzheimers disease is it a lifelong "calciumopathy"? *Neuroscientist* **13**, 546-559.
- Suñol, C., Babot, Z., Fonfría, E., Galofré, M., García, D., Herrera, N., Iraola, S., and Vendrell, I. (2008). Studies with neuronal cells: from basic studies of mechanisms of neurotoxicity to the prediction of chemical toxicity. *Toxicol. In vitro.* **22**, 1350-1355.
- Tai, H.C., and Lim, C. (2006). Computational studies of the coordination stereochemistry, bonding, and metal selectivity of mercury. *J Phys Chem A*, **110**, 452-62.
- Takayama, C., and Inoue, Y. (2004). Transient expression of GABA_A receptor α 2 and α 3 subunits in differentiating cerebellar neurons. *Dev Brain Res* **148**, 169-177.
- Takayama, C., and Inoue, Y. (2006). Developmental localization of potassium chloride co-transporter 2 in granule cells of the early postnatal mouse cerebellum with special reference to the synapse formation. *Neuroscience* **143**, 757-767.

- Takeuchi T. (1968) Pathology of Minamata disease. In Minamata Disease, Study Group of Minamata disease, pp. 141–228. Kumamoto University, Shuhan Co., Japan.
- Takeuchi, T., Morikawa, N., Matsumoto, H., and Shiraishi, Y. (1962). A pathological study of Minamata Disease in Japan. *Acta Neuropathologica* **2**, 40-57.
- Tanaka, Y., Tanaka, Y., Furuta, T., Yanagawa, Y., and Kaneko, T. (2008). The effects of cutting solutions on the viability of GABAergic interneurons in cerebral cortical slices of adult mice. *J. Neurosci. Methods* **171**, 118-125.
- Tang, S.C., Arumugam, T.V., Cutler, R.G., Jo, D.G., Magnus, T., Chan, S.L., Mughal, M.R., Telljohann, R.S., Nassar, M., Ouyang, X., Calderan, A., Ruzza, P., Guiotto, A., and Mattson, M.P. (2007). Neuroprotective actions of a histidine analogue in models of ischemic stroke. *J. Neurochem.* **101**, 729-36.
- Tashiro, A., Aaron, G., Aronov, D., Cossart, R., Dumitriu, D., Fenstermaker, V., Goldberg, J., Hamzei-Sichani, F., Ikegaya, Y., Konur, S., MacLean, J., Nemet, B., Nikolenko, V., Portera-Cailliau, C., and Yuste R. (2006). Imaging brain slices. In Handbook of Biological Confocal Microscopy (J.B. Pawley, ed.), 3rd ed., pp.722-735. Springer Science+Business Media, New York, NY.
- Thévenaz, P., Ruttimann, U.E., and Unser, M. (1998). A pyramid approach to subpixel registration based on intensity. *IEEE Trans on Image Proc* **7**, 27-41.
- Toescu, E.C., and Vreugdenhil, M. (2010). Calcium and normal brain aging. *Cell Calcium* **47**, 158-164.
- Tokuomi, H., Uchino, M., Imamura, S., Yamanaga, H., Nakanishi, R., and Ideta, T. (1982) Minamata Disease (organic mercury poisoning): neurologic and electrophysiologic studies. *Neurology* **32**, 1369-1375.
- Traxinger, D., and Atchison, W.D. (1987). Comparative effects of divalent cations on the methylmercury-induced alterations of acetylcholine release. *JPET* **240**, 451-459.
- Tretter, V., Mukherjee, J., Maric, H., Schindelin, H., Sieghart, W., and Moss, S.J. (2012). Gephyrin, the enigmatic organizer at GABAergic synapses. *Frontiers in Cell. Neurosci.* **6.23**, 1-16.
- Tsang, S.Y., Ng, S.K., Xu, Z., and Xue, H. (2007). The evolution of GABAA receptor-like genes. *Mol. Biol. Evol.* **24**, 599-610.

- Tsetlin, V., Kuzmin, D., and Kasheverov, I. (2010) Assembly of nicotinic and other Cys-loop receptors. *J Neurochem.* **116**, 734-741.
- Tymianski, M., Charlton, M.P., Carlen, P.L., and Tator, C.H. (1993). Secondary Ca²⁺ overload indicates early neuronal injury which precedes staining with viability markers. *Brain Res.* **607**, 319-323.
- Uchino, M., Tanaka, Y., Ando, Y., Yonehara, T., Hara, A., Mishima, I., Okajima, T., and Ando, M. (1995). Neurologic features of chronic minamata disease (organic mercury poisoning) and incidence of complications with aging. *J. Environ. Sci. Health B* **30**, 699-715.
- US EPA, (1997). Methylmercury study report to congress. EPA-452/R-97-006.
- Usuki, F., Yasutake, A., Umehara, F., Tokunaga, H., Matsumoto, M., Eto, K., Ishiura, S., Higuchi, I. (2001). In vivo protection of a water-soluble derivative of vitamin E, Trolox, against methylmercury-intoxication in the rat. *Neurosci. Lett.* **304**, 199-203.
- Vale, C., Fonfría, E., Bujons, J., Messeguer, A., Rodríguez-Farré, E., and Suñol, C. (2003). The organochlorine pesticides γ -hexachlorocyclohexane (lindane), α -endosulfan and dieldrin differentially interact with GABAA and glycine-gated chloride channels in primary cultures of cerebellar granule cells. *Neuroscience.* **117**, 397-403.
- Varagic, Z., Wimmer, L., Schnürch, M., Mihovilovic, M.D., Huang, S., RallaPalli, S., Cook, J.M., Mirheydari, P., Ecker, G.F., Sieghart, W., and Ernst, M. (2013). Identification of novel positive allosteric modulators and null modulators at the GABAA receptor α + β -interface. *Brit. J. Pharmacol.* **169**, 371-383.
- Vendrell, I., Carrascal, M., Vilaró, M., Abián, J., Rodríguez-Farré, E., and Suñol C. (2007). Cell viability and proteomic analysis in cultured neurons exposed to methylmercury. *Human & Exp. Toxicol.* **26**, 263-272.
- Vendrell, I., Carrascal, M., Campos, F., Abián, J., and Suñol C. (2010). Methylmercury disrupts the balance between phosphorylated and non-phosphorylated cofilin in primary cultures of mice cerebellar granule cells A proteomic study. *Toxicol and Applied Pharmacol.* **242**, 109-118.
- Veng, L.M., Mesches, M.H., and Browning, M.D. (2003). Age-related working memory impairment is correlated with increases in the L-type calcium channel protein alpha1D (Cav1.3) in area CA1 of the hippocampus and both are ameliorated by chronic nimodipine treatment. *Brain Res. Mol. Brain Res.* **110**, 193-202.

- Vitalone, A., Catalani, A., Cinque, C., Fattori, V., Matteucci, P., Zuena, A.R., and Costa, L.G. (2010) Long-term effects of developmental exposure to low doses of PCB 126 and methylmercury. *Toxicol Lett.* **197**, 38-45.
- Volpe, J.J. (2009). Cerebellum of the premature infant: rapidly developing, vulnerable, clinically important. *J Child Neurol.* **24**,1085-104.
- Wafford, K.A., Thompson, S.A., Thomas, D., Sikela, J., Wilcox, A.S., and Whiting, P.J. (1996). Functional characterization of human gamma-aminobutyric acidA receptors containing the alpha 4 subunit. *Mol. Pharmacol.* **50**, 670-678.
- Wall, M.J. (2002). Furosemide reveals heterogeneous GABA(A) receptor expression at adult rat Golgi cell to granule cell synapses. *Neuropharmacology* **43**, 737-749.
- Wall, M.J. (2005). A role for zinc in cerebellar synaptic transmission? *Cerebellum* **4**, 224-229.
- Wang, Z., Danscher, G., Kim, Y.K., Dahlstrom, A., Mook Jo, S. (2002). Inhibitory zinc-enriched terminals in the mouse cerebellum: double-immunohistochemistry for zinc transporter 3 and glutamate decarboxylase. *Neurosci. Lett.* **321**, 37-40.
- Wankerl, K., Weise, D., Gentner, R., Rumpf, J.J., and Classen, J. (2010). L-type voltage-gated Ca²⁺ channels: a single molecular switch for long-term potentiation/long-term depression-like plasticity and activity-dependent metaplasticity in humans. *J. Neurosci.* **30**, 6197-6204.
- Weiss, B. (1990). Risk assessment: the insidious nature of neurotoxicity and the aging brain. *Neurotoxicology* **11**, 305-313.
- Weiss, B. (2010). Lead, manganese, and methylmercury as risk factors for neurobehavioral impairment in advanced age. *Int. J. Alzheimers Dis.* **2011**, 607543.
- Weiss, B., Clarkson, T.W., and Simon, W. (2002). Silent latency periods in methylmercury poisoning and in neurodegenerative disease. *Environ. Health Perspect.* **110 Suppl. 5**, 851-854.
- Weiss, B., Stern, S., Cox, C., and Balys, M. (2005). Perinatal and lifetime exposure to methylmercury in the mouse: behavioral effects. *Neurotoxicology* **26**, 675-690.
- Westenbroek, R.E., Sakurai, T., Elliott, E.M., Hell, J.W., Starr, T.V.B., Snutch, T.P., and Catterall W.A. (1995). Immunochemical identification and subcellular distribution of the α 1A subunits of brain calcium channels. *J. Neurosci.* **15**, 6403-6418.

- Wisden, W., Cope, D., Klausberger, T., Hauer, B., Sinkkonen, S.T., Tretter, V., Lujen, R., Jones, A., Korpi, E.R., Mody, I., Sieghart, W., and Somogyi, P. (2002). Ectopic expression of the GABAA receptor $\alpha 6$ subunit in hippocampal pyramidal neurons produces extrasynaptic receptors and an increased tonic inhibition. *NEuropharmacology*. **43**, 530-549.
- Wong, L.C., Lu, B., Tan, K.W., and Fivaz, M. (2010) Fully-automated image processing software to analyze calcium traces in populations of single cells. *Cell Calcium*. **48**, 270-274.
- Workman, A.D., Charvet, C.J., Clancy, B., Darlington, R.B., Finlay, B.L. (2013). Modeling transformations of neurodevelopmental sequences across mammalian species. *J Neurosci*. **33**, 7368-7383.
- Wu, X., Wu, Z., Ning, G., Guo, Y., Ali, R., Macdonald, R.L., De Blas, A.L., Luscher, B., and Chen, G. (2012). γ -aminobutyric acid type A (GABAA) receptor α subunits play a direct role in synaptic *versus* extrasynaptic targeting. *J. Biol. Chem.* **287**, 27417-27430.
- Xu, J., Mashimo, T., and Sudhof T.C. (2007). Synaptotagmin-1, -2, and -9: Ca(2+) sensors for fast release that specify distinct presynaptic properties in subsets of neurons. *Neuron* **64**, 667-681.
- Xu, M., Yan, C., Tian, Y., Yuan, X., and Shen, X. (2010). Effects of low level of methylmercury on proliferation of cortical progenitor cells. *Brain Res.* **1359**, 272-290.
- Xu, X., Weber, D., Carvan, M.J.3rd, Coppens, R., Lamb, C., Goetz, S., and Schaefer, L.A. (2012). Comparison of neurobehavioral effects of methylmercury exposure in older and younger adult zebrafish (*Danio rerio*). *NeuroToxicology*, **33**, 1212-1218.
- Yaginuma-Sakurai, K., Murata, K., Iwai-Shimada, M., Nakai, K., Kurokawa, N., Tatsuta, N., Satoh, H. (2012). Hair-to-blood ratio and biological half-life of mercury: experimental study of methylmercury exposure through fish consumption in humans. *J. Toxicol. Sci.* **37**, 123-130.
- Yamada, J., Okabe, A., Toyoda, H., Kilb, W., Luhmann, H.J., and Fukuda, A. (2004). Cl⁻ uptake promoting depolarizing GABA actions in immature rat neocortical neurones is mediated by NKCC1. *J Physiol* **557**, 829-841.
- Yasutake, A., Nakano, A., Miyamoto, K., and Eto, K. (1997). Chronic effects of methylmercury in rats. I. Biochemical aspects. *Tohoku J Exp. Med.* **182**, 197-205.

- Yee, S., Choi, B.H. (1994). Methylmercury poisoning induces oxidative stress in the mouse brain. *Exp. Mol. Pathol.* **60**, 188-196.
- Yee, S., and Choi, B.H. (1996). Oxidative stress in neurotoxic effects of methylmercury poisoning. *Neurotoxicology* **17**, 17-26.
- Yin, Z., Milatovic, D., Aschner, J.L., Syversen, T., Rocha, J.B., Souza, D.O., Sidoryk, M., Albrecht, J., and Aschner, M. (2007). Methylmercury induces oxidative injury, alterations in permeability and glutamine transport in cultured astrocytes. *Brain Res.* **1131**, 1-10.
- Yoshida, M., Shimizu, N., Suzuki, M., Watanabe, C., Satoh, M., Mori, K., and Yasutake, A. (2008). Emergence of delayed methylmercury toxicity after perinatal exposure in metallothionein-null and wild-type C57BL mice. *Environ. Health Perspect.* **116**, 746-751.
- Yorifuji, T., Tsuda, T., Inoue, S., Takao, S., and Harada, M. (2011). Long-term exposure to methylmercury and psychiatric symptoms in residents of Minamata, Japan. *Environ. Int.* **37**, 907-913.
- Yuan, Y., and Atchison, W.D. (1997). Action of methylmercury on GABA(A) receptor-mediated inhibitory synaptic transmission is primarily responsible for its early stimulatory effects on hippocampal CA1 excitatory synaptic transmission. *J Pharmacol Exp Ther* **282**, 64-73.
- Yuan, Y., and Atchison, W.D. (1999). Comparative effects of methylmercury on parallel-fiber and climbing-fiber responses of rat cerebellar slices. *J Pharmacol Exp Ther.* **288**, 1015-25.
- Yuan, Y., and Atchison, W.D. (2003). Methylmercury differentially affects GABA_A receptor-mediated spontaneous IPSCs in Purkinje and granule cells of rat cerebellar slices. *J Physiol* **550.1**, 191-204.
- Yuan, Y., and Atchison, W.D. (2007). Methylmercury-induced increase of intracellular Ca²⁺ increases spontaneous synaptic current frequency in rat cerebellar slices. *Mol Pharmacol* **71**, 1109-1121.
- Yuan, Y., Otero-Montañez, J.K., Yao, A., Herden, C.J., Sirois, J.E., and Atchison, W.D. (2005). nwardly rectifying and voltage-gated outward potassium channels exhibit low sensitivity to methylmercury. *Neurotoxicology* **26**, 439-454.

- Yuste, R., MacLean, J., Vogelstein, J. and Paninski, L. (2011). Imaging action potentials with calcium indicators. *Cold Spring Harb. Protoc.* **2011**, 985-989.
- Zariwala, H.A., Borghuis, B.G., Hoogland, T.M., Madisen, L., Tian, L., De Zeeuw, C.I., Zeng, H., Looger, L.L., Svoboda, K., and Chen, T.-W. (2012). A Cre-dependent CGaMP3 reporter mouse for neuronal imaging *in vivo*. *J. Neurosci.* **32**, 3131-3141.
- Zheng, J.Q., and Poo, M. (2007). Calcium signaling in neuronal motility. *Annu. Rev. Cell Dev. Biol.* **23**, 23375–23404.
- Zheng, T., Santi, M.R., Bovolin, P., Marlier, L.N.J., and Grayson, D.R. (2003). Developmental expression of the $\alpha 6$ GABA_A receptor subunit mRNA occurs only after cerebellar granule cell migration. *Dev Brain Res* **75**, 91-103.
- Zhou, X., Wei, J., Song, M., Francis, K., and Yu, S.P. (2010). Novel role of KCNQ2/3 channels in regulating neuronal cell viability. *Cell Death Differ.* **18**, 493-505.
- Zhuchenko, O., Bailey, J., Bonnen, P., Ashizawa, T., Stockton, D.W., Amos, C., Dobyns, W.B., Subramony, S.H., Zoghbi, H.Y., and Lee, C.C. (1997). Autosomal dominant cerebellar ataxia (SCA6) associated with small polyglutamine expansions in the alpha 1A-voltage-dependent calcium channel. *Nat. Genet.* **15**, 62-69.
- Zimmer, B., Kuegler, P.B., Baudis, B., Genewsky, A., Tanavde, V., Koh, W., Tan, B., Waldmann, T., Kadereit, S., and Leist, M. (2010). Coordinated waves of gene expression during neuronal differentiation of embryonic stem cells as basis for novel approaches to developmental neurotoxicity testing. *Cell Death Differ.* **18**, 383-395.